

EXHIBIT 3

LETTERS

An siRNA-based microbicide protects mice from lethal herpes simplex virus 2 infection

Deborah Palliser^{1,2}, Dipanjan Chowdhury^{1,2}, Qing-Yin Wang³, Sandra J. Lee⁴, Roderick T. Bronson⁵, David M. Knipe³ & Judy Lieberman^{1,2}

Herpes simplex virus 2 (HSV-2) infection causes significant morbidity¹ and is an important cofactor for the transmission of HIV infection². A microbicide to prevent sexual transmission of HSV-2 would contribute substantially to controlling the spread of HIV and other infections^{3,4}. Because RNA interference (RNAi) provides effective antiviral defence in plants and other organisms, several studies have focused on harnessing RNAi to inhibit viral infection⁵. Here we show that vaginal instillation of small interfering RNAs (siRNAs) targeting HSV-2 protects mice from lethal infection. siRNAs mixed with lipid are efficiently taken up by epithelial and lamina propria cells and silence gene expression in the mouse vagina and ectocervix for at least nine days. Intravaginal application of siRNAs targeting the HSV-2 *UL27* and *UL29* genes (which encode an envelope glycoprotein and a DNA binding protein⁶, respectively) was well tolerated, did not induce interferon-responsive genes or cause inflammation, and protected mice when administered before and/or after lethal HSV-2 challenge. These results suggest that siRNAs are attractive candidates for the active component of a microbicide designed to prevent viral infection or transmission.

Most mammalian cells do not take up siRNAs without a transfection reagent. We instilled fluorescein isothiocyanate (FITC)-labelled siRNAs complexed with a transfection lipid into the mouse vagina. The vaginal and ectocervical epithelium, underlying lamina propria and stroma efficiently took up the fluorescent siRNAs (Fig. 1a). When siRNAs targeting enhanced green fluorescent protein (*EGFP*) were administered intravaginally with lipid to transgenic GFP mice that express *EGFP* in every cell from the β -actin promoter⁷, GFP expression three days later was down-modulated throughout the vagina and cervix of GFP siRNA-treated mice, but not in control mice (Fig. 1b). Intravaginal siRNAs did not cause systemic silencing in distant organs such as the liver. Silencing persisted without diminution for at least nine days (the total length of the experiments) under conditions in which epithelial turnover was reduced by treatment with medroxyprogesterone acetate (Fig. 1c). Further studies are required to determine how long silencing persists and to assess the effect of menstrual variation on durability. Nonetheless, the extent and persistence of silencing suggests that siRNAs are attractive candidates for the active component of a microbicide. Moreover, their durability suggests that an RNAi-based microbicide might not need to be administered just before sexual intercourse, mitigating one of the main problems with microbicides: compliance.

To determine whether topical siRNA application could protect against sexually transmitted infection, seven siRNAs targeting three essential HSV-2 genes—*UL5* (a component of the helicase-prime complex), *UL27* (envelope glycoprotein B) and *UL29* (a DNA-binding protein)⁶—were designed using the Dharmacon design program⁸. After overnight incubation, siRNA-treated NIH3T3

(Fig. 2a) and Vero (Fig. 2b) cells were infected with HSV-2 strain 186 at a multiplicity of infection (MOI) of 1, and viral replication was assessed by plaque assay 24 h later. *UL5*, *UL27* and *UL29* siRNAs significantly reduced viral titre, but GFP siRNA and inverted *UL29* siRNA did not (Fig. 2b, c).

UL29 was the most effective siRNA, suppressing viral replication by 62-fold in NIH3T3 cells and 25-fold in Vero cells. Viral replication by *UL29* was inhibited at siRNA concentrations of 25 nM, and reached a plateau at 100 nM siRNA (Fig. 2c and data not shown). Gene silencing was specific for the targeted gene. When *UL27* and *UL29* messenger RNAs were quantified by real-time polymerase chain reaction with reverse transcription (RT-PCR) in Vero cells transfected one day earlier with *UL27*, *UL29* or GFP siRNA and infected with HSV-2, peak *UL27* expression (6 h after infection) was significantly downregulated in response to *UL27*, but not to *UL29* or GFP siRNA ($P < 0.004$). Conversely, *UL29*, which is expressed earlier than *UL27*, was significantly downregulated both at 4 h and 6 h, and only in response to *UL29* siRNA ($P < 0.0001$ compared with GFP siRNA) (Fig. 2d). One day later, when infection had amplified by cell-to-cell spread, the expression of all four viral genes examined (siRNA-targeted *UL5*, *UL27* and *UL29* as well as the viral thymidine kinase *TK*) was reduced by siRNAs targeting any of the viral genes (Fig. 2e). These differences were all highly statistically significant. Even the least effective siRNA (*UL29.1*) reduced viral replication (that is, *TK* expression; $P < 0.002$ compared with GFP siRNA). Control GFP siRNA did not affect viral gene transcription. Viral gene silencing roughly paralleled the inhibition of viral replication, with *UL29.2* siRNA proving the most effective, suppressing relative viral gene expression by 4–5-fold ($P < 0.001$ compared with GFP siRNA). *UL5.2* and *UL27.2* siRNAs each inhibited viral gene expression by ~3-fold ($P < 0.002$ for *UL5.2*, $P < 0.001$ for *UL27.2* compared with GFP).

To investigate whether siRNAs could protect mice from HSV-2 infection, groups of 5–10 medroxyprogesterone-pretreated mice were given lipid-complexed *UL29.2* intravaginally 2 h before and 4 h after vaginal challenge with 2LD_{50} (2×10^4 plaque-forming units, p.f.u.) of HSV-2 wild-type virus. Mice treated with <250 pmol *UL29.2* siRNA were not protected, mice treated with 250 pmol siRNA were partially protected, and 500 pmol siRNA gave optimal protection (data not shown). We therefore administered 500 pmol siRNA in subsequent experiments.

UL29.2 siRNA provided highly significant protection, as assessed daily by a clinical disease scoring system or by survival (Fig. 3a, b). Although 75% of infected mice treated with GFP siRNA (15/20) or no siRNA (13/17) died, only 25% of mice treated with *UL29.2* (5/20) died (time to death comparison by log-rank test; $P < 0.001$ versus no treatment, $P < 0.003$ versus GFP siRNA). Although 55% of *UL29.2*-treated mice developed some signs of infection, surviving

¹CBR Institute for Biomedical Research, ²Department of Pediatrics, ³Department of Microbiology and Molecular Genetics, ⁴Dana Farber Cancer Institute and ⁵Department of Pathology, Harvard Medical School, Boston, Massachusetts 02115, USA.

mice were free of clinical disease by day 11. A longitudinal regression analysis of disease severity over time and between groups showed robust protection in UL29.2-treated mice ($P < 0.001$ versus no treatment, $P < 0.006$ versus GFP siRNA when analysed with respect to time course; $P < 0.001$ versus either control when analysed between groups).

Mice treated with UL27.2, which was less effective *in vitro*, were less effectively protected. Sixty per cent (6/10) of mice survived the lethal vaginal challenge ($P < 0.009$ compared with untreated, $P = 0.10$ compared with GFP siRNA). UL27.2 protection from disease severity was significant by longitudinal regression analysis ($P < 0.001$ compared with untreated, $P < 0.005$ compared with GFP siRNA with respect to time; $P < 0.01$ and $P = 0.05$ when analysed between the respective groups). The clinical advantage was also evident by quantifying shed virus six days after infection

(Fig. 3c). Although all infected mice not given siRNAs shed virus on day six, no virus was detected in 70% of UL29.2- and 50% of UL27.2-treated mice. No virus was isolated from three out of nine GFP siRNA-treated mice, but this was not significantly different from mice not treated with siRNAs. Comparison of virus recovered from UL29.2 siRNA-treated mice with GFP siRNA-treated mice also was not significant ($P = 0.09$ by Wilcoxon rank sum test). However, the geometric mean viral titre was reduced from $1,226 \text{ p.f.u. ml}^{-1}$ in untreated mice to $7.9 \text{ p.f.u. ml}^{-1}$ in mice that received UL29.2 ($P < 0.01$). Viral shedding at day six predicted survival, as 18 out of 19 mice from which virus was cultured died, whereas none out of 15 mice with undetectable virus died.

One concern about using RNAi against viruses is escape from RNAi by mutation of the targeted sequence. Escape mutation has been shown for polio, HIV and hepatitis C¹¹. We cloned and

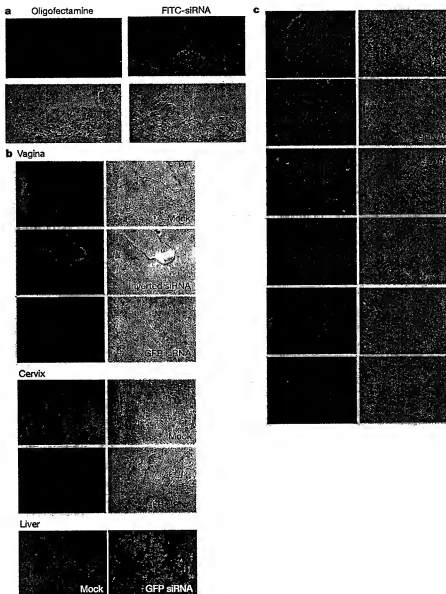


Figure 1 | siRNAs administered intravaginally are efficiently taken up by vaginal tissue and durably silence endogenous EGFP expression.

a, FITC-siRNA mixed with Oligofectamine is efficiently taken up throughout the mucosa and submucosa. Sections were obtained 24 h after administration. b, siRNA targeting EGFP, but not an inverted control sequence, silences EGFP expression throughout the mouse vagina and cervix

in GFP transgenic mice three days after administration. Liver EGFP expression is unaffected. c, Silencing persists for at least nine days in the vagina of GFP transgenic mice treated with GFP siRNAs. Data are representative of at least two experiments. An siRNA targeting an irrelevant gene (Set) was administered to control mice.

sequenced HSV-2 DNA from the day 6 vaginal swab from one UL29.2-treated mouse that died and from one control mouse. No mutations were found in 150-nucleotide stretches of *UL29*, which included the targeted sequence, in 24 sequences analysed from each mouse. Escape mutation is not anticipated to be as problematic for DNA viruses (such as HSV-2) as for RNA viruses.

The cervicovaginal mucosa of siRNA-treated, HSV-2-infected mice at day 6 was also spared (Fig. 3d). In control infected mice that were pretreated with no siRNA or GFP siRNA, the mucosal epithelium was partially denuded, and dying cells and inflammatory infiltrates were prominent. Multinucleated cells with intranuclear inclusion bodies—a hallmark of HSV-2 infection—were also evident. In contrast, in UL27.2 or UL29.2 siRNA-treated mice, the epithelium

was intact and there were few apoptotic bodies and scarcely any inflammatory cells.

To investigate the effects of delaying siRNA treatment until after HSV-2 exposure, 500 pmol of UL27.2 or UL29.2, or a mixture of both (250 pmol each), was administered intravaginally 3 and 6 h after infection. Mice receiving UL27.2 or UL29.2 alone had no survival advantage compared with mice given GFP siRNA (2/6 survived) or no siRNA (1/6 survived) (Fig. 3e). However, 5/6 mice given both UL27.2 and UL29.2 siRNA survived ($P = 0.11$ compared with GFP siRNA; $P < 0.04$ compared with no siRNA). Therefore, post-exposure treatment might be effective. Targeting multiple genes will probably work better than targeting a single gene.

Under certain circumstances, siRNAs can induce the interferon (IFN) pathway and trigger inflammation^{17–19}. We therefore analysed vaginal tissue for inflammatory infiltrates (Fig. 4a) and induction of interferon and interferon-responsive genes 24 and 48 h after siRNA treatment (Fig. 4b). siRNA treatment did not cause an inflammatory infiltrate. Moreover, *Ifnb* and the principal interferon-responsive genes, *Oas1* and *Stat1*, were not significantly induced when analysed by quantitative RT-PCR. As expected, HSV-2 infection in the absence of siRNAs (used as a positive control) activated interferon-responsive genes.

Vaginal instillation of siRNAs targeting essential viral genes protects mice from vaginal challenge with a lethal dose of HSV-2. The treatment was well-tolerated without causing inflammation or inducing interferon-responsive genes. This efficient and lasting silencing deep in the vaginal tissue was unexpected, and augurs well for using siRNAs to prevent or treat sexually transmitted viral and parasitic infections. Our results, together with impressive results in lung models of viral infection^{16–20}, suggest that siRNA uptake at mucosal surfaces may be particularly efficient and involve mechanisms not present in internal organs.

Much work needs to be done to develop siRNAs as the basis for a microbicide. These experiments were done without optimizing the siRNAs for silencing efficiency or chemical modifications that enhance resistance to endogenous RNases²¹. siRNAs would also need to be formulated in a vehicle acceptable for vaginal retention. The effect of menstrual variation on protection, especially on the durability of silencing, needs to be evaluated. Viral sequence variability also needs to be addressed. However, by targeting relatively well-conserved viral sequences in essential viral genes or by combining siRNAs that target multiple viral genes, the related problems of viral sequence diversity and potential escape mutation might be mitigated. Although we did not find evidence of escape mutation, this might take longer than six days to develop. Any extension of our results to the designing of an HIV microbicide would also require demonstrating silencing in resident tissue macrophages, dendritic cells and T cells, which are rare in normal, uninfamed vaginal tissue.

Finally, cost is an important consideration for a microbicide designed for global use. Only 500 pmol siRNA was required to protect mice in this study. The manufacturing cost of a single application for humans, crudely estimated on the basis of scaling up by weight and current costs, is \$8. If silencing is durable and treatments can be spaced, this is a realistic cost. Given the devastating global epidemic and the unlikelihood of there being an effective HIV-1 vaccine soon, we feel that investigating whether RNAi can be harnessed for use in microbicides is a sensible approach.

Note added in proof: In the advance online publication of this Letter, in the second sentence of the fourth paragraph ‘25 μM’ and reached a plateau at 100 μM’ should read ‘25 nM’, and reached a plateau at 100 nM’. In addition, the x axis of Fig. 2c should read ‘siRNA concentration (nM)’. These errors have been corrected for print.

METHODS

Mice. BALB/c mice (5–8 weeks old) were obtained from Taconic Farms; FVB-Tg(GFP)-Nagy mice were from Jackson Laboratories²². Mice were

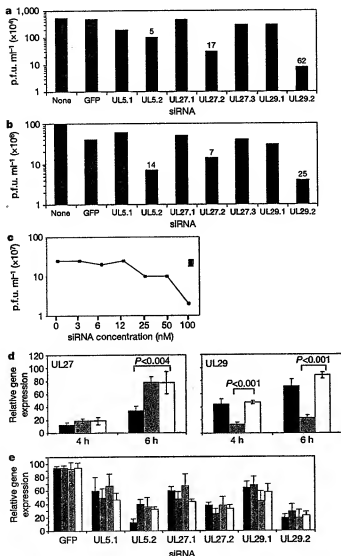


Figure 2 | siRNAs targeting HSV-2 reduce viral replication. NIH3T3 (a) or Vero (b–e) cells were transfected overnight with siRNA, then infected with HSV-2 and harvested 20 h later. Values above bars show fold reduction in viral plaques. Data are representative of five independent experiments. c, Dose-response curve, showing effect of treatment with UL29.2 (filled circles), inverted UL29.2 (filled square) or GFP (filled triangle) siRNA. d, e, Gene silencing by real-time RT-PCR was specific at 4 h or 6 h, that is, before cell-to-cell spread (UL27.2, dark grey; UL29.2, light grey; GFP, white) (d), but expression of all viral genes (UL5.1, black; UL27.1, dark grey; UL29.1, light grey; TK, white) was suppressed at 24 h (e). Data show mean \pm s.d. from one of two experiments.

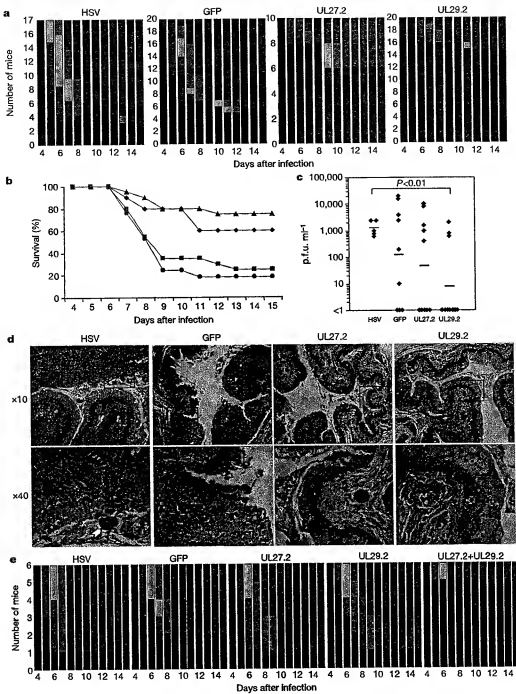


Figure 3 | siRNAs protect mice from lethal HSV-2 infection. **a-d.** Mice given lipid-complexed siRNA intravaginally 2 h before and 4 h after infection with $\sim 2 \text{ LD}_{50}$ HSV-2 were analysed for disease severity (**a**) (see colour code provided in Methods), survival (**b**) (HSV only, red; GFP, green; UL27.2, light blue; UL29.2, dark blue), viral shedding on day 6 (**c**) and cervicovaginal histopathology on day 6 (**d**). **a, b** show data from three experiments. Transfection of lipid alone did not affect HSV-2 disease (not shown).

subcutaneously injected with 2 mg medroxyprogesterone acetate (Sicor), and then 1 week later were infected vaginally with 2×10^6 p.f.u. ($\sim 2 \text{ LD}_{50}$) HSV-2 strain 186 (ref. 22). siRNA (500 pmol) was complexed with Oligofectamine (Invitrogen) according to the manufacturer's protocol, and was then administered intravaginally (in a maximum volume of 12 μl) either 2 h and 4 h after HSV-2 infection or 3 h and 6 h after HSV-2 infection. Clinical signs of infection were graded according to a five-point scale: 0, no signs of infection (purple); 1, slight genital erythema and oedema (blue); 2, moderate genital inflammation (green); 3, purulent genital lesions (yellow); 4, hind limb paralysis

(orange); 5, death (red)²². Viral shedding was determined by swabbing the vaginal cavity (using a Microtip swab, Purify Inc.) on day 6 after infection, and titrating the virus on Vero cells. In some cases, the vagina was dissected at the indicated times and either fixed in 10% formalin (Sigma) for paraffin embedding and sectioning, or stored in RNAlater (Qiagen) for RNA isolation.

Viruses and transfection assays. For *in vitro* studies, 186AKpn, a replication-competent, TK-negative mutant of strain 186syn + (ref. 23) was grown in Vero cells as described²⁴. Vero or NIH3T3 cells (ATCC) (4×10^4 cells per well in 6-well plates in 1 ml of complete medium, plated one day earlier), were treated

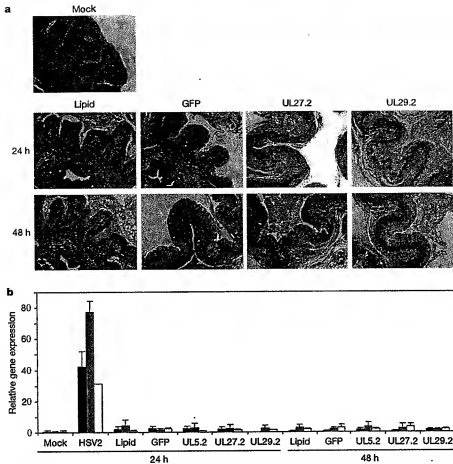


Figure 4 | Topical lipid-complexed siRNAs do not activate inflammation or interferon-responsive genes. **a,** Vaginal tissue, dissected 24 h or 48 h after administering 500 pmol of lipid-complexed siRNA, was assessed by haematoxylin-eosin staining for inflammation (**a**, $\times 10$ magnification) and by quantitative RT-PCR for expression of *Ifnb* (black) and the interferon-responsive genes *Stat1* (grey) and *Oasl* (white) relative to the control gene

Gapdh (**b**). HSV-2 infection was used as a positive control for interferon induction. In siRNA-treated mice, no HSV-2 was administered. None of the siRNAs induced a significant change in interferon-responsive gene expression compared to mock-treated mice given only PBS intravaginally. Data show mean \pm s.d.

with 100 pmol or the indicated concentration of siRNA. The siRNA had been complexed with TransIT-TKO (Mirus) to transfet Vero cells or with TransIT-siQuest (Mirus) for NIH3T3 cells, according to the manufacturer's instructions. The medium was replaced after overnight incubation at 37 °C, and 2 h later HSV-2 186ΔKpn was added at an MOI of 1. After 1 h at 37 °C, the medium was again replaced. Cells were harvested 24 h later and viral titres determined by plaque assay on Vero cells. For mouse experiments, wild-type HSV-2 strain 186syn + virus was used²³. An aliquot of virus used for each mouse experiment was also assayed by plaque assay to confirm viral titre.

siRNAs. siRNAs (Dharmacon) were prepared according to the manufacturer's instructions. FITC-labelled siRNA was a previously described sequence targeting CD4 (ref. 26). The sequence for silencing *EGFP* has been described²⁴. The sequences for HSV-2 (Genbank accession number NC_001798) siRNAs were: UL5.1 (nt 12838–12856) sense 5'-CUACGGCAUCAGCUCCAAA-3', antisense 5'-UUUGGAGCGUAGGCGGUAG-3'; UL5.2 (nt 12604–12622) sense 5'-UGUGGUCAUUGCUAUUA-3', antisense 5'-UUAAUAGACAAUAGACCACA-3'; UL27.1 (nt 54588–54606) sense 5'-GUUUGAGUUAUACCAACAU-3', antisense 5'-UAUGGUGGUAGUACGUAAAC-3'; UL27.2 (nt 54370–54388) sense 5'-ACCGUAGCUCGGACAGUC-3', antisense 5'-GAGUUCUGACGAGCAUCGU-3'; UL27.3 (nt 54097–54115) sense 5'-UGACCCGAAUACAUCA-3', antisense 5'-AUGUGAUGGUACGGUGA-3'; UL29.1 (nt 59715–59733) sense 5'-CACUUGGAGUACAUUCAA-3', antisense 5'-UAUGGAUGUACGUAGUGG-3'; UL29.2 (nt 60324–60342) sense 5'-CUUUCGGCAUUAUCCAA-3', antisense 5'-AACCUUAAUCUACGGCUUUC-3', antisense 5'-GAAAGGGUAGUAGUAGGUU-3'.

Quantitative RT-PCR. Total RNA (1 µg) was isolated using the RNeasy RNA isolation kit (Qiagen) and reverse transcribed using Superscript III (Invitrogen)

and random hexamers, according to the manufacturer's protocol. Real-time PCR was performed on 0.2 µl of complementary DNA, or a comparable amount of RNA with no reverse transcriptase, using Platinum Taq Polymerase (Invitrogen) and a BioRad iCycler. SYBR green (Molecular Probes) was used to detect PCR products. Reactions were performed in 25 µl in triplicate. Primers were: *Gapdh* forward 5'-TTCACCCACATGGAAAGGG-3', *Gapdh* reverse 5'-GGCATGGACTGTGTCATGG-3', *TX* forward 5'-CGATCTACTCGCCA CACGGTG-3', *TX* reverse 5'-GAACGGGAAACAGGCAAACAG-3', *UL5* forward 5'-TCCGTGGACTCACCTTGGAC-3', *UL5* reverse 5'-CGAACCT GTGCCTCACACATCGC-3', *UL27* forward 5'-CAAAGACGTGACCGCTGTGG CAG-3', *UL27* reverse 5'-GGGGTTGGCTCCATGTGTTCC-3', *UL29* forward 5'-CGCAGGAGATGGAGCTGTGTTCC-3', *UL29* reverse 5'-CGGGCTGT CATCGTCCGAAG-3', *Stat1* forward 5'-TTTCCCAGACTCGACCTCTCG-3', *Stat1* reverse 5'-GGGTGCAAGTTGGGATTCAC-3', *Oasl* forward 5'-GGAGGTGCAAGTCCAAACGAA-3', *Oasl* reverse 5'-TGAAGGGAGGAG GGGCATAAAC-3', *Ifnb* forward 5'-CTGGAGGAGCTGAATGGAAA-3', *Ifnb* reverse 5'-CTTGAAGTCCGCCCTGTAGGT-3'.

PCR parameters consisted of 5 min Taq activation at 95 °C, followed by 40 cycles of 95 °C \times 20 s, 60 °C \times 30 s, and 69 °C \times 20 s. Standard curves were generated and the relative amount of mRNA was normalized to *Gapdh* mRNA. Specificity was verified by melt curve analysis and agarose gel electrophoresis.

Tissue sections and microscopy. For fluorescence microscopy, dissected tissue was placed in optimal cutting temperature compound (TissueTek) and snap-frozen in LN₂. For haematoxylin-eosin stained sections, tissues were fixed in 10% formalin and paraffin-embedded. Microscopy was performed and scored (by an operator blind to the treatment condition) on a Zeiss Axiovert 200M microscope using Slidebook acquisition and analysis software (Intelligent Imaging).

Statistical analysis. *In vitro* data were analysed by Student's t-test. Survival distribution was calculated using the Kaplan and Meier method¹¹, and the univariate comparison of survival for control versus treated groups was tested using a log-rank test, comparing two groups at a time¹². The approach of generalized estimating equations was used to model disease scores collected over time and to compare disease severity of control versus treated groups¹³. All P-values are for two-tailed significance tests.

Received 12 July; accepted 26 September 2005.

Published online 23 November 2005.

- Whitley, R. J. in *Field's Virology* (eds Knipe, D. M. & Howley, P. M.) 2461–2510 (Lippincott, Williams and Wilkins, Philadelphia, 2001).
- Wald, A. & Link, K. Risk of human immunodeficiency virus infection in herpes simplex virus type 2 seropositive persons: a meta-analysis. *J. Infect. Dis.* 185, 45–52 (2002).
- Celum, C., Levine, R., Weaver, M. & Wald, A. Genital herpes and human immunodeficiency virus double trouble. *Bull. World Health Organ.* 82, 447–453 (2004).
- Pichler, H. Starting to gel. *Nature* 430, 138–140 (2004).
- Shankar, P., Manjunath, N. & Lieberman, J. The prospect of silencing disease using RNA interference. *J. Am. Med. Assoc.* 293, 1367–1373 (2005).
- Roizman, B. & Knipe, D. M. in *Field's Virology* (eds Knipe, D. M. & Howley, P. M.) 2399–2440 (Lippincott, Williams and Wilkins, Philadelphia, 2001).
- Hadjantonakis, A. K., Gertstein, M., Iwasa, M., Okabe, M. & Nagy, A. Generating green fluorescent mice by germline transmission of green fluorescent ES cells. *Med. Dev.* 76, 79–90 (1998).
- Khorova, A., Reynolds, A. & Jayasena, S. D. Functional siRNAs and miRNAs exhibit strand bias. *Cell* 115, 209–216 (2003).
- Boden, D., Pusch, O., Lee, F., Tucker, L. & Ramananam, R. Human immunodeficiency virus type 1 escape from RNA interference. *J. Virol.* 77, 11531–11535 (2003).
- Gitlin, L., Stone, J. K. & Andino, R. Poliovirus escape from RNA interference: short interfering RNA-target recognition and implications for therapeutic approaches. *J. Virol.* 79, 1027–1035 (2005).
- Wilson, J. A. & Richardson, C. D. Hepatitis C virus replicons escape RNA interference induced by a short interfering RNA directed against the NS5B coding region. *J. Virol.* 79, 7050–7058 (2005).
- Sledz, C. A., Holko, M., de Veer, M. J., Silverman, R. H. & Williams, B. R. Activation of the interferon system by short-interfering RNAs. *Nature Cell Biol.* 5, 834–839 (2003).
- Heidel, J. D., Hu, S., Liu, X. F., Triche, T. J. & Davis, M. E. Lack of interferon response in animals to naked siRNAs. *Nature Biotechnol.* 22, 1579–1582 (2004).
- Hornung, V. et al. Sequence-specific potent induction of IFN- α by short interfering RNA in plasmacytoid dendritic cells through TLR7. *Nature Med.* 11, 263–270 (2005).
- Judge, A. D. et al. Sequence-dependent stimulation of the mammalian innate immune response by synthetic siRNA. *Nature Biotechnol.* 23, 457–462 (2005).
- Ge, Q. et al. Inhibition of influenza virus production in virus-infected mice by RNA interference. *Proc. Natl. Acad. Sci. USA* 101, 8676–8680 (2004).
- Tompkins, S. M., Lo, C. Y., Turnpenny, T. M. & Epstein, S. L. Protection against lethal influenza virus challenge by RNA interference in vivo. *Proc. Natl. Acad. Sci. USA* 101, 8682–8686 (2004).
- Bikò, V., Musiyenko, A., Shulyayeva, O. & Barik, S. Inhibition of respiratory viruses by nasally administered siRNA. *Nature Med.* 11, 50–55 (2005).
- Zhang, W. et al. Inhibition of respiratory syncytial virus infection with intranasal siRNA nanoparticles targeting the viral NS1 gene. *Nature Med.* 11, 56–62 (2005).
- Li, B. J. et al. Using siRNA in prophylactic and therapeutic regimens against SARS coronavirus in Rhesus macaque. *Nature Med.* 11, 944–951 (2005).
- Manoharan, M. RNA interference and chemically modified small interfering RNAs. *Curr. Opin. Chem. Biol.* 8, 570–579 (2004).
- Morrison, L. A., Da Costa, X. J. & Knipe, D. M. Influence of mucosal and parenteral immunization with a replication-defective mutant of HSV-2 on immune responses and protection from genital challenge. *Virology* 243, 178–187 (1998).
- Jones, C. A., Taylor, T. J. & Knipe, D. M. Biological properties of herpes simplex virus 2 replication-defective mutant strains in a murine nasal infection model. *Virology* 278, 137–150 (2000).
- Gao, M. & Knipe, D. M. Genetic evidence for multiple nuclear functions of the herpes simplex virus ICP8 DNA-binding protein. *J. Virol.* 63, 5258–5267 (1989).
- Spang, A. E., Godowski, P. J. & Knipe, D. M. Characterization of herpes simplex virus 2 temperature-sensitive mutants whose lesions map in or near the coding sequences for the major DNA-binding protein. *J. Virol.* 45, 332–342 (1983).
- Novina, C. D. et al. siRNA-directed inhibition of HIV-1 infection. *Nature Med.* 8, 681–686 (2002).
- Kaplan, E. L. & Meier, R. Non-parametric estimation from incomplete observation. *J. Am. Stat. Assoc.* 53, 457–481 (1958).
- Mantel, N. Evaluation of survival data and two new rank order statistics arising in its consideration. *Cancer Chemother. Rep.* 50, 163–170 (1966).
- Zeger, S. L. & Liang, K. Y. Longitudinal data analysis for discrete and continuous outcomes. *Biometrics* 42, 121–130 (1986).

Acknowledgements We thank R. Colgrove, T. Taylor, E. Torres-Lopez, D. Brown and S. White for advice. This work was supported by grants from the NIH to D.M.K. and J.L., and by postdoctoral fellowships from the Harvard Center for AIDS Research and amfAR to D.P. and the Leukemia and Lymphoma Society to D.C.

Author Information Reprints and permissions information is available at npg.nature.com/reprintsandpermissions. The authors declare competing financial interests: details accompany the paper at www.nature.com/nature. Correspondence and requests for materials should be addressed to J.L. (lieberman@cbr.med.harvard.edu).

EXHIBIT 4

ORIGINAL ARTICLE

Suppression of ocular neovascularization with siRNA targeting VEGF receptor 1

J Shen¹, R Samul¹, RL Silva¹, H Akiyama¹, H Liu¹, Y Saishin¹, SF Hackett¹, S Zinnen², K Kossen²,

K Fosnaugh², C Vargeese², A Gomez², K Bouhana², R Aitchison², P Pavco² and PA Campochiaro¹

¹The Departments of Ophthalmology and Neuroscience, The Johns Hopkins University School of Medicine, Baltimore, MD, USA and

²Sirna Therapeutics, Inc., Boulder, CO, USA

In this study, we used small interfering RNA (siRNA) directed against vascular endothelial growth factor receptor 1 (vegfr1) mRNA to investigate the role of VEGFR1 in ocular neovascularization (NV). After evaluating many siRNAs, Sirna-027 was identified; it cleaved vegfr1 mRNA at the predicted site and reduced its levels in cultured endothelial cells and in mouse models of retinal and choroidal neovascularization (CNV). Compared to injection of an inverted control sequence, quantitative reverse transcriptase-PCR demonstrated statistically significant reductions of 57 and 40% in vegfr1 mRNA after intravitreous or periocular injection of Sirna-027, respectively. Staining showed uptake of 5-bromodeoxyuridine-labeled Sirna-027 in retinal cells that

lasted between 3 and 5 days after intravitreous injection and was still present 5 days after periocular injection. In a CNV model, intravitreous or periocular injections of Sirna-027 resulted in significant reductions in the area of NV ranging from 45 to 66%. In mice with ischemic retinopathy, intravitreous injection of 1.0 µg of Sirna-027 reduced retinal NV by 32% compared to fellow eyes treated with 1.0 µg of inverted control siRNA. These data suggest that VEGFR1 plays an important role in the development of retinal and CNV and that targeting vegfr1 mRNA with siRNA has therapeutic potential.

Gene Therapy (2006) 13, 225–234. doi:10.1038/sj.gt.3302641; published online 29 September 2005

Keywords: age-related macular degeneration; angiogenesis; choroidal neovascularization; diabetic retinopathy; ischemic retinopathy; retinal neovascularization; small interfering RNA

Introduction

Vascular endothelial growth factor (VEGF-A) plays a central role in the development of several types of neovascularization (NV), including retinal and choroidal neovascularization (CNV).^{1–4} These data suggest that the VEGF pathway may be an important therapeutic target and results from clinical trials using an aptamer⁵ or an antibody fragment⁶ that binds VEGF-A have supported this contention. Blocking VEGF receptors is another strategy for antagonizing VEGF-A that has the potential advantage of blocking multiple VEGF family members at once.

There are multiple VEGF receptors (VEGFR) and their role in angiogenesis is not completely clear. Mutated VEGFs that bind VEGFR2, but not VEGFR1, have full activity as stimulators of endothelial cell proliferation and migration, and stimulate corneal angiogenesis and vascular leakage in skin, whereas VEGFs that bind VEGFR1, but not VEGFR2, lack these activities.⁷ Therefore, for endothelial cells *in vitro*, and for cornea and skin

in vivo, VEGFR2 is essential for VEGF-mediated activity. In fact, it has been postulated that VEGFR1 is a decoy receptor that negatively regulates the activity of VEGFR2,⁸ and during developmental angiogenesis this appears to be the case, because *vegfr1* –/– mice show excessive proliferation of angioblasts, a sign of VEGF-A overaction.⁹ However, in other settings, VEGFR1 appears to play proangiogenic and propermeability roles, effects that may be mediated by placental growth factor (PIGF), which binds VEGFR1, but not VEGFR2.¹⁰ Also, stimulation of VEGFR1 may cause vascular endothelium in some vascular beds to release tissue-specific growth factors.¹¹ Therefore, investigations in the vascular bed of interest must be carried out to determine the roles of VEGFR1 and VEGFR2 in particular disease processes.

Small interfering RNAs (siRNAs) provide a useful means to selectively reduce mRNAs and probe the function of gene products. In this study, we used Sirna-027, an siRNA that specifically reduces vegfr1 mRNA, to explore the role of VEGFR1 in ocular NV.

Results

siRNA-mediated reduction of vegfr1 mRNA in cultured cells

Candidate siRNAs targeting vegfr1 mRNA were designed using a bioinformatics-based approach with one

Correspondence: Dr PA Campochiaro, Departments of Ophthalmology and Neuroscience, The Johns Hopkins University School of Medicine, Maumenee 719, 600 N. Wolfe Street, Baltimore, MD 21287-9277, USA.

E-Mail: pcampo@jhmi.edu

Received 13 June 2005; revised 26 July 2005; accepted 4 August 2005; published online 29 September 2005

selection criterion being conservation of the siRNA target site in the human, mouse, and rat *vegfr1* sequences. This constraint supports direct animal testing of siRNAs that are also suitable for human clinical trials. Chemical modifications of the siRNA were included that enhance stability and support their use *in vivo*. These include inverted abasic moieties at the 5' and 3' ends of the sense strand oligonucleotide and a single phosphorothioate linkage between the last two nucleotides at the 3' end of the target-complementary (antisense) strand. These modifications significantly extend the *in vivo* half-life in vitreous and ocular tissue following intraocular injection into rabbit eye (manuscript in preparation).

The lead candidate Sirna-027 was first identified from a panel of stabilized siRNAs by its ability to reduce NV in a rat corneal pocket model of VEGF-induced angiogenesis (data not shown). To determine if treatment with Sirna-027 specifically reduced its endogenous target mRNA, cell culture studies were carried out in human aortic endothelial cells (HAEs). When quantified by reverse transcriptase (RT)-PCR, cellular levels of *vegfr1* mRNA were reduced by 71% following treatment with 12.5 nM Sirna-027 relative to treatment with the inverted control siRNA (Figure 1a). No effect of Sirna-027 was noted on the level of *vegfr2* mRNA (Figure 1b). While these two VEGF receptors share considerable homology, the Sirna-027 target site is not present in *vegfr2* mRNA. Significant reduction of *vegfr1* mRNA and lack of activity on *vegfr2* mRNA support the specificity of Sirna-027 cleavage.

The potency of Sirna-027 was evaluated using a luciferase-reporter assay in cultured HeLa cells. A reporter plasmid was constructed by ligating ~80 nucleotides of human *vegfr1* sequence into the 3' untranslated region of the *Renilla* luciferase gene. The reporter plasmid also contained a Firefly luciferase gene for use as a normalization control. When this reporter plasmid and Sirna-027 were cotransfected into HeLa cells, RNAi activity directed against the *vegfr1* target appended to the *Renilla* mRNA resulted in a reduction of *Renilla* luciferase activity. As shown in Figure 1c, the IC_{50} for Sirna-027 in this system is ~50 pm. The dose-response curve reaches saturation at approximately 1 nM Sirna-027 with a >95% reduction in the ratio of *Renilla*:Firefly luciferase activity. These data demonstrate that Sirna-027 is effective at extremely low concentrations.

Experiments in a HeLa cell extract confirmed that Sirna-027 acts by an RNAi mechanism to direct cleavage of *vegfr1* sequence at the expected site. The site of siRNA-directed target cleavage is defined by the 5' end of the siRNA antisense strand and results in site-specific strand scission between the target nucleotides annealed to the 10th and 11th positions of the target complementary sequence.¹² As shown in Figure 2, incubation of an ~100 nucleotide 5'-³²P-labeled transcript of *vegfr1* sequence with Sirna-027 in a HeLa cell extract resulted in specific cleavage predominantly at the expected position. The amount of product formed increased with time; after 2 h approximately 25% of the target RNA was converted to product. No cleaved product was observed when the target was incubated with a control siRNA with the same stabilizing modifications. Thus, Sirna-027 acts via an RNAi mechanism and directs the site-specific cleavage of *vegfr1* mRNA.

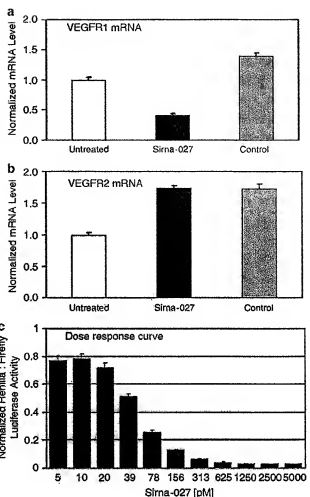


Figure 1 Sirna-027 specifically reduces *vegfr1* mRNA. Cultured HAEs were left untreated or transfected with LP2K complexes containing 12.5 nM Sirna-027 or the inverted control siRNA. Total RNA isolated at 24 h post-transfection was analyzed by RT-PCR for either *vegfr1* (a) or *vegfr2* (b) mRNA. Normalized RNA levels for the untreated samples were set to 1 to facilitate comparison. Treatment with Sirna-027 reduced the level of *vegfr1* by 71% ($P=0.0001$) compared to treatment with the inverted control siRNA, but had no effect on the level of *vegfr2*. Note that in this cell culture system siRNA transfection conditions alone significantly increased the level of both VEGF receptor mRNAs. Compared to untreated cells, treatment with the inverted control resulted in a 40–75% increase in *vegfr1* ($P=0.0026$) and *vegfr2* ($P=0.0038$), respectively. As this effect is likely due to the use of the lipid transfection agent, it is appropriate to state the activity of Sirna-027 relative to treatment with the inverted control siRNA. (c) A dose-response curve (5–5000 pm) for Sirna-027 was obtained in a luciferase reporter system in HeLa cells in which cleavage at the Sirna-027 target site resulted in decreased *Renilla* luciferase activity (normalized to activity of Firefly luciferase located on the same plasmid reporter). Curve fit of the data using Kaleidograph software (Synergy Software, Reading, PA, USA) revealed an IC_{50} of ~50 pm. For (a–c), means (+s.e.m.) were calculated from three replicate transfections.

Intravitreous or periocular injection of Sirna-027 significantly reduces *vegfr1* mRNA and protein in the eye

Experiments were designed to determine how effectively Sirna-027 is able to reduce expression of *vegfr1* mRNA in two mouse models of ocular NV. In a mouse model of

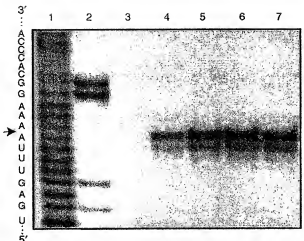
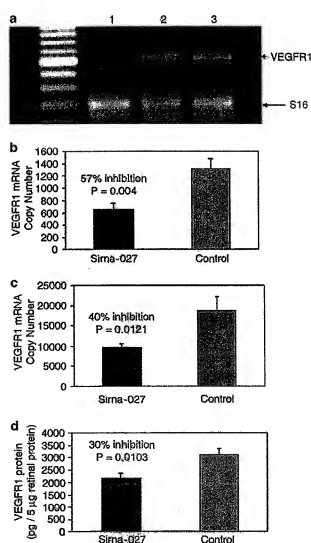


Figure 2 Sirna-027 directs site-specific cleavage of target vegfr1 RNA. A radiolabeled transcript of vegfr1 RNA sequence containing the Sirna-027 target site was generated for use as the substrate for an siRNA-induced cleavage assay in HeLa cell extract. The sequence of the Sirna-027 target site is shown to the left of RNA markers generated from the radiolabeled transcript by alkaline hydrolysis (lane 1, nucleotide ladder) or RNase T1 (lane 2, digestion at guanosine residues). The remaining lanes contain products following a 2 h incubation with either the negative control siRNA (lane 3, no cleavage products) or Sirna-027 for 30, 60, 90, and 120 min (lanes 4–7, respectively). The predominant Sirna-027 cleavage product is observed at the expected location within the substrate as indicated with A'IA in the sequence. Secondary products, one or more nucleotides shorter, may result from substrate heterogeneity or target RNA degradation prior to or subsequent to cleavage.

CNV due to laser-induced rupture of Bruch's membrane, mice were given one intravitreous injection of 1.5 μ g of Sirna-027, 1.5 μ g of a control siRNA with inverted sequence, or phosphate-buffered saline (PBS) immediately after laser. After 7 days, RT-PCR was carried out using total RNA isolated from whole eyes and *vegfr1* specific primers. Compared to the level of *vegfr1* mRNA amplified from eyes injected with inverted control siRNA (Figure 3a, lane 2) or PBS (lane 3), only a very faint band for *vegfr1* mRNA was visible from eyes injected with Sirna-027 (lane 1).

A similar study was carried out in mice with oxygen-induced ischemic retinopathy. In this case, mice were given an intravitreous injection of 3 μ g of Sirna-027 in one eye and 3 μ g of inverted control siRNA in the other eye at P12, the beginning of the ischemic period. At P15, real-time PCR demonstrated that injection of Sirna-027 resulted in a 57% reduction in *vegfr1* mRNA (Figure 3b) compared to intravitreous injection of inverted control siRNA. Periodic injection of Sirna-027 also significantly reduced the level of *vegfr1* mRNA in the retinas of mice with ischemic retinopathy (Figure 3c). Periodic injection of 7.5 μ g of Sirna-027 at P12, P14, and P16 resulted in



a 40% reduction in *vegfr1* mRNA at P17 compared to fellow eyes injected with inverted control siRNA.

To assess the impact on VEGFR1 protein levels, P12 mice with ischemic retinopathy were given an intravitreous injection of 5 µg of Sirna-027 in one eye and 5 µg of inverted control siRNA in the other eye. At P15, ELISA results showed that the level of VEGFR1 in the retinas of Sirna-027-treated eyes was reduced by 30% compared to retinas of eyes injected with inverted control siRNA (Figure 3d).

Distribution of siRNA in the eye at several time points after intravitreous or periocular injection

5-Bromodeoxyuridine (BrdU)-labeled Sirna-027 was used to evaluate distribution of siRNA in the mouse eye over time after injection. 6 h after intravitreous injection of 5 µg of BrdU-labeled Sirna-027, there was staining for BrdU in ganglion cells, some cells in the inner nuclear layer, and a strip along the external limiting membrane (Figure 4). At 12 and 24 h after injection, most of the staining was in the ganglion cells and inner nuclear layer. By 48 h, there is also prominent staining in photoreceptors. At 5 days after injection, it appeared that most of the BrdU-labeled siRNA had been cleared from the retina.

At 6 h after periocular injection of 25 µg of BrdU-labeled Sirna-027, there was staining of some ganglion cells, a few cells in the inner nuclear layer, and the region

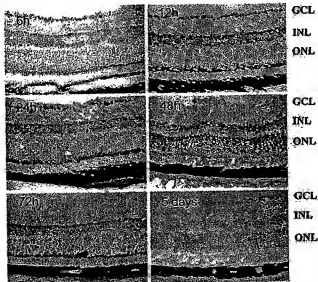


Figure 4 Distribution of BrdU-labeled Sirna-027 in the retina at various times after intravitreous injection. In all, 5 µg of BrdU-labeled Sirna-027 was injected into the vitreous cavity of mice and, at 6, 12, 24, or 48 h (h) or 5 days after injection, mice were euthanized and ocular frozen sections were immunohistochemically stained for BrdU. At 6 h after injection, staining was limited to ganglion cells, a few cells in the inner nuclear layer, and the region of the external limiting membrane. At 12 and 24 h after injection, there was strong staining in ganglion cells and the inner nuclear layer. At 48 h and beyond, there was no longer staining in ganglion cells. There was widespread strong staining in photoreceptor cell bodies at 48 h that was less at earlier and later time points. By 5 days after injection, there was no longer staining for BrdU in the retina. GCL = ganglion cell layer; INL = inner nuclear layer; ONL = outer nuclear layer.

of the external limiting membrane (Figure 5). The staining in ganglion cells, the inner nuclear layer, and the strip along the external limiting membrane increased at 12 h, seemed to peak at 24 h, and decreased at later time points although it was still detectable at 5 days after injection. The staining in photoreceptor cell bodies peaked at 12–24 h and was back to baseline by 72 h. These results demonstrate that siRNAs rapidly access all layers of the retina after either intravitreous or periocular injection and are detectable for several days after injection.

Intravitreous or periocular injection of Sirna-027 suppresses CNV

The effect of Sirna-027 *in vivo* was assessed using a laser-induced model of CNV in adult female C57BL/6 mice. One group of mice was treated on days 1 and 7 with an intravitreous injection of 1.5 µg of Sirna-027 in one eye and 1.5 µg of inverted control siRNA in the fellow eye. A second group of mice received injection of 0.5 µg of Sirna-027 in one eye and PBS in the fellow eye on days 1 and 7. At 14 days after rupture of Bruch's membrane, eyes that received intraocular injections of inverted siRNA or PBS developed large areas of CNV (Figure 6a and b). Compared to the control eyes, eyes treated with 1.5 or 0.5 µg of Sirna-027 had significantly smaller areas of CNV (Figure 6c–e). Reductions in CNV lesion size of 56 and 66% vs 1.5 µg inverted control siRNA or PBS, respectively, were noted.

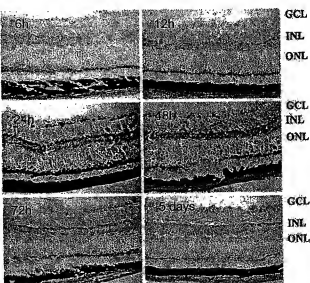


Figure 5 Distribution of BrdU-labeled Sirna-027 in the retina at various times after periocular injection. In all, 5 µg containing 25 µg of BrdU-labeled Sirna-027 was injected into the periocular space of mice and, at 6, 12, 24, or 48 h (h) or 5 days after injection, mice were euthanized and ocular frozen sections were immunohistochemically stained for BrdU. At 6 h after injection, staining was limited to ganglion cells, a few cells in the inner nuclear layer, and the region of the external limiting membrane. The staining in ganglion cells, the inner nuclear layer, and the strip along the external limiting membrane increased at 12 h, seemed to peak at 24 h, and decreased at later time points although it was still detectable at 5 days after injection. The staining in photoreceptor cell bodies peaked at 12–24 h and was back to baseline by 72 h. GCL = ganglion cell layer; INL = inner nuclear layer; ONL = outer nuclear layer.

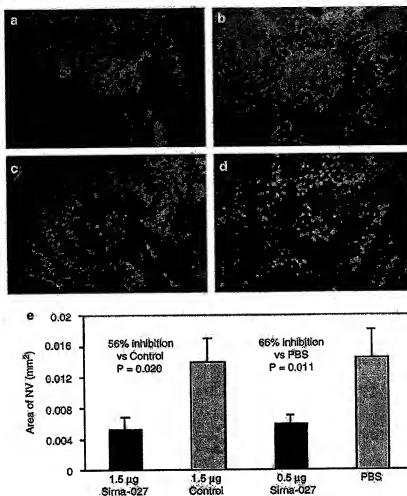


Figure 6 Intravitreous injection of Sirna-027 suppresses choroidal NV. Ruptures in Bruch's membrane were induced at three locations in each eye on day 1. On days 1 and 7, mice received a 1 μ l intravitreous injection of 1 μ g Sirna-027 in one eye and 1.5 μ g inverted control siRNA in the fellow eye, or 0.5 μ g Sirna-027 in one eye and PBS in the fellow eye. On day 14, mice were perfused with fluorescein-labeled dextran and choroidal flat mounts were examined by fluorescence microscopy. There were large areas of choroidal NV at Bruch's membrane rupture sites in eyes injected with 1.5 μ g inverted control siRNA (a) or PBS (b), while eyes injected with 0.5 μ g (c) or 1.5 μ g of Sirna-027 (d) had small areas of choroidal NV. Measurement of the area of choroidal NV by image analysis (e) demonstrated that eyes injected with Sirna-027 had significantly smaller choroidal NV areas than fellow eye controls. Data are expressed as the averaged CNV area (+s.e.m.). (P = 0.020 for difference between 1.5 μ g Sirna-027 (n = 6) and 1.5 μ g inverted control siRNA (n = 16), P = 0.011 for difference between 0.5 μ g Sirna-027 (n = 5) and PBS (n = 5)).

The effect of periocular injections of Sirna-027 was also investigated. After rupture of Bruch's membrane, mice were given 5 μ l containing 7.5 μ g of either Sirna-027 or inverted control siRNA every 3 days for 2 weeks by periocular injection. Eyes treated with Sirna-027 had significantly smaller areas of CNV compared to those treated with inverted siRNA (Figure 7). CNV area was reduced by 45%.

Intravitreous injection of Sirna-027 suppresses retinal NV

The effect of Sirna-027 on NV was also assessed in a model of ischemia-induced retinal NV. In this model, areas of retinal ischemia due to closure of retinal blood vessels result in sprouting of new vessels that grow through the internal limiting membrane into the vitreous cavity, similar to the situation seen in humans with retinopathy of prematurity or proliferative diabetic

retinopathy. Mice with ischemic retinopathy were given an intravitreous injection of 1 μ l containing 1 μ g of Sirna-027 in one eye and inverted control siRNA in the fellow eye at P12. At P17, the amount of retinal NV was significantly reduced in eyes injected with Sirna-027 compared to those injected with inverted siRNA (Figure 8). Following this single injection, the area of retinal NV was reduced by 32%.

Discussion

Several lines of evidence suggest that VEGFR2 plays a primary role in VEGF signaling, but the action of VEGFR1 is less established and appears to be context-dependent. During developmental angiogenesis, VEGFR1 acts as a negative regulator of VEGF activity,¹³ but in adult mice with Lewis lung carcinoma, tumor

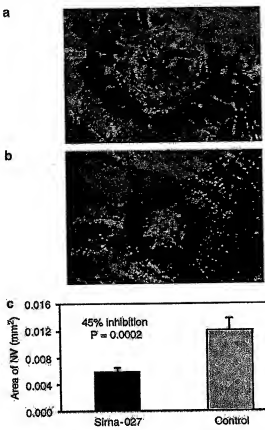


Figure 7 Periorcular injection of Sirna-027 suppresses choroidal NV. Bruch's membrane was ruptured at three locations in each eye on day 1. On days 1, 4, 7, 10, and 13, mice received periorcular injections of 7.5 μg of Sirna-027 or inverted control siRNA. On day 14, mice were perfused with fluorescein-labeled dextran and choroidal flat mounts were examined by fluorescence microscopy. There were large areas of choroidal NV at Bruch's membrane rupture sites in eyes injected with inverted siRNA (a), while eye injected with Sirna-027 had smaller areas of choroidal NV (b). Measurement of the area of choroidal NV by image analysis (c) demonstrated that, compared to the area of choroidal NV at Bruch's membrane rupture sites ($n=13$) in eyes injected with inverted siRNA, there was a 45% reduction in the area of choroidal NV at rupture sites ($n=12$) in eyes treated with Sirna-027 ($P=0.0002$). Data are expressed as the averaged CNV area ($\pm \text{s.e.m.}$).

angiogenesis was stimulated through VEGFR1.¹⁴ Also, inhibition of VEGFR1 with an anti-VEGFR1 antibody suppressed ischemia-induced retinal NV.¹⁰ Moreover, some proangiogenic effects may be mediated by PIGF specifically through VEGFR1 and not VEGFR2.¹⁶ In this study, we used Sirna-027, a chemically stabilized siRNA directed against *vegfr1* mRNA, to reduce specifically the levels of retinal VEGFR1. Either intravitreous or periorcular injection of Sirna-027 caused significant reduction of *vegfr1* mRNA and significantly suppressed CNV or retinal NV; therefore, VEGFR1 is a positive regulator of both CNV and retinal NV.

In addition to VEGFR1 and VEGFR2, the neuropilins (Npns), Npn1 and Npn2, participate in VEGF signaling and both play important roles in pathologic ocular NV.¹⁵⁻¹⁸ Intravitreous injection of an anti-Npn1 antibody suppresses ischemia-induced retinal NV and mice deficient in Npn2 have markedly reduced ischemia-induced and VEGF-induced retinal NV. Thus, it appears that all four

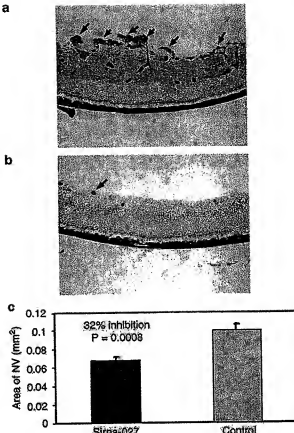


Figure 8 Sirna-027 reduces retinal NV in mice with oxygen-induced ischemic retinopathy. Litters of neonatal C57BL/6 mice were placed in 75% oxygen at P7. At P12, mice were removed to room air and were given an intravitreous injection of 1 μg of Sirna-027 or inverted control siRNA. At P17, the mice were euthanized and ocular frozen sections were stained with GSA. Mice treated with inverted siRNA ($n=8$) showed extensive preretinal NV (a, arrows). However, mice treated with Sirna-027 ($n=8$; b, arrows) had significantly less preretinal NV. (c) Data are represented as the average NV area ($\pm \text{s.e.m.}$) and demonstrated that Sirna-027 treatment reduced preretinal NV by 32% relative to treatment with inverted control ($P=0.0008$).

VEGF receptors, VEGFR1, VEGFR2, Npn1, and Npn2, play important nonoverlapping roles in pathologic ocular NV, and each provides a target for therapeutic intervention.

In addition to demonstrating that VEGFR1 is a potential target for treatment of CNV, this study also suggests that a viable strategy for attacking that target is to knock down *vegfr1* mRNA with Sirna-027. Labeled Sirna-027 was detected in the retina for 4–5 days following intravitreous injection, suggesting that it is taken up and retained within retinal cells for a substantial period of time. After periorcular injection, labeled Sirna-027 was able to pass through the sclera and choroid and was detectable within retinal cells for at least 5 days. With either route of delivery, there was sufficient reduction of *vegfr1* mRNA to significantly suppress CNV. Also, intravitreous injection of Sirna-027 significantly suppressed ischemia-induced retinal NV, with corresponding reductions in *vegfr1* mRNA and protein. These data suggest that both intravitreous and periorcular

injection of Sirna-027 deserve further testing as potential treatment approaches for ocular NV.

Previous studies have demonstrated that VEGF is a critical stimulus for CNV and an important therapeutic target. Two VEGF antagonists, an aptamer and an antibody fragment, reduce vision loss in patients with CNV when given by repeated intravitreous injections.^{5,6} Identifying additional VEGF pathway antagonists with improved characteristics, such as a prolonged duration of effect or a less-invasive route of delivery, is an important goal. The ability to reduce more than one target in a pathway may be especially useful and could be accomplished using bi- or multifunctional siRNAs designed to target more than one mRNA. Thus, the identification and use of chemically stabilized siRNAs that can specifically target one or more members of the VEGF pathway may be a viable alternative, or an adjunct, to more traditional therapeutic approaches. A phase I clinical trial investigating the safety of a single intravitreous injection of several different doses of Sirna-027 in patients with neovascular age-related macular degeneration is underway. The effect of a single intravitreous injection may be too brief to achieve a sustained therapeutic effect; so, if the safety profile for Sirna-027 is good, it is planned to perform a phase II trial to investigate the efficacy of multiple intravitreous injections of Sirna-027 in patients with neovascular AMD. Additional preclinical studies are also needed to investigate strategies for sustained delivery of siRNAs to the eye, which would not only be useful for treatment with Sirna-027 but also could be the basis for using siRNAs to treat a variety of ocular disorders in the future.

Materials and methods

Mice

Pathogen-free female C57BL/6 mice were purchased from Charles Rivers Laboratories, Inc. (Wilmington, MA, USA) and were treated in accordance with the requirements of the Committee on Animal Welfare of the Johns Hopkins University School of Medicine and the guidelines of the Association for Research in Vision and Ophthalmology for the use of animals in Research.

siRNA synthesis and structure

RNA single strands were synthesized at Sirna Therapeutics, Inc. by standard procedures.¹⁹ Complementary sense and antisense single strands were annealed, desaltsed, and lyophilized to provide the final siRNA duplex. The integrity and purity of the siRNA was confirmed by HPLC, and MALDI-TOF MS methodologies. Lyophilized duplex was reconstituted in PBS.

The sequences of the two oligonucleotide strands of the Sirna-027 siRNA duplex are as follows: sense, 5'-BCU GAG UUU AAA AGG CAC CCT TB-3'; antisense, 5'-GGG UGC CUU UUA AAC UCA GT₃T-3'. Modifications are unpaired deoxythymidines (T), one phosphorothioate linkage (S) and two inverted 2'-deoxy abasic nucleotides (B).²⁰ The sense strand is identical in sequence to the target site in *vegfr1* mRNA; the antisense strand directs cleavage of *vegfr1* mRNA when bound in the RNA-induced silencing complex (RISC). The Sirna-027 target sequence is present in *vegfr1* mRNA for human

(GenBank accession no. NM_002019.1, nucleotides 349–368), mouse (NM_010228.1), rat (NM_019306.1), as well as in the pig and monkey *vegfr1* genes. RNA was isolated from pig and monkey tissue and used to synthesize cDNA for *vegfr1*, which was sequenced to confirm the presence of the Sirna-027 target site. A negative control siRNA with the same stabilizing modifications as Sirna-027 was used. This inverted control is an siRNA with an inverted Sirna-027 sequence as follows: sense, 5'-BCC CAC GGA AAA UUU GAG UCT TB-3'; antisense, 5'-GAC UCA AAU UUU CCG UGG GT₃T-3'.

BrdU labeling

A single BrdU nucleotide was introduced at the 3'-end of the antisense strand replacing the penultimate nucleotide. BrdU-labeled Sirna-027 was made by annealing this antisense strand with its complementary sense strand to form the duplex.

Measurement of vegfr1 mRNA in Sirna-027-treated HAECs

HAECs (Cambrex Corp., East Rutherford, NJ, USA) were seeded in the 24 inner wells of 48-well plates and grown to 60–75% confluence in endothelial cell growth medium (EGM-2; Cambrex Corp., East Rutherford, NJ, USA) at 37°C, 5% CO₂. siRNAs were mixed with 100 µl Opti-MEM (Invitrogen, Carlsbad, CA, USA) without serum to a concentration of 125 nM. The siRNA solution was then combined 1:1 with a diluted solution of Lipofectamine 2000 (LF2K; Invitrogen, Carlsbad, CA, USA), gently mixed, and incubated for 30 min at room temperature to allow formation of siRNA/LF2K complexes. The diluted LF2K was prepared by mixing 2.0 µl LF2K and 98 µl Opti-MEM. For transfection, the EGM-2 was aspirated from the cells and replaced with 200 µl of Opti-MEM without serum. siRNA/LF2K complexes (50 µl/well) were added to treatment wells for a final concentration of 12.5 nM, mixed gently, and plates were incubated at 37°C, 5% CO₂. After 4 h, the transfection medium was replaced with 200 µl EGM-2 and plates were incubated at 37°C, 5% CO₂ for an additional 20 h. Transfections were performed in triplicate.

At 24 h after addition of siRNA to cells, total RNA was isolated with the Invitrik Inviscreen RNA HTS 96-Kit/C (Invitrik, Berlin, Germany) using the manufacturer's instructions. Quantitative RT-PCR was performed in ABI Prism 7000 or 7500 Sequence Detectors (Applied Biosystems, Foster City, CA, USA) using a SuperScript III Platinum One-Step qRT-PCR System and RNaseOut Ribonuclease Inhibitor (Invitrogen, Carlsbad, CA, USA) to measure *vegfr1* or *vegfr2* mRNA and compare it to GAPDH mRNA levels for normalization. Reactions contained 5 µl RNA in 50 µl. Primers used for *vegfr1* were 5'-GAG CTA AAA ATC TTG ACC CAC ATT G-3' (forward) and 5'-CAG TAT TCA ACA ATC ACC ATC AGA G-3' (reverse) with 5'-FAM-CTG GGA GCC TGC ACC AAG CAA GGA-TAMRA-3' for the probe. For *vegfr2*, primers were 5'-TCT GCC TAC CTC ACC TGT TIC C-3' (forward) and 5'-TGA CTG ATT CCT GCT GTG TTG TC-3' (reverse) with 5'-FAM-ATG GAG GAG GAA GTA TGT GAC CCC A-TAMRA-3' for the probe. Primers used for GAPDH were 5'-GAA ATC CCA TCA CCA TCT TCC A-3' (forward) and 5'-CGT ACT

CAG CGC CAG CAT C-3' (reverse) with 5'-FAM-AGC GAG ATC CCT CCA AAA TCA AGT GGG-TAMRA-3' for the probe.

Testing Sirna-027 activity in a luciferase reporter/HeLa cell culture system

A luciferase reporter plasmid was made by inserting a fragment of the human vegfr1 gene (nucleotides 326–403) between the *Xba*I and *Nol*I sites of the pSICHECK-2™ luciferase reporter plasmid (Promega, Madison, WI, USA). Ligation into this site placed the vegfr1 target sequence in the 3'-untranslated region of the Renilla luciferase gene, while the Firefly luciferase control gene in the pSICHECK-2 plasmid was unaltered. The insertion was confirmed by sequencing in both directions.

In all, 15 000 HeLa S3 cells were plated in each well of a Costar 3603 black 96-well plate (Corning Incorporated, Corning, NY, USA) in 75 µl Iscove's Modified Dulbecco's Medium (Invitrogen, Carlsbad, CA, USA) supplemented with 10% bovine calf serum (Hyclone, Logan, UT, USA). Plates were incubated overnight at 37°C (5% CO₂). The reporter plasmid and siRNA were cotransfected into HeLa cells using LF2K. Each well received 50 µl of OPTI-MEM (Invitrogen, Carlsbad, CA, USA) containing 100 ng of reporter plasmid, 0.5 µl LF2K, and siRNA (0.005–5 nM) in a final volume of 125 µl. Transfections were performed in triplicate. Following transfection, cells were incubated as above for approximately 17 h. Renilla and Firefly luciferase activities were determined using Dual-Glo luciferase reagents (Promega, Madison, WI, USA) according to the manufacturer's instructions. Data were acquired on a Luminoskan Ascent luminometer (Thermo Labsystems, Helsinki, Finland). The ratio of Renilla:Firefly luciferase activity was normalized to that observed in HeLa cells cotransfected with a control siRNA and the reporter plasmid. The IC₅₀ was determined using Kaleidograph software (Synergy Software, Reading, PA, USA).

Testing of Sirna-027 activity in HeLa cell extracts

HeLa cytosol was prepared as described previously.²¹ A transcript of human vegfr1 (GenBank Accession number NM_002019, nucleotides 313–415) was produced by T7 transcription from a DNA template²² and 5'-end labeled using guanylyl transferase (Ambion, Austin, TX, USA) and α-³²P-GTP (Perkin-Elmer, Boston, MA, USA). Reactions including HeLa cell extract, ³²P-labeled vegfr1 RNA target, and 100 nM Sirna-027 were assembled in 50 µl by the method of Martinez and Tuschl.²¹ Reactions were incubated at 37°C and aliquots were quenched into two volumes of stop buffer (7 M urea, 1× TBE, xylene cyanol, bromophenol blue, pH 7) at 30, 60, 90, or 120 min, denatured for 5 min at 95°C, and resolved on a 12% denaturing polyacrylamide gel with appropriate markers. To generate RNA size markers, the ³²P-labeled transcript was subjected to RNase T₁ digestion under denaturing conditions.²³ An RNA size ladder was generated by alkaline hydrolysis of the ³²P-labeled transcript.²⁴ The gel was dried and exposed to a phosphorimager screen. Results were visualized with a Molecular Dynamics Storm 860 phosphorimager and analyzed using ImageQuant (Molecular Dynamics, Piscataway, NJ, USA).

Assessment of distribution of siRNA in the retina after intravitreous or periocular injections

Mice were anesthetized and given an intravitreous injection of 1 µl or a periocular injection of 5 µl of PBS containing 5 µg/µl BrdU-labeled Sirna-027. Mice were euthanized at several different time points after injection and eyes were frozen in optimal cutting temperature embedding compound (OCT; Miles Diagnostics, Elkhart, IN, USA). Frozen sections (10 µm) were fixed in 4% paraformaldehyde, and incubated for 2 h in a 1:50 dilution of a rat antibody that specifically recognizes BrdU (Serotec, Oxford, UK) in 0.05 M Tris-buffered saline (TBS), pH 7.6. Slides were washed and incubated in mouse anti-rat IgG conjugated to biotin (Jackson ImmunoResearch Laboratories, Inc., West Grove, PA, USA) for 90 min at room temperature. Slides were washed and incubated with 1:100 avidin D coupled to horseradish peroxidase (Vector Laboratories, Burlingame, CA, USA) for 45 min. After washing with 0.05 M TBS, slides were incubated with 3,3'-diaminobenzidine tetrahydrochloride dihydrate to give a brown reaction product. The sections were covered with a standard glass coverslip and examined by light microscopy.

Mice with oxygen-induced ischemic retinopathy

Ischemic retinopathy was produced by a previously described method.²⁵ At postnatal day (P) 7, mice were placed in 75±3% oxygen for 5 days and then returned to room air at P12. Treatments were instituted at P12 and consisted of intravitreous or periocular injection of Sirna-027 in one eye and injection of vehicle (PBS) or inverted control siRNA in the fellow eye. For analysis of vegfr1 mRNA after siRNA treatment, mice were either given a 1 µl intravitreous injection containing 3 µg of Sirna-027 or inverted control siRNA or a 5 µl periocular injection containing 7.5 µg Sirna-027 or the inverted control. Retinas were harvested on P15 or P17, respectively. For analysis of VEGFR1 protein after siRNA treatment, mice were given a 1 µl intravitreous injection containing 5 µg of Sirna-027 or inverted control siRNA. Retinas were harvested on P15. To assess retinal NV in this model, mice were treated at P12 with a 1 µl intravitreous injection containing 1 µg of Sirna-027 or inverted control siRNA. Retinal NV was measured as described below using eyes harvested on P17.

Measurement of the amount of retinal NV

Serial sections (10 µm) were cut through the entire eye, starting with sections that included the iris root on one side of the eye and proceeding to the iris root on the other side. Every tenth section, roughly 100 µm apart, was stained with biotinylated *Griffonia simplicifolia* lectin B4 (GSA, Vector Laboratories, Burlingame, CA, USA), which selectively binds to vascular cells. Slides were incubated in methanol/H₂O₂ for 10 min at 4°C, washed with 0.05 M TBS, pH 7.6, and incubated for 30 min in 10% normal porcine serum. Slides were incubated for 2 h at room temperature with biotinylated GSA and after rinsing with 0.05 M TBS, they were incubated with avidin coupled to peroxidase (Vector Laboratories) for 45 min at room temperature. After being washed for 10 min with 0.05 M Tris buffer, pH 7.6, slides were incubated with diaminobenzidine (Research Genetics, Huntsville, AL, USA) to give a brown reaction product, and mounted

with Cytoseal (Stephens Scientific, Riverdale, NJ, USA). Slides were examined with an Axioskop microscope, and images were digitized using a 3 CCD color video camera and a frame grabber. Image-Pro Plus software was used to delineate GSA-stained cells on the surface of the retina and their area was measured. The mean of the measurements from each eye was used as a single experimental value.

Measurement of retinal vegfr1 mRNA

Retinas were dissected and total RNA was isolated using an RNeasy kit (Qiagen Inc., Chatsworth, CA, USA). After quantification of RNA concentration using Gene SpecII (Hitachi, Japan), 1 µg was treated with DNase I (Ambion Inc., Austin, TX, USA) to remove any contaminating genomic DNA and cDNA was synthesized with RT (SuperScript II; Life Technologies, Gaithersburg, MD, USA) and 5.0 µM oligo(dT) primer. Samples of cDNA were aliquoted and stored at -80°C.

For visualization of mRNA, amplification was performed using primers specific for vegfr1 mRNA: 5'-AAG ATG CCA GCC GAA GGA GA-3' (forward) and 5'-GGC TCG GCA CCT ATA GA CA-3' (reverse). Titration was determined to ensure that PCR was performed in the linear range of amplification. Mouse S16 ribosomal protein primers, 5'-CAC TGC AAA CGG GGA AAT GG-3' (forward) and 5'-TGA GAT GGA CTG TCG GAT GG-3' (reverse), were used to provide an internal control for the amount of template in the PCR reactions. In all, 20 µL of PCR product was loaded and electrophoresed on a 1% agarose gel and visualized using ethidium bromide. The gel was photographed using a Kodak Gel Logic 200 gel imaging system (Rochester, NY, USA).

To quantify levels of vegfr1 mRNA, quantitative RT-PCR was performed and analyzed using the SYBR Green I format on the LightCycler rapid thermal cycler system (Roche Molecular Biochemicals, Indianapolis, IN, USA). Reactions were performed in a 20-µL volume using the FastStart Master SYBR Green I reaction mix (Roche Molecular Biochemicals) with 0.5 mM primers and MgCl₂ concentration optimized between 2 and 5 mM. Cyclophilin A was used as a standard for normalization. The sequences of the PCR primer pairs used were: VEGFR1, 5'-CTG CCC TAT GAT GCC AGC AA-3' (forward) and 5'-ACG CTT CGG TCT TCA GGG AA-3' (reverse); cyclophilin A, 5'-CAG ACG CCA CTG TCG CCT T-3' (forward) and 5'-TGT CTT TGG AAC TTT GTC TGC AA-3' (reverse). Murine vegfr1 and cyclophilin A mRNA were amplified with Pfu Taq polymerase (Stratagene, La Jolla, CA, USA). PCR products were purified with a gel extraction kit (Qiagen, Chatsworth, CA, USA), and mRNA copy numbers were calculated according to the Roche quantification technique manual. Standard curves for each gene were plotted with quantified cDNA template during each RT-PCR reaction. Target gene mRNA copy number was normalized to 10⁶ copies of cyclophilin A.

Enzyme-linked immunoabsorbent assays

The retinas were removed and placed in 200 µL lysis buffer (50 µL 1 M Tris-HCl (pH 7.4), 50 µL 10% sodium dodecyl sulfate, 5 µL 100 nM phenylmethane sulfonyl and 5 mL sterilized, de-ionized water). Retinas were homogenized by pipetting, sonicated at 4°C for 5 s, and centrifuged at 13 K for 5 min at 4°C. The pellet was

discarded and the supernatant was transferred to a fresh tube. The protein concentration of supernatants was measured using a Bio-Rad Protein Assay Kit (Bio-Rad, Hercules, CA, USA). ELISAs were performed using the Quantikine VEGFR1 assay kit (R & D Systems, Minneapolis, MN, USA) using the manufacturer's instructions. Serial dilutions of recombinant VEGFR1 were assayed to generate a standard curve with the limit of detection at 125 pg/mL.

Model of laser-induced CNV

CNV was generated by modification of a previously described technique.²⁶ Briefly, 4–5-week-old female C57BL/6 mice were anesthetized and the pupils were dilated with 1% tropicamide. Three burns of 532 nm diode laser photoocoagulation (75 µm spot size, 0.1 s duration, 120 mW) were delivered to each retina using the slit lamp delivery system of an OcuLight GL Photocoagulator (Iridex, Mountain View, CA, USA) and a hand-held cover slide as a contact lens. Burns were performed in the 9, 12, and 3 o'clock positions of the posterior pole of the retina. Production of a bubble at the time of laser, which indicates rupture of Bruch's membrane, is an important factor in obtaining CNV,²⁶ so only burns in which a bubble was produced were included in the study. Mice were treated with Sirna-027 by intravitreous injections on the day of laser (day 1) and day 7 or periocular injections on days 1, 4, 7, 10, and 13. For intravitreous injections, mice were given 0.5 or 1.5 µg of Sirna-027 in one eye and an equivalent amount of inverted control siRNA or vehicle in the fellow eye. For each periocular injection, mice were given 7.5 µg of Sirna-027 in one eye and inverted siRNA in the fellow eye. Mice were euthanized 14 days after laser for measurement of the area of CNV at Bruch's membrane rupture sites.

Measurement of CNV area

The area of CNV at Bruch's membrane rupture sites was measured in choroidal flat mounts.²⁷ Mice were anesthetized and perfused with 1 mL of PBS containing 50 mg/mL of fluorescein-labeled dextran (2x10⁶ average mw, Sigma, St Louis, MO, USA) as described previously.²⁸ The eyes were removed and fixed for 1 h in 10% phosphate-buffered formalin. The cornea and lens were removed and the entire retina was carefully dissected from the eyecup. Radial cuts (4–7, average 5) were made from the edge to the equator and the eyecup was flat mounted in Aquamount with the sclera facing down. Flat mounts were examined by fluorescence microscopy on an Axioskop microscope (Zeiss, Thornwood, NY, USA) and images were digitized using a three-color CCD video camera (IK-TU40A, Toshiba, Tokyo, Japan) and a frame grabber. Image-Pro Plus software (Media Cybernetics, Silver Spring, MD, USA) was used to measure the total area of hyperfluorescence associated with each burn, corresponding to the total fibrovascular scar. The areas within each eye were averaged to give one experimental value per eye for plotting the areas in the figures.

Statistical analyses

Data are presented graphically as mean±s.e.m. For *in vivo* studies, comparisons between Sirna-027-treated and control-treated fellow eyes were analyzed using a

two-way analysis of variance or paired *t*-tests. Each animal served as its own control. For *in vitro* studies, a one-way analysis of variance or unpaired *t*-tests were used for comparisons among groups. Data were log-transformed for analysis. *P*-values were not adjusted for multiple comparisons; all *P*-values are two-tailed.

Acknowledgements

This work was supported by a grant from Sirna Therapeutics, Inc. PAC is the George S and Dolores Dore Eccles Professor of Ophthalmology and Neuroscience. PAC is a consultant for Sirna Therapeutics, Inc., which is monitored by the Conflict of Interest Committee of the Johns Hopkins University School of Medicine.

References

- Okamoto N, Tobe T, Hackett SF, Ozaki H, Vinores MA, LaRochelle W et al. Transgenic mice with increased expression of vascular endothelial growth factor in the retina: a new model of intraretinal and subretinal neovascularization. *Am J Pathol* 1997; 151: 281-291.
- Seo M-S, Kwak N, Ozaki H, Yamada H, Okamoto N, Yamada E et al. Dramatic inhibition of retinal and choroidal neovascularization by oral administration of a kinase inhibitor. *Am J Pathol* 1999; 154: 1743-1753.
- Ozaki H, Seo M-S, Ozaki K, Yamada H, Yamada E, Okamoto N et al. Blockade of vascular endothelial cell growth factor receptor signaling is sufficient to completely prevent retinal neovascularization. *Am J Pathol* 2000; 166: 679-707.
- Kwak N, Okamoto N, Wood JM, Campochiaro PA. VEGF is an important stimulator in a model of choroidal neovascularization. *Invest Ophthalmol Vis Sci* 2000; 41: 3158-3164.
- Gragoudas ES, Adams AF, Cunningham JR ET, Feinsod M, Guyer DR. Pegaptanib for neovascular age-related macular degeneration. *N Engl J Med* 2004; 351: 2805-2816.
- Rosenfeld PJ, Villante N, Feuer WJ, Pulaifito CA, McCluskey ER, RhuFav V2 (anti-VEGF antibody fragment) in neovascular AMD: safety, tolerability, and efficacy of multiple, escalating dose intravitreal injections. *Invest Ophthalmol Vis Sci* 2003; 44 (Suppl): 970.
- Gille H, Kowalski J, Li B, LeCouter J, Moffat B, Zioncheck TF et al. Analysis of biological effects and signaling properties of Flt-1 (VEGFR-1) and KDR (VEGFR-2). *J Biol Chem* 2001; 276: 3222-3230.
- Park JE, Chen HH, Winer J, Houck KA, Ferrara N. Placenta growth factor. Potentiation of vascular endothelial growth factor bioactivity, *in vitro* and *in vivo*, and high affinity binding Flt-1 but not to Flk-1/KDR. *J Biol Chem* 1994; 269: 25646-25654.
- Fong GH, Zhang L, Bryce DM, Peng J. Increased hemangioblast commitment, not vascular disorganization, is the primary defect in flt-1 knockout mice. *Development* 1999; 126: 3015-3025.
- Luitton A, Tjwa M, Moons L, Wu Y, Angelillo-Scherrer A, Liao F et al. Revascularization of ischemic tissues by PIGF treatment, and inhibition of tumor angiogenesis, arthritis and atherosclerosis by anti-Flt1. *Nat Med* 2002; 8: 831-839.
- LeCouter J, Moritz DR, Bing L, Phillips GL, Liang XH, Gerber H-P et al. Angiogenesis-independent endothelial protection of liver: role of VEGFR-1. *Science* 2003; 299: 890-893.
- Elbashi SM, Martinez J, Patkaniowska A, Lendeckel W, Tuschl T. Functional anatomy of siRNAs for mediating efficient RNAi in *Drosophila melanogaster* embryo lysate. *EMBO J* 2001; 20: 6877-6888.
- Hiratsuka S, Minowa O, Kuno J, Noba T, Shibuya M. Flt-1 lacking the tyrosine kinase domain is sufficient for normal development and angiogenesis in mice. *Proc Natl Acad Sci USA* 1998; 95: 9349-9354.
- Hiratsuka S, Maru Y, Okada A, Seiki M, Noda T, Shibuya M. Involvement of Flt-1 tyrosine kinase (vascular endothelial growth factor receptor-1) in pathological angiogenesis. *Cancer Res* 2001; 61: 1207-1213.
- Ishida S, Shinoda K, Kawashima S, Oguchi Y, Okada Y, Ikeda E. Coexpression of VEGF receptors VEGFR-2 and neuropilin-1 in proliferative diabetic retinopathy. *Invest Ophthalmol Vis Sci* 2000; 41: 1649-1656.
- Ishihama H, Ohbayashi M, Kurosova N, Kitsukawa T, Matsuzawa O, Miyake Y et al. Colocalization of neuropilin-1 and Flk-1 in retinal neovascularization in a mouse model of retinopathy. *Invest Ophthalmol Vis Sci* 2001; 42: 1172-1178.
- Oh H, Takagi H, Otani A, Koyama S, Kemmonchi S, Uemura A et al. Selective induction of neuropilin-1 by vascular endothelial growth factor (VEGF): a mechanism contributing to VEGF-induced angiogenesis. *Proc Natl Acad Sci USA* 2002; 99: 383-388.
- Shen J, Samuel R, Zimmer J, Liu H, Liang X, Hackett SF et al. Deficiency of neuropilin-2 suppresses VEGF-induced retinal neovascularization. *Mol Med* 2004; 10: 12-18.
- Wincott F, Di Renzo A, Shaffey C, Grimm S, Tracz D, Workman C et al. Synthesis, deprotection, analysis, and purification of RNA and ribozymes. *Nucleic Acids Res* 1995; 23: 2677-2684.
- Peracchi A, Beigelman L, Usman N, Herschlag D. Rescue of abasic hammerhead ribozymes by exogenous addition of specific bases. *Proc Natl Acad Sci USA* 1996; 93: 11522-11527.
- Martinez J, Patkaniowska A, Urlaub H, Luhrmann R, Tuschl T. Single-stranded antisense siRNAs guide target RNA cleavage in RNAi. *Cell* 2002; 110: 563-574.
- Milligan JE, Grobe DR, Witherell FW, Uhlenbeck OC. Oligoribonucleotide synthesis using T7 RNA polymerase and synthetic DNA templates. *Nucleic Acids Res* 1987; 15: 8783-8798.
- Vourakis JN, Celantano J, Finn M, Lockard RE, Mitra T, Pavlakis G et al. Sequence and structure analysis of end-labeled RNA with nucleases. In: Chirikjian GG, Papas TS (eds) *Gene Amplification and Analysis*. New York: Elsevier/North Holland, 1981, pp. 267-298.
- Levin RJ, Krummel B, Chamberlin MJ. Isolation and properties of transcribing ternary complexes of *Escherichia coli* RNA polymerase positioned at a single template base. *J Mol Biol* 1987; 196: 85-100.
- Smith LEH, Wesolowski E, McLellan A, Kostyk SK, D'Amato R, Sullivan R et al. Oxygen-induced retinopathy in the mouse. *Invest Ophthalmol Vis Sci* 1994; 35: 101-111.
- Tobe T, Ortega S, Luna JD, Ozaki H, Okamoto N, Derevjanik NL et al. Targeted disruption of the FGF2 gene does not prevent choroidal neovascularization in a murine model. *Am J Pathol* 1998; 153: 1641-1646.
- Edelman JL, Castro MR. Quantitative image analysis of laser-induced choroidal neovascularization in rat. *Exp Eye Res* 2000; 71: 523-533.
- Tobe T, Okamoto N, Vinores MA, Derevjanik NL, Vinores SA, Zack DJ et al. Evolution of neovascularization in mice with overexpression of vascular endothelial growth factor in photoreceptors. *Invest Ophthalmol Vis Sci* 1998; 39: 180-188.

EXHIBIT 5

Small interfering RNA (siRNA) targeting *VEGF* effectively inhibits ocular neovascularization in a mouse model

Samuel J. Reich, Joshua Fosnot, Akiko Kuroki, Waixing Tang, Xiangyang Yang, Albert M. Maguire, Jean Bennett, Michael J. Tolentino

F.M. Kirby Center for Molecular Ophthalmology, Department of Ophthalmology, Scheie Eye Institute, University of Pennsylvania, Philadelphia, PA

Purpose: RNA interference mediated by small interfering RNAs (siRNAs) is a powerful technology allowing the silencing of mammalian genes with great specificity and potency. The purpose of this study was to demonstrate the feasibility of RNA interference mediated by siRNA in retinal cells in vitro and in the murine retina in vivo.

Methods: siRNAs specific for enhanced green fluorescent protein (*EGFP*) and murine and human vascular endothelial growth factor (*VEGF*) were designed. In vitro studies in human cell lines entailed modulation of endogenous VEGF levels through chemically induced hypoxia. Effects of siRNA treatment on these levels were measured by ELISA. In vivo studies evaluating effects of siRNA on levels of *EGFP* and *VEGF* were performed by co-injecting recombinant viruses carrying *EGFP* or *hVEGF* cDNAs along with the appropriate siRNAs subretinally in mice. Additional studies aimed at blocking production of endogenous *hVEGF* were performed using laser-induced choroidal neovascularization (CNV) in mice. Effects of in vivo treatments were evaluated ophthalmoscopically. Retinal/choroidal flat mounts were evaluated after perfusion with dextran-fluorescein. Alternatively, retinas were evaluated in histological sections or VEGF levels were measured in intact eyes using ELISA.

Results: Successful delivery of siRNA to the subretinal space was confirmed by observing significantly reduced levels of *EGFP* in eyes treated with Ad CM *VEGFP* plus *EGFP*-directed siRNA. siRNAs directed against *hVEGF* effectively and specifically inhibit hypoxia-induced VEGF levels in human cell lines and after adenoviral induced *hVEGF* transgene expression in vivo. In addition, subretinal delivery of siRNA directed against murine *Vegf* significantly inhibited CNV after laser photocoagulation.

Conclusions: Delivery of siRNA can be used in vitro and in vivo to target specific RNAs and to reduce the levels of the specific protein product in the targeted cells. This work suggests that RNA interference has potential for application to studies of retinal biology and for the treatment of a variety of retinal diseases, including those involving abnormal blood vessel growth.

RNA interference (RNAi) is a process conserved throughout many eukaryotic organisms, in which the presence of double stranded RNA (dsRNA) in a cell results in the destruction of mRNAs whose sequences share homology to the dsRNA. This phenomenon is now being exploited as a powerful tool for reverse genetics, and shows great promise for therapeutic applications. Elbashir et al. [1] have shown that synthetic RNAs of 21 and 22 nucleotides in length are able to mediate cleavage of the target RNA. These RNAs are termed small interfering RNA (siRNA). This group has also shown that siRNAs are involved in degrading homologous RNAs in mammalian cells [1]. Recently it was demonstrated that RNA interference mediated by siRNAs can specifically target sequence from hepatitis C virus in living mice [2,3].

Technology that allows the downregulation of expression of specific genes expressed in the retina would have numerous applications ranging from improving our understanding of the basic biology of the retina to providing therapy for blinding diseases. As a first step in evaluating the potential of retinal delivery of siRNA, we selected three target genes for study:

the reporter gene, enhanced green fluorescent protein (*EGFP*) and both human (*h*) and murine (*m*) vascular endothelial growth factor (*VEGF*). We designed siRNAs directed specifically against these genes and tested their abilities to mediate RNA interference in vitro in human cell lines and in vivo in mice. The ability of siRNA molecules to silence endogenous *VEGF* gene expression was also evaluated in an animal model for age-related macular degeneration (AMD): the murine laser-induced model of choroidal neovascularization (CNV) [4]. CNV, found in the "wet" form of AMD, is characterized by the growth of new blood vessels below the retina. While multiple pro-angiogenic proteins may be involved in CNV, VEGF has been shown in both clinical and bench research studies to play a critical role in the pathophysiology of this blinding condition [5-14]. *VEGF* is known to be upregulated in the laser photocoagulation model of CNV [15]. Our studies demonstrate that siRNA can be used to downregulate the expression of two different genes expressed in the retinal pigment epithelium (RPE). We also show that siRNA targeting *Vegf* can be used to decrease the extent of CNV in the laser photocoagulation model. These findings suggest that delivery of siRNA directed against *VEGF* may be a useful approach with which to treat retinal diseases with a neovascular component.

Correspondence to: Michael J. Tolentino, Scheie Eye Institute, 51 North 39th Street and Myrin Circle, Philadelphia, PA, 19104; Phone: (215) 662-8675; email: mtolent95@aol.com

METHODS

siRNA design: Selection of siRNAs was based on the characterization of siRNA by ElBashir et al [1,16]. An hVEGF5.siRNA targeting the sequence 5'-AAA CCU CAC CAA GGC CAG CAC-3' was selected. This siRNA consisted of an RNA duplex containing a sense strand 5'-ACC UCA CCA AGG CCA GCA C_dTd-3' and an antisense strand 5'-G UGC UGG CCU UGG UGA GGdUTd-3'. For rescue of the CNV model an siRNA was designed that targets mouse *Vegf* mRNA at the sequence 5'-AAC GAU GAA GCC CUG GAG UGC-3'. The sense strand of this molecule, in Vegf1.siRNA, was 5'-CGA UGA AGC CCU GGA GUG C_dTd-3' and the antisense strand was 5'-GCA CUC CAG GGC UUC AUC GdUTd-3'. The siRNA used to downregulate EGFP expression targeted the following sequence in EGFP mRNA: 5'-GGC UAC GUC CAG GAG CGC ACC-3'. The sense strand of this molecule, EGFP1.siRNA, was 5'-P GGC UAC GUC CAG CGC ACC-3' and the antisense strand was 5'-P U GCG CUC CUG GAC GUA GCC UU-3' (Pre-synthesized control siRNA green fluorescent protein duplex, Dharmacon Research Inc (Lafayette, CO)). The EGFP1.siRNA was also used as a control for studying the effects of hVEGF5.siRNA and mVegf1.siRNA. All synthetic RNA sequences were synthesized and purified by Dharmacon Research, Inc.

Preparation of recombinant adenoviruses: Serotype 5, E1-deleted replication defective adenovirus vectors were prepared and used as described [17,18]. Transgenes were driven by the cytomegalovirus (CMV) promoter. The viruses were prepared in human embryonic kidney '293' cells, purified by double CsCl density gradient centrifugation and stored in 10% glycerol at -70 °C prior to use.

siRNA transfection and hypoxia induction in vitro: Human cell lines (human embryonic kidney '293' and HeLa cells, ATCC, Manassas, VA) were seeded into 24 well plates one day prior to transfection. At the time of transfection with siRNA, the cells were about 50% confluent in 250 µl of complete DMEM medium. Transfections of siRNA (at 13 nM) were performed in all cell lines using the Transit TKO Transfection reagent (Mirus, Madison, WI; using guidelines provided by the manufacturer). Controls included transfection reagent lacking siRNA, and nonspecific siRNA (EGFP1.siRNA). 24 h after transfection, hypoxia was induced in the cells by the addition of desferrioxamine to a final concentration of 130 mM in each well as described [19]. 48 h post transfection the supernatant was removed from all wells and a human VEGF ELISA (R & D systems, Minneapolis, MN) was performed on the cell supernatants as described in the Quantikine human VEGF ELISA protocol. ELISA results were read on a Wallac Victor2 ELISA plate reader (Perkin Elmer Life Sciences, Inc., Boston, MA). Experiments were repeated four times using 293 cells and three times using HeLa cells. The Student's t-test was used for statistical analysis using the combined data from each of the replicates.

In vivo studies and tissue analysis: Animal experiments were performed in accordance with institutional guidelines for the care and use of animals in research. Both adenovirus and

siRNA were delivered subretinally to five adult C57Bl/6 mice (Jackson Labs, Bar Harbor, ME) as described previously [17]. The mixture injected contained about 1x10⁸ particles of Ad CMVEGFP, generously provided by Dr. J. Wilson (Dept. of Medical Genetics, University of Pennsylvania), and 20 picomoles of EGFP1.siRNA conjugated with transit TKO reagent (Mirus). As positive control, contralateral eyes received a mixture containing the same amount of Ad CMV.EGFP and 20 picomoles of hVEGF5.siRNA conjugated with transit TKO reagent (Mirus). Production of EGFP was detected by ophthalmoscopy 48-60 h after injection as described [20]. Animals were sacrificed and the eyes were enucleated and fixed in 4% paraformaldehyde. Eyes were prepared as either flat mounts (4 animals/8 eyes) or 10 µm cryosections for fluorescent microscopy (1 animal/2 eyes). Microscopic examinations were performed with a Zeiss fluorescent dissecting microscope and with a Leica DMR microscope (Wetzlar, Germany) equipped with epifluorescence illumination. Images were captured using a Hamamatsu CCD camera (Hamamatsu Photonics, Bridgewater, NJ) using OpenLab 2.2 software (Improvision, Boston, MA).

Inhibition of human VEGF in vivo: Ad.CMV.hVEGF, generously provided by Dr. M. Herlyn (Molecular and Cellular Oncogenesis, University of Pennsylvania), was injected subretinally and bilaterally in eyes of five C57Bl/6 mice. One eye of each animal was co-injected with mVegf1.siRNA and contralateral eyes were co-injected with EGFP1.siRNA as control. Two days later, eyes were snap frozen in liquid N₂ following enucleation. All eyes were homogenized in lysis buffer (Roche, Basel, Switzerland) and total protein was measured using a Bradford assay. The samples were all normalized for total protein prior to assaying for human VEGF by ELISA. The ELISA was performed according to the manufacturers recommendations (R & D systems).

Laser induced CNV model studies: Adult (8-15 week old) female C57Bl/6 mice (n=30) were anesthetized with averin (2,2,2-tribromoethanol) and pupils were dilated with 1% tropicamide. Laser photocoagulation was performed bilaterally using a diode laser photocogulator (IRIS Medical, Mountain View, CA) and slit lamp system with a cover slip as a contact lens. Laser photocoagulation (140 mW, 75 µm spot size, 0.1 s duration) was applied to the 8 and 10 o'clock positions in the right eye and 2 and 4 o'clock positions in the left eye, 2 to 3 disk diameters from the optic nerve. Since the rupture of Bruch's membrane is necessary to create significant CNV [4], bubble formation at the time of photocoagulation was used as an indication of the rupture of Bruch's membrane. Laser burns that did not induce a rupture in Bruch's membrane were excluded from the study. Lesions in which two laser spots became confluent were also excluded from the study.

Approximately 36 h after laser treatment, siRNA was delivered to both eyes by subretinal injection. A mixture containing about 1x10⁸ particles of Ad.CMV.LacZ, generously provided by Dr. J. Wilson, and 20 picomoles of mVegf1.siRNA conjugated with transit TKO reagent (Mirus) was injected. As control, contralateral eyes received a mixture of the same

molecules except that mVegf1 siRNA was replaced with EGFP1 siRNA. Two weeks after laser photoocoagulation, animals were perfused with high molecular weight dextran-fluorescein (Molecular Probes, Eugene, OR) to label the retinal/choroidal vasculature and eyes were harvested. The area of CNV was measured in choroidal flat mount preparations by a masked individual using modifications of methods described previously [4,21]. These modifications are as follows: Microscopic examinations were performed with a Leica DMR microscope (Wetzlar, Germany) equipped with epifluorescence illumination. Lesions in the dextran-fluorescein-perfused flat mount preparations were identified as circular fluorescent (fluorescein positive) areas corresponding with the area previously exposed to the laser light. Images of the lesions were captured using a black and white Hamamatsu CCD camera (Hamamatsu Photonics, Bridgewater, NJ) coupled to a Apple Macintosh G4 computer (Cupertino, CA) equipped with OpenLab 2.2 software. Images for calibration were obtained from a slide with a grating of known size. The hyperfluorescent fluorescein-dextran labeled blood vessels within the area of the laser burn were selected as a "region of interest" (ROI) using OpenLab software and this software was used to calculate the area (μm^2) occupied by the white pixels in the ROIs. The ROIs were selected after collecting the images under identical integration settings. They were selected by using the Openlab "magic wand" tool to identify pixels in the laser burn site at a range of 2000-4090 intensity units (The intensity units are defined within the OpenLab software. The units selected represented levels measured in normal fluorescein-perfused vasculature. For reference, the intensity of background, non-fluorescent, areas was <450 intensity units.) The ROIs were generally well-circumscribed by a region lacking fluorescence. After measuring the areas of CNV, images were colorized in OpenLab by applying an intensity ramp at 515 nm (the wavelength at which the image data were captured) using the "Apply wavelength" function. This intensity ramp was applied to all of the pixels in the image and made the whitest pixels the brightest green color. The images were then exported to Adobe Photoshop software for presentation purposes. Situations in which there was no evidence of a laser burn after bright field analysis of choroidal flatmounts were excluded. Statistical analysis of the results was performed using a one-tailed distribution, two sample unequal variance Student's t-test.

RESULTS

Hypoxia-induced upregulation of human VEGF is halted by siRNA application in vitro. The ability of hVEGF5 siRNA to target human VEGF mRNA was tested in vitro in a system whereby exposure to desferrioxamine results in the induction of hypoxia-signaling events. That, in turn, induces VEGF expression [19].

Prior to hypoxia induction, two different human cell lines (embryonic kidney ["293"] cells and ovarian carcinoma [HeLa] cells) were transfected with hVEGF5 siRNA. As control, additional cells were transfected with an siRNA (EGFP1 siRNA) designed to target the reporter gene, EGFP, or with buffer alone. VEGF upregulation occurs due to a desferrioxamine-

mediated induction of the HIF-1 hypoxic signaling pathway within 24 h [19]. To upregulate VEGF via this method, cells were exposed to desferrioxamine 24 h post-transfection. A human VEGF ELISA was performed on cell supernatants 24 h after desferrioxamine withdrawal in order to measure the effects of siRNA treatment on hVEGF levels. The hypoxia-mediated increase in hVEGF protein was reduced significantly in the presence of hVEGF5 siRNA (Figure 1). Exposure to the non-specific siRNA (EGFP1 siRNA) or to buffer lacking siRNA had minimal effect on hVEGF levels. EGFP1 siRNA

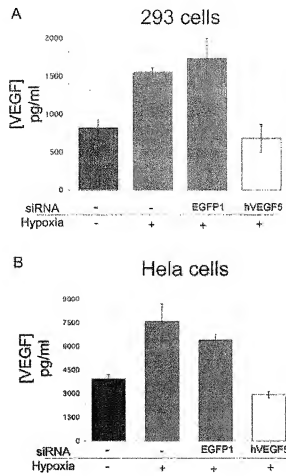


Figure 1. RNA interference disrupts desferrioxamine induced up-regulation of VEGF in vitro. The hVEGF5 siRNA or control reagents were transfected into 293 cells (A) and HeLa cells (B) prior to inducing hypoxia with desferrioxamine. VEGF levels were measured in cell supernatants by ELISA 24 h after hypoxia induction. Hypoxia induced VEGF expression. In both 293 cells and HeLa cells, exposure to hVEGF5 siRNA reduced the amount of VEGF produced after hypoxia ($p<0.01$ for both cell types). There was no significant difference in the amount of VEGF produced by hypoxic cells when control reagents (EGFP1 siRNA) or no siRNA were delivered. The error bars represent the standard errors of the mean of 4 or 3 replicates, respectively, for the 293 and HeLa cells.

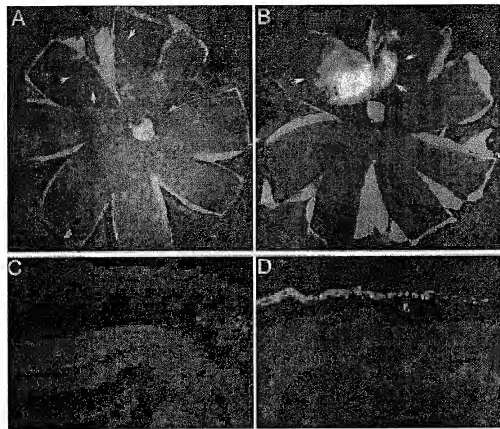


Figure 2. Effect of EGFP1 siRNA on *EGFP* expression in RPE cells *in vivo*. Eyes of mice were injected subretinally with Ad.CMV.EGFP in the presence of either EGFP1 siRNA (A,C) or hVEGF5 siRNA (B,D). Levels of EGFP were low in the injected portion of EGFP1 siRNA-treated eyes on inspection of flat mount preparations (A) and cryosections (C). No EGFP was detectable in the un.injected portions of these retinas. In comparison, high levels of EGFP were present in the region of injection in flat mounts (B) or cryosections (D) of eyes exposed to the control hVEGF5 siRNA. Arrows point to boundaries of injection blebs. Sections within the regions demarcated by the arrows in panels A and B are shown in panels C and D, respectively.

had no significant inhibitory effect on the concentration of hVEGF after exposure to hypoxic conditions in both 293 cells (Figure 1A; $p=0.22$) and HeLa cells (Figure 1B; $p=0.15$). There was no significant difference in hVEGF levels comparing normoxic and hypoxic, hVEGF5 siRNA-treated 293 cells ($p=0.17$). Human VEGF levels were significantly lower in the hypoxia plus hVEGF5 siRNA-treated cells than in cells treated with normoxia alone ($p<0.01$).

The ability to down-regulate VEGF production with an siRNA *in vitro* prompted us to explore the *in vivo* application of siRNA in the retina.

In vivo delivery of siRNAs to murine retinal pigment epithelial cells: Retinal pigment epithelial cells are thought to be the cells that, through abnormal VEGF production, initiate the process that leads to pathologic neovascularization (i.e. CNV) in AMD [12-14]. To determine whether siRNAs can be effectively delivered to the RPE, we expressed *EGFP* in those cells *in vivo* using a recombinant adenovirus, a virus that targets these cells efficiently and nearly exclusively after subretinal injection in adult mice. Recombinant adenovirus also results in a rapid onset of transgene expression [17,22]. In this system, we tested the possibility that EGFP1 siRNA would reduce levels of EGFP protein. Five mice received bilateral subretinal injections with Ad.CMV.hVEGF, an E1/E3-deleted recombinant adenovirus delivering the *EGFP* cDNA driven by the CMV promoter. In the right eyes EGFP1 siRNA was also injected and in the contralateral eyes an siRNA unre-

lated to *EGFP* (hVEGF5 siRNA) was injected as a non-specific control. Ophthalmoscopy was performed 48 h post injection, the time at which adenovirus-mediated transgene expression in this system is maximal [17]. Ophthalmoscopy in-

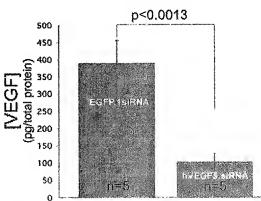


Figure 3. RNA interference significantly diminishes levels of hVEGF *in vivo*. Ad.CMV.hVEGF was delivered by subretinal injection bilaterally in 5 animals in the presence of either hVEGF5 siRNA or, in contralateral eyes, EGFP1 siRNA as control. Animals were sacrificed 48 h post-injection, and the eyes were removed and processed for VEGF ELISA. Bars represent the means, the error bars represent the standard errors of the mean. Injection of hVEGF5 siRNA results in significant reduction in levels of hVEGF compared to injection of EGFP1 siRNA ($p<0.0013$).

dicated that levels of EGFP were significantly lower in 4 of the 5 eyes co-injected with EGFP1 siRNA compared to the 5 eyes co-injected with hVEGF5 siRNA (not shown). The mice were sacrificed 48-60 h post-injection, and the eyes were harvested and evaluated for presence and amount of EGFP by inspection of retinal flat mounts and histological preparations. Figure 2A,B is representative of the flat mount results. There were only low levels of EGFP-specific fluorescence in whole

mount preparations of the eyes that had received EGFP1 siRNA (Figure 2A) whereas EGFP was intensely fluorescent in retinas co-injected with hVEGF5 siRNA (Figure 2B). Uninjected portions of the eyes showed only background levels of fluorescence. Histological analyses revealed faint levels of EGFP in occasional cells of the injected portions of the retinas co-injected with EGFP1 siRNA (Figure 2C) but high levels of EGFP in the analogous regions of the contralateral eyes co-injected with hVEGF5 siRNA (Figure 2D).

Adenoviral expression of human VEGF silenced by siRNA in murine retina in vivo: Having demonstrated delivery of siRNA to RPE cells and significant diminution in levels of a marker protein, we sought to inhibit expression of a biologically relevant molecule in the retina *in vivo*. *VEGF* is an ideal candidate as this molecule is known to play a significant role in retinal neovascular disease [8-11]. Ad.CMV.hVEGF was used to deliver *hVEGF* as this virus can upregulate pharmacological levels of *hVEGF* and is capable of producing CNV when injected in the subretinal space [23,24].

One eye of each of 5 animals was co-injected with Ad.CMV.hVEGF and hVEGF5 siRNA while contralateral eyes were co-injected with Ad.CMV.hVEGF and EGFP1 siRNA as control. The animals were sacrificed 60 h post-injection and the eyes were processed for a human VEGF ELISA. There was a significant attenuation of VEGF levels in eyes that had received hVEGF5 siRNA as compared to the control

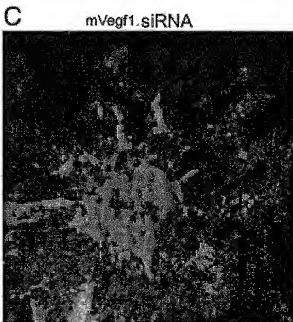
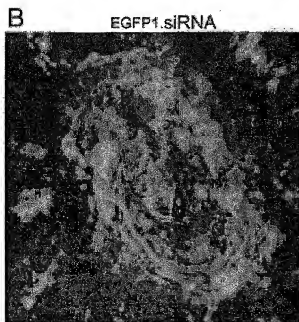
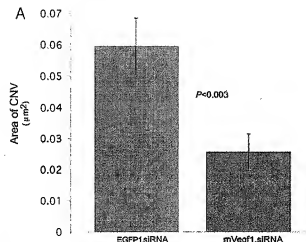


Figure 4. The extent of CNV is significantly reduced after subretinal delivery of *mVegf1* siRNA. Thirty-six hours following laser photoagulation, *mVegf1* siRNA was delivered subretinally in one eye of each of 30 mice. Contralateral eyes were injected with a control (EGFP1) siRNA. Animals were perfused with dextran-fluorescein and the areas of CNV were measured in choroidal flat mounts 14 days after laser treatment. There is a significant difference ($p<0.003$) in mean areas of CNV between eyes injected with *mVegf1* siRNA versus EGFP1 siRNA (panel A). Representative areas of CNV in eyes of a dextran-fluorescein-perfused animal that had received EGFP1 siRNA in one eye but *mVegf1* siRNA in the other are shown in the colorized panels B and C, respectively. The CNV lesions were generally well-circumscribed by a region lacking fluorescence (as in panel B). CNV was identified by observing dextran-fluorescein-filled blood vessels on the choroidal/retinal interface, which are normally absent.

EGFP1.siRNA (Figure 3). The data demonstrate that the hVEGF siRNA is effective in decreasing levels of hVEGF in murine RPE cells *in vivo*.

Inhibition of choroidal neovascularization using siRNA directed at murine Vegf. To determine whether siRNA can inhibit CNV in an animal model, we tested the effects of delivery of an siRNA directed against murine *Vegf* (m*Vegf1*.siRNA) in a laser induced model of CNV. We delivered m*Vegf1*.siRNA by subretinal injection to the RPE of mice 36 h after laser treatment. The areas of m*Vegf1*.siRNA injection encompassed all of the laser spots as well as untreated retina adjacent to these spots. Contralateral eyes received siRNA targeting EGFP1 (EGFP1.siRNA) as control. The mice were perfused with dextran-fluorescein 14 days after the laser treatment, the time of maximal neovascularization, and the areas of neovascularization were measured using digital image capture around the burn spots. The majority of lesions (75% for the EGFP1.siRNA-treated eyes and 80% for the Vegf1.siRNA-treated eyes) met the criteria for analysis (see Methods). The locations of these neovascular areas exactly coincided with the sites initially exposed to laser. Neovascularization was not observed in portions of the retina that had not been exposed to laser. The areas of neovascularization in animals that received m*Vegf1*.siRNA were, on average, one quarter of the area of the control-treated spots (Figure 4, p<0.003). These data show that siRNA targeting m*Vegf* is capable of inhibiting CNV in the laser photocoagulation model.

DISCUSSION

The data presented here represent the application of a technology to inhibit expression of genes in the retina, specifically to inhibit the expression of *VEGF*. To our knowledge, the data presented here describe the first successful application of siRNA to the retina. siRNA was used to significantly decrease levels of exogenous expression of transgenes both *in vitro* and *in vivo*. Results shown here from *in vitro* studies using siRNA directed against *VEGF* revealed a significant reduction in the amount of VEGF protein produced under hypoxic conditions. Even more impressive due to the high levels of protein produced after delivery of recombinant adenovirus, siRNA directed against *VEGF* significantly reduced VEGF protein levels after delivery of Ad.CMV.hVEGF *in vivo*. Finally, a test for relevance of *VEGF*-directed siRNA towards human retinal disease comes from studying its effect in an *in vivo* model of CNV. In accord with the *in vitro* and the *in vivo* Ad.CMV.hVEGF data, application of a *Vegf*-directed siRNA significantly reduced the extent of neovascularization in the murine laser photocoagulation model of CNV. The results provide an encouraging first step in application of siRNA technology to the retina.

As with any new technology, the data from the siRNA studies presented here invite many questions. For example: how can this technology be applied to other (non RPE) retinal cell types? While these data demonstrate delivery of functional siRNA to the RPE they do not explore delivery of the molecules to other retinal cells. Subretinal delivery of adenovirus

efficiently targets the RPE and occasional Müller cells, but not other layers of the adult retina [17]. Because the reporter protein was only expressed in the RPE we cannot currently assess the delivery of siRNA to other retinal cell types. We are currently employing other assays to address efficient delivery to the photoreceptors, Müller cells and ganglion cells. What is the stability of the effect? Is there any toxicity induced by the delivery or the composition of the siRNAs? Although there was no qualitative evidence of acute toxicity in the small number of samples we evaluated, it will be important to formally evaluate both acute and chronic toxicity of the treatment/siRNA in a larger number of eyes. In the case of laser photoocoagulation/CNV, how efficacious is the effect of VEGF1.siRNA when it is administered at different stages of the disease? Will siRNA-mediated therapy be effective in other animal models of retinal neovascularization? VEGF siRNA-mediated rescue of additional models of ocular neovascularization such as the murine retinopathy of prematurity model [25] and models in larger animals are currently being studied in pursuit of answers to these questions.

The stability of the siRNA-induced interference effect on retinal cells is unknown at present. Experiments in progress aim to characterize the timecourse and magnitude of the effect after siRNA transfection. If this effect is found to be short-lived, there are other modifications that could be used to achieve a more sustained effect. For example, the combination of siRNA technology with recombinant viral vector techniques is a particularly promising avenue. Virus-mediated delivery of siRNA would allow delivery of therapeutic siRNA molecules that are replenished over time. Regardless of the mode of delivery, the potential of siRNA for contributing to a diverse set of applications is exciting. The possibilities range from using this technology to define developmental and physiological processes in the retina to testing approaches that might result in therapy for a diverse set of ocular diseases, including those involving ocular neovascularization.

ACKNOWLEDGEMENTS

This work was funded by the Juvenile Diabetes Foundation International, NEI KO8 EY 131410, NIH RO1-EY10820, RO1-EY12156, P30 DK47757, Foundation Fighting Blindness, Research to Prevent Blindness, International Retinal Research Foundation, the LIFE Foundation, the Steinbach Foundation, the Paul and Evanna Mackall Foundation Trust and the F.M. Kirby Foundation. MJT and SJR hold equity in Acuity Pharmaceuticals, Inc.

REFERENCES

- Elbashir SM, Lendeckel W, Tuschl T. RNA interference is mediated by 21- and 22-nucleotide RNAs. *Genes Dev* 2001; 15:188-200.
- McCaffrey AP, Meuse L, Pham TT, Conklin DS, Hamon GJ, Kay MA. RNA interference in adult mice. *Nature* 2002; 418:38-9.
- Song E, Lee SK, Wang J, Ince N, Ouyang N, Min J, Chen J, Shankar P, Lieberman J. RNA interference targeting Fas protects mice from fulminant hepatitis. *Nat Med* 2003; 9:347-51.
- Tobe T, Ortega S, Luna JD, Ozaki H, Okamoto N, Derevjanik NL, Vinores SA, Basilico C, Campochiaro PA. Targeted disruption

of the FGF2 gene does not prevent choroidal neovascularization in a murine model. *Am J Pathol* 1998; 153:1641-6.

- Iu M, Adamis AP. Vascular endothelial growth factor gene regulation and action in diabetic retinopathy. *Ophthalmol Clin North Am* 2002; 15:69-79.
- Campochiaro PA. Retinal and choroidal neovascularization. *J Cell Physiol* 2000; 184:301-10.
- Kwak N, Okamoto N, Wood JM, Campochiaro PA. VEGF is major stimulator in model of choroidal neovascularization. *Invest Ophthalmol Vis Sci* 2000; 41:3158-64.
- Ajello LP, Avery RL, Arrigg PG, Keyt BA, Jampel HD, Shah ST, Pasquale LR, Thieme H, Iwamoto MA, Park JE, et al. Vascular endothelial growth factor in ocular fluid of patients with diabetic retinopathy and other retinal disorders. *N Engl J Med* 1994; 331:1480-46.
- Krzystolik MG, Alshari MA, Adamis AP, Gaudreault J, Gragoudas ES, Michaud NA, Li W, Connolly E, O'Neill CA, Miller JW. Prevention of experimental choroidal neovascularization with intravitreal anti-vascular endothelial growth factor antibody fragment. *Arch Ophthalmol* 2002; 120:338-46.
- Tolentino MJ, McLeod DS, Tatomoto M, Otsuji T, Adamis AP, Linty GA. Pathologic features of vascular endothelial growth factor-induced retinopathy in the nonhuman primate. *Am J Ophthalmol* 2002; 133:373-85.
- Adamis AP, Shima DT, Tolentino MJ, Gragoudas ES, Ferrara N, Folkman J, D'Amore PA, Miller JW. Inhibition of vascular endothelial growth factor prevents retinal ischemia-associated iris neovascularization in a nonhuman primate. *Arch Ophthalmol* 1996; 114:66-71.
- Grossniklaus HE, Ling JX, Wallace TM, Dithmar S, Lawson DH, Cohen C, Elmer VM, Elmer SG, Sternberg Jr. Macrophage and retinal pigment epithelium expression of angiogenic cytokines in choroidal neovascularization. *Mol Vis* 2002; 8:119-26.
- Hofman P, Blaauwgeerts HG, Tolentino MJ, Adamis AP, Nunes Cardozo BJ, Vrensen GF, Schlingemann RO. VEGF-A induced hyperpermeability of blood-retinal barrier endothelium in vivo is predominantly associated with pinocytotic vesicular transport and not with formation of fenestrations. Vascular endothelial growth factor-A. *Curr Eye Res* 2000; 21:637-45.
- Lopez PF, Sippy BD, Lambert HM, Thach AB, Hinton DR. Transdifferentiated retinal pigment epithelial cells are immunoreactive for vascular endothelial growth factor in surgically excised age-related macular degeneration-related choroidal neovascular membranes. *Invest Ophthalmol Vis Sci* 1996; 37:855-68.
- Shen WY, Yu MJ, Barry CJ, Constable JJ, Rakoczy PE. Expression of cell adhesion molecules and vascular endothelial growth factor in experimental choroidal neovascularisation in the rat. *Br J Ophthalmol* 1998; 82:1063-71.
- Elbashti SM, Martinez J, Patkanowksa A, Lendeckel W, Tuschl T. Functional anatomy of siRNAs for mediating efficient RNAi in *Drosophila melanogaster* embryo lysate. *EMBO J* 2001; 20:6877-88.
- Bennett J, Wilson J, Sun D, Forbes B, Maguire A. Adenovirus vector-mediated in vivo gene transfer into adult murine retina. *Invest Ophthalmol Vis Sci* 1994; 35:2535-42.
- Gruss CJ, Satyamoorthy K, Berkng C, Lininger J, Nesbit M, Schaeider H, Liu ZJ, Oka M, Hsu MY, Shirakawa T, Li G, Bogennroder T, Carmeliet P, El-Deyri WS, Eck SL, Rao JS, Baker AH, Bennett JT, Cronbleholme TM, Velazquez O, Karmacharya J, Margolis DJ, Wilson JM, Detmar M, Skubitz M, Robbins PD, Buck C, Herlyn M. Stroma formation and angiogenesis by overexpression of growth factors, cytokines, and proteolytic enzymes in human skin grafted to SCID mice. *J Invest Dermatol* 2003; 120:683-92.
- Jiang BH, Zheng JZ, Leung SW, Roe R, Semenza GL. Transactivation and inhibitory domains of hypoxia-inducible factor 1alpha. Modulation of transcriptional activity by oxygen tension. *J Biol Chem* 1997; 272:19253-60.
- Bennett J, Duan D, Engelhardt JF, Maguire AM. Real-time, noninvasive in vivo assessment of adenovirus-mediated retinal transduction. *Invest Ophthalmol Vis Sci* 1997; 38:2857-63.
- Edelman JL, Castro MR. Quantitative image analysis of laser-induced choroidal neovascularization in rat. *Exp Eye Res* 2000; 71:523-33.
- Li T, Adamian M, Roof DJ, Berson EL, Dryja TP, Roessler BJ, Davidson BL. In vivo transfer of a reporter gene to the retina mediated by an adenoviral vector. *Invest Ophthalmol Vis Sci* 1994; 35:2543-9.
- Spilsbury K, Garrett KL, Shen WY, Constable JJ, Rakoczy PE. Overexpression of vascular endothelial growth factor (VEGF) in the retinal pigment epithelium leads to the development of choroidal neovascularization [published erratum appears in *Am J Pathol* 2000; 157:1413]. *Am J Pathol* 2000; 157:135-44.
- Baffi J, Byrnes G, Chan CC, Csaky KG. Choroidal neovascularization in the rat induced by adenovirus mediated expression of vascular endothelial growth factor. *Invest Ophthalmol Vis Sci* 2000; 41:3582-9.
- Smith LE, Wesolowski E, McLellan A, Kostyk SK, D'Antonio R, Sullivan R, D'Amore PA. Oxygen-induced retinopathy in the mouse. *Invest Ophthalmol Vis Sci* 1994; 35:101-11.

EXHIBIT 6

RNA interference targeting transforming growth factor- β type II receptor suppresses ocular inflammation and fibrosis

Hiroshi Nakamura,¹ Shahid S. Siddiqui,² Xiang Shen,¹ Asrar B. Malik,² Jose S. Pulido,¹ Nalin M. Kumar,² Beatrice Y. J. T. Yue¹

(The first two authors contributed equally to this publication)

Departments of ¹Ophthalmology and Visual Sciences, and ²Pharmacology, College of Medicine, University of Illinois at Chicago, Chicago, IL

Purpose: Transforming growth factor- β (TGF- β) is an important mediator of wound healing responses. In the eye, TGF- β activity has been implicated in causing corneal haze after laser surgery and subconjunctival scarring following glaucoma surgery. The purpose of the study was to determine whether small interference RNAs (siRNAs) targeting the type II receptor of TGF- β (T β RII) could be used to suppress the TGF- β action.

Methods: T β RII specific siRNAs designed from the human gene sequence were transfected into cultured human corneal fibroblasts. The protein and transcript levels of the receptor were determined by immunofluorescence, western blotting, and real time PCR. Immunofluorescence and immunoblotting were carried out to examine fibronectin assembly. A wound closure assay was used to assess cell migration in *in vitro* fibroblast cultures. In addition, the *in vivo* effects of T β RII siRNA were evaluated in a mouse model of ocular inflammation and fibrosis generated by subconjunctival injection of phosphatase buffered saline and latex beads. Mouse T β RII siRNA was introduced into experimental eyes. Cellularity on tissue sections was evaluated after staining with hematoxylin and eosin. Collagen deposition was visualized by picrosirius red staining.

Results: T β RII siRNAs abrogated the receptor transcript and protein expression in cultured corneal fibroblasts. The gene knockout inhibited fibronectin assembly and retarded cell migration. In the mouse model, introduction of T β RII specific siRNAs significantly reduced the inflammatory response and matrix deposition.

Conclusions: T β RII specific siRNAs were efficacious both *in vitro* and *in vivo* in knocking down the TGF- β action. A direct application of siRNA into eyes to downregulate T β RII expression may provide a novel therapy for preventing ocular inflammation and scarring.

Transforming growth factor- β (TGF- β), a family of structurally related multifunctional cytokines, has wide biological actions including cell growth, differentiation, apoptosis, and fibrogenesis [1-3]. TGF- β typically is secreted in a latent form and is activated through a complex process of proteolytic activation and dissociation of latency protein subunits [4]. The action of TGF- β is mediated by TGF- β receptors types I (T β RI) and II (T β RII), both of which are serine and threonine kinases. Signal transduction is initiated by TGF- β binding to T β RII, followed by its association with T β RI [4]. T β RII phosphorylates multiple serines and threonines in the TTSGSGSGSG sequence of the cytoplasmic region of T β RII [4]. The activated T β RI in turn phosphorylates and activates the transcription factors, Smads [4,5].

TGF- β has emerged as a key mediator of the fibrotic response to wounding. It is upregulated during different types of wound healing in the eye, liver, and skin [3,6-8]. Of the three human isoforms (TGF- β 1, TGF- β 2, and TGF- β 3), TGF- β 2 is the predominant form in the eye [9,10]. TGF- β s have

been shown to be important in ocular scarring in conditions including proliferative vitreoretinopathy [11], cataract formation [12], corneal opacities [13], and subconjunctival scarring, a complication of filtration surgery in glaucoma [14,15]. TGF- β also has been implicated in choroidal neovascularization [16,17].

In glaucoma filtration surgery, postoperative scarring at the wound site is a critical determinant of the surgical outcome [18,19]. Although anti-scarring agents such as mitomycin C and 5-fluorouracil can prevent post-operative scarring and improve surgical outcome [20,21], they do so by causing widespread fibroblast cell death and are associated with severe and potentially blinding complications [22,23]. The important role of TGF- β in the wound repair has led to other strategies [15] such as the use of anti-TGF- β antibody [24,25] and antisense oligonucleotides [26] to block the TGF- β action. These studies have, in general, targeted the ligand rather than the receptor.

In the current study, we used the RNA interference (RNAi) strategy to target the TGF- β pathway. Gene silencing is a process by which double stranded RNA triggers the destruction of mRNAs sharing the same sequence. RNAi is initiated by the conversion of double stranded RNA into 21-23 nucleotide

Correspondence to: Dr. Beatrice Yue, Department of Ophthalmology and Visual Sciences, University of Illinois at Chicago, 1855 West Taylor Street, Chicago, IL, 60612; Phone: (312) 996-6125; FAX: (312) 996-7773; email: Beatyuc@uic.edu

fragments, termed small interfering RNAs (siRNAs), that direct the degradation of the target RNAs [27-29]. siRNAs have been shown to be of great value in knocking down genes in a variety of biological systems [30-32].

Since the ligand engagement by TβRII appears to be a major limiting step in cellular activation, we designed siRNAs targeting this receptor. In experiments described herein, the siRNAs induced a marked reduction in the TGF-β-mediated matrix deposition and retarded the migration of cultured human corneal fibroblasts. In addition, siRNA specific for TβRII was shown in an *in vivo* mouse model to reduce inflammation and the complications of wound repair in the eyes.

METHODS

Cell cultures: Normal human corneas from donors aged 13, 29, 34, 45, and 47 years were obtained from the Illinois Eye Bank (Chicago, IL). The procurement of tissues was approved by the Institutional Review Board at the University of Illinois at Chicago in compliance with the declaration of Helsinki. Corneal fibroblasts were derived from the stromas isolated from the corneas. The cells were maintained in serum containing media as previously described [33].

T_BRII siRNA sequences: siRNAs were derived from the coding sequence of the human T_BRII gene (MR5079). The siRNA selection was based on the program at Ambion (Austin, TX), choosing 21 nucleotide sequences that start with AA and have a 30 to 70% GC content. Sequences identified were BLASTed against the Genbank database. Four sequences that cover different regions of the T_BRII coding sequence and contain no homology to the non-T_BRII sequence were custom synthesized by Dharmacon Research (Lafayette, CO). The target sequences (5' to 3') and the siRNA duplexes for these 4 siRNA duplexes, designated as hT1, hT2, hT3, and hT4, are shown in Table 1, with the position of the first nucleotide in the human T_BRII sequence shown in parentheses.

In addition, a nonspecific, scrambled siRNA duplex

TABLE 1. TARGET AND DUPLEX SEQUENCES FOR TbRII SPECIFIC siRNAs

Four siRNAs, designated as hT1, hT2, hT3, and hT4, were designed from the coding sequence of the human TBRII gene. The target sequences (5'-3') and the siRNA duplex sequences are listed, with the position of the first nucleotide in the human TBRII sequence shown in parentheses. siRNA from the similar region as hT1 of the mouse TBRII sequence was also designed and the target sequence of the mouse T1 (mT1) siRNA is shown. There is one nucleotide difference (small letter) between the human and mouse TBRII sequences.

(Scramble II duplex), used as a control, and a Cy3 labeled luciferase GL2 duplex, used to determine optimal conditions for siRNA transfection, were purchased from Dharmacon. siRNA from the similar region as hT1 of the mouse T β RII sequence (AF406755), was also synthesized and tested for efficacy in vivo in an inflammatory/fibrosis mouse model. The target sequence of the mouse T1 (mT1) siRNA is shown in Table 1. There is one nucleotide difference (small letter) between the human and mouse T β RII sequences.

Transfection of siRNA duplexes: Normal human corneal fibroblasts were transfected with TBRII specific siRNA duplex (25, 50, 100, or 200 nM final concentration) or scrambled (control) siRNA (100 or 200 nM) using TransIT-TKO reagent (Takara Mirus, Madison, WI), following the manufacturer's protocol. The cells were harvested 16, 24, 48, or 72 h after transfection for analyses. Also as controls, corneal fibroblasts were either untreated or treated only with TransIT-TKO.

Immunofluorescence staining: After transfection, cells were fixed in 2% formaldehyde, permeabilized with 0.1% Triton X-100, and stained with rabbit anti-TBRII antibody (1:100, SC1700, Santa Cruz Biotechnology, Santa Cruz, CA) and FITC conjugated goat anti-rabbit IgG (1:250, Southern Biotechnology, Birmingham, AL). The nuclei of the cells were counterstained with 4',6'-diamidino-2-phenylindole dihydrochloride (DAPI). To observe the fibronectin network, cells were fixed in cold methanol, and immunostained with rabbit anti-human fibronectin (1:100, BD Biosciences, Lexington, KY) and FITC-goat anti-rabbit IgG (1:200; Jackson ImmunoResearch, West Grove, PA).

Western blotting: After siRNA transfection, corneal fibroblasts were lysed in a Triton lysis buffer. Equal amount of protein (20 µg/lane) was resolved on a 10% sodium dodecyl sulfate (SDS)-polyacrylamide gel. The proteins were then transferred to nitrocellulose membranes for probing with rabbit anti-TPRII antibody (1:1000) and horseradish peroxidase (HRP) conjugated goat anti-rabbit IgG (1:5000; Jackson ImmunoResearch). Signals were detected by chemiluminescence and analyzed by densitometry.

For secreted fibronectin, cells (48 h after transfection) were incubated with serum-free media for 24 h. After normalizing against the protein content in cell lysates, equal aliquots of media samples were electrophoresed on 10% SDS polyacrylamide gels under reducing conditions. Immunoblotting was performed using rabbit anti-human fibronectin (1:5000) and HRP-goat anti-rabbit IgG (1:10,000; Jackson ImmunoResearch).

Real time PCR: Total RNA was extracted with Trizol (Invitrogen, Carlsbad, CA) from cells 48 and 72 h after transfection. RNA (100 ng) was converted into cDNA using the Thermoscript RT-PCR system (Invitrogen) with oligo dT and random hexamers.

Primer pairs for the T_BRII gene were as described [34]. PCR amplification was performed using a Cepheid SmartCycler. The PCR mixture contained cDNA, Ex Taq R-PCR polymerase (Takara Mirus), 3 mM MgCl₂, dNTP, SYBR-Green (Molecular Probes, Portland, OR), and 0.5 μM of each gene specific primer. To normalize samples, real time PCR

reactions containing primers for 18S rRNA (number 1717, Ambion) were also performed. Amplification of PCR products was monitored via intercalation of SYBR-Green. A no template control and a no reverse transcription control were included. Agarose gel electrophoresis was used to verify that the T β RII PCR product was of the correct 75 bp size and that no primer dimers were formed. The C_i values were normalized to 18S rRNA to obtain a mean, normalized T β RII value using the Q-gene software (Version 1) as previously described [35].

Cell migration assay: Corneal fibroblasts after transfection were scratched with a sterile P20 pipet tip [36]. The migration of cells into the wound was examined by phase contrast microscopy 7 h after wounding. Total area of the wound in each 10x field and the area covered by the migrating cells within the wound were measured using an Image Processing Tool Kit (Version 3.0, Reindeer Graphics, Asheville, NC). At least 10 fields were analyzed and the mean percentage of wound area covered by cells was calculated. Student's t test was used for the statistical analysis.

Mouse model of subconjunctival inflammation and fibrosis: The experimental protocol was approved by the animal care committee at the University of Illinois at Chicago. Animal care guidelines comparable to those published by the US Public Health Service were followed. C57BL6 mice underwent general anesthesia with intraperitoneal injections of ketamine and xylazine. The subconjunctival scarring model was generated similar to that reported previously [37], with modifications. Instead of sterile phosphate buffered saline (PBS) alone, 30 μ l of PBS containing latex beads (1.053 μ m diameter, 300 μ g/ml; Polysciences, Warrington, PA) was injected to the temporal subconjunctival space of mouse eyes. For siRNA effects, the left eyes of mice were injected in a masked manner with 30 μ l of PBS/beads mixed with 0.1 μ l of TransIT-TKO and 200 nM mT1 or scrambled siRNA. To serve as controls, the left eyes of other mice were uninjected, or injected with PBS/latex beads alone or with TransIT-TKO reagent. All the right eyes were untouched. Mice were sacrificed by cervical dislocation 2, 4, 7, and 14 days after injection. At least 4 mice were used for each treatment/time point.

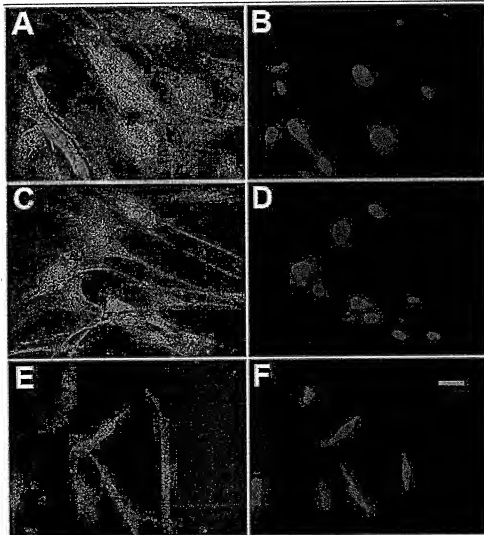


Figure 1. siRNA inhibits T β RII expression. Immunofluorescence analysis of human corneal fibroblasts, untreated (A,B), treated for 48 h with scrambled siRNA (C,D), or with 100 nM hT1 (E,F) was performed. T β RII expression is shown in A,C, and E. Staining of nuclei with DAPI (blue) is shown in B, D, and F. Note the reduction in T β RII staining of cells treated with hT1 siRNA (E) compared to control cells (A,C). The morphology after the siRNA treatment was somewhat altered. The bar represents 10 μ m.

Enucleated eyes were fixed with 10% buffered formalin and 5 µm thick paraffin sections were prepared. The sections were stained with hematoxylin and eosin to assess the inflammatory reaction and picrosirius red to demonstrate collagen

deposition [37]. The number of inflammatory cells in subconjunctival areas in the sections was counted. The value was normalized to number of inflammatory cells per 2500 µm² area underneath the conjunctival epithelium.

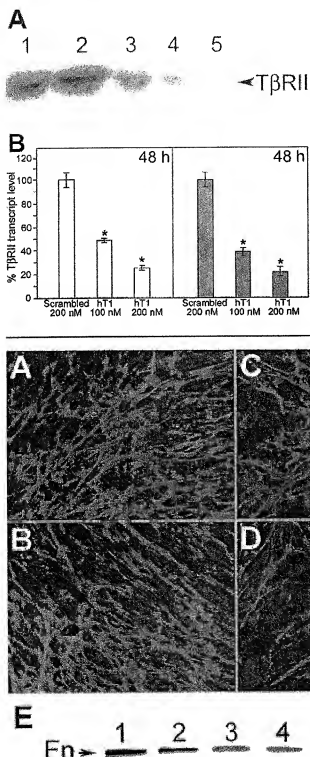


Figure 2. siRNAs suppress TβRII protein expression in corneal fibroblasts. Total cell lysates from human corneal fibroblasts treated with hT1 siRNA or control, scrambled siRNA for 48 h were separated on 10% SDS polyacrylamide gels and immunoblotted with a TβRII specific antibody. Lane 1 contains lysate from cells incubated with TransIT-TKO reagent alone (no siRNA). Lane 2 contains lysate from cells treated with 100 nM scrambled siRNA. Lanes 3 and 4 contain lysates of cells treated with hT1 siRNA at a final concentration of 100 nM (lane 3) or 200 nM (lane 4). In lane 5, the TβRII antibody was preincubated with antigenic peptide before probing the normal cell lysate. The TβRII band is indicated. **B** siRNAs reduce levels of TβRII transcript. RNA was prepared from cells treated with scrambled siRNA or hT1 siRNA for 48 or 72 h at either 100 or 200 nM concentration. Following conversion to cDNA, the samples were analyzed by real time PCR using primers to TβRII or 18S rRNA. The bar graphs show the mean expression levels of TβRII transcript normalized to 18S RNA relative to that of scrambled siRNA treated controls. Asterisks indicate that the data are significantly different from the scrambled controls ($p<0.0002$, $n=3$, Student's *t* test).

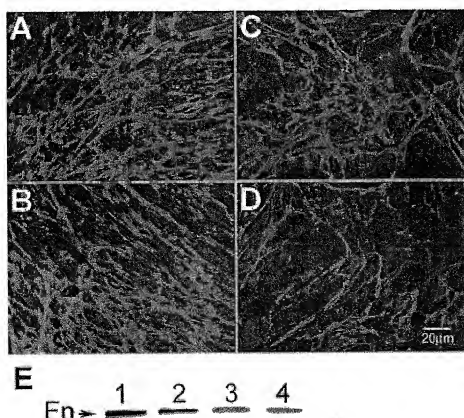


Figure 3. TβRII siRNA interferes with fibronectin production. Immunofluorescence analysis of fibroblasts untreated (A), treated for 48 h with scrambled siRNA (B), 100 nM hT1 (C), or 200 nM hT1 (D) was performed to visualize the fibronectin matrix (in green). Nuclei stained with DAPI are seen in blue. E: The level of fibronectin secreted to the culture media was analyzed by western blotting. Samples were from cultures untreated (lane 1), treated with scrambled RNA (lane 2), or 100 nM (lane 3) or 200 nM (lane 4) hT1. The fibronectin (Fn) bands are labeled.

RESULTS

Suppression of T β RII protein and mRNA expression: Using the TransIT-TKO reagent, we transfected human corneal fibroblasts with all four siRNAs (hT1-4) designed from the human T β RII gene sequence. The cellular uptake of oligoribonucleotides was initially determined using a Cy3 labeled luciferase siRNA. The transfection was efficient in that greater than 90% of the cells displayed red fluorescence of the luciferase siRNA (data not shown). Immunofluorescence showed punctate staining of T β RII on the surface of untreated control corneal fibroblasts (Figure 1A). The staining was in addition observed in the cytoplasm, particularly in the perinuclear area. When treated with 100 nM hT1 for 48 h, the T β RII staining intensity was markedly reduced (Figure 1E). At 100 nM, hT2, hT3, and hT4 likewise suppressed the T β RII staining intensity (data not shown). The inhibitory effect was also observed to varying degrees for all four siRNAs with other concentrations (50 and 200 nM) and time points (24 and 72 h). This response however was not evident at the lowest concentration (25 nM) and the shortest time point (16 h) tested. Overall, hT1 and hT2 resulted in a greater inhibition than hT3 and hT4. Cells treated with scrambled siRNA (Figure 1C) exhibited a similar staining intensity and pattern as the untreated control cells (Figure 1A).

Western blotting (Figure 2A) yielded a 73-75 kDa band immunoreactive to anti-T β RII in the vehicle treated control and scrambled siRNA transfected samples. The protein band was diffuse as T β RII is a glycoprotein. At 48 h, 100 and 200 nM hT1 siRNA induced a marked decrease in signal intensity for T β RII compared to vehicle or scrambled RNA treated con-

trols. Densitometric analysis indicated a 70-85% reduction of T β RII expression in the siRNA treated samples. When the T β RII antibody was preincubated with the antigenic peptide before probing, the immunoreactive band disappeared (Figure 2A, lane 5) confirming the specificity of the antibody.

T β RII transcript levels were examined by real time PCR using 18S rRNA to normalize the data. Figure 2B shows the mean normalized T β RII gene expression as determined by the method of Muller et al [35]. Compared to scrambled siRNA, hT1 at 100 and 200 nM reduced ($p<0.0002$) the level of T β RII transcripts at both 48 and 72 h time points. There was also a dose dependent response as the 200 nM concentration was more effective than 100 nM.

T β RII siRNA impairs fibronectin assembly and fibronectin secretion: Visualized by immunofluorescence, untreated control and scrambled siRNA treated corneal fibroblasts exhibited robust fibronectin deposition and a dense fibrillar network over cells (Figure 3A,B). The fibronectin deposition was clearly reduced in cells 48 h after transfection with both 100 and 200 nM of hT1 siRNA (Figure 3C,D). Cell density was similar in the various specimens and thus the decreased fibronectin assembly was not related to reduction in cell number.

Western blotting was carried out to determine whether the effect of siRNAs on the fibronectin fibrilllogenesis was a reflection of decreased fibronectin secretion. Corneal fibroblasts, 48 h after transfection, were incubated in serum-free medium for 24 h. Proteins in the media were subjected to electrophoresis and immunoblotting (Figure 3E). A 220 kDa fibronectin band was observed in all samples. Consistent with

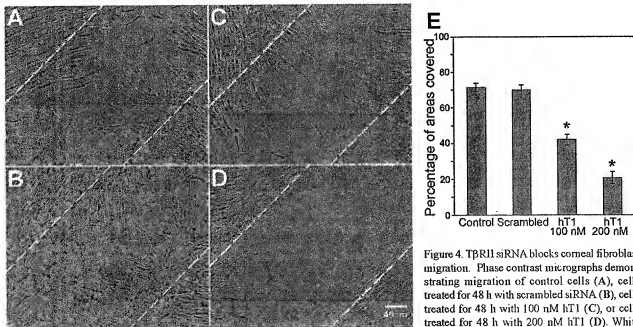


Figure 4. T β RII siRNA blocks corneal fibroblast migration. Phase contrast micrographs demonstrating migration of control cells (A), cells treated for 48 h with scrambled siRNA (B), cells treated for 48 h with 100 nM hT1 (C), or cells treated for 48 h with 200 nM hT1 (D). White dotted lines mark the wound edges. E: Bar graph showing mean percentage of wound area covered by migrating corneal fibroblasts in each specimen ($n=10$), error bars represent the standard error of the mean. Asterisks denote values significantly different from those of scrambled RNA treated controls ($p<0.0001$). Experiments were repeated 3 times, yielding similar results.

the immunofluorescence data, treatment with 100 nM hT1 (Figure 3E, lane 3) and 200 nM hT1 (Figure 3E, lane 4) resulted in decreased fibronectin secretion into the culture media. The siRNA elicited a greater effect with 200 (66% reduction compared to the scrambled siRNA treated sample) than 100 nM (40% reduction).

T β RII siRNA blocks corneal fibroblast migration: Wound scratch assays indicated that corneal fibroblasts migrated into the wounded area (Figure 4A). Within 7 h, untreated control

and scrambled RNA transfected cells filled 71.8±4.3% and 69.3±5.8% of the pipette tip generated wound area (Figure 4E), respectively. By contrast, the percent wound area covered by 100 nM hT1 (42.3±10.2%) and 200 nM hT1 (21.9±3.9%) transfected cells was significantly decreased ($p<0.0001$).

T β RII siRNA markedly reduces ocular inflammation and fibrosis in a mouse model: To generate a mouse model of inflammation and fibrosis, PBS and latex beads were injected

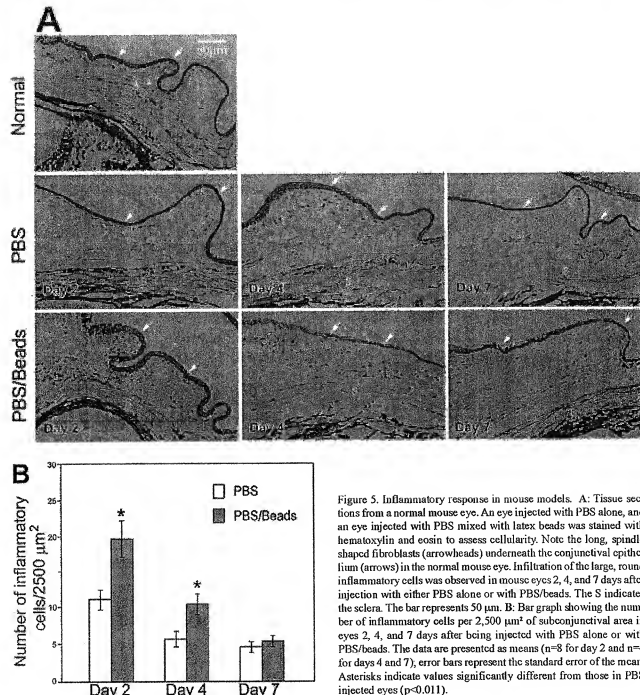


Figure 5. Inflammatory response in mouse models. A: Tissue sections from a normal mouse eye. An eye injected with PBS alone, and an eye injected with PBS mixed with latex beads was stained with hematoxylin and eosin to assess cellularity. Note the long, spindle shaped fibroblasts (arrowheads) underneath the conjunctival epithelium (arrows) in the normal mouse eye. Infiltration of the large, round inflammatory cells was observed in mouse eyes 2, 4, and 7 days after injection with either PBS alone or with PBS/beads. The S indicates the sclera. The bar represents 50 μ m. B: Bar graph showing the number of inflammatory cells per 2,500 μm^2 of subconjunctival area in eyes 2, 4, and 7 days after being injected with PBS alone or with PBS/beads. The data are presented as means ($n=8$ for day 2 and $n=4$ for days 4 and 7), error bars represent the standard error of the mean. Asterisks indicate values significantly different from those in PBS injected eyes ($p<0.01$).

into the subconjunctival space of mice. A model has been described previously using only PBS for injections [37], in which the inflammatory response was observed between days 1 and 3 and collagen deposition was seen on day 14 following injections. In the PBS/beads model, round and large inflammatory cells (Figure 5A), contrasting the long, spindle shaped fibroblasts (Figure 5A, arrowheads), were observed after hematoxylin and eosin staining in the subconjunctival space within 2 days of injection. The number of inflammatory cells per $2,500 \mu\text{m}^2$ area underneath the conjunctival epithelium was significantly greater ($p<0.01$) in the PBS/latex beads injected eyes than with PBS alone (Figure 5B). The inflammatory response observed on day 2 subsided on days 4 and 7 (Figure 5A,B). Since subconjunctival injection of PBS/beads augmented the inflammatory response, this model was used to test the siRNA effects.

siRNA with mouse sequences corresponding to those of hT1 (designated as mT1), or scrambled siRNA was introduced into mouse eyes together with PBS/latex beads in a masked manner. Two days following the injection, numerous inflammatory cells were observed underneath the conjunctival epithelium in the scrambled RNA treated and PBS/latex beads

injected control eyes. In comparison, the infiltration of inflammatory cells was significantly less ($p<0.015$) in mT1 treated eyes (Figure 6A,B). On post-injection day 14, picrosirius red staining showed thick collagen deposition underneath the conjunctival epithelium of scrambled RNA treated eyes (Figure 6C). The fibrotic response was markedly repressed by treatment with mT1 siRNA (Figure 6C).

DISCUSSION

The present study demonstrates that siRNAs specific to human T β RII knocked down the receptor expression in cultured human corneal fibroblasts. Immunofluorescence staining, western blotting, and real time PCR analyses showed the effectiveness of the dose and time dependent inhibition; that is, at concentrations ranging from 25 to 200 nM and time points from 16 to 72 h. We showed that two (hT1 and hT2) of the four siRNAs tested were more efficacious. The confidence of the data is established since gene silencing is produced from siRNAs designed from different regions of the T β RII gene.

Corneal fibroblasts constitutively express TGF- β [38], which induces the expression of matrix molecules such as fibronectin and collagen type I [38,39] and facilitates the mi-

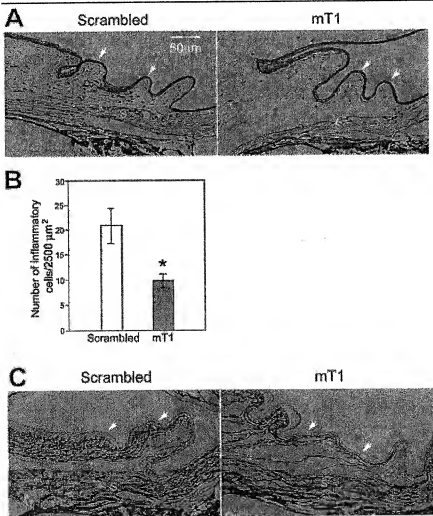


Figure 6. Suppression of inflammatory response and collagen deposition by T β RII siRNA. A: Hematoxylin and eosin stained tissue sections from mouse eyes 2 days after injection with PBS/latex beads along with 200 nM scrambled or mT1 siRNA. Arrows indicate the conjunctiva and S indicates the sclera. The bar represents 50 μm . B: Bar graph showing the number of inflammatory cells per $2,500 \mu\text{m}^2$ of subconjunctival area in eyes injected with 200 nM of mT1 compared to those treated with scrambled siRNA. Data are presented as means ($n=5$), error bars represent the standard error of the mean. The asterisk indicates values significantly different from those of scrambled RNA treated controls ($p<0.015$). C: Tissue sections from eyes 14 days after injection were stained with picrosirius red to demonstrate deposition of collagen that appears as pink fibrillar structures. Note the thick subconjunctival collagen layers in the scrambled siRNA treated mouse eye. Arrows indicate the conjunctival epithelium and S indicates the sclera.

gration of corneal fibroblasts [39,40]. Both of these are critical steps in the wound repair process [41]. In the current study, we showed that fibronectin secretion and deposition were reduced and corneal fibroblast migration was markedly retarded with the siRNA treatment. These findings are consistent with the disruption of the TGF- β signaling pathway by the siRNA directed against T β RII.

The siRNA effect was also demonstrated in a mouse model of ocular inflammation and fibrosis. Our model is similar to that described by Reichel, et al. [37], but instead of injecting PBS alone into the subconjunctival space, we injected PBS mixed with latex beads into mouse eyes. This resulted in a marked augmentation of the inflammatory response. Even in this severe inflammatory model, we observed that nT1 siRNA at 200 nM was effective in blocking the inflammatory and fibrotic responses in the mouse eyes. The reduced fibrosis may be related to the reduced inflammation, impeded fibroblast migration, or diminished matrix deposition. It is also noteworthy that while adenovirus and other vectors may be employed for long term inhibition of inflammation, transient knockdown by synthetic siRNAs allows a better dosage control and may minimize potential side effects. Certainly in our mouse model, a one-time administration of siRNA at a very early phase was sufficient to control the inflammatory process.

Ocular fibrotic wound response is a major cause of impaired vision and blindness, especially following surgical treatment for glaucoma [18,19]. Excessive post-operative scarring often leads to failure of filtration surgery. While the use of antimetabolites such as mitomycin C and 5-fluorouracil as conjunctival anti-scarring treatments benefits a number of patients, these agents are associated with potentially blinding complications including hypotony, inculopathy, and infection [20-23]. Therefore, sequestering of mature TGF- β is an important target in preventing inflammation and fibrosis. Antibodies to TGF- β 2 have been reported to reduce conjunctival scarring [24,25]. In addition, antisense oligonucleotides [26,42] or ribozymes [43] to TGF- β were shown to be effective in wound healing in animal and cell culture studies. However, the neutralizing antibody approach exhibits relatively weak effects in general as it may not gain full access to the targeted TGF- β molecules [43]. Antisense phosphorothioate oligonucleotides and ribozymes can be successful, but their effectiveness [44], stability, and specificity are still in debate. The concentrations needed are also generally in the μ M range, whereas as the present study indicates, the nT1 siRNA is efficacious at 200 nM. Additionally, our approach of targeting the TGF- β receptor [45] rather than the ligand allows for more specific and effective knockdown of the cytokine function.

In summary, the current study demonstrates that downregulation of the T β RII gene by local application of siRNA prevents ocular inflammation and fibrosis. Our results underscore the potential of a novel therapy for preventing the inflammatory response and scarring in ocular diseases and after glaucoma filtration surgery. This approach may also have applications for other surface tissues, including the skin.

DISCLOSURE

Shahid S. Siddiqui, Asrar B. Malik, Jose S. Pulido, Nalin M. Kumar, and Beatrice Y. J. T. Yue have filed a patent application based on the work described in this manuscript.

ACKNOWLEDGEMENTS

The authors thank Stanley Moskal, Hiroshi Sakai, Haripriya Rajani, and Yaseen Khan for technical assistance. This work was supported by grant EY03890 (BYJTY), EY05628 (BYJTY), EY013605 (NMK), HL 64573 (ABM), and core grant EY01792 from the National Institutes of Health, Bethesda, MD, and by an unrestricted grant from Research to Prevent Blindness, New York, NY.

REFERENCES

- Massague J, Cheifetz S, Laiho M, Ralph DA, Weis FM, Zentella A. Transforming growth factor-beta. *Cancer Surv* 1992; 12:81-103.
- Piek E, Heldin CH, Ten Dijke P. Specificity, diversity, and regulation in TGF-beta superfamily signaling. *FASEB J* 1999; 13:2105-24.
- Border WA, Noble NA. Transforming growth factor beta in tissue fibrosis. *N Engl J Med* 1994; 331:1286-92.
- Massague J. TGF-beta signal transduction. *Annu Rev Biochem* 1998; 67:753-91.
- Massague J. How cells read TGF-beta signals. *Nat Rev Mol Cell Biol* 2000; 1:169-78.
- Coulier TB Jr, Roberts AB, Sporn MB, Danielpour D, Dart LL, Michels RG, de Bustros S, Enger C, Kato H, Lansing M, Hayashi H, Glaser BM. Correlation of fibrosis and transforming growth factor-beta type 2 levels in the eye. *J Clin Invest* 1989; 83:1661-6.
- McCormick LL, Zhang Y, Tootell E, Gilliam AC. Anti-TGF-beta treatment prevents skin and lung fibrosis in murine scleroderma graft-versus-host disease: a model for human scleroderma. *J Immunol* 1999; 163:5693-9.
- Shah M, Foreman DM, Ferguson MW. Neutralisation of TGF-beta 1 and TGF-beta 2 or exogenous addition of TGF-beta 3 to cutaneous rat wounds reduces scarring. *J Cell Sci* 1995; 108 (Pt 3):985-1002.
- Lutty GA, Merges C, Threlkeld AB, Crone S, McLeod DS. Heterogeneity in localization of isoforms of TGF-beta in human retina, vitreous, and choroid. *Invest Ophthalmol Vis Sci* 1993; 34:477-87.
- Pasquale LR, Domman-Pease ME, Lutty GA, Quigley HA, Jampl HD. Immunocalocalization of TGF-beta 1, TGF-beta 2, and TGF-beta 3 in the anterior segment of the human eye. *Invest Ophthalmol Vis Sci* 1993; 34:23-30.
- Kon CH, Oceleston NL, Aylward GW, Khaw PT. Expression of vitreous cytokines in proliferative vitreoretinopathy: a prospective study. *Invest Ophthalmol Vis Sci* 1999; 40:705-12.
- Hales AM, Chamberlain CG, McAvoy JW. Cataract induction in lenses cultured with transforming growth factor-beta. *Invest Ophthalmol Vis Sci* 1995; 36:1709-13.
- Chen C, Michelini-Norris B, Stevens S, Rowsey J, Ren X, Goldstein M, Schultz G. Measurement of mRNAs for TGF β and extracellular matrix proteins in corneas of rats after PRK. *Invest Ophthalmol Vis Sci* 2000; 41:4108-16.
- Cordeiro MF. Role of transforming growth factor beta in conjunctival scarring. *Clin Sci (Lond)* 2003; 104:181-7. Erratum in: *Clin Sci (Lond)*. 2003; 105:723.

15. Cordeiro MF. Beyond Mitomycin: TGF- β ta and wound healing. *Prog Retin Eye Res* 2002; 21:75-89.
16. He S, Jin ML, Worpel V, Hinton DR. A role for connective tissue growth factor in the pathogenesis of choroidal neovascularization. *Arch Ophthalmol* 2003; 121:1283-8.
17. Yamamoto R, Ogata N, Yamamoto C, Matsushita M, Matsuzaki K, Uyama M, Matsumoto M. Expression of transforming growth factor-beta factors in normal rat retina and experimental choroidal neovascularization. *Jpn J Ophthalmol* 2002; 46:525-32.
18. Migdal C, Gregory W, Hitchings R. Long-term functional outcome after early surgery compared with laser and medicine in open-angle glaucoma. *Ophthalmology* 1994; 101:1651-6, discussion 1657.
19. Addicks EM, Quigley HA, Green WR, Robin AL. Histologic characteristics of filtering blebs in glaucomatous eyes. *Arch Ophthalmol* 1983; 101:795-8.
20. Khaw PT, Doyle JW, Sherwood MB, Grierson I, Schultz G, McGorrity S. Prolonged localized tissue effects from 5-minute exposures to fluorouracil and mitomycin C. *Arch Ophthalmol* 1993; 111:263-7.
21. Cordeiro MF, Reichel MB, Gay JA, D'Esposito F, Alexander RA, Khaw PT. Transforming growth factor- β 1, - β 2, and - β 3 in vivo: effects on normal and mitomycin C-modulated conjunctival scarring. *Invest Ophthalmol Vis Sci* 1999; 40:1975-82.
22. Crowston JG, Akbar AN, Constable PH, Ocleston NL, Daniels JT, Khaw PT. Antimetabolite-induced apoptosis in Tenon's capsule fibroblasts. *Invest Ophthalmol Vis Sci* 1998; 39:449-54.
23. Stanhope RL, McMenemy MG, Lieberman MF. Hypotonous maculopathy after trabeculectomy with subconjunctival 5-fluorouracil. *Am J Ophthalmol* 1992; 114:544-53.
24. Cordeiro MF, Gay JA, Khaw PT. Human anti-transforming growth factor- β 2 antibody: a new glaucoma anti-scarring agent. *Invest Ophthalmol Vis Sci* 1999; 40:2225-34.
25. Mead AJ, Wong TT, Cordeiro MF, Anderson IK, Khaw PT. Evaluation of anti-TGF- β 2 antibody as a postoperative anti-scarring agent in glaucoma surgery. *Invest Ophthalmol Vis Sci* 2003; 44:3394-401.
26. Cordeiro MF, Mead A, Ali RR, Alexander RA, Murray S, Chen C, York-Defalco C, Dean NM, Schultz GS, Khaw PT. Novel antisense oligonucleotides targeting TGF- β ta inhibit in vivo scarring and improve surgical outcome. *Genther* 2003; 10:59-71.
27. Elbasir SM, Harborth J, Lendeckel W, Yalcin A, Weber K, Tuschl T. Duplexes of 21-nucleotide RNAs mediate RNA interference in cultured mammalian cells. *Nature* 2001; 411:494-8.
28. Fire A, Xu S, Montgomery MK, Kostas SA, Driver SE, Mello CC. Potent and specific genetic interference by double-stranded RNA in *Caenorhabditis elegans*. *Nature* 1998; 391:806-11.
29. Hannon GJ. RNA interference. *Nature* 2002; 418:244-51.
30. Reich SJ, Fonott J, Kuroki A, Tang W, Yang X, Maguire AM, Bennett J, Tolentino MJ. Small interfering RNA (siRNA) targeting VEGF effectively inhibits ocular neovascularization in a mouse model. *Mol Vis* 2003; 9:210-6.
31. Song E, Lee SK, Wang J, Ince NJ, Ouyang N, Min J, Chen J, Shankar P, Lieberman J. RNA interference targeting Fas protects mice from fulminant hepatitis. *Nat Med* 2003; 9:347-51.
32. Dykshorn DM, Novina CD, Sharp PA. Killing the messenger: short RNAs that silence gene expression. *Nat Rev Mol Cell Biol* 2003; 4:457-67.
33. Yue BY, Baum JL. Studies of corneas in vivo and in vitro. *Vision Res* 1981; 21:41-3.
34. Huang C, Kim Y, Caramori ML, Fish AJ, Rich SS, Miller ME, Russell GB, Mauer M. Cellular basis of diabetic nephropathy: II. The transforming growth factor- β ta system and diabetic nephropathy lesions in type 1 diabetes. *Diabetes* 2002; 51:3577-81.
35. Muller PY, Janovjak H, Miserez AR, Dobie Z. Processing of gene expression data generated by quantitative real-time RT-PCR. *BioTechniques* 2002; 32:1372-4, 1376, 1378-9. Erratum in: *BioTechniques* 2002; 33:514.
36. Mostafavi-Pour Z, Askan JA, Parkinson SJ, Parker PJ, Ng TT, Humphries MJ. Integrin-specific signaling pathways controlling focal adhesion formation and cell migration. *J Cell Biol* 2002; 161:155-77.
37. Reichel MB, Cordeiro MF, Alexander RA, Cire IA, Bhattacharya SS, Khaw PT. New model of conjunctival scarring in the mouse eye. *Br J Ophthalmol* 1998; 82:1072-7.
38. Song QH, Singh RP, Richardson TP, Nugent MA, Trinkaus-Randall V. Transforming growth factor- β ta expression in cultured corneal fibroblasts in response to injury. *J Cell Biochem* 2000; 77:186-99.
39. Massague J. The transforming growth factor- β ta family. *Annu Rev Cell Biol* 1990; 6:597-641.
40. Andreescu JL, Ledet T, Ehlers N. Keratocyte migration and peptide growth factors: the effect of PDGF, bFGF, EGF, IGF-I, aFGF and TGF- β ta on human keratocyte migration in a collagen gel. *Curr Eye Res* 1997; 16:605-13.
41. Clark RAF. Cutaneous wound repair. In: Goldsmith LA, editor. *Physiology, Biochemistry, and Molecular Biology of the Skin*. 2nd ed. New York: Oxford University Press; 1991. p. 576-601.
42. Shen ZJ, Kim SK, Kwon OS, Lee YS, Moon BJ. Specific inhibition of transforming growth factor- β ta expression in human osteoblast cells by antisense phosphorothioate oligonucleotides. *Eur J Biochem* 2001; 268:2331-7.
43. Yamamoto K, Morishita R, Tomita N, Shimozato T, Nakagami H, Kikuchi A, Aoki M, Higaki J, Kaneda Y, Ogihara T. Ribozyme oligonucleotides against transforming growth factor- β ta inhibited neointimal formation after vascular injury in rat model: potential application of ribozyme strategy to treat cardiovascular disease. *Circulation* 2000; 102:1308-14.
44. Stein CA. The experimental use of antisense oligonucleotides: a guide for the perplexed. *J Clin Invest* 2001; 108:641-4.
45. Shi Y, Massague J. Mechanisms of TGF- β ta signaling from cell membrane to the nucleus. *Cell* 2003; 113:685-700.

EXHIBIT 7

ORIGINAL RESEARCH ARTICLE

siRNA-mediated knockdown of the serotonin transporter in the adult mouse brain

DR Thakker¹, F Natt², D Hüskens², H van der Putten¹, R Maier¹, D Hoyer^{1,3} and JF Cryan¹

¹Psychiatry Program, Neuroscience Research, Novartis Institutes for Biomedical Research, Novartis Pharma AG, Basel, Switzerland; ²Functional Genomics, Novartis Institutes for Biomedical Research, Novartis Pharma AG, Basel, Switzerland;

³The Harold L Dorris Neurological Research Center, Department of Neuropharmacology, The Scripps Research Institute, La Jolla, CA, USA

Selective serotonin reuptake inhibitors (SSRIs) are widely used antidepressant drugs that increase the extracellular levels of serotonin by blocking the reuptake activity of the serotonin transporter (SERT). Although SSRIs elevate brain serotonergic neurotransmission acutely, their full therapeutic effects involve neurochemical adaptations that emerge following chronic drug administration. The adaptive downregulation of SERT has recently been implicated in the therapeutic response of SSRIs. Interestingly, studies using *SERT*-knockout mice reveal somewhat paradoxical depression-related effects, probably specific to the downregulation of SERT during early development. However, the behavioral significance of SSRI-mediated downregulation of SERT during adulthood is still unknown. We investigated whether somatic gene manipulation, triggered by infusing short interfering RNA (siRNA) into the ventricular system, would enable the downregulation of SERT in the adult mouse brain. Infusing the *SERT*-targeting siRNA, for 2 weeks, significantly reduced the mRNA levels of SERT in raphe nuclei. Further, a significant, specific and widespread downregulation of SERT-binding sites was achieved in the brain. In contrast, 2-week infusion of the SSRI, citalopram, produced a widespread downregulation of SERT-binding sites, independent of any alterations at the mRNA level. Irrespective of their mechanisms for downregulating SERT in the brain, infusions of *SERT*-siRNA or citalopram elicited a similar antidepressant-related behavioral response in the forced swim test. These results signify a role for the downregulation of SERT in mediating the antidepressant action of SSRIs in adults. Further, these data demonstrate that siRNA-induced widespread knockdown of gene expression serves as a powerful tool for assessing the function of endogenous genes in the adult brain.

Molecular Psychiatry (2005) 10, 782–789. doi:10.1038/sj.mp.4001687; published online 10 May 2005

Keywords: RNA interference; depression; forced swim test; citalopram; *in vivo*; dopamine transporter

The serotonin transporter (SERT) controls the temporal and spatial activity of extracellular serotonin by facilitating a rapid and high-affinity reuptake of this neurotransmitter into presynaptic terminals.¹ SERT is also a primary molecular target for the most widely prescribed antidepressant drugs, the selective serotonin reuptake inhibitors (SSRIs).² SSRIs readily inhibit SERT activity and elevate the serotonergic tone in the brain. However, full therapeutic benefits ensue only after chronic use of SSRIs, requiring the manifestation of long-term adaptations, secondary to the blockade of serotonin reuptake.^{3,4}

Emerging studies reveal downregulation of SERT as an adaptive consequence of sustained and high occupancy by chronically administered SSRIs.^{5–8} The

downregulation of SERT favorably potentiates the SSRI-mediated increase in the brain serotonergic neurotransmission.^{6–7} Further, the lag time required by SSRIs to produce a substantial downregulation of SERT correlates well with the time needed for eliciting a full therapeutic response. Therefore, downregulation of SERT has been implicated in the antidepressant action of SSRIs.⁷

Recently, *SERT*-deficient mice were used to ascertain the role of SERT in the etiology of depression vs the antidepressant action of SSRIs.^{9,10} Consequently, the depression-related behavior illustrated by these mice has been attributed to the developmental changes that result from early-life absence of SERT.^{10–12} Indeed, an elevated propensity toward abnormal emotional behavior is noted in adult animals chronically treated with antidepressants during early development,^{12–14} or in individuals genetically expressing low levels of SERT.^{15–18} Therefore, although *SERT*-knockout mice represent a useful model for investigating disorders involving genetic alterations in SERT during early life,^{11,19} they are less appropriate

Correspondence: Dr JF Cryan, PhD, Psychiatry program, Neuroscience Research, Novartis Institutes for Biomedical Research, Novartis Pharma AG, Basel, CH4002, Switzerland.

E-mail: john.f.cryan@novartis.com

Received 14 January 2005; revised 14 March 2005; accepted 30 March 2005

for studying the partial SERT downregulation observed following chronic use of SSRIs. Moreover, these mice fail to establish the functional relevance of downregulating SERT during adulthood.

In an effort to obtain a specific downregulation of *SERT* in the adult mouse brain, we employed nonviral RNA interference (RNAi) methodology, which we have recently validated *in vivo*.²⁰ RNAi is a cellular surveillance mechanism that destroys the endogenous mRNAs containing sequences complementary to a double-stranded RNA (dsRNA) trigger.²¹ Short interfering RNAs (siRNAs) mimic the cleavage products of dsRNA and produce sequence-specific gene-knockdown in mammalian cells, without eliciting the lethal dsRNA-interferon response.^{22,23} Recently, we demonstrated that intracerebroventricularly (i.c.v.) infused siRNAs can efficiently produce a widespread downregulation of gene expression in the adult mouse brain.²⁰ Here, we compare the neurochemical as well as the behavioral consequences of infusing a SERT-targeting siRNA vs the SSRI, citalopram, in the brain.

Materials and methods

Animals

Male BALB/c mice (19–29 g; Iffa Crédo, France) were housed two/cage for at least 1 week before surgery, and thereafter one/cage, in a temperature- and humidity-controlled room with 12–12 h light–dark cycle (lights on at 0600 A.M.). Food pellets and tap water were available *ad libitum*, except during behavioral testing. Animal handling and experimentation were performed during the light cycle, in accordance with the Veterinary Authority of Basel-Stadt, Switzerland.

Drug/siRNA administration in mouse brain

The sequences of SERT-targeting siRNAs were checked for theoretical specificity against the mouse transcriptome using the Smith Watermann algorithm. In all, 12 different siRNA sequences were accepted, with at least two nonconsecutive and nonterminal mismatches against any other transcript. siRNAs were screened for their *in vitro* knockdown efficiency in a reporter assay, consisting of the cotransfection of siRNAs with a plasmid coding for a SERT-YFP fusion mRNA, as previously described for antisense oligonucleotides.²⁴ The target sequence for each siRNA (GenBank accession no. NM_010484), and its efficiency in reducing the mRNA levels from 100% to the value in parentheses, along with the corresponding coefficient of variation, is indicated as follows: nt 429–449 (27%, 4.4), 528–548 (43%, 7.3), 643–663 (20.8%, 13.8), 648–668 (45.7%, 4.7), 801–821 (14.3%, 8.9), 1230–1250 (10.4%, 4.8), 1233–1253 (16.5%, 7.5), 1239–1259 (19.8%, 4.3), 1455–1475 (23.6%, 1.7), 1459–1479 (24.8%, 6.5), 1725–1745 (25.2%, 4.4) and 2061–2081 (12.4%, 12.1). Subsequently, the siRNA, targeting nt 1230–1250, that revealed a consistently maximal knockdown of ~90% was chosen for all *in vivo* experiments. A

corresponding 3-nit-mismatch siRNA (mmRNA; guide, 5'-UUGUGGAACGUGUGGUAGCdTdT-3'; complement, 5'-CCUACACACAGUUCACAAAdTdT-3') served as a control. The guide and complement strands of each siRNA were annealed in an isotonic RNAi buffer as described previously.^{20,25} Citalopram.HBr was also dissolved in the same RNAi vehicle. Osmotic minipumps (Alzet model 1002, Durect Corporation, Cupertino, CA, USA) were filled in order to infuse vehicle (6 µl/day), citalopram (20 µg/day), SERT-siRNA or mmRNA (0.4 mg/day) for 2 weeks. This duration of infusion was chosen based on our previous studies showing that a maximally effective RNAi response requires 2 weeks of siRNA infusion.²⁰ A maximally effective dose of siRNA was used that was well tolerated with no signs of neurotoxicity (hind-limb paralysis, vocalization, food intake or neuroanatomical damage) following i.c.v. application for 2 weeks. Implantation of the cannula for infusion into the dorsal third ventricle (AP: -0.5 mm; ML: 0 mm, DV: -3 mm, relative to bregma),²⁶ from the subcutaneously-implanted minipump, was performed as described previously.²⁰

Behavioral assessment

Forced swim test was conducted as described previously,^{27,28} 14 days after implanting the cannula-minipump assembly. Briefly, mice were individually placed into plexiglas cylinders (24 cm high × 21 cm internal diameter) filled with water (25.4 ± 0.7°C) to a depth of 15 cm. Test sessions were recorded by a video camera positioned directly above the cylinders. A well-trained observer, blinded to the treatment groups, scored these videotapes for the duration of mouse immobility during the last 4 min of the 6 min test period. A mouse was judged to be immobile when making only those movements necessary to keep its head above water. We chose the forced swim test, which is the most widely used paradigm for assessing depression- or antidepressant-related behavior in mice,^{29,30} and also because it was sensitive to the partial knockdown of SERT in *SERT*^{+/-} mice.⁹

Locomotor activity was assessed in a novel environment as described previously,²⁸ for 60 min between 08:00 and 11:30, ~24 h after conducting the forced swim test.

Processing of the brain for mRNA and protein analysis Mice were decapitated immediately after their locomotor activity trial. Brains were removed and serial coronal sections of 10 µm thickness were obtained at the following AP coordinates, in mm, relative to bregma:²⁶ 2.46 (prefrontal cortex), 1.18 (caudate putamen, nucleus accumbens, olfactory tubercle, lateral and medial septum), -0.22 (globus pallidus), -0.46 (to confirm the site of injection), -1.58 (cerebral cortex, hippocampus, thalamus, hypothalamus, amygdala), -3.08 (substantia nigra, ventral tegmental area), -4.36 (superior colliculus, dorsal and median raphe), -5.34 (locus caeruleus) and -7.2 (brainstem). Sections were thaw-mounted onto poly-L-lysine-

coated slides, coded for a blind analysis of mRNA and protein, and stored at -80°C until use.

In situ hybridization was performed as described,³¹ using [³⁵S]-labeled antisense riboprobes, in order to detect the SERT or neuron-specific enolase (NSE) mRNA on adjacent brain sections. Hybridizing brain sections with the corresponding [³⁵S]-labeled sense riboprobes did not reveal any mRNA signal and served as a control for each probe. The DNA templates, for riboprobe synthesis, were generated from cDNA fragments of mouse SERT (nt 187–637; GenBank accession no. NM_010484) or NSE (nt 2089–2290; GenBank accession no. X52380). At the end of the *in situ* hybridization procedure, slides were dipped in liquid nuclear emulsion and the optical density (OD) of silver grains, positive for the probed mRNA, was quantified as described previously.³¹

Quantitative autoradiography was performed on brain sections as described previously,^{30,32} with minor modifications, in order to determine changes in densities of SERT- or dopamine transporter (DAT)-binding sites following various treatments. Briefly, sections were subjected to two washes in an aqueous buffer (120 mM NaCl, 0.1 M sucrose, 10 mM sodium phosphate) for 1 h followed by incubation with a nonsaturating concentration of [¹²⁵I]RTI-55 (10 pM, 2200 Ci/mmol, Perkin-Elmer, Boston, MA, USA) in fresh buffer for 2 h. [¹²⁵I]RTI-55 selectively labeled SERT, provided the binding to DAT was occluded with 10 μM GBR-12909. The same radioligand was used to label DAT upon inhibition of SERT binding with 50 nM citalopram. By using tissue-calibrated data from the coexpressed radioactive standards, OD values of autoradiograms were transformed to levels of radioactivity bound (nCi/mg tissue protein) to specific brain regions in tissue sections. Nonspecific binding was determined in adjacent brain sections by using 50 nM citalopram and 10 μM GBR-12909, in addition to the radioligand, and was equivalent to the autoradiographic film background.

Results

siRNA-induced specific knockdown of SERT mRNA and protein in the brain

We recently demonstrated the ability of siRNAs, infused into the dorsal third ventricle, to knockdown genes expressed in caudal brain regions as far as the substantia nigra and ventral tegmental area.²⁹ Here, we tested if a similar protocol could be used to target SERT expressed further away from the site of infusion, specifically in the serotonergic neurons of the dorsal and median raphe nuclei.⁵ A maximally effective RNAi response requires 2 weeks of siRNA infusion, irrespective of the half-life of the target protein.²⁰ The same infusion period is also required by SSRIs in order to produce a substantial downregulation of SERT.^{5,7} Therefore, mice were infused with the SERT-targeting siRNA, a corresponding mmRNA, citalopram or vehicle for 2 weeks into the ventricular

system. *In situ* hybridization analysis revealed a significant downregulation of SERT mRNA in the dorsal as well as median raphe of mice receiving siRNA (Figure 1a). SERT mRNA levels were unaltered

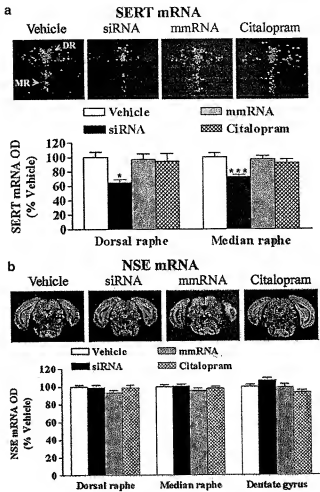


Figure 1 siRNA-induced specific knockdown of SERT mRNA in the dorsal and median raphe nuclei. Mice received a 2-week infusion of vehicle, SERT-targeting siRNA, mmRNA or citalopram into the dorsal third ventricle. (a) SERT mRNA infusion significantly reduced the mRNA levels of SERT specifically expressed in the dorsal and median raphe nuclei, DR and MR, respectively. (b) NSE mRNA levels in the same regions, and the dentate gyrus, were unaffected by any treatment. At the top of each panel are low magnification, dark-field photomicrographs illustrating representatives of *in situ* hybridization with SERT (a) or NSE (b) riboprobes in adjacent, coronal brain sections followed with emulsion-dipping of slides. The extent of siRNA-induced knockdown is revealed by expressing the densitometric quantification of mRNA positive grains as % OD values of those in corresponding regions from vehicle-treated mice. Bars represent means \pm SEM of 12–26 observations (2–4 observations/animal, depending on the brain region, and 6–7 animals/group). * $P < 0.05$, *** $P < 0.001$, significantly different from all other treatments; raw OD values were analyzed using one-way ANOVA followed by Tukey's *post hoc* test.

with infusion of mmRNA or citalopram as compared to those in vehicle-infused mice (Figure 1a). mRNA levels of the neuronal marker, NSE, were quantified in the same regions of adjacent brain sections. None of the treatments, including siRNA, produced a significant change in raphe levels of NSE mRNA (Figure 1b). The dentate gyrus is the most susceptible region to the gene-knockdown effect of i.c.v. siRNA.²⁰ However, SERT-siRNA or any other treatment had no effect on NSE mRNA levels in this region, indicative of a SERT-specific action of siRNA (Figure 1b).

SERT protein is localized not only in the soma and dendrites of neurons originating in the raphe nuclei but also is transported down the axons to serotonergic projection areas widespread in the brain.¹ [¹²⁵I]RTI-55

autoradiography was performed for quantification of SERT-binding sites in 18 regions along the rostral-caudal axis of the brain. Infusing the SSRI, citalopram, for 2 weeks produced a significant decrease, by ~40–50%, in the density of SERT-binding sites in almost all brain regions analyzed (Figure 2). Infusion of siRNA, but not mmRNA, also led to a significant downregulation of SERT in all these brain regions, except the nucleus accumbens and olfactory tubercle (Figure 2). The extent of siRNA-mediated SERT downregulation varied across brain regions: a maximal 60% effect observed in the hippocampus and thalamus, while only 18% decrease noted in the prefrontal cortex, locus coeruleus and brainstem (Figure 2). All other brain regions exhibited a

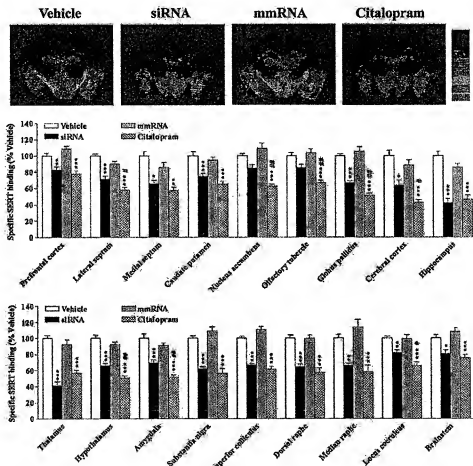


Figure 2 Widespread down regulation of SERT-binding sites following infusion of siRNA or citalopram in the brain. Infusion of the SERT-targeting siRNA or citalopram led to an extensive downregulation of SERT in the brain as compared with infusions of vehicle or mmRNA. (Top) Representative autoradiograms of [¹²⁵I]RTI-55 binding to SERT in sections showing maximum number of brain regions with siRNA- and citalopram-induced downregulation of SERT. The microscale bars from top to bottom represent binding values of 0.74, 1.26 and 2.52 nCi/mg. (Bottom) Densitometric analysis of specific SERT binding is presented as % binding in the corresponding region of vehicle-infused mice, in order to illustrate the extent of siRNA- or citalopram-induced SERT downregulation in each region. Bars represent mean \pm SEM of 12–52 observations (2–8 observations/animal, varying with the brain regions analyzed, and 6–7 animals/group). Raw values were analyzed using one-way ANOVA followed by Tukey's *post hoc* test. * $P<0.05$, ** $P<0.01$, *** $P<0.001$, significantly different from vehicle- or mmRNA-treated mice in each brain region; * $P<0.05$, ** $P<0.01$, significantly different from siRNA treatment in the same region.

moderate decline of ~33% in the density of SERT-binding sites following siRNA treatment (Figure 2). Citalopram-induced downregulation of SERT was marginally, yet significantly, greater than that induced by siRNA in some regions, including the lateral septum, nucleus accumbens, olfactory tubercle, globus pallidus, cerebral cortex, hypothalamus, amygdala and locus coeruleus (Figure 2). Differences in basal levels of SERT binding may possibly account for differences observed among brain regions in siRNA-induced downregulation of SERT. However, this possibility was ruled out due to a lack of any significant correlation ($r=0.02$, $P=0.93$) illustrated in the binding levels of DAT, a protein closely related to SERT, following infusions of vehicle, SERT-siRNA, mmRNA or citalopram. DAT-binding sites throughout the brain were unaffected by any treatment, again, suggesting a SERT-specific effect of siRNA as well as of citalopram (Figure 3).

Antidepressant-like response in mice receiving SERT-targeting siRNA

The forced swim test is the best characterized and most widely used model for assessing alterations in depression- or antidepressant-related behavior in mice following genetic or drug-induced manipulations.^{29,30} The behavioral readout is the duration for which the mouse remains immobile following initial escape-intended movements when subjected to this test. In this case, immobility is thought to reflect a behavioral despair that disengages the mouse from

actively coping with stressful stimuli, also known as 'entrainment' in clinical depression.³⁰ This model was employed to test if mice displayed a depression- or antidepressant-like phenotype following 2-week infusions of vehicle, SERT-siRNA mmRNA or citalopram. One-way ANOVA revealed a significant effect of treatment on the duration of immobility in the forced swim test ($F_{3,36}=4.08$, $P=0.014$). Consistent with the antidepressant action of SSRIs, mice infused with citalopram demonstrated a significant decrease in immobility as compared to those receiving vehicle or mmRNA (Figure 4a). Interestingly, the duration of immobility was also significantly reduced to the same extent for siRNA-treated mice (Figure 4a). Further, we tested if the antidepressant-like phenotype, exhibited by citalopram- or siRNA-infused mice in the forced swim test, was confounded by a possible hyperactivity in these mice. A two-way repeated measures ANOVA failed to reveal any significant effect of treatment on locomotor activity ($F_{3,36}=1.425$, $P=0.252$, Figure 4b). A significant effect of time ($F_{11,396}=28.188$, $P<0.001$) was noted, however, with no significant treatment \times time interaction ($F_{33,396}=0.712$, $P=0.882$), indicating that all animals equally habituated to the behavioral assessment, irrespective of their treatments.

Discussion

In the present study, we describe a nonviral, *in vivo* RNAi method for downregulating SERT in the adult mouse brain. Recently, we demonstrated that siRNA

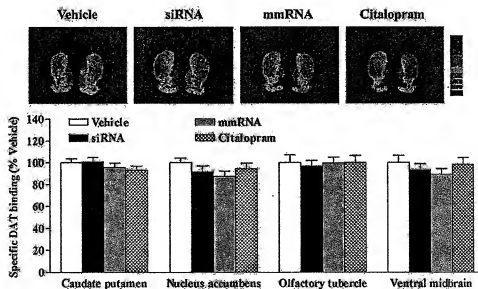


Figure 3 DAT binding levels in the brain are unaltered with SERT-siRNA or citalopram treatment. (Top) Representative autoradiograms of [³H]RTI-55 binding to DAT in the caudate putamen, nucleus accumbens and olfactory tubercle. Microscale bars from top to bottom represent binding values of 0.74, 1.26, 2.52 and 5.36 nCi/mg. (Bottom) Densitometric analysis of specific DAT binding presented as % binding in the corresponding region of vehicle-infused mice. Infusing the vehicle, SERT-targeting siRNA, mmRNA or citalopram for 2 weeks had no significant effect on DAT binding in any brain region. Bars represent mean \pm SEM of 22–26 observations (3–4 observations/animal and 6–7 animals/group).

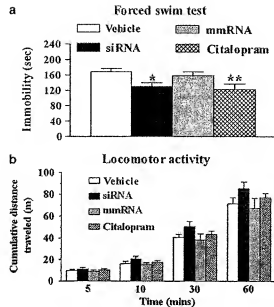


Figure 4 Antidepressant-like response in mice treated with SERT-targeting siRNA or the SSRI, citalopram. (a) Mice infused with citalopram demonstrated a significantly decreased immobility in the forced swim test as compared to mice infused with vehicle or mmRNA. A similar antidepressant response was noted for siRNA-infused mice. (b) Locomotor activity of these mice was assessed, ~24 h later, as the distance traveled (m) in 5 min intervals upto 60 min. None of the treatments had a significant effect on mouse locomotor activity as shown with the cumulative distance traveled in a 5, 10, 30 or 60 min period. Bars represent mean \pm SEM values from 10 animals/group. * P <0.05, ** P <0.01, significantly different from vehicle, using one-way (a) or two-way repeated measures (b) ANOVA followed by Fisher's *post hoc* test.

infusion into the dorsal third ventricle can knockdown gene expression in regions as far rostral as the prefrontal cortex and as caudal as the substantia nigra.²⁰ Here, we efficiently target *SERT* expression in the dorsal and median raphe nuclei, ~1 mm caudal to the substantia nigra (~5 mm from the infusion site), which further extends the potential utility of our RNAi protocol to downregulate genes in a broader expanse of the brain.

We compared the neurochemical consequences of infusing a SERT-targeting siRNA vs the SSRI, citalopram. Infusion of citalopram i.c.v., for 2 weeks, produced a significant downregulation of SERT, by a magnitude equivalent to that previously reported with subcutaneous infusions of SSRIs.^{5,7} Further, citalopram-induced downregulation of SERT was independent of any changes at the mRNA level, consistent with previous studies using other SSRIs.^{5,6} In contrast, 2-week infusion of SERT-siRNA specifically reduced the mRNA levels of SERT in the dorsal and median raphe nuclei. It may be argued that this effect on SERT mRNA is rather modest, and a longer

infusion period is required in order to obtain a substantial knockdown at the mRNA level. However, siRNA-induced specific knockdown of *SERT* was also noted at the protein level to an extent comparable to that produced by citalopram in most of the brain regions analyzed. Further, the possibility of achieving a greater magnitude of SERT knockdown, with extended siRNA infusions, seems unlikely considering the half-life of SERT is ~3 days.^{33,34}

The behavioral consequence of downregulating SERT, following infusion of siRNA, was an anti-depressant-related response in the forced swim paradigm, the most widely used model for assessing antidepressant-related behavior in rodents.³⁰ The siRNA-induced antidepressant response was similar to that elicited by the SSRI, citalopram, in this test. Further, this antidepressant response was not due to any hyperactivity *per se*, as the locomotor activity of these mice was unaltered when placed in a novel environment. In marked contrast to the antidepressant-related response of mice infused with either SERT-siRNA or citalopram, a depression-related behavior has been illustrated by the *SERT* heterozygous mice in addition to full knockout mice, using the same forced swim paradigm.⁹ *SERT* heterozygous knockouts display reduced levels of SERT during early development as opposed to the downregulated SERT in adult mice obtained using SERT-siRNA or citalopram in this study. Therefore, a depression-like behavior of the heterozygous knockouts implies that downregulation of SERT during early developmental stages may have a negative influence on emotional behavior. Previous studies have reported an abnormal emotional behavior in animals subjected to an early-life regimen of SSRIs or other less-SSRIs.¹²⁻¹⁴ More recently, an increased risk of abnormal emotional behavior was also documented in pediatric patients taking SSRIs.³⁵ Therefore, it remains to be verified if such deleterious effects result from downregulation of SERT following early-life exposure to SSRIs. Interestingly, a downregulation of SERT has been reported in the brains of depressed patients.³⁶⁻³⁸ Therefore, on the surface these findings are incongruent with our current data and that of Frazer and colleagues.⁹⁻⁸ However, genetically-mediated downregulation of SERT during early life could also explain for the apparent discrepancy between the antidepressant-related outcome of siRNA- or SSRI-induced downregulation of SERT and the downregulation reported in the brains of depressed patients.³⁶⁻³⁸ Whether these depressed patients were, indeed, genetically predisposed to expressing low levels of SERT remains unknown. Clearly, a more comprehensive analyses of an association between the downregulation of SERT with polymorphisms in the *SERT* gene and the vulnerability to affective disorders is warranted.

In conclusion, we demonstrate the efficiency of our nonviral RNAi protocol to produce a specific and widespread downregulation of SERT in the adult mouse brain. Using this technique, we highlight the functional significance of SERT downregulation in

mediating the antidepressant response of SSRIs during adulthood. With an emerging knowledge of mechanisms underlying the regulation of SERT levels at presynaptic nerve terminals,³⁹ we anticipate that targeting the mechanisms that facilitate a downregulation of SERT would not only advance our understanding of how SSRI antidepressants work but also potentially lead to the development of more rapid-acting antidepressant agents.

Acknowledgements

We gratefully acknowledge Sabine Leonhard, Hugo Bürki, Dominique Fehlmann, Dora Khar, David Kirk and Jose Crespo for their excellent technical assistance, and Dr Graeme Bilbe (Head of Neuroscience Research, Novartis Institutes of BioMedical Sciences) for his continuous support of our RNAi projects.

References

- Blakely RD, De Felice LJ, Hartzell HC. Molecular physiology of norepinephrine and serotonin transporters. *J Exp Biol* 1994; **196**: 263–281.
- Frazer A. Antidepressants. *J Clin Psychiatry* 1997; **58**: 9–25.
- Duman RS, Malberg J, Thome J. Neural plasticity to stress and antidepressant treatment. *Biol Psychiatry* 1999; **46**: 1181–1191.
- Nestler EJ, Barrot M, Dilione RJ, Eisch AJ, Gold SJ, Monteggia LM. Neurobiology of depression. *Neuron* 2002; **34**: 13–25.
- Benmansour S, Cecchi M, Morilak DA, Gerbarg GA, Javors MA, Gould GG et al. Effects of chronic antidepressant treatments on serotonin transporter function, density, and mRNA level. *J Neurosci* 1999; **19**: 10494–10501.
- Benmansour S, Owens WA, Cecchi M, Morilak DA, Frazer A. Serotonin clearance *in vivo* is altered to a greater extent by antidepressant-induced downregulation of the serotonin transporter than by acute blockade of this transporter. *J Neurosci* 2002; **22**: 6766–6772.
- Frazer A, Benmansour S. Delayed pharmacological effects of antidepressants. *Mol Psychiatry* 2002; **7**: S23–S28.
- Gould GG, Pardon MC, Morilak DA, Frazer A. Regulatory effects of reboxetine treatment alone, or following paroxetine treatment, on brain noradrenergic and serotonergic systems. *Neuropsychopharmacology* 2003; **28**: 1633–1641.
- Holmes A, Yang RJ, Murphy DL, Crawley JN. Evaluation of antidepressant-related behavioral responses in mice lacking the serotonin transporter. *Neuropsychopharmacology* 2002; **27**: 914–923.
- Lira A, Zhou M, Castanon N, Ansorge MS, Gordon JA, Francis JH et al. Altered depression-related behaviors and functional changes in the dorsal raphe nucleus of serotonin transporter-deficient mice. *Biol Psychiatry* 2003; **54**: 953–959.
- Holmes A, Murphy DL, Crawley JN. Abnormal behavioral phenotypes of serotonin transporter knockout mice: parallels with human anxiety and depression. *Biol Psychiatry* 2003; **54**: 953–959.
- Ansorge MS, Zhou M, Lira A, Hen R, Gingrich JA. Early-life blockade of the 5-HT transporter alters emotional behavior in adult mice. *Science* 2004; **306**: 879–881.
- Mirman M, van der Pol NE, Corner MA, van Ooyen HG, Bour HL. Suppression of active sleep by chronic treatment with chlorimipramine during early postnatal development: effects upon adult sleep and behavior in the rat. *Brain Res* 1981; **204**: 129–146.
- Vogel G, Neill D, Hagler M, Kors D. A new animal model of endogenous depression: a summary of present findings. *Neurosci Biobehav Rev* 1990; **14**: 85–91.
- Battersby S, Ogilvie AD, Smith CA, Blackwood DH, Muir WJ, Quinn JP et al. Structure of a variable number tandem repeat of the serotonin transporter gene and association with affective disorder. *Psychiatr Genet* 1996; **6**: 177–181.
- Lesch KP, Bengel D, Heils A, Sabol SZ, Greenberg BD, Petri S et al. Association of anxiety-related traits with a polymorphism in the serotonin transporter gene regulatory region. *Science* 1996; **274**: 1527–1531.
- Caspi A, Sugden K, Moffitt TE, Taylor A, Craig IW, Harrington H et al. Influence of life stress on depression: moderation by a polymorphism in the 5-HTT gene. *Science* 2003; **301**: 386–389.
- Kaufman J, Yang BZ, Douglas-Palumberi H, Houshyar S, Lipschitz D, Krystal JH et al. Social supports and serotonin transporter gene moderate depression in maltreated children. *Proc Natl Acad Sci USA* 2004; **101**: 17316–17321.
- Murphy DL, Uhl GR, Holmes A, Ren-Patterson , Hall FS, Sora I et al. Experimental gene interaction studies with SERT mutant mice as models for human polygenic and epistatic traits and disorders. *Genes Brain Behav* 2003; **2**: 350–364.
- Thakker DR, Natt F, Hüskens D, Maier R, Müller M, van der Putten H et al. Neurochemical and behavioral consequences of widespread gene knockdown in the adult mouse brain using non-viral RNA interference. *Proc Natl Acad Sci USA* 2004; **101**: 17270–17275.
- Fair A, Xu S, Mengmeyer MK, Kostas SA, Driver SE, Mello CC. Potent and specific genetic interference by double-stranded RNA in *Ceutorhynchus elegans*. *Nature* 1998; **391**: 806–811.
- Caplen NJ, Parish S, Imani F, Fire A, Morgan RA. Specific inhibition of gene expression by small double-stranded RNAs in invertebrate and vertebrate systems. *Proc Natl Acad Sci USA* 2001; **98**: 9742–9747.
- ElBashir S, Harborth J, Lendeckel W, Yalcin A, Weber K, Tuschl T. Duplexes of 21-nucleotide RNAs mediate RNA interference in cultured mammalian cells. *Nature* 2001; **411**: 494–498.
- Hüskens D, Asselbergs F, Kinzel B, Natt F, Weiller J, Martin P et al. mRNA fusion constructs serve in a general cell-based assay to profile oligonucleotide activity. *Nucleic Acids Res* 2003; **31**: e102.
- Dorn G, Patel S, Wotherspoon G, Hemmings-Mieszczak M, Barclay J, Natt FJC et al. siRNA relieves chronic neuropathic pain. *Nucleic Acids Res* 2004; **32**: e9.
- Paxinos G, Franklin KB. *The mouse brain in stereotaxic coordinates*, 2nd edn. Academic Press: London, UK, 2001.
- Cryan JF, Dalvi A, Jin SH, Hirsch BR, Lucki I, Thomas SA. Use of dopamine- β -hydroxylase-deficient mice to determine the role of norepinephrine in the mechanism of action of antidepressant drugs. *J Pharmacol Exp Ther* 2001; **298**: 651–657.
- Mombereau C, Kaupmann K, Froestl W, Sansig G, van der Putten H, Cryan JF. Genetic and pharmacological evidence of a role for GABA_A receptors in the modulation of anxiety- and antidepressant-like behavior. *Neuropharmacology* 2004; **49**: 1050–1062.
- Lucki I, Dalvi A, Mayorga AJ. Sensitivity to the effects of pharmacologically selective antidepressants in different strains of mice. *Psychopharmacology (Berl)* 2001; **155**: 315–322.
- Cryan JF, Mombereau C. In search of a depressed mouse: utility of models for studying depression-related behavior in genetically modified mice. *Mol Psychiatry* 2004; **9**: 326–357.
- Bischoff S, Barhanin J, Bettler B, Bladt S, Heinemann S. Spatial distribution of kainate receptor subunit mRNA in the mouse basal ganglia and ventral mesencephalon. *J Comp Neurol* 1997; **379**: 541–562.
- Sellings LHL, Clarke PBS. Segregation of amphetamine reward and locomotor stimulation between nucleus accumbens medial shell and core. *J Neurosci* 2003; **23**: 6295–6303.
- Vicente A, Battaglia G, Carroll FI, Kuhar MJ. Serotonin transporter production and degradation rates: studies with RTI-76. *Brain Res* 1999; **841**: 1–10.
- Kimmel H, Vicente A, Kuhar MJ. Neurotransmitter transporters synthesis and degradation rates. *Life Sci* 2001; **68**: 2181–2185.
- Garland EJ. Facing the evidence: antidepressant treatment in children and adolescents. *CMAJ* 2004; **170**: 489–491.
- Malison RT, Price LH, Berman R, van Dyck CH, Pelton GH, Carpenter L et al. Reduced brain serotonin transporter availability in major depression as measured by [¹¹C]-26-carboxymethoxy-3-(4-iodophenyl)tropane and single photon emission computed tomography. *Biol Psychiatry* 1998; **44**: 1090–1098.

37 Willeit M, Praschak-Rieder N, Neumeister A, Pirker W, Asenbaum S, Vitouch O *et al.* [^{123}I]- β -CIT SPECT imaging shows reduced brain serotonin transporter availability in drug-free depressed patients with seasonal affective disorder. *Biol Psychiatry* 2000; **47**: 482-489.

38 Arango V, Underwood MD, Mann JJ. Serotonin brain circuits involved in major depression and suicide. *Prog Brain Res* 2002; **136**: 443-453.

39 Blakely RD, Bauman AL. Biogenic amine transporters: regulation in flux. *Curr Opin Neurobiol* 2000; **10**: 328-336.

EXHIBIT 8

Methodology

Open Access

An efficient intrathecal delivery of small interfering RNA to the spinal cord and peripheral neurons

Miaw-Chyi Luo¹, Dong-Qin Zhang¹, Shou-Wu Ma¹, Yuan-Yuan Huang¹, Sam J Shuster², Frank Porreca¹ and Josephine Lai^{*1}

Address: ¹Department of Pharmacology, The University of Arizona Health Sciences Center, Tucson, AZ 85724, USA and ²Neuromics, Minneapolis, MN 55438, USA

Email: Miaw-Chyi Luo - mluo@arizona.edu; Dong-Qin Zhang - dozhang@email.arizona.edu; Shou-Wu Ma - shouwu@email.arizona.edu; Yuan-Yuan Huang - huang1@email.arizona.edu; Sam J Shuster - sam@neuromics1.com; Frank Porreca - frankp@email.arizona.edu; Josephine Lai^{*} - lai@u.arizona.edu

* Corresponding author

Published: 28 September 2005

Received: 24 June 2005

Accepted: 28 September 2005

Molecular Pain 2005, 1:29 doi:10.1186/1744-8069-1-29

This article is available from: <http://www.molecularpain.com/content/1/1/29>

© 2005 Luo et al; licensee BioMed Central Ltd.

This is an Open Access article distributed under the terms of the Creative Commons Attribution License (<http://creativecommons.org/licenses/by/2.0>), which permits unrestricted use, distribution, and reproduction in any medium, provided the original work is properly cited.

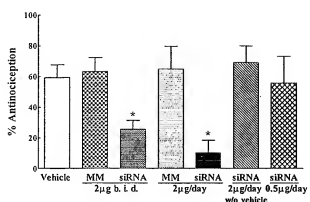
Abstract

We have developed a highly effective method for *in vivo* gene silencing in the spinal cord and dorsal root ganglia (DRG) by a cationic lipid facilitated delivery of synthetic, small interfering RNA (siRNA). A siRNA to the delta opioid receptor (DOR), or a mismatch RNA, was mixed with the transfection reagent, i-Fect™ (vehicle), and delivered as repeated daily bolus doses (0.5 μg to 4 μg) via implanted intrathecal catheter to the lumbar spinal cord of rats. Twenty-four hours after the last injection, rats were tested for antinociception by the DOR selective agonist, [D-Ala², Glu⁴]deltorphin II (DELT), or the mu opioid receptor (MOR) selective agonist, [D-Ala², N-Me-Phe⁴, Gly-ol⁵]enkephalin (DAMGO). Pretreatment with the siRNA, but not the mismatch RNA or vehicle alone, blocked DELT antinociception dose-dependently. The latter was concomitant with a reduction in the spinal immunoreactivity and receptor density of DOR, and in DOR transcripts in the lumbar DRG and spinal dorsal horn. Neither siRNA nor mismatch RNA pretreatment altered spinal immunoreactivity of MOR or antinociception by spinal DAMGO, and had no effect on the baseline thermal nociceptive threshold. The inhibition of function and expression of DOR by siRNA was reversed by 72 hr after the last RNA injection. The uptake of fluorescence-tagged siRNA was detected in both DRG and spinal cord. The low effective dose of siRNA-i-Fect™ complex reflects an efficient delivery of the siRNA to peripheral and spinal neurons, produced no behavioral signs of toxicity. This delivery method may be optimized for other gene targets.

Background

RNA interference (RNAi) is an endogenous mechanism of RNA dependent degradation of specific mRNA by a protein complex called the RNA induced silencing complex (RISC) [1]. This mechanism was first characterized in the

nematode *Caenorhabditis elegans* as an intrinsic protective response against invaded viral RNA [2]. The sequence specific substrate selectivity of RISC is dictated by its complex formation with certain double stranded, small interfering RNA (siRNA) that, in the nematode, is generated from

**Figure 1**

Dose effect of intrathecal siRNA to DOR on the antinociceptive effect of the delta opioid agonist [D-Ala², Glu⁴]Deltorphin II (DELT). DELT was given intrathecally (30 µg). The antinociceptive efficacy of DELT is defined as % antinociception measured 30 min after drug administration ($n = 6$ rats/group). Intrathecal DELT antinociception was significantly blocked after 3 consecutive daily dose of siRNA at a daily dose of 4 µg (2 µg b.i.d.) or 2 µg (* $p < 0.05$), when compared with that observed in the vehicle control group. Mismatch RNA at the same doses had no effect on DELT antinociception. The 2 µg daily dose of siRNA, when administered without i-Fect™, did not block intrathecal DELT antinociception. The 0.5 µg dose of the siRNA in i-Fect™ did not have any effect on intrathecal DELT antinociception. Statistical analysis was carried out by one-way ANOVA following Dunnett's multiple comparisons.

viral RNA by an enzyme complex called DICER [3]. Subsequently, it was demonstrated that RNAi could be achieved in cultured mammalian cells by transfecting them with chemically synthesized siRNA [4], or by plasmid generated siRNA [5], thus establishing a new technology for functional genomics as well as drug target validation. In vertebrate experimental models, RNAi has been successfully applied to target exogenous and endogenous gene expression in organ systems such as liver, spleen, kidney, lung, and pancreas via systemic delivery [6-10]. However, this novel technology is not readily amenable to targeting nervous system genes because siRNA does not easily cross the blood brain barrier, and its uptake by neurons *in vitro* is poor [11]. While chemical modification of siRNA may enhance the efficiency of uptake of these molecules in cultured neurons as demonstrated recently [12], only a few studies to date succeeded in knocking down target genes in the central nervous system (CNS) [13-16]. We proposed that the limited advance made in the latter could be improved by establishing a

paradigm that efficiently delivers the siRNA to the CNS and can be optimized for a variety of targets.

We have previously shown that the delta opioid receptor (DOR) can be effectively knocked down *in vitro* [17] and *in vivo* [18,19] by antisense oligodeoxynucleotide (ODN) treatment. *In vivo*, an antisense ODN to the DOR, at a dose of 12.5 µg (1.6 nmol), given twice daily, produced a robust inhibition, by day 3, of antinociception of the DOR selective agonist, [D-Ala², Glu⁴]deltorphin II (DELT) when given intracerebroventricularly [18] or intrathecally [19]. We thus postulate that the DOR is a suitable prototypic nervous system gene target for the purpose of optimizing *in vivo* RNAi by siRNA based on our prior experience with delivery and dosing of ODN, time course of the knockdown and turnover rate of the DOR. Another critical advantage is the well-established protocols and reagents for measuring the expression and function of DOR. We show here that a low dose of 2 µg of siRNA when mixed with a transfection agent, i-Fect™, and given once daily by the intrathecal route, effectively abolishes the function of DOR in the lumbar spinal cord. A selective reduction in the transcript and protein level of DOR in the lumbar dorsal root ganglia (DRG) and in the lumbar dorsal horn of the spinal cord suggests that the inhibitory effect of the siRNA on DOR is specific to its knockdown of DOR expression. The uptake of the siRNA by cells in the DRG and the spinal cord is consistent with its site of action. The effect of the siRNA is abolished by scrambling its sequence, or by discontinuing the siRNA treatment. The effective dose of the siRNA requires the use of i-Fect™, which facilitates the uptake of the siRNA into target tissues.

Results

Intrathecal administration of a siRNA to DOR blocked spinal DELT antinociception

The siRNA that was designed was first evaluated for its effect on DOR expression *in vitro*. This was accomplished by transfecting the siRNA/i-Fect™ complexes into NG108-15 cells that express endogenous DOR (the DOR in the NG108-15 cells has the mouse genotype; while the siRNA sequence was designed based on the rat DOR sequence, it cross-reacts with the mouse sequence). Quantitative RT-PCR analysis of total RNA extracts from these cells harvested 48 hr after transfection showed an $82.4 \pm 9.2\%$ knockdown of the DOR transcripts compared with that in control, non-transfected cells. For *in vivo* delivery, an initial experiment was conducted to determine the dose response of the siRNA, or mismatch RNA on intrathecal DELT antinociception (Fig. 1). Rats were given vehicle, the siRNA or mismatch RNA once daily for 3 consecutive days, and spinal DELT antinociception was measured 24 hr after the last injection. In the vehicle pretreated rats, intrathecal DELT produced $60 \pm 8\%$ MPE, which was con-

sistent with that previously published [19]. The siRNA at 2 µg and 4 µg (as two 2 µg doses, one at 0900 and one at 1600 hr) daily dose both significantly attenuated the antinociception of DELT when compared with DELT antinociception in the vehicle control, while a 0.5 µg daily dose had no effect. The antinociception by DELT observed in the 2 µg and 4 µg siRNA pretreated groups were not significantly different from each other ($10 \pm 8\%$ MPE, $25 \pm 5\%$ MPE, respectively; $P > 0.05$). The mismatch RNA treated groups did not differ significantly from the vehicle control irrespective of dosage of the mismatch RNA. These data established the 2 µg daily as the approximate minimum effective dose of this siRNA. However, if this dose of the siRNA was given without the vehicle i-Fect™, the subsequent antinociceptive effect of intrathecal DELT was robust, and was not significantly different from that observed in the vehicle pretreated group, or mismatch RNA treated groups (Fig. 1). Notably, none of the RNA treatments had any effect on the baseline thermal nociceptive threshold when compared with that of the vehicle control group. The baseline thermal latencies for paw withdrawal in the vehicle, siRNA (2 µg/day for 3 days), and mismatch RNA groups prior to treatment were: 20 ± 1.5 sec, 21 ± 1.1 sec, and 20 ± 1.1 sec, respectively. Twenty-four hours after the last injection, the baseline thermal latencies were 20 ± 1.0 sec, 19 ± 1.5 sec, and 20 ± 1.0 sec, respectively. Neither vehicle nor RNA treatment precipitated overt signs of behavioral toxicity or motor impairment in the animals. All subsequent siRNA or mismatch RNA treatment employed the 3 consecutive daily dose of 2 µg given with i-Fect™.

The inhibitory effect of siRNA treatment on DELT antinociception is transient and reversible

Whereas spinal DELT antinociception was attenuated after siRNA treatment, determined at 24 hr after the last siRNA injection, when the animals were tested again 48 hr later (i.e., 72 hr after the last injection), DELT antinociception was not different when compared with that in mismatch RNA and vehicle control groups (Fig. 2).

Knockdown of DOR in the spinal dorsal horn by the siRNA
 Figure 3 shows the saturation analysis of DOR in the spinal dorsal horn by the selective antagonist, [³H]naltindole. SiRNA, but not mismatch RNA, produced a significant reduction in the density of the DOR measured as the maximum specific binding (B_{max}) of the radioligand and when compared with that in the vehicle treated controls. The reduction represents ~70% knockdown of the DOR density after siRNA treatment. The dissociation constant (K_d) for [³H]naltindole was not different in the three treatment groups. Immunohistochemical analysis using an anti-DOR antibody showed a significant reduction of immunoreactivity for DOR in the superficial laminae of the dorsal horn of the lumbar spinal cord from

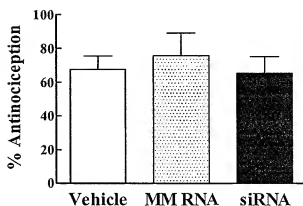


Figure 2
Spinal DELT antinociception tested 72 hours after the last RNA or vehicle injection ($n = 6/group$). There is no significant difference in the % antinociception among the three pretreatment groups ($p > 0.05$).

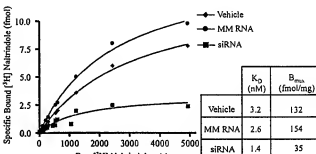


Figure 3
Saturation [³H]naltindole binding in membranes prepared from rat dorsal lumbar spinal cord ($n = 3$ rats/group). The B_{max} value in the siRNA group, but not the mismatch RNA group, was significantly lower than that in the vehicle treated group. The K_d values are not significantly different among the 3 groups ($p > 0.05$). Data are representative of 3 independent experiments.

siRNA treated rats, but not from the mismatch RNA treated rats (Fig. 4). Lumbar spinal dorsal horn harvested from siRNA treated rats 72 hr after the last siRNA injection showed strong DOR immunoreactivity, which was not different from the vehicle or from the mismatch RNA controls. The recovery of DOR immunoreactivity by 72 hr after the last siRNA injection is consistent with the observed recovery of DELT antinociception in the siRNA treated rats at this time point shown in Fig. 2.

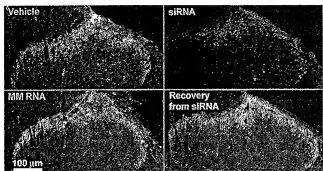


Figure 4
DOR-immunoreactivity in the dorsal horn of the spinal cord after vehicle, siRNA or mismatch (MM) RNA treatment. The immunoreactivity of DOR was predominantly found in laminae I/II of the dorsal horn. The immunolabeling was significantly lower in tissue from siRNA treated rats. Tissues taken 72 hours after the last siRNA injection (siRNA recovery) show similar level of immunoreactivity for DOR when compared with vehicle or MM RNA controls. Each image is representative of multiple sections from 3 rats per treatment group.

siRNA treatment reduced the level of DOR transcripts in the DRG and the spinal dorsal horn

The mRNA levels of DOR in the lumbar spinal cord and L4/L5 DRGs were determined by quantitative RT-PCR at 24 hr after the last siRNA injection. In the siRNA treated group, there was a 38% reduction in DOR transcripts in the DRG ($61.9 \pm 5.7\%$ of vehicle control), and 62% reduction in the lumbar spinal cord ($38 \pm 17.7\%$ of vehicle control). Mismatch RNA pretreatment did not significantly alter the DOR mRNA level in either the DRG ($109 \pm 2.0\%$ of vehicle control) or the lumbar spinal cord ($90 \pm 0.01\%$ of vehicle control).

siRNA was taken up by DRG and spinal cord cells

AlexaFluor546-tagged siRNA fluorescence was clearly detected in both the lumbar DRG and spinal cord 24 hr after intrathecal delivery of 2 μ g of the tagged RNA (Fig. 5A, B). In the DRG, fluorescence was present in cell bodies of various sizes. The labeling was punctate, perinuclear, and varied in intensity among the cells (Fig. 5A). In the spinal cord cross sections, fluorescence could be seen distributed over the entire cross sections, labeling a large number of cells in both the dorsal and the ventral horn, as well as the area around the central canal. Figure 5B shows an example of a $40 \times$ magnification of the labeled spinal cord cells in the superficial laminae of the dorsal horn. The fluorescence is seen in the cytoplasm of the labeled cells, while nuclei typically appear as dark, unlabeled areas in the center of these cells. The localization of the

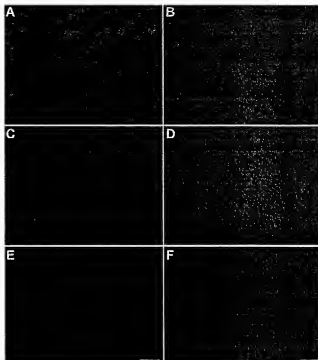


Figure 5
AlexaFluor546-tagged siRNA uptake in lumbar DRG (A, C, E) and spinal cord (B, D, F). Vehicle (10 μ L) (C, D), siRNA with vehicle (2 μ g/10 μ L) (A, B), or siRNA without vehicle (2 μ g/10 μ L of aqueous annealing buffer) (E, F) was given intrathecally as a single injection. Tissues were harvested and processed 24 hr later. Images of the DRG were taken using a 20 \times objective lens and that of the spinal cord taken using a 40 \times objective lens. In all the fluorescence labeled cells, the labeling was punctate and peri-nuclear, and labeling intensities varied among cells. In the spinal cord (B), labeled cells were distributed widely in both the dorsal horn and the ventral horn. The images in B, D, F were taken from laminae I/II of the dorsal horn. Scale bar for the DRG images shown in panel E is 50 μ m; scale bar for the spinal cord images shown in panel F is 25 μ m.

fluorescence strongly suggests that the labeling is intracellular and thus due to the uptake of the tagged siRNA by the DRG and the spinal cord cells. Autofluorescence of the tissue sections was negligible under these imaging conditions when tissue sections from vehicle-injected rats were analyzed (Fig. 5C, D). Notably, when fluorescence-tagged siRNA was delivered into rats without i-Fect™, its uptake in the lumbar DRG (Fig. 5E) as well as in the lumbar spinal cord (Fig. 5F) was extremely poor.

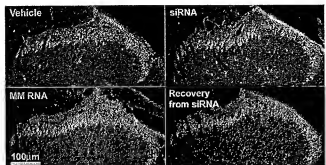


Figure 6
MOR-immunoreactivity in the dorsal horn of the spinal cord after vehicle, siRNA (to DOR) or mismatch (MM) RNA treatment. The MOR immunoreactivity is predominantly localized to laminae III of the dorsal horn. No significant difference in the immunoreactivity for MOR was seen among the 3 treatment groups. Tissue taken 72 hours after the last siRNA injection (siRNA recovery) also showed similar MOR immunoreactivity as the control groups. Each image is representative of multiple sections processed from 3 rats used in each group. The sections used in this figure and those used for DOR labeling shown in Figure 4 were from the same animals.

sensory primary afferent [15]. While both studies demonstrated that siRNA attenuated the intended gene target, the former was a short intervention (3.5 hr) while the experimental subject was under general anesthesia, whereas the latter required very high concentration and continuous infusion of siRNA (400 μ g/day for up to 7 days) to elicit a modest knockdown of the target. It is not clear whether the high dose of siRNA needed to effect reflects an inefficient RNAi mechanism in neurons or whether the modulation of gene function cannot be sustained over time.

Our data show that in the presence of a suitable transfection agent, the siRNA to the DOR is highly effective at a low concentration of 2 μ g, or 0.14 nmol, given once a day. This dose is 23 times lower than the amount of antisense ODN required to elicit a knock down of the DOR as previously published [18], and is substantially lower than the effective dose reported for the knock down of the P2X3 receptors in the DRG [15]. The siRNA treatment delivered without the transfection reagent was without effect, suggesting that the transfection reagent significantly enhanced the uptake of the siRNA into target cells, as verified by the detection of fluorescence uptake of spinal cord and DRG tissues after injecting the tagged siRNA. This observation is consistent with recent evidence that the uptake of siRNA by neurons in culture is likely a key limiting step in the siRNA mediated gene silencing [12]. The amount of RNA delivered as a bolus dose in transfection reagent tends to be limited by the solubility of the RNA. The transfection reagent used in the present study was i-FectTM, which is a cationic lipid mixture that has been optimized for the delivery of short oligonucleotides in vitro [24]. This reagent was chosen for the present study because the RNA/lipid complexes remain in suspension at a fairly high concentration in a volume that is suitable for intrathecal delivery. A maximum of 2 μ g of RNA can be given in a 10 μ L injection volume. Should a daily dose of >2 μ g is desired, the delivery can be adjusted by giving multiple doses.

siRNA to DOR did not alter the function or expression of MOR

In vehicle-pretreated rats, DAMGO (0.5 μ g) produced 66 \pm 16% MPE, which is consistent with that previously published [20]. Neither siRNA to DOR, nor mismatch RNA treatment, had any effect on intrathecal DAMGO antinociception when compared with the vehicle control (79 \pm 11% MPE, 73 \pm 10% MPE, respectively to 66 \pm 16% MPE; $P > 0.05$). There was also no significant difference in the MOR immunoreactivity in the dorsal horn of the spinal cord between siRNA, mismatch RNA, and vehicle treated groups (Fig. 6).

Discussion

The advances made recently toward the *in vivo* applications of RNAi in vertebrate systems are critical towards developing siRNA as therapeutics [21-23]. These *in vivo* applications, however, do not yet apply to central nervous system function because siRNA do not readily cross the blood brain barrier (BBB) via systemic delivery. Because drugs may bypass the BBB by delivering them directly into the CSF, such delivery routes may be exploited in order to determine whether neurons and other cells in the nervous system may be amenable to RNAi by siRNA *in vivo*. Two recent reports used intrathecal delivery to prevent hypoxia-induced expression of brain derived neurotrophic factor in the spinal cord [14], or to knockdown the expression of the purinergic receptor subtype, P2X3, in

A significant knockdown of DOR transcripts by siRNA treatment is consistent with the proposed mechanism of action of RNAi [25,26]. In this regard, the knockdown of the DOR transcripts was observed in both the dorsal horn of the spinal cord as well as the lumbar DRG, demonstrating that the siRNA interferes with the synthesis of both the presynaptic and the postsynaptic populations of DOR, which is also highly consistent with the uptake pattern of the tagged siRNA. The effects of siRNA culminate in a significant reduction of DOR immunoreactivity and ligand binding capacity in the superficial laminae of the dorsal horn of the spinal cord where the functional receptors are predominantly located. The loss of functional DOR is evident by the loss of antinociceptive activity of the DOR selective agonist, DELT, given intrathecally.

Together, these results justify our conclusion that we have established an effective method for delivering siRNA that interferes efficiently with the expression and function of target genes in both the peripheral nervous system (i.e., sensory primary afferent) and the central nervous system (i.e., spinal cord).

The use of a mismatch RNA confirms the specificity of the siRNA sequence for the DOR. The siRNA treatment had no effect on the expression or the function of the highly homologous receptor type, MOR, further supporting the target specificity of the siRNA employed here. Finally, the effect of the siRNA is fully reversible; thus the observed effects of the siRNA are specific to the use of siRNA, and the treatment paradigm does not precipitate any long-term effects due to toxicity such as motor impairment. This paradigm can be easily adjusted for dosage and duration of treatment, and is based on a well-established, relatively non-invasive method of drug delivery that has general applications for spinal and peripheral targets. The reagents required are minimal and economical, and can be adapted for other gene targets. Our findings support the hypothesis that siRNA can be effectively applied to modulate nervous system function. The significant knockdown of the target transcripts in both the DRG and the spinal cord conforms with the established mechanism of siRNA mediated gene silencing, and is consistent with the uptake of siRNA seen in both the peripheral neurons (i.e., DRG) and the central nervous system (i.e., spinal cord). The low dose of siRNA further suggests that the efficacy of RNAi depends critically on the efficient delivery of the siRNA to the target tissues. Unlike antisense oligodeoxyribonucleotides, siRNA may be delivered systemically [23]. Thus, chemical modifications that enhance systemic stability and facilitate siRNA transport across the BBB or the uptake of siRNA by neurons would greatly advance the potential of siRNA as therapeutic.

Methods

siRNA preparation

The siRNA sequence for the DOR (accession no. U00475, the only gene sequence that is defined as delta opioid receptor to date) was from nucleotides 364 to 384 relative to the start codon. The sequences were as follows: sense 5'-GGCUGUGCCUCUCAUUGACUUU-3'; antisense 5'-GUCAAUGGAGAGCACAGCCUU-3'. A scrambled sequence was designed as a mismatch control: sense 5'-GGCGUGUCUCUUCUUACGACUUU-3' and antisense 5'-GUCGUAAAGAGAGACACGCCUU-3'. BLAST search of the nucleotide sequences in the GenBank database showed no substantial homology with other genes. These 21-nucleotide RNA oligonucleotides were synthesized individually, deprotected and purified by RNase-free HPLC (Midland Certified Reagent Company). siRNA and mismatch RNA duplexes were formed in a concentration of

200 μ M in annealing buffer as described [4] for 3 min at 90°C followed by 1 h at 37°C. The siRNA stocks were aliquoted and stored at -80°C. For fluorescence labeling of the siRNA, AlexaFluor 546 was conjugated at the 5' end of the sense strand by solid phase synthesis and the tagged siRNA was purified by HPLC (Qiagen) and resuspended to a concentration of 200 μ M in annealing buffer.

In vitro analysis of knock down of DOR in NG108-15 cells by the siRNA

NG108-15 Cells were cultured in 5% fetal calf serum/ 5% newborn calf serum/ 45% Ham's F-12/ 45% DMEM/ 100 μ M⁻¹ penicillin/ 100 μ g mL⁻¹ streptomycin (Invitrogen). Cells were maintained in 75 cm² flasks in a humidified atmosphere with 95% air and 5% CO₂. For experiments, cells were seeded in 6-well plates at 3 \times 10⁵ cells/well 24 hr before the siRNA treatment. Cells were transfected with 2 μ g of siRNA-iFect™ complexes in 1:4 ratio (w/v) per well. Forty-eight hours after transfection, cells were harvested and total RNA was isolated. DOR transcripts were detected by real-time RT-PCR (see below).

Quantitative RT-PCR

Total RNA was isolated from the lumbar dorsal spinal cord, the L4 and L5 dorsal root ganglia using Aurum™ total RNA mini kit (Bio-Rad). Quantitative RT-PCR was performed using the iCycler iQ Multicolor Real-Time PCR Detection System with iScript cDNA Synthesis Kit and iQ SYBR Green Supermix (Bio-Rad). All samples were run in triplicate using an annealing temperature of 60°C. Primers for the amplification of DOR were: forward primer: 5'-GTTCACCAAGCATCTCAGG -3'(nuc. 396-414); reverse primer: 5'-TGCATACCACTGCTCCATC -3'(nuc. 577-595). That for GAPDH were: forward primer: 5'-ATCATCCCTGCATCCACTG-3'(nuc. 610-628); reverse primer: 5'-GCCTGCTTACCACTTC -3'(nuc. 771-788). All primers were synthesized by Midland Certified Reagent Company, Inc. PCR efficiencies for DOR and GAPDH were 97% and 98%, respectively, with correlation coefficient of 0.999. Expression of DOR was normalized to expression of GAPDH. The differences of DOR mRNA expression between treatments were analyzed using the Comparative C_T Method (ABI Prism 7700 Sequence Detection System User Bulletin #2, p11-15, 2001). The threshold cycle (C_T) is defined as the cycle at which the amount of amplified PCR product from the target cDNA reaches a fixed threshold. In each treatment, $\Delta C_T = C_T$ for the target, DOR - C_T for the endogenous reference, GAPDH. $\Delta\Delta C_T = \Delta C_{T,treatment} - \Delta C_{T,control}$. The equation, 2 ^{$\Delta\Delta C_T$} , denotes the ratio of the level of DOR transcripts in the treated group and that of the control group. This number is converted to percent of control, where control is set at 100.

Animal surgery and RNA administration

Male Sprague-Dawley rats, weighing between 200–220 g, were used in these experiments. All the procedures used in these experiments have been approved by the Institutional Animal Care and Use Committee. Rats were implanted with intrathecal (*i.th.*) catheters and allowed 7 days to recover from surgery prior to treatment. The rats were divided into siRNA, mismatch RNA and vehicle groups, with at least 6 rats per group. siRNA or mismatch RNA complexes were prepared immediately prior to administration by mixing the RNA solution (200 μ M in annealing buffer) with a transfection reagent, i-Fect™ (Neuromics), in a ratio of 1:4 (w/v) [24]. At this ratio, the final concentration of RNA as an RNA/lipid complex was 2 μ g in 10 μ L siRNA or mismatch RNA, or i-Fect™ alone (defined as vehicle) in 10 μ L was delivered to the lumbar region of the spinal cord via the *i.th.* catheters. Injections were given daily for 3 consecutive days. Nociceptive testing and tissue harvest were carried out at 24 hr and 72 hr after the last injection. The fluorescence tagged siRNA was mixed with i-Fect™ and injected in the same manner as for the untagged RNA, except that only one injection was given and tissue harvested 24 hr later.

Nociceptive testing

Radiant heat paw withdrawal test using a movable infrared light source was employed as the nociceptive stimulus. The experimenter who conducted the nociceptive testing was blinded to the pretreatment of the experimental groups. The baseline latency for withdrawal of the left hindpaw was recorded from the experimental animals 24 hr prior to RNA or vehicle administration. Twenty-four hr following the last injection, the baseline latency was recorded again. The rats then received either 30 μ g of [D-Ala²]deltorphin II (DELT) or 0.5 μ g of [D-Ala², N-Me-Phe⁴, Gly-ol]enkephalin (DAMGO) (Sigma) intrathecally and the thermal latency were measured at 15-min interval over 60 min. A maximal cutoff latency of 33 s was used to prevent potential tissue injury. The % antinociceptive effect of DELT or DAMGO was defined as: [(treatment-baseline)]/(cutoff-baseline)] × 100. The testing was repeated at 72 hr after the last injection.

Saturation analysis of DOR by [³H]naltrexole

Crude membranes were prepared from the lumbar dorsal spinal cords pooled from the rats in each treatment group, resuspended in 50 mM Tris buffer, pH7.2, and the protein content measured as previously described [18]. Saturation analysis of [³H]naltrexole (20 Ci/mmol, PerkinElmer) was carried out using 10 concentrations of [³H]naltrexole (31.3 pM to 5 nM), done in triplicates, incubated with 50 μ g of membranes per assay tube in 0.5 mL buffer, at a total volume of 1.0 mL, in a shaking water bath at 25°C for 3 hr. Non-specific binding of the radioligands was defined by that in the presence of 10 μ M naloxone.

The reactions were terminated by rapid filtration through Whatman GF/B filters, followed by five washes with 4 mL of ice-cold saline. The radioactivity was determined by liquid scintillation counting. Data were analyzed by non-linear least squares regression analysis using GraphPad Prism 4 (GraphPad software).

Immunohistochemical analysis of DOR and MOR and fluorescence imaging

Rats were deeply anesthetized with ketamine HCl/xylazine (Sigma). The heart was exposed and transcardially perfused with 10 mM sodium phosphate-buffered saline (PBS, pH 7.4) until exudate ran clear, then switched to 10% buffered formalin for a further 15 min. Lumbar spinal cord and the L4 and L5 DRG were isolated and post-fixed in 10% buffered formalin for 24 hr and cryoprotected with 30% sucrose in 10 mM PBS. After pre-blocking with 10% normal goat serum (Vector Laboratories), frontal sections (20 μ m) of the spinal cord were incubated with either a rabbit anti-rat primary antibody for DOR (1:2000) or a rabbit anti-rat primary antibody for MOR (1:5000) at 4°C for 48 hr (both antibodies were from Neuromics). Slides were rinsed with 2.5% normal goat serum/PBS and then incubated with a secondary antibody (AlexaFluor 594-conjugated goat anti-rabbit IgG (1:1000, Molecular Probes) for 1 hour at room temperature. Slides were again rinsed 3 times with the same buffer, dried, and mounted for microscopy. Fluorescent imaging of the samples was carried out using Nikon E800 fluorescence microscope equipped with 10 \times , 20 \times and 40 \times objective lenses and standard filters for Y-2E/C TRX RED, coupled to a Hamamatsu C5810 color CCD camera (Hamamatsu Photonic System) for digital image acquisition using Adobe Photoshop software on a PC workstation. The same system was used for the imaging of slide mounted lumbar spinal cord and L4/L5 DRG (20 μ m longitudinal sections) from animals that have been injected with the tagged siRNA, except that the filters for TRITC was used.

Statistical analysis

Significant differences among paw withdrawal latencies at 30-min time point after DELT or DAMGO injection were determined by ANOVA followed by the *post hoc* least significant differences test. Unpaired *t*-test was used for all other between group comparisons.

Abbreviations

RNAi RNA interference

siRNA Small interfering RNA

MM RNA Mismatch RNA

i.th. Intrathecal

DOR Delta opioid receptor
 DELT [D-Ala²]deltrophin II
 MOR Mu opioid receptor
 DAMGO [D-Ala², N-Me-Phe⁴, Gly-ol⁵]enkephalin
 DRG Dorsal root ganglia

Competing interests

The author(s) declare that they have no competing interests.

Acknowledgements

The authors thank Dr. David Bumcrot for critical review and discussion of the manuscript, and Wen-Jun Zhang for technical assistance. This work is supported by the National Institute on Drug Abuse Grant P01 DA06284.

References

- Hammond SM, Bernstein E, Beach DL, Hannan GJ: A genetic link between co-suppression and RNA interference in *C. elegans*. *Nature* 2000, 404:293-296.
- Fritz A, Xu S, Montgomery MK, Koester SA, Driver SE, Mello CC: Potent and specific genetic interference by double-stranded RNA in *C. elegans*. *Nature* 1998, 391:906-811.
- Bernstein E, Caudy AA, Hammond SM, Hannan GJ: Role for a bidentate ribonuclease in the initiation step of RNA interference. *Nature* 2001, 409:363-366.
- Elshabani SM, Harborth J, Lendeckel W, Yalcin A, Weber K, Tuschl T: Duplexes of 21-nucleotide RNAs mediate RNA interference in cultured mammalian cells. *Nature* 2001, 411:494-497.
- Brummelkamp TR, Bernards R, Agami R: A system for stable expression of short interfering RNAs in mammalian cells. *Science* 2002, 296:550-553.
- McCaffrey AP, Meuse L, Pham T-T, Conklin DS, Hannan GJ, Kay MA: Gene expression: RNA interference in adult mice. *Nature* 2002, 419:38-39.
- Song E, Lee S-K, Wang J, Ince N, Quyuan N, Min J, Chen J, Shankar P, Lieberman J: RNA Interference targeting Fas protects mice from fulminant hepatitis. *Nat Med* 2003, 9:347-351.
- Sorensen DR, Leirdal M, Stoudt M: Gene silencing by systemic delivery of synthetic siRNAs in adult mice. *J Mol Biol* 2003, 327:761-766.
- Zender L, Huker S, Liedtke C, Tillmann HL, Zender S, Mundt B, Waltemathe M, Gosling T, Flemming P, Maleki NP, Trautwein C, Manns MP, Kühlnd F, Kühlnd C: Caspase 8 small interfering RNA prevents acute liver failure in mice. *Proc Natl Acad Sci USA* 2003, 100:7797-7802.
- Kobayashi N, Matsui Y, Kawase A, Hirata K, Miyagishi M, Taira K, Nishikawa M, Takakura Y: Vector-based in vivo RNA Interference: dose and time-dependent suppression of transgene expression. *J Pharmacol Exp Ther* 2004, 308:688-693.
- Trübsch B, Wood M: Application of nucleic acid technology in the CNS. *J Neurochem* 2004, 88:257-265.
- Davidson TJ, Harel S, Arboleda VA, Prunell GF, Shulanski ML, Greene LA, Troy CM: Highly efficient small interfering RNA delivery to primary mammalian neurons induces microRNA-like effects before mRNA degradation. *J Neurosci* 2004, 24:10040-10046.
- Makimura H, Mizuno TM, Mastaitis JV, Agami R, Robbins CV: Reducing hypothalamic AGRP by RNA interference increases metabolic rate and decreases body weight without influencing food intake. *BMC Neurosci* 2002, 3:18-23.
- Baker-Herman TL, Fuller DD, Davis RW, Zabka AG, Goldner FJ, Doperański NJ, Johnson RA, Watters JJ, Mitchell GS: BDNF is necessary and sufficient for spinal respiratory plasticity following intermittent hypoxia. *Nat Neurosci* 2003, 7:48-55.
- Dorn G, Patel S, Wotherspoon G, Hemmings-Miesczak M, Barday J, Nazr FJC, Martin P, Bevan S, Fox A, Ganju P, Wishart V, Hall Jonathian: siRNA relieves chronic neuropathic pain. *Nucleic Acids Res* 2004, 32:e549.
- Thakker DR, Nazr F, Husken D, Maier R, Müller M, van der Putten H, Hoyer D, Cryan JF: Neurochemical and behavioral consequences of widespread gene knockdown in the adult mouse brain by using nonviral RNA interference. *Proc Natl Acad Sci* 2004, 101:17270-17275.
- Lai J, Crook TJ, Payne A, Lynch RM, Porreca F: Antisense targeting of delta opioid receptors in NG108-15 cells: direct correlation between oligodeoxyribonucleotide uptake and receptor density. *J Pharmacol Exp Ther* 1997, 281:589-596.
- Bilsky BJ, Bernman RN, Hrbzy VJ, Rothman RB, Lai J, Porreca F: Characterization of antinociception to opioid receptor selective agonists after antisense oligodeoxyribonucleotide-mediated "knock-down" of opioid receptor in vivo. *J Pharmacol Exp Ther* 1996, 277:491-501.
- Bilsky BJ, Wang T, Lai J, Porreca F: Selective blockade of peripheral delta opioid receptor-induced antinociception by intradermal administration of delta opioid receptor antisense oligodeoxyribonucleotide. *Neurosci Lett* 1996, 220:155-158.
- Vanderlaan TW, Gardner LR, Burgess SE, Ibrahim M, Dogru A, Zhong C-M, Zheng E-T, Man PTP, Oospov M-H, Lai J, Porreca F: Dynorphin promotes abnormal pain and spinal opioid antinociceptive tolerance. *J Neurosci* 2000, 20:7074-7079.
- Wood MJA, Trübsch B, Abdellatif A, Besson D: Therapeutic gene silencing in the nervous system. *Hum Mol Genet* 2003, 12:R279-R284.
- Rossi JI: A cholesterol connection in RNAi. *Nature* 2004, 427:155-156.
- Soutschek J, Alkins A, Bramlage B, Charisse K, Consten R, Donguigue M, Elbasir S, Geidka A, Hadwiger P, Harborth J, John M, Kessavam V, Levine G, Pandey RK, Racine T, Rajeev KG, Röhl I, Touđarska I, Wang G, Wuschko S, Buncrop D, Kotolsiansky Y, Limmer S, Manoharan M, Vornlocher H-P: Therapeutic silencing of an endogenous gene by systematic administration of modified siRNAs. *Nature* 2004, 432:173-178.
- More information about this reagent may be obtained on line at <http://www.neuroomics.com>.
- Hannan GJ: RNA Interference. *Nature* 2002, 418:244-251.
- Novina CD, Sharp PA: The RNAi revolution. *Nature* 2004, 430:161-164.

Publish with BioMed Central and every scientist can read your work free of charge

"BioMed Central will be the most significant development for disseminating the results of biomedical research in our lifetime."

Sir Paul Nurse, Cancer Research UK

Your research papers will be:

- available free of charge to the entire biomedical community
- peer reviewed and published immediately upon acceptance
- cited in PubMed and archived on PubMed Central
- yours — you keep the copyright

Submit your manuscript here:
http://www.biomedcentral.com/info/publishing_adv.asp



EXHIBIT 9

Research article

Open Access

Reducing hypothalamic AGRP by RNA interference increases metabolic rate and decreases body weight without influencing food intakeHideo Makimura^{1,2}, Tooru M Mizuno^{1,2}, Jason W Mastaitis^{1,2}, Reuven Agami³ and Charles V Mobbs*^{1,2}

Address: ¹Fishberg Center for Neurobiology, Neurobiology of Aging Laboratories, Mount Sinai School of Medicine, One Gustave L. Levy Place, Box 1639, New York, New York, 10029, USA, ²Department of Geriatrics and Adult Development, Mount Sinai School of Medicine, One Gustave L. Levy Place, New York, New York, 10029, USA and ³Division of Tumor Biology, The Netherlands Cancer Institute, 121 Plesmanlaan 1066 CX, Amsterdam, The Netherlands

E-mail: Hideo.Makimura - Hideo.Makimura@mssm.edu; Tooru M Mizuno - Tooru.Mizuno@mssm.edu; Jason W Mastaitis - Jason.Mastaitis@mssm.edu; Reuven Agami - r.agami@nki.nl; Charles V Mobbs* - Charles.Mobbs@mssm.edu

*Corresponding author

Published: 7 November 2002

Received: 20 August 2002

BMC Neuroscience 2002, 3:18

Accepted: 7 November 2002

This article is available from: <http://www.biomedcentral.com/1471-2202/3/18>

© 2002 Makimura et al; licensee BioMed Central Ltd. This article is published in Open Access: verbatim copying and redistribution of this article are permitted in all media for any purpose, provided this notice is preserved along with the article's original URL.

Abstract

Background: Several lines of evidence strongly suggest that agouti-related peptide (AGRP) plays a key role in the regulation of metabolic function but ablation of the AGRP gene has no apparent effect on metabolic function. Since specific pharmacological antagonists of AGRP do not presently exist, we assessed if reduction of hypothalamic AGRP mRNA by RNA interference (RNAi) would influence metabolic function, an outcome suggesting that pharmacological antagonists might constitute useful reagents to treat obesity.

Results: The RNAi protocol specifically reduced hypothalamic expression of AGRP mRNA by 50% and resulted in reduction of AGRP peptide immunoreactivity. Physiologically, the reduction in AGRP levels was associated with increased metabolic rate and reduced body weight without changes in food intake.

Conclusion: AGRP can function to increase body weight and reduce metabolic rate without influencing food intake. The present study demonstrates that RNAi protocols can be used to assess physiological function of neuronal genes *in vivo*.

Background

Agouti-related peptide (AGRP) gene expression is elevated by fasting and in obesity due to leptin insufficiency [1,2], while reversal of obese phenotypes by adrenalectomy reverses the elevation of AGRP mRNA [3]. Injections of synthetic analogs of AGRP, and of AGRP itself, also stimulate food intake and body weight [4,5]. Together with the observation that transgenic over-expression of the AGRP

gene leads to hyperphagia and obesity [1], these data suggest that antagonism of AGRP may reduce food intake and body weight, thus potentially serving as a therapy for obesity.

RNAi produces sequence-specific reduction of gene expression in various mammalian *in vitro* systems [6] and most recently, RNAi was shown to suppress the expression

a. Synthetic siRNA against AGRP:

5'-CUGAGUUGUGUUUCUGCUUGTT-3'
3'-TTGACUCAACACAAGACGACAAC-5'

b. Representative Northern blot bands

	GFPi	AGRPI
(cont'l)	(exp't)	

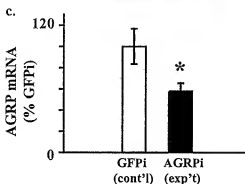


Figure 1

Small interfering RNA (siRNA) particles decreases AGRP mRNA. (a) Synthetic siRNA particle designed against AGRP mRNA. (b) Representative bands from the Northern blot 24 hours after injection shows decreased levels of AGRP mRNA in the group injected with AGRP-siRNA particle compared to the control GFPi-siRNA injections. (c) Quantification of the Northern blot results yields a statistically significant decrease in expression of 50% with the AGRP-siRNA particle. Data are expressed as a mean percentage \pm SEM of GFPi mRNA levels ($n = 16$; $p < 0.05$).

and activity of a luciferase transgene in adult mice [7], suggesting that RNAi may become a valuable molecular and possibly clinical tool for use *in vivo*. A major advantage of RNAi over a similar protocol, using antisense oligonucleotides, is that the use of antisense oligonucleotides to assess chronic effects requires constant or repetitive infusion, is expensive and generally impractical for more than a few days. In contrast, RNAi can be used to study long-term phenotypes (including body weight and memory functions) due to the development of a DNA plasmid-based system to deliver short double-stranded RNA sequences *in vivo*[8]. While RNAi has been extensively used to assess physiological functions of specific genes in *C. elegans* and *Drosophila* [9,10] and a single recent paper has reported that RNAi can reduce gene expression *in vivo* (in liver) [7], the applicability of RNAi to assess physiological

or neuronal function in mammals has not yet been demonstrated.

Here we show, using both small interfering RNA (siRNA) particles and the plasmid based RNAi delivery system, pSUPER-RNAi, that decreasing endogenous hypothalamic AGRP levels in the central nervous system leads to significant physiological responses including an increase in metabolic rate and a decrease in body weight.

Results and Discussion

Effects of small interfering RNA particles against AGRP

SiRNA particles against both AGRP and GFP were designed based on reports by Elbashir et al. [6] (Fig. 1a). Injection of these siRNA particles into the arcuate nucleus of the hypothalamus reduced AGRP mRNA about 50% 24 hours after injection, compared to the control group injected with siRNA particles targeted to GFP (Fig. 1b and 1c). The 50% decrease in expression level is similar to previously reported effects of RNAi to reduce gene expression from 40–80% both *in vitro*[6] and *in vivo*[7] in mammalian systems. Since the construct targeted to AGRP reduced AGRP expression relative to the construct targeted to GFP, this result indicates specific down-regulation by the AGRP RNAi construct.

The decrease in AGRP mRNA was associated with a striking increase in metabolic rate. Both heat production (Fig. 2a; $p < 0.0001$) and oxygen consumption, VO_2 (Fig. 2b; $p < 0.0003$) were elevated one day after infusion of the AGRPi construct. Metabolic rate continued to be elevated during day 2 (heat production $p < 0.0001$; VO_2 $p < 0.0494$). However, by 3 days after infusion, metabolic rate returned to control levels. This result indicates that AGRP normally acts to reduce metabolic rate, consistent with conclusions from indirect evidence based on pair-fed animals treated with AGRP [11].

The decrease in AGRP mRNA and increase in metabolic rate was associated with a trend to decrease body weight, but this effect was not significant over the 48 hours after injection (body weight loss of -1.72 ± 0.66 g for the GFPi control mice compared to a loss of -2.85 ± 0.52 g for the AGRPi mice). Surprisingly, decrease in AGRP mRNA did not significantly influence food intake compared to controls (mean intake of 5.0 ± 0.7 g/day for the GFPi control mice compared to 5.3 ± 0.6 g/day for the AGRPi mice). Since both the AGRPi and the control GFPi mice were still recovering from the effects of the surgery and anesthesia at 48 hours, it is not surprising that the effects on body weight were not statistical at this time. Nevertheless the lack of an effect on food intake was unexpected since treatment with synthetic AGRP peptides has profound effects on food intake [4,5].

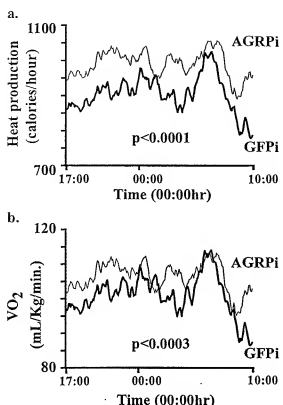


Figure 2
Reducing AGRP levels with siRNA increases metabolic rate. (a) Heat production for AGRP-siRNA injected mice was found to be significantly and dramatically elevated one day following surgery compared to the control injected GFP-siRNA mice ($n = 16$; $p < 0.0001$). (b) Oxygen consumption, VO_2 , was also significantly elevated one day after surgery for mice injected with the AGRP-siRNA particles ($n = 16$; $p < 0.0003$).

Effects of the plasmid based RNAI protocol against AGRP
Since it was anticipated that double-stranded RNAI particles, like antisense oligonucleotides, would produce only very transient reduction in mRNA levels, and indeed the effect on physiological function was only transient, we next assessed effects of AGRP RNAI using a plasmid-based system, pSUPER [8] (Fig. 3a), which leads to the transcription of a short double stranded RNA product with a hairpin loop *in vivo*. Using luciferase as a reporter we observed that liposome-mediated transfection of plasmids into brain parenchyma allows significant gene expression for more than one week after infusion [12]. Transfection of neurons in the arcuate nucleus of the hypothalamus led to a decrease in AGRP peptide immunoreactivity, whereas transfection with the control plasmid targeted to GFP had

no effect on AGRP immunoreactivity (Fig. 3b,3c). The effect of RNAI to reduce AGRP gene expression was therefore also associated with decreased expression of the AGRP peptide.

The persistent effect of the pSUPER vector to reduce the levels of AGRP peptide was associated with a significant reduction in body weight that persisted over six days (Fig. 4a; $p < 0.0001$). While the control group recovered body weight initially lost due to surgery, the pSUPER-AGRPI group did not regain the body weight lost. In contrast, as with the double-stranded RNAI construct, infusion of the plasmid-based AGRP RNAI construct did not significantly reduce food intake compared to infusion of the plasmid-based GFP RNAI construct (Fig. 4b; $p = 1.6992$). Food intake was minimal immediately following surgery, however, both groups of mice recovered to consume four to five grams of food per day. The loss of body weight, without changes in food intake is consistent with increases in metabolic rate observed with the siRNA protocol. This result supports the hypothesis that tonic hypothalamic AGRP reduces metabolic rate independent of food intake, and indeed that metabolic rate may be even more dependent on AGRP tone than is food intake.

Conclusions

In summary, the present report represents the first demonstration that RNA interference can be used to reduce expression of an endogenous gene in adult mammals. This protocol has allowed us to assess the physiological function of an endogenous neuronal gene. This study also directly indicates that hypothalamic AGRP regulates metabolic rate. The observation that reduction of AGRP mRNA would produce more profound effects on metabolic rate than on food intake was surprising since infusion of AGRP peptide produces profound effects on food intake [4,5]. However, since neither AGRP mRNA nor peptide was completely ablated, it seems likely that effects on food intake would become more apparent with a more dramatic manipulation. Although ablation of the AGRP gene was reported to have no effect on metabolic phenotype [13], our results suggest that complete ablation of the gene may have produced metabolic compensation. Thus reducing (but not ablating) AGRP expression in adult mice may have identified a metabolic role for AGRP not apparent from complete ablation of the gene, suggesting that agents antagonizing the effect of AGRP may be useful to treat obesity without producing unacceptable loss of appetite. Consistent with previous findings in mammalian systems [6–8] and unlike other systems such as *C. elegans* and *Drosophila* [9,10], RNAI reduced but did not eliminate expression of AGRP. However, improvements in delivery systems, especially in conjunction with viral-based gene transfer protocols [14], could result in greater and even longer-term reduction of target gene expression

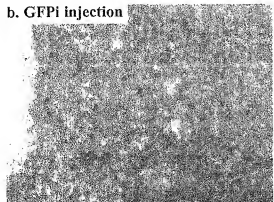
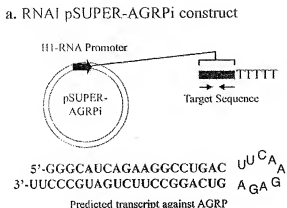


Figure 3
pSUPER-AGRPI construct decreases AGRP immunoreactivity. (a) Overall design of the pSUPER-RNAI plasmid construct targeted against AGRP and the predicted transcript with the hairpin loop. (b and c) Immunocytochemistry of fasted mice transfected with the (b) control pSUPER-GFPi vector compared to (c) mice transfected with the pSUPER-AGRPI vector shows decreased AGRP immunoreactivity with the RNAI plasmid construct targeted to AGRP.

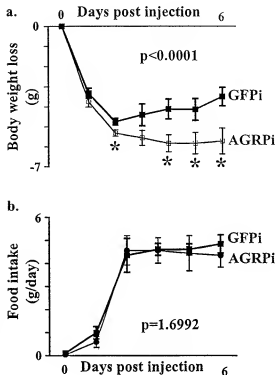


Figure 4
Decreasing AGRP levels by pSUPER-AGRPI construct decreases body weight (a) Mice transfected with the pSUPER-AGRPI construct shows persistent loss of body weight after transfection while the mice transfected with the control vector recover body weight over a course of six days ($n = 14$; $p < 0.0001$). (b) pSUPER-RNAI targeted to AGRP has no effect on mean daily food intake ($n = 14$; $p = 1.6992$).

suggesting that RNAi will prove to be a useful tool to assess physiological functions of mammalian genes *in vivo*, especially those expressed in the brain, as RNAi has been so useful in functional mapping of genes in non-mammalian systems.

Methods

Animal and RNAI protocols

The appropriate Institutional Animal Review Board had approved all studies. To study the effects of RNAi, C57BL/6J mice retired breeders were obtained from The Jackson Laboratory (Bar Harbor, ME). Mice were individually housed with free access to food and water under 12:12 h light-dark cycle (lights on at 07:00 h). Stereotaxic surgery was performed under anesthesia (2.5% 2-2-2-tribromoethanol, 0.015–0.017 ml/g body weight, i.p.). The RNAI constructs were injected bilaterally using a 1 ul

Hamilton syringe placed on a stereotaxic frame into the following coordinates from bregma: anterior-posterior -0.12; lateral \pm 0.02; vertical -0.6. Double-stranded siRNA particles to reduce expression of AGRP were designed based on Elbashir et al. [6] (Fig. 1a). The siRNA oligonucleotides were designed from the beginning of exon 1 of both AGRP and CFP genes and ordered gel-purified and annealed from Oligos Etc. (Wilsonville, OR). SIRNA particles were re-suspended in RNase-free water to a concentration of 1 mM and 0.5 μ l was injected over 2 minutes by stereotaxic surgery bilaterally. The pSUPER-RNAI plasmid constructs were re-suspended in lipofectin (Invitrogen Corp. Carlsbad, CA) to a concentration of 1 μ g/ μ l, and 1 μ l of the mixture was injected bilaterally over five minutes using the same coordinates as for the siRNA particles. Body weight and food intake was monitored daily.

Metabolic rate was monitored continuously by indirect calorimetry for three days following surgery. Air from each cage was sampled every five minutes, and oxygen and carbon dioxide concentrations from each sample were measured independently. From the change in oxygen, VO_2 or oxygen consumption can be calculated after normalizing to body weight. Heat production can then be calculated using the following formula: Heat (cal/hour) = $((4.33 + 0.67 \times (\text{VCO}_2/\text{VO}_2)) \times \text{VO}_2 \times (\text{Body weight}) \times 60$). Therefore, the parameter VO_2 is normalized to body weight, whereas heat production is not normalized to body weight.

For Northern blot analysis, all mice were sacrificed toward the end of the light period (between 17:00 and 19:00 h) by decapitation after a brief exposure to carbon dioxide. Brains were quickly removed and the hypothalamus was dissected out, frozen on dry ice and stored at -70°C until use. For immunocytochemistry, mice were perfused with cold PBS followed by 4% paraformaldehyde. Brains were removed, post-fixed in paraformaldehyde then preserved in 30% sucrose solution for 48 hours.

Northern blot analysis

Total RNA was extracted from tissue using TRIzol (GIBCO BRL, Gaithersburg, MD). Concentration of the samples were measured by UV spectrophotometer and normalized to 1 μ g/ μ l. Uniform concentration and integrity of the samples were verified by agarose gel electrophoresis prior to Northern blot analysis. Six micrograms of total RNA from hypothalamus was subjected to Northern blot analysis, as described previously, to measure AGRP mRNA [15,16,2,3]. Briefly, RNA was denatured by incubating with glyoxal and dimethyl sulfoxide for 1 hour at 50°C and separated on a 1.5% agarose 10 mM NaPO₄ (pH = 7.0) gel for 1 hour at 100 V. The RNA was then transferred to an Immobilon S (Millipore) membrane by capillary elution overnight in 20 \times standard saline citrate (SSC)

buffer. Membranes were briefly washed in 6 \times SSC, baked at 80°C and cross-linked by UV light. The membranes were prehybridized in Ultrahyb buffer (Ambion) at 68°C for 2 hours and hybridized overnight with 3.5×10^6 DPM/ml of probe at 42°C. The blots were probed with single-stranded internally labeled DNA probe as described previously [17]. The membranes were washed twice in 1 \times SSC/0.1% SDS solution for 15 minutes at room temperature, followed by 0.1 \times SSC/0.1% SDS solution for 15 minutes at room temperature twice and then for 3 hours at 42°C. The membranes were then exposed to phosphoimager screen overnight. The total integrated densities of hybridization signals were determined by phosphoimager (STORM 860, Molecular Dynamics, Sunnyvale, CA). To monitor RNA loading, membranes were re-probed and hybridized with a ³²P-labeled probe encoding 18S ribosomal RNA.

Immunocytochemistry

Cryopreserved brains were cut to a thickness of 30 μ m in a cryostat at -20°C and stored in PBS-B buffer (10 mM PO₄ in 0.9% NaCl) containing 0.1% sodium azide at 4°C. Immunocytochemistry was performed with a rabbit polyclonal primary antibody to AGRP peptide diluted 1 to 10,000 (Phoenix Pharmaceuticals, Belmont, CA) followed by Vectastain ABC kit (Vector Laboratories, Burlingame, CA). The immunoreactivity was visualized with the Vector VIP kit (Vector Laboratories, Burlingame, CA). Sections were mounted on microscopic slides, air-dried and cover slipped with VectaMount (Vector Laboratories, Burlingame, CA).

Statistical Analysis

Statistical analysis for the Northern blot was performed by student's t-test, using the JMP statistical package implemented on the Macintosh operating system. A p-value of less than 0.05 was considered significant. For the analysis of the metabolic cage data, a two-way ANOVA (time \times RNAI construct) was performed using the JMP statistical package. For analysis of food intake and body weight, a two-way ANOVA (time \times RNAI construct) followed, where indicated, by student's t-test ($p < 0.05$ was considered significant) was performed to compare each independent time point.

Authors' contributions

HM participated in the design and coordination of the study, implemented the molecular biological cloning of the RNAI constructs, carried out the animal protocols, processed the tissues, performed Northern blot analysis and immunocytochemistry, performed statistical analysis and drafted the manuscript. TMM participated in the design of the study and the animal protocols. JWM participated in the animal protocols and immunocytochemistry. RA provided the pSUPER construct and provided useful

discussion. CVM conceived of the study, participated in the design and coordination of the study and drafted the manuscript.

All authors read and approved the final manuscript.

Acknowledgements

The authors would like to thank I-Wei Shu for his expertise in immunocytochemistry and Chintia L. Pullin for her help in cloning.

References

- Ollmann MM, Wilson BD, Yang YK, Kerns JA, Chen Y, Gantz I, Barsh GS: Antagonism of central melanocortin receptors in vitro and in vivo by agouti-related protein. *Science* 1997, 278(5335):135-138.
- Mizuno TM, Mobbs CV: Hypothalamic agouti-related protein messenger ribonucleic acid is inhibited by leptin and stimulated by fasting. *Endocrinology* 1999, 140(2):814-817.
- Makimura H, Mizuno TM, Roberts J, Silverstein J, Beasley J, Mobbs CV: Adrenalectomy reverses obese phenotype and restores hypothalamic melanocortin tone in leptin-deficient ob/ob mice. *Diabetes* 2000, 49(11):1917-1923.
- Fair W, Boston BA, Kesterson RA, Hobby VJ, Cone RD: Role of melanocortinergic neurons in feeding and the agouti obesity syndrome. *Nature* 1997, 389(6651):165-169.
- Rossi M, Kim MS, Morgan DG, Small CJ, Edwards CM, Sunter D, Abu-shanab S, Copley RR, AP, Russell SH, Stanley SA, Smith DM, Yagle K, Ghatei MA, Bloom SR: A C-terminal fragment of Agouti-related protein increases feeding and antagonizes the effect of alpha-melanocyte stimulating hormone in vivo. *Endocrinology* 1998, 139(10):4428-4431.
- Elshabani SM, Harborth J, Lendeckel W, Yalcin A, Weber K, Tuschl T: Duplexes of 2'-nucleotide RNAs mediate RNA interference in cultured mammalian cells. *Nature* 2001, 411(6834):494-498.
- McCaffrey AP, Meiss L, Pham T-TT, Conklin DS, Hannon GJ, Kay MA: RNA Interference In Adult Mice. *Nature* 2002, 418(July):38-39.
- Brummelkamp TR, Bernards R, Agami R: A system for stable expression of short interfering RNAs in mammalian cells. *Science* 2002, 296(5567):S50-S53.
- Fire A, Xu S, Montgomery MK, Kostas SA, Driver SE, Mello CC: Potent and specific genetic interference by double-stranded RNA in *Caenorhabditis elegans*. *Nature* 1998, 391(6669):806-811.
- Misquita L, Paterson BM: Targeted disruption of gene function in *Drosophila* by RNA interference (RNA-i): a role for nauvatus in embryonic somatic muscle formation. *Proc Natl Acad Sci USA* 1999, 96(4):1451-1456.
- Small CJ, Kim MS, Stanley SA, Mitchell JR, Murphy K, Morgan DG, Ghatei MA, Bloom SR: Effects of chronic central nervous system administration of agouti-related protein in pair-fed animals. *Diabetes* 2001, 50(2):248-254.
- Katsel PL, O'Connell B, Mizuno TM, Mobbs CV, Greenstein RJ: Liposomes mediated gene transfer into GH3 cells, and rat brain, liver and gut: comparison of different polar or aliphatic domains. *Int J Surg Res Biol* 2000, 1(5):415-426.
- Qian S, Chen JY, Weinger M, Trambauer ME, Novi DE, Guan X, Yu H, Shen Z, Fehling Y, Frazier E, Chen A, Camacho RE, Shearman LP, Goparaju S, MacNeil DJ, Van der Ploeg LH, Marsh DJ: Neither agouti-related protein nor neuropeptide Y is critically required for the regulation of energy homeostasis in mice. *Mol Cell Biol* 2002, 22(14):5027-5035.
- Kapitz MG, Makimura H: Defective viral vectors as agents for gene transfer in the nervous system. *J Neurosci Methods* 1997, 71(1):125-132.
- Mizuno TM, Kleopoulos SP, Bergen HT, Roberts JI, Priest CA, Mobbs CV: Hypothalamic pro-opiomelanocortin mRNA is reduced by fasting and in ob/ob and db/db mice, but is stimulated by leptin. *Diabetes* 1998, 47(2):294-297.
- Mizuno TM, Makimura H, Silverstein J, Roberts JL, Lopincio T, Mobbs CV: Fasting regulates hypothalamic neuropeptide Y, agouti-related peptide, and proopiomelanocortin in diabetic mice independent of changes in leptin or insulin. *Endocrinology* 1999, 140(10):4551-4557.
- Mizuno TM, Bergen H, Funabashi T, Kleopoulos SP, Zhong YG, Bau-man WA, CV Mobbs: Obese gene expression: reduction by fasting and stimulation by insulin and glucose in lean mice, and persistent elevation in acquired (diet-induced) and genetic (yellow agouti) obesity. *Proc Natl Acad Sci USA* 1996, 93(8):3434-3438.

Publish with **BioMed Central** and every scientist can read your work free of charge

"BioMedCentral will be the most significant development for disseminating the results of biomedical research in our lifetime."

Paul Nurse, Director-General, Imperial Cancer Research Fund

Publish with BMC and your research papers will be:

- available free of charge to the entire biomedical community
- peer reviewed and published immediately upon acceptance
- cited in PubMed and archived on PubMed Central
- yours - you keep the copyright

Submit your manuscript here:
<http://www.biomedcentral.com/submit/>



editorial@biomedcentral.com

EXHIBIT 10

Inhibition of HPV 16 E6 oncogene expression by RNA interference *in vitro* and *in vivo*

X.-Y. NIU*, Z.-L. PENG*, W.-Q. DUAN†, H. WANG* & P. WANG*

*Department of Obstetrics and Gynecology, Sichuan University Huaxi the Second Hospital, Chengdu, Sichuan Province, China; and †Department of Burn and Plastic, Huaxi Hospital of Sichuan University, Chengdu, Sichuan Province, China

Abstract. Niu X-Y, Peng Z-L, Duan W-Q, Wang H, Wang P. Inhibition of HPV 16 E6 oncogene expression by RNA interference *in vitro* and *in vivo*. *Int J Gynecol Cancer* 2006;16:743–751.

Substantial studies have demonstrated that the initiation and progression of cervical cancer were closely associated with human papillomavirus (HPV) E6 and E7 oncogenes. The therapeutic strategy with ribozyme or antisense oligonucleotides to inhibit the expression of HPV E6 or E7 oncogenes showed effect to some degree, but problems such as low efficiency, short-period maintenance, and high cost still remain. The aim of this study was to investigate *in vitro* and *in vivo* the effect of HPV 16 E6 small interfering RNA (HPV 16 E6 siRNA) on cervical cancer cell line CaSki cells. The specific siRNA of HPV 16 E6 was synthesized and transfected into CaSki cells by liposome. The number of apoptotic cells, HPV 16 E6 messenger RNA (mRNA) level, and E6 protein expression were measured before and after the transfection by flow cytometry, reverse transcriptase–polymerase chain reaction, and Western blot, respectively. Cervical cancer in nude mice was established, and siRNA was injected directly into the nude mice peritoneal cavity or subcutaneous tumor. The efficiency of siRNA was evaluated by tumor volume change, HPV 16 E6 protein expression, and apoptosis of tumor cells. Apoptosis rate of CaSki cells at days 1, 2, 5, and 9 after siRNA transfection were 7.7%, 11.8%, 37.4%, and 12.6%, respectively. The mRNA level of HPV 16 E6 at the same time points were reduced by 77%, 83%, 59%, and 41%, respectively. But the mRNA level of β-actin, as an internal control, showed no significant change. The inhibition rates of E6 protein synthesis at days 1, 2, 5, and 9 after the transfection were 79.7%, 80.4%, 71.3%, and 57.4%, respectively, whereas the protein levels of Lamin A/C, as internal control, had no change. *In vivo*, E6 siRNA administration groups showed a dramatic effect in inhibiting tumor growth, suppressing expression of E6 protein, and inducing tumor necrosis and apoptosis as compared with the control group. Direct injection of siRNA into subcutaneous tumor resulted in tumor suppression effect similar to that via the peritoneal cavity, and with additional injection better results could be achieved in cervical cancer CaSki cells. RNA interference exists, and the interference to HPV 16 E6 is specific and highly efficient both *in vitro* and *in vivo*.

KEYWORDS: CaSki cell, cervical cancer, gene therapy, HPV 16 E6, RNA interference.

Several studies suggested that the initiation and the progress of malignant progression in human cervical cancer were closely linked with high-risk types of human papillomavirus (HPV), namely HPV 16 and HPV 18. Among them, HPV 16/18 E6/E7 have been recognized as oncogenes, which could downregulate antioncogene p53, activate telomerase, hold the pro-

duction of interferon, add the integration and mutation of exogenous genes, inhibit programmed cell death, and make cell eternity^[1,2]. Over recent years, antisense oligonucleotides of HPV E6/E7 have been transfected into cervical cancer cells by virus to upregulate p53, release cytochrome c into cytoplasm, activate procaspase-9 and procaspase-3, inhibit the activity of telomerase, and induce cell apoptosis; as a result, tumor cells appear to stop dividing rapidly and revert to a normal state. However, this technique was not as good as expected, having problems such as low efficiency, short-period maintenance, and high cost^[3–5].

Address correspondence and reprint requests to: Niu Xiao-Yu, MD, Department of Obstetrics and Gynecology, Sichuan University Huaxi the Second Hospital, Ren Ming Nan Lu San Duan 20, Chengdu, Sichuan Province 610041, China. Email: clemay@sohu.com

RNA interference (RNAi) has recently been recognized as a powerful weapon to inhibit gene expression, in which double-stranded RNA targets homologous messenger RNA (mRNA) sequence for endonucleolytic cleavage and degradation^(6,7). This process was originally discovered to exist in diverse species of living organisms and could be inherited in non-mammalian system, including plants, *Caenorhabditis elegans*, and *Drosophila*^(8,9). Later on, a further study indicated that it could lead to posttranscriptional gene silence in mammalian system by RNA duplexes of 21–23 nucleotides (called siRNA), and the effect was several orders of magnitude higher than using antisense or ribozyme^(7,10–12). RNAi distributes widely and specifically inhibits gene expression. It provides a simple and cost-effective method. In addition, RNAi has more potential for high-throughput analysis of gene function in the postgenomic era^(12,13).

However, experiences are not enough in this new technology. Our current study was to investigate whether interfering HPV 16 E6 transcription by RNAi could lead to the silence of the oncogene, thus reverse the HPV infection, and prevent or stop the progression of cervical cancer.

Materials and methods

Cell culture and transfection

Human cervical cancer cell line CaSki (purchased from Classic Specimen Culture and Storage Centre in Wuhan University) contains about 600 copies of integrated HPV 16 genome. CaSki cells were cultured in Roswell Park Memorial Institute 1640 plus 10% fetus calf serum at 37°C in 5% CO₂ for 4–5 days and then trypsinized and subcultured at 5 × 10⁵ cells per well into six-well tissue culture plates. After 48 h of culture, the cells were transfected with HPV 16 E6 siRNA formulated into liposomes according to the manufacturer's instructions (TransMessenger™, Qiagen, Valencia, CA). siRNA concentration was 0.5 µg per well, and the final volume of culture medium was 2 mL per well. The cells were harvested for analysis at days 1, 2, 5, and 9 after the transfection, respectively. The experiment at each time point was executed three times in parallel.

Measurement of apoptosis

Apoptotic cells at various time points indicated above, before, and after the transfection were identified by the use of flow cytometry (Elite Type, Coulter, Fullerton, CA) following the manufacturer's protocol.

RNA preparation and mRNA quantification

Twenty-one-nucleotide RNAs were synthesized and purified via polyacrylamide gel electrophoresis by Proligo (Paris, France). The negative control of HPV 16 E6 siRNA was also synthesized (the nucleotide bases were arranged randomly and do not share sequence similarity with the exons of any human genes). Sequences of siRNA were as follows: HPV 16 E6 sense strand: 5'-CUGUUCGUUGCAGUACACATT-3'; anti-sense strand: 5'-UGUGUACUGCAAGAACAGTT-3'; negative control sense strand: 5'-GCUUUGGUGUACAUCCAATT-3'; antisense strand: 5'-UUGGAUGUACACCAAGACTT-3'.

Total cellular RNA was extracted using the RNeasy Kit (Takara, Shiga, Japan). For reverse transcriptase-polymerase chain reaction, the Access RT-PCR System (Promega, Beijing, China) was used. Reverse transcription was carried out with 0.5 µg total RNA. For E6 mRNA amplification, the primers 5'-TCA AAA GCC ACT GTG TCC TG-3' and 5'-CGT GTT CTT GAT GAT CTG CA-3' were used with the following parameters for amplification: 45 min at 48°C; 2 min at 94°C; followed by 40 cycles of 30 s at 94°C, 1 min at 58°C, and 2 min at 68°C; with the last cycle concluding with a reaction 7 min at 68°C.

Protein measurement

The changes of protein expression at various time points was detected by Western blot analysis before and after HPV 16 E6 siRNA transfection. After the cell pellets were added with 1× sodium dodecyl sulphate sample buffer, protein fractions obtained were resolved on 12% sodium dodecyl sulphate-polyacrylamide gel electrophoresis gels and then the gels were electroblotted onto nitrocellulose membrane for visualization by immunostaining. Anti-HPV 16 E6 primary antibody (diluted 1:500, Santa Cruz, Santa Cruz, CA) and the secondary antibody (diluted 1:1000, Santa Cruz) were used.

Flow cytometry was used to quantify a change in protein expressions at days 1, 2, 5, and 9 before and after HPV 16 E6 siRNA transfection.

Inhibiting rate of protein expression was calculated by the following formula: (1 – [the fluorescent level of protein after transfection-negative control]/[the fluorescent level of protein before transfection-negative control]) × 100%.

In vivo studies

Twenty female nude mice, aged 4–6 weeks, were purchased from the Animal Center of Sichuan University

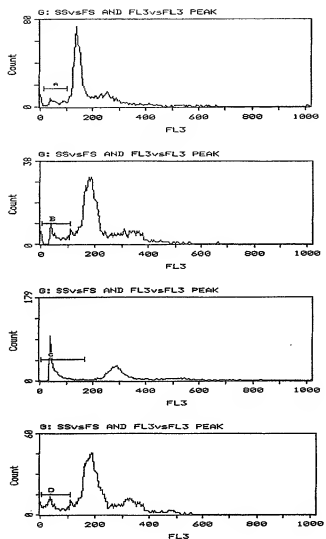


Figure 1. The cellular apoptosis at various times after HPV 16 E6 siRNA transfection (A, B, C, D represented the apoptotic peaks of 24 h, 48 h, fifth, and ninth day after transfection).

Huaxi Medical Center. The mice were divided into five groups, each of which consisted of four mice.

A total of 5×10^6 CaSkI cells were injected into the subcutaneous tissue of the right front limb of a mouse. Four weeks later, the tumor mass, which grew to approximately 2121 mm^3 in diameter, was collected from which pieces 2 mm in diameter were cut. Each piece of the tumor was transplanted into the subcutaneous tissue of a new mouse's right front limb. Two weeks later, the volumes of all the tumors reached approximately $130-150 \text{ mm}^3$ in diameter (the tumor volume was calculated by the following formula: $V = \pi/6 \times \text{longest diameter} \times \text{shortest diameter}^2$); then the injection experiments were carried out in each group outlined as follows.

Control group: Two mice were given injection directly into peritoneal cavity, the other two were injected into subcutaneous tumor, and the injection fluid was negative control siRNA 2 μg in a solution of 12 μL TransMessenger Transfection Reagent.

Experimental group 1: HPV 16 E6 siRNA 2 μg in a solution of 12 μL TransMessenger Transfection Reagent was injected into the peritoneal cavity of the mice for 5 days and then the tumor was cut off for tests.

Experimental group 2: HPV 16 E6 siRNA 2 μg in a solution of 12 μL TransMessenger Transfection Reagent was injected into the peritoneal cavity of the mice for 12 days and then the tumor was cut off for tests.

Experimental group 3: HPV 16 E6 siRNA 2 μg in a solution of 12 μL TransMessenger Transfection Reagent was injected into the subcutaneous tumor of the mice for 5 days and then the tumor was cut off for tests.

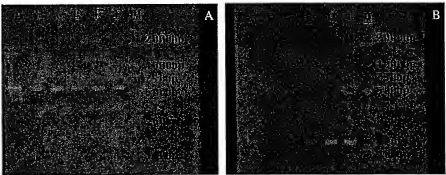


Figure 2. RT-PCR results of HPV 16 E6 and β -actin before and after HPV 16 E6 siRNA transfection into CaSkI cells. A: RT-PCR result of β -actin mRNA as internal control. Bands at 587 bp are β -actin. (A: 24 h after transfection; B: 48 h after transfection; C: 5 d after transfection; D: 9 d after transfection) E: HPV 16 E6 siRNA negative control; F: before transfection; M: DL2000 marker. B: RT-PCR result of HPV 16 E6 mRNA. Bands at 120 bp are HPV 16 E6 (A: 24 h after transfection; B: 48 h after transfection; C: 5 d after transfection; D: 9 d after transfection; E: HPV 16 E6 siRNA negative control; F: before transfection; M: DL2000 marker)



Figure 3. HPV16 E6 protein expressions at various times before and after E6 siRNA transfection in Western blot. Lamin A/C as the internal control. (C/c: 24 h after transfection; D/d: 48 h after transfection; E/e: fifth day after transfection; F/f: ninth day after transfection; A/a: E6 siRNA negative control; B/b: before E6 siRNA transfection.)

Experimental group 4: HPV 16 E6 siRNA 2 μ g in a solution of 12 μ L TransMessenger Transfection Reagent was injected into the subcutaneous tumor twice, with a 5-day interval between the injections, and then 7 days after the second injection, the tumor was cut off for consecutive tests.

The transfection agent was dissolved in a solution of 500 μ L Roswell Park Memorial Institute 1640 without antibiotic and serum and injected directly into the peritoneal cavity of the mice or the solution of 100 μ L injected directly into the tumor. In different groups, we measure a tumor size on the 3rd, 5th, 10th, and 12th day after the injection of SiRNA and also cut off the tumor at day 5 or day 12 for histopathologic examination according to the design of different groups.

Immunohistochemistry (IHC) in tumor tissue of mice was carried out using biotin peroxidase complex (SAB)

method. When doing semiquantitative analysis of HPV 16 E6 positive cells, five images ($\times 200$) of each slide were collected by the CCD Camera. The index of opacity density was used as a parameter to evaluate the E6 positive expression in different groups. Apoptosis of tumor cells coming from the treated mice was measured by terminal deoxynucleotidyl transferase-mediated dUTP nick-end labeling using *In Situ* Cell Death Detection Kit (Roche, Shanghai, China). During the process, fluorescence images of apoptotic tumor cells were taken to calculate the mean apoptotic cells based on ten fields ($\times 100$).

Statistical analysis

Statistical analysis was performed by using SPSS software (version 10.0) for *t* test, linear regression, correlation, and one-way ANOVA. Statistical significance

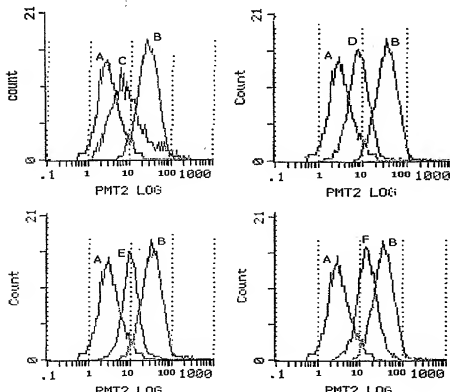


Figure 4. HPV 16 E6 protein expressions at various times before and after E6 siRNA transfection to CaSki cells. (A: negative control; B: E6 protein before transfection; C: E6 protein at 24 h after transfection; D: E6 protein at 48 h after transfection; E: E6 protein at fifth day after transfection; F: E6 protein at ninth day after transfection.)

Table 1. HPV 16 E6 protein expressions at various time points before and after E6 siRNA transfection into CaSkI cells

	Before transfection (n = 3)	Negative control (n = 3)	24 h after transfection (n = 3)	48 h after transfection (n = 3)	Fifth day after transfection (n = 3)	Ninth day after transfection (n = 3)
PFD (M ± SD)	27.8 ± 3.18	3.52 ± 1.30	8.45 ± 2.84	8.27 ± 1.21	10.5 ± 2.62	13.8 ± 2.17
PIR (%)	—	—	79.7 ± 2.93	80.4 ± 1.49	71.3 ± 2.77	57.4 ± 2.31

PFD, protein fluorescent density; PIR, protein inhibiting rate.

was accepted when the probability of occurrence by chance was <0.05.

Results

Apoptosis after HPV16 E6 siRNA transfection

There was a steady increase in the apoptotic rates from days 1 and 2 to day 5 (7.7%, 11.8%, and 37.4%, respectively) after transfection. On day 9, the apoptotic rate decreased to 12.6% (Fig. 1).

The HPV 16 E6 mRNA expression after siRNA transfection

Both experimental samples and negative control for the HPV 16 E6 mRNA expression before E6 siRNA transfection were about the same level. The HPV 16 E6 mRNA at days 1, 2, 5, and 9 after transfection was reduced by 77%, 83%, 59%, and 41%, respectively. But the mRNAs of β-actin, as internal control, have no change (estimated from densitometry, see Fig. 2).

The HPV 16 E6 protein expressions after siRNA transfection

The HPV 16 E6 protein expressions in Western blot were dramatically reduced at days 1, 2, 5, and 9 after E6 siRNA transfection, while the protein expression at 48 h reached the lowest level. Later on, the E6 protein levels gradually raised again. Both experimental samples and negative control before the transfection showed the same protein expression level. The protein expressions of Lamin A/C, as internal control, have no change (Fig. 3).

HPV 16 E6 protein level before and after the transfection were also measured by flow cytometry. The inhibiting rates of E6 protein expression after the transfection were over 70% at days 1, 2, and 5, while the inhibiting rate of E6 protein at day 9 was reduced but still over 50% (Fig. 4 and Table 1).

The changes of tumor volume

Table 2 and Figure 5 showed the changes of tumor volumes in different groups, and Table 3 showed the linear regression and correlation between tumor volume and time of injection. The tumor volumes of the four experimental groups were obviously inhibited, whereas tumor volume of the control group grew fast. The tumor volume and time of injection showed a strong correlation (Table 3). The result of regression analysis revealed the inhibiting effects of five groups in the following orders: group 4 > group 1 > group 3 > group 2 > control group. The regression coefficient of the four experimental groups differed significantly from that of control group ($P < 0.05$). In addition, among the four experimental groups, only group 4 was differing from each of three others ($P < 0.05$).

Pathologic changes

Experimental groups showed a greater degree of tumor necrosis compared to control group on hematoxylin-eosin staining results. The slices of mice liver did not show abnormal in all groups, which suggested that no obvious toxic reactions were induced for the route of administration, dosage, and time interval.

HPV 16 E6 positive reaction was seen in tumor tissue, which exhibited accumulated brown particles

Table 2. The tumor volume changes of different groups before and after injection

Tumor volume (mm ³)	Control group (n = 4)	Group 1 (n = 4)	Group 2 (n = 4)	Group 3 (n = 4)	Group 4 (n = 4)
Before inj.	131.94 ± 12.14	179.59 ± 10.22	150.79 ± 17.65	176.97 ± 22.16	205.64 ± 13.33
3 days after inj.	236.23 ± 18.36	196.32 ± 12.66	198.84 ± 20.12	231.27 ± 18.23	259.66 ± 14.26
5 days after inj.	520.19 ± 23.67	264.88 ± 14.18	241.14 ± 16.38	294.69 ± 31.32	262.12 ± 20.17
10 days after inj.	1123.56 ± 45.98		318.12 ± 12.29		289.13 ± 28.41
12 days after inj.	1358.91 ± 61.17		382.36 ± 25.45		302.48 ± 33.72

inj., injection.

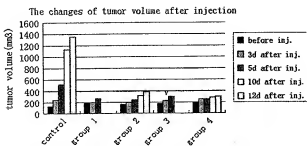


Figure 5. The changes to tumor volume before and after injection.

appearing in cell nucleus by IHC. The E6 expression of the control group was uneven in staining, with 70% of cells positive, whereas only 20% of cells were positive in group 2, and almost all cells were negative in groups 3, 4, and 5 (Fig. 6). Images were recorded and analyzed using an image analyzing software, and index of opacity density was calculated ($\times 400$, 20 fields in total). One-way ANOVA was used to compare between groups among five groups (Table 4). Significant difference was observed when the experimental groups were compared with the control group ($P < 0.05$), but there was no difference among the four experimental groups ($P > 0.05$).

Figure 7 showed apoptosis in tumor tissue measured by terminal deoxynucleotidyl transferase-mediated dUTP nick-end labeling (green fluorescence spots were apoptotic cells). The mean apoptotic cells were 21, 42, 39, 53, and 78 for control group, groups 1, 2, 3, and 4, respectively. The apoptotic cells in the four experimental groups were significantly increased when compared with that in control group ($P < 0.05$, one-way ANOVA).

Discussion

The critical factors for successful RNA interfering in mammalian system

Recent studies have demonstrated that the housekeeping genes in some mammalian cells could be interfered with RNAi, which greatly caught the scientists' attraction^(6-9,11,12). Because RNAi was highly specific and

efficient in inhibiting target genes, it is becoming the focus of recent studies to make it a new tool for curing tumor, infectious, and hereditary diseases⁽¹⁴⁾. Since double-strand structure and 3' overhanging region protect siRNA against endonuclease, RNAi could be superior to antisense oligonucleotides and ribozyme⁽¹⁵⁾. Many other factors are critical in the success: for example, the homogeneity of siRNA sequences to target gene, the degradation, mutation and secondary structure of target mRNA, and the proteins enclosing the mRNA to transfer it in cells, etc⁽¹⁶⁾. In our study, BLAST software was used to determine the best siRNA sequences to HPV 16 E6 target gene, a 19-nucleotide sequence from 193 to 212 bp in its mRNA sequence, and avoid exon sequence of human genes to ensure the specificity and efficiency of RNAi.

There were also a lot of other factors influencing the success of RNAi *in vivo*, such as mode of the drug administration, dosage, frequency and formula of medication; drug absorbability, sensitivity, and resistance; local and system circular immunity state of animals; pharmacokinetics and toxicity in animals, etc. All of these factors match or mismatch will affect the outcome *in vivo* test greatly⁽¹⁷⁻¹⁹⁾. HPV-associated lesions of skin and mucosa have provided relatively accessible locations to minimize problem of drug delivery. Since it was difficult to establish a model for the study of cervical cancer at the site of uterine cervix, we created a mass of tumor at the subcutaneous tissue of right front limb of mice, which was easily spotted and observed during the experiments. Injection of 2 μ g siRNA plus transfection agent was directly conducted once or twice at peritoneal cavity or subcutaneous tumor of mice, respectively. Tumor volume, HPV 16 E6 IHC of tumor slice, apoptosis, and necrosis of tumor cells were all measured to evaluate the effect of siRNA. The experimental groups showed better outcome than control group in inhibiting tumor growth, inhibiting E6 protein expression, increasing tumor necrosis, and apoptosis. In addition, two-time administration of siRNA was better than once. Report indicated that it was more effective through peritoneal cavity administration of siRNA than by venous or

Table 3. The linear regression and correlation between tumor volume and injection time

Parameters	Control group	Group 1	Group 2	Group 3	Group 4
Correlation coefficient R	0.990	0.505	0.964	0.630	0.646
Regression coefficient B	117.447	7.915	16.116	12.126	7.195
Regression coefficient t test	29.338	2.294	15.395	2.564	3.592
P value	<0.001*	0.042*	<0.001*	0.028*	0.002*
Regression equation F value	860.714	5.596	237.011	6.574	12.904
P value	<0.001*	0.042*	<0.001*	0.028*	0.002*

* $P < 0.05$.

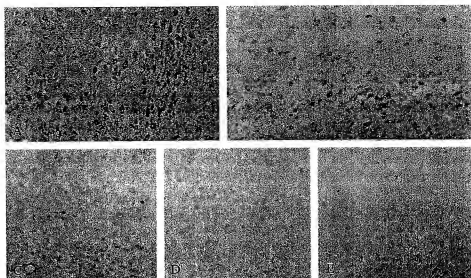


Figure 6. IHC image of HPV 16 E6 of nude mice tumor tissue in different groups. $\times 200$. (A: E6 positive stain as brown color in the cytoplasm of CaSki cells in control group; B: E6 partially positive stain as brown color in the cytoplasm of CaSki cells in the group 1; C, D, and E: E6 negative stain as no brown color in the cytoplasm of CaSki cells in the group 2, group 3, and group 4.)

subcutaneous mode, and it was not effective by tumor injection directly⁽²⁰⁾. However, our current study showed that direct injection into tumor gave effects as good as through peritoneal cavity, and injection twice or more led to better results. This might give hope to offer an interesting alternative way for drug delivery in future.

The specificity and efficiency of RNAi in CaSki cells

The efficiency of RNAi in mammalian cells is usually high. The inhibition of RNA expression and protein synthesis has shown over 50% rate, but seldom to 100%; therefore, RNAi technology is recognized as gene knockout not gene knockout⁽¹⁴⁾. CaSki cell was used in our experiment due to its high copy (about 600 copies) of HPV 16. In contrast, SiHa cells only have 1–2 copies. Several researches concerning E6 protein expression in SiHa cell or HeLa cell have

been carried out, in which E6 was not measurable directly, just relying on detecting p53 or P21 protein levels to know E6 expressions indirectly^(21–24). We detected the E6 mRNA and its protein levels in CaSki cells directly, which has given us more accurate data to evaluate the function of targeting E6 by E6 siRNA. According to our results, the inhibiting rates of E6 mRNA expression by siRNA at days 1, 2, 5, and 9 after transfection were 77%, 83%, 59%, and 41%, respectively, while that of the E6 protein expression were 79.7%, 80.4%, 71.3%, and 57.4%, respectively. Neither the negative control nor Lamin A/C, an internal control, showed any significant change in the mRNA and protein expression. Based on these, RNAi exists in CaSki cells, and exogenous viral gene has been interfered specifically and highly efficiently. In animal models, even the lowest dose and single injection could lead to dramatic results, as experimental groups showed inhibiting tumor growth and E6 protein expression, and increasing tumor necrosis and apoptosis after siRNA transfection. The randomly

Table 4. HPV16 E6 IHC images analysis

	Control group	Group 1	Group 2	Group 3	Group 4
Index of opacity density ($M \pm SD$)	19.03 ± 4.29	7.73 ± 1.29	4.33 ± 1.59	5.15 ± 2.00	6.90 ± 2.01
P value ^a		<0.001*	<0.001*	<0.001*	<0.001*
P value ^b			0.173	0.288	0.729
P value ^c				0.728	0.288
P value ^d					0.462

^aCompare with control group.

^bCompare with group 1.

^cCompare with group 2.

^dCompare with group 3.

*P < 0.05.

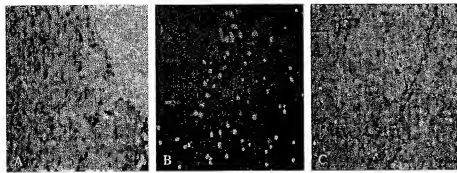


Figure 7. TUNEL fluorescence photos of nude mice tumor tissue of different groups. $\times 100$. (A: injection into peritoneal cavity in group 1; B: injection once into tumor in group 3; C: injection twice into tumor in group 4) TUNEL, terminal deoxynucleotidyl transferase-mediated dUTP nick-end labeling.

arranged nucleotide bases of siRNA in control group have no effect, which further proved the high efficiency and specificity of interference.

In contrast, Jiang and Milner^(21,22) showed that targeting HPV 16 E6 by synthetic E6 siRNAs resulted in only a very weak growth inhibition of HPV16-positive cancer cells, with no signs of significant cell death. In another study, Butz *et al.*⁽²³⁾ reported that targeting viral E6 oncogene in HeLa and SiHa cell lines either by synthetic or vector-borne siRNA had a dramatic induction of apoptosis following treatment against E6, whereas E7 had not been affected. The inconsistent results in above studies may have resulted from the varied efficiency of siRNA due to the target sequence and a less suitable region of E6 chosen for siRNA sequence. Our findings suggested that the molecular targeting of E6 by siRNA represents a promising novel approach for the development of specific therapeutic strategies against HPV-positive cancers and dysplasias. Hall and Alexander⁽²⁴⁾ reported different results using the E7 cognate siRNA species which reduced the expression of both E6 and E7 in HeLa cell line. Whether there was a designing problem for E7 siRNA has not been determined yet, and this question remains to be elucidated in future.

Reports indicated that HPV E6/E7 was associated with multidrug resistance in cervical cancer therapy⁽²⁵⁾. The HPV E6/E7 RNAi was not only capable of inhibiting the tumor growth directly but also overcoming the drug resistance to result in better outcome in the treatment. Studies indicated that siRNA could interfere with several oncogenes in a consecutive manner, and thus can be used to block the initiation and progression of tumor. For tumor prevention and treatment, RNAi might be a promising therapeutic approach for the patients.

The time efficiency of RNAi in CaSki cells

A few reports addressed the time efficiency of targeting E6 with siRNA; one of them showed that peak

efficiency of E6 or E7 siRNA was roughly at 48 h after the transfection. This aspect was one of our main parts of focus in this study. Some reports demonstrated that the persistence of RNAi in mammalian system by synthesized siRNA occurred for a short period of time, and inhibiting the genes' expression reached peak level within 48–72 h after siRNA transfection depending on the half-life of protein targeted. What is more, most of the protein expressions stored to the stable levels within 5–7 days after the transfection^(11,26). The short-period effect of the inhibition was associated with cell proliferation double time required, not related to the degradation of siRNA. The apoptotic CaSki cells and the inhibiting E6 protein expression by siRNA in our study have been reversed at day 9 after E6 siRNA transfection, which were more effective than those reported by others in mammalian cells. The main reasons for short-period effect in our experiment might be due to (1) The transfection rate was not 100%; therefore, non-transfected CaSki cells could proliferate doubly to induce the E6 protein expression increase and the apoptotic cells decrease proportionally. How to improve the efficiency of transfection warrants further study. (2) RNAi does not interfere with the recovery of cellular regulatory systems reported previously in studies for inhibition by viral gene expression^(21,22), which suggested that other anti-apoptotic factors may be involved in this process. (3) siRNA used in this study was a simple, double-stranded structure synthesized biochemically and transferred by liposome. If the double-stranded RNA is made up of stem-loop structure, just like hair-pin structure (small hair-pin RNA, shRNA), RNAi can be achieved in regions in diverse promoters, such as H1 and U6 belonging to RNAIII polynuclease family. If the shRNA is integrated into virus plasmid, a novel, established stable cell line could inhibit protein expression for a rather long time. Several successful tests have been reported^(10,27–29).

The prospect of RNAi

RNAi appears to be a critical tool for biologists and clinicians for functional genomics research. The success of RNAi to inhibit HPV virus genes expression has provided an alternative way for genetic treatment of cervical cancer. In spite of this, however, many problems remained to be tackled, including transferring nucleotides into definite cells or tissues with the less toxicity and higher efficiency. It is believed that with various modes of delivery of siRNA, RNAi might be more effective than any other technologies developed for the downregulation of gene expression. With a thorough and deeper understanding of RNAi, it may play an important role for treating and curing cancers, as well as infectious disease and dominant genetic disorders.

Acknowledgment

We thank Prof. Wei YuQuan (Sichuan University Huaxi Hospital) for instructing lab work and thank Prof. Bai Huai (Sichuan University Huaxi the second Hospital) for revising the article. This work was funded by a program grant (30371483) from National Science Funding of China to Prof. Zhi-Lan Peng.

References

- Lee CJ, Sub Ej, Kang HT et al. Induction of senescence-like state and suppression of telomerase activity through inhibition of HPV E6/E7 gene expression in cells immortalized by HPV 16 DNA. *Exp Cell Res* 2002;277:173-82.
- Tai TM, Ting RC. In vitro and in vivo inhibition of human papillomavirus type 16 E6 and E7 genes. *Cancer Res* 1995;55:4599-605.
- Zheng YF, Rao ZG, Zhang JR. Effects of anti-HPV16 E6-ribozyme on the proliferation and apoptosis of human cervical cancer cell line CaSki. *J First Mil Med Univ (Chinese)* 2002;22:496-8.
- Choo CK, Ling MT, Suen CK et al. Retrovirus-mediated delivery of HPV 16 E7 antisense RNA inhibited tumorigenicity of Caski cells. *Gynecol Oncol* 2000;78(Pt 1):293-301.
- Storey A, Oates D, Banks L et al. Anti-sense phosphorothioate oligonucleotides have both specific and non-specific effects on cells containing human papillomavirus type 16. *Nucleic Acids Res* 1999;19:4109-14.
- Waterhouse PM, Wang MB, Lough T. Gene silencing as an adaptive defense against viruses. *Nature* 2001;411:834-42.
- Paul CP, Good PD, Winer I et al. Effective expression of small interfering RNA in human cells. *Nat Biotechnol* 2002;20:505-8.
- Smallheiser NR, Manev H, Costa E. RNAi and brain function: was McConnell on the right track? *Trends Neurosci* 2001;24:216-8.
- Liu Y, Jiang Y, Qiao DR et al. The mechanism and utilization of posttranscriptional gene silencing. *Chin J Biotechnol (Chinese)* 2002;18:140-3.
- Sui G, Soohoo C, Affar el B et al. A DNA vector-based RNAi technology to suppress gene expression in mammalian cells. *Proc Natl Acad Sci U S A* 2002;99:5515-20.
- ElBashir SM, Harborth J, Weber K et al. Analysis of gene function in somatic mammalian cells using small interfering RNAs. *Methods* 2002;26:199-213.
- ElBashir SM, Harborth J, Lendeckel W et al. Duplexes of 21-nucleotide RNAs mediate RNA interference in cultured mammalian cells. *Nature* 2001;411:494-8.
- Dornze P, Picard D. RNA interference in mammalian cells using siRNAs synthesized with T7 RNA polymerase. *Nucleic Acids Res* 2002;30:e46.
- Caplen NJ. RNAi as a gene therapy approach. *Expert Opin Biol Ther* 2003;3:575-86.
- Bass BL. RNA interference: the short answer. *Nature* 2001;411:428-9.
- Orphanides G, Reinberg D. A unified theory of gene expression. *Cell* 2002;108:439-51.
- McManus AF, Meissner L, Pham TT et al. RNA interference in adult mice. *Nature* 2004;418:838-9.
- Xia H, Mao Q, Paulson HL et al. siRNA-mediated gene silencing in vitro and in vivo. *Nat Biotechnol* 2002;20:1006-10.
- Lewis DL, Hagstrom JE, Loomis AG et al. Efficient delivery of siRNA for inhibition of gene expression in prostate cancer. *Nat Genet* 2002;32:107-8.
- Filleur S, Courtin A, Alt-St-Ali S et al. siRNA-mediated inhibition of vascular endothelial growth factor severely limits tumor resistance to antiangiogenic thrombospondin-1 and slows tumor vascularization and growth. *Cancer Res* 2003;63:919-22.
- Jiang M, Milner J. Selective silencing of viral gene expression in HPV-positive human cervical carcinoma cells treated with siRNA, a primer of RNA interference. *Oncogene* 2002;21:6041-8.
- Jiang M, Milner J. Selective silencing of viral gene E6 and E7 expression in HPV-positive human cervical carcinoma cells using small interfering RNAs. *Methods Mol Biol* 2004;292:401-20.
- Butz K, Ristriani T, Hengstermann A et al. siRNA targeting of the viral B6 oncogene efficiently kills human papillomavirus-positive cancer cells. *Oncogene* 2003;22:5938-45.
- Hall AH, Alexander KA. RNA interference of human papillomavirus type 18 B6 and E7 induces senescence in HeLa cells. *J Virol* 2003;77:6066-9.
- Padilla LA, Leung BS, Carson LR. Evidence of an association between human papilloma-virus and impaired chemotherapy-induced apoptosis in cervical cancer cells. *Gynecol Oncol* 2002;85:59-66.
- Novina CD, Murray MF, Dykxhoorn DM et al. siRNA-directed inhibition of HIV-1 infection. *Nature Med* 2002;8:681-6.
- Brummelkamp TR, Bernards R, Agami R. A system for stable expression of short interfering RNAs in mammalian cells. *Science* 2002;296:550-3.
- Paddison PJ, Caudy AA, Bernstein E et al. Short hairpin RNAs (shRNA) induce sequence-specific silencing in mammalian cells. *Genes Dev* 2002;16:648-58.
- Yu JY, Deriuier SL, Turner DL. RNA interference by expression of short-interfering RNAs and hairpin RNAs in mammalian cells. *Proc Natl Acad Sci U S A* 2002;99:6047-52.

Accepted for publication February 2, 2005

EXHIBIT 11

RNA Interference-Mediated Gene Silencing of Pleiotrophin Through Polyethylenimine-Complexed Small Interfering RNAs *In Vivo* Exerts Antitumoral Effects in Glioblastoma Xenografts

MARIUS GRZELINSKI,^{1,*} BEATA URBAN-KLEIN,^{1,*} TOBIAS MARTENS,² KATRIN LAMSZUS,² UDO BAKOWSKY,³ SABRINA HÖBEL,¹ FRANK CZUBAYKO,¹ and ACHIM AIGNER¹

ABSTRACT

RNA interference (RNAi) is a powerful strategy to inhibit gene expression through specific mRNA degradation mediated by small interfering RNAs (siRNAs). *In vivo*, however, the application of siRNAs is severely limited by their instability and poor delivery into target cells and target tissues. Glioblastomas are the most frequent and malignant brain tumors with, so far, limited treatment options. To develop novel and more efficacious therapies, advanced targeting strategies against glioblastoma multiforme (GBM)-relevant target genes must be established *in vivo*. Here we use RNAi-based targeting of the secreted growth factor pleiotrophin (PTN), employing a polyethylenimine (PEI)/siRNA complex strategy. We show that the complexation of chemically unmodified siRNAs with PEI leads to the formation of complexes that condense and completely cover siRNAs as determined by atomic force microscopy (AFM). On the efficient cellular delivery of these PEI/siRNA complexes, the PTN downregulation in U87 glioblastoma cells *in vitro* results in decreased proliferation and soft agar colony formation. More importantly, *in vivo* treatment of nude mice through systemic application (subcutaneous or intraperitoneal) of PEI-complexed PTN siRNAs leads to the delivery of intact siRNAs into subcutaneous tumor xenografts and a significant inhibition of tumor growth without a measurable induction of siRNA-mediated immunostimulation. Likewise, in a clinically more relevant orthotopic mouse glioblastoma model with U87 cells growing intracranially, the injection of PEI-complexed PTN siRNAs into the CNS exerts antitumoral effects. In conclusion, we present the PEI complexation of siRNAs as a universally applicable platform for RNAi *in vitro* and *in vivo* and establish, also in a complex and relevant orthotopic tumor model, the potential of PEI/siRNA-mediated PTN gene targeting as a novel therapeutic option in GBM.

OVERVIEW SUMMARY

The inhibition of gene expression through RNA interference (RNAi) relies on small interfering RNAs (siRNAs). Major limitations are their instability and poor cellular delivery especially *in vivo*. Glioblastomas are the most frequent and malignant brain tumors with, so far, limited treatment options, which emphasizes the need to develop novel therapeutic approaches including advanced gene-targeting strategies. Here we establish a polyethylenimine (PEI)/siRNA complexation method for RNAi-based targeting of the growth factor pleiotrophin (PTN). On com-

plexation with PEI, siRNAs are completely protected and efficiently internalized by cells. The PEI/siRNA-mediated PTN downregulation in U87 glioblastoma cells *in vitro* results in decreased proliferation and soft agar colony formation. *In vivo* treatment of nude mice through subcutaneous, intraperitoneal, or intrathecal application of PEI-complexed PTN siRNAs significantly inhibits the growth of tumor xenografts in subcutaneous and orthotopic tumor models. Hence, PEI/siRNA complexation represents a promising strategy for RNAi-based gene targeting, and PTN targeting is a novel therapeutic option in glioblastoma multiforme.

¹Department of Pharmacology and Toxicology, Philipps-University School of Medicine, D-35033 Marburg, Germany.

²Department of Neurosurgery, University Hospital Hamburg-Eppendorf, D-20246 Hamburg, Germany.

³Department of Biopharmacy and Pharmaceutical Technology, Philipps-University School of Medicine, D-35033 Marburg, Germany.

*M.G. and B.U.-K. contributed equally to this work.

INTRODUCTION

RNA interference (RNAi) offers great potential not only for *in vitro* target validation, but also *in vivo* as a novel therapeutic strategy based on the highly specific and efficient silencing of a target gene, for example, in tumor therapy (for review see, e.g., Hannon and Rossi, 2004). The main issue, however, is the delivery of therapeutically active siRNAs, which are the mediators of RNAi-induced specific mRNA degradation (Elbashir *et al.*, 2001), into the target tissue/target cells *in vivo* (for review see, e.g., Howard, 2003; Hannon and Rossi, 2004). For safety reasons, strategies based on (viral) vector delivery may be of only limited clinical use. The more desirable approach is to directly apply catalytically active siRNAs. So far, however, only a few studies on siRNA-mediated gene silencing *in vivo* exist, often relying on high amounts of siRNAs, describing particular applications in certain target organs and/or using siRNAs with chemical modifications (for review see Shankar *et al.*, 2005; Uprichard, 2005; Aigner, 2006). Clearly, there is the need for a broad method platform that allows the therapeutic use of siRNAs through direct systemic application.

Polyethylenimines (PEIs) are synthetic branched polymers with a protonable amino group in every third position and a high cationic charge density (Boussif *et al.*, 1995; Behr, 1997). Thus, PEIs are able to form with DNA noncovalent interpolyelectrolyte complexes (Boussif *et al.*, 1995), which are small colloidal particles allowing efficient cellular uptake through endocytosis. On this basis, certain PEIs have been used as transfection reagent in a variety of cell lines and in animals for DNA delivery (for review see Kichler, 2004; Wagner *et al.*, 2004; and references therein). More recently, we showed that the complexation with PEIs also represents an efficient method for the protection of RNA molecules from nucleolytic degradation and leads to the delivery of intact and bioactive RNA molecules including ribozymes and siRNAs (Aigner *et al.*, 2002a; Urbanc-Klein *et al.*, 2005) into tumor cells.

Glioblastoma multiforme (GBM) accounts for a high proportion of intracranial human tumors with, despite aggressive treatment, a poor prognosis (Davis *et al.*, 2001) and nearly all GBM patients die within 1 year (Holland, 2000). Despite some progress the therapeutic options are, unfortunately, rather limited and, clearly, novel therapeutic strategies are needed. Targeting, for example, of disease-specific molecules involved in the proliferation, apoptosis, angiogenesis, or migration of the tumor cells may offer a high potential for the development of more effective therapies against GBM.

Besides other aberrations, the deregulated expression of polypeptide growth factors and their receptors has been shown to be one of the key mechanisms for the malignant growth and metastatic spread of tumor cells. In GBM a variety of growth factors is expressed with, for example, vascular endothelial growth factor (VEGF) being an attractive target gene driving tumor neoangiogenesis (see, e.g., Jensen, 1998). Here, we explore the therapeutic potential of targeting another growth factor, pleiotrophin (PTN), which has been shown previously to be overexpressed and functionally relevant in glioblastoma (see below).

PTN, also referred to as heparin-binding growth-associated molecule (HB-GAM), heparin-binding growth factor-8, heparin-binding neurotrophic factor (HBNF), or osteoblast-specific

factor-1 (OSF-1), is a 15.3-kDa secreted protein that was originally purified from human breast cancer cells (Wellstein *et al.*, 1992), bovine uterus (Milner *et al.*, 1989), as well as neonatal rat brain (Rauvala, 1989; Li *et al.*, 1990), and that exerts pleiotropic stimulating actions on a wide variety of different cell types (e.g., fibroblasts, endothelial cells, neurons, and epithelial cells) (Rauvala, 1989; Li *et al.*, 1990; Courty *et al.*, 1991; Fang *et al.*, 1992; Laaroubi *et al.*, 1994; Choudhuri *et al.*, 1997; Bowden *et al.*, 2002). PTN is a developmentally regulated cytokine that is highly expressed in embryonic rodent tissues, whereas its expression drops dramatically after the perinatal phase. In the adult rodent brain, for example, only a few structures such as the hippocampus and cerebral cortex have detectable PTN expression levels (Czubayko *et al.*, 1995; Kurtz *et al.*, 1995; Zhang and Deuel, 1999; Muramatsu, 2002).

On the other hand, expression of PTN and its receptors, anaplastic lymphoma kinase (ALK) and receptor protein tyrosine phosphatase- ζ (RPTP ζ), is found in tumors originating from neuroectodermal lineages including GBM and melanoma. cDNA arrays (Muller *et al.*, 2003) as well as enzyme-linked immunosorbent assay (ELISA) and immunohistochemistry (Urbicht *et al.*, 2003) revealed that PTN expression is upregulated in glioblastomas as compared with normal human brain tissue and that all WHO grade III and IV gliomas and glioma cells are positive for PTN (Mentein and Held-Feindt, 2002; Lu *et al.*, 2005). Moreover, RNAi knockdown studies have established the functional role of RPTP ζ in GBM cell motility (Muller *et al.*, 2003), and ribozyme targeting of ALK has shown that ALK expression is rate limiting in the growth of GBM cell lines (Powers *et al.*, 2002). Although the PTN stimulation of ALK still remains controversial in the literature (Moog-Lutz *et al.*, 2005; and references therein), two naturally occurring forms of PTN with distinct biological activities have been described (Lu *et al.*, 2005). Furthermore, the rate-limiting role of PTN in glioblastoma has been firmly established (Grzelinski *et al.*, 2005).

So far, most studies exploring strategies to establish PTN as a putative attractive target have used anti-PTN antisense (Satyamoorthy *et al.*, 2000) or ribozyme targeting (Czubayko *et al.*, 1996) in melanoma cell lines. Inhibition of PTN expression on stable transfection of 1205 melanoma cells with plasmid-based ribozyme expression vectors led to reduced subcutaneous tumor growth of 1205 cells in athymic nude mice and decreased metastatic spread to the lungs (Czubayko *et al.*, 1996). Furthermore, two studies using 37-nucleotide-long hammerhead ribozymes showed that systemic intraperitoneal or intravenous delivery of RNA-based drugs was able to inhibit the subcutaneous tumor growth of 1205 melanoma cells in athymic nude mice, demonstrating the general feasibility of anti-PTN targeted tumor therapies (Aigner *et al.*, 2002a; Malerczyk *et al.*, 2005). Most recently, plasmid-based ribozyme targeting in glioblastoma cell lines revealed the rate-limiting role of pleiotrophin in glioblastoma growth and angiogenesis (Grzelinski *et al.*, 2005).

The aims of the present study were (1) to establish the application of PEI-complexed, PTN-specific siRNAs in glioblastoma cells as a complex tool for PTN targeting *in vitro* and *in vivo*, (2) to assess the antitumoral effects of this PEI/siRNA-mediated PTN depletion strategy in GBM cells regarding decreased cell proliferation *in vitro* and reduced subcutaneous tumor growth in athymic nude mice *in vivo*, and hence (3) to

establish the therapeutic potential of PEI/siRNA-based PTN targeting in GBM. To this end, most importantly, our goal was (4) to test in a clinically more relevant orthotopic mouse tumor model whether intracranial administration of PEI-complexed PTN-targeted siRNA could inhibit intracranial glioblastoma growth.

We found that the systemic intraperitoneal or subcutaneous administration of anti-PTN PEI/siRNA complexes efficiently delivered intact siRNAs into subcutaneous U87 tumor xenografts, leading to the reduction of intratumoral PTN levels and to the significant inhibition of tumor growth. Furthermore, in a more complex and more relevant orthotopic glioblastoma model, intracranial application of therapeutic PEI-complexed anti-PTN siRNAs again exerted antitumoral effects, indicating the potential of PEI/siRNA-mediated gene targeting as a novel therapeutic option in GBM.

MATERIALS AND METHODS

Tissue culture, siRNAs, animals, and PEI complexation

The glioblastoma cell line U87 was obtained from the American Type Culture Collection (ATCC, Manassas, VA) and cultivated under standard conditions (37°C, 5% CO₂) in Iscove's modified Dulbecco's medium (IMDM; PAA Laboratories, Cölbe, Germany) supplemented with 10% fetal calf serum (FCS) unless indicated otherwise. For PTN targeting, PTN siRNA 43 strands (GUGAAAAGUCUGACUGGdTdT/CACAGUCAGACUUCUUCACtTdT) were chemically synthesized and annealed (Ambion, Austin, TX) while an unrelated siRNA directed against luciferase (pGL2; Dharmacon, Lafayette, CO) served as negative control. Immunocompetent mice (C57BL/129sv) and athymic nude mice (*nu/nu*) (Charles River Laboratories, Wilmington, MA) were used as indicated.

For PEI complexation, 100 pmol of siRNA was dissolved in 200 μl of 10 mM HEPES–150 mM NaCl, pH 7.4, and incubated for 10 min. joPEI (4 ×, 1.25 μl; Qbiogene, Wiesbaden, Germany) was dissolved in 200 μl of the same buffer, and after 10 min was pipetted into the siRNA solution. This resulted in an siRNA:PEI (N/P) ratio of 10 as suggested for DNA by the manufacturer and as determined as optimal for siRNAs in pilot experiments (data not shown). After vortexing, the mixture was incubated for 1 hr at room temperature before use. To keep the complex concentration constant, amounts of complex to be used in different experiments were adjusted according to the volumes or sizes of the wells *in vitro* or according to the estimated distribution volume *in vivo*.

For PEI/siRNA treatment, U87 cells were seeded in 6 wells at 2 × 10⁶ cells per well or in 24 wells at 6 × 10⁵ cells per well 24 hr before the start of the experiment. Transfections were performed by the addition of the PEI/siRNA complex (80 pmol of siRNA per well of a 6-well plate or 10 pmol of siRNA per well of a 24-well plate, respectively) in IMDM–2% FCS for 4 hr. For RNA quantitation, cells were harvested 48 hr after transfection.

Growth assays

Studies of anchorage-dependent proliferation were carried out essentially as described previously (Abuharbeid *et al.*, 2004). Briefly, cells were plated into a 96-well plate at 200 cells

per well and cultivated in IMDM–2% FCS in a humidified incubator under standard conditions. PEI/siRNA complexes corresponding to 2 pmol of specific or nonspecific siRNA per well were added to the wells, and at the time points indicated the numbers of viable cells in eight wells were determined in a colorimetric assay according to the manufacturer's protocol (cell proliferation reagent WST-1; Roche Molecular Biochemicals, Mannheim, Germany).

Anchorage-independent proliferation was studied in soft agar assays essentially as described previously (Wellstein *et al.*, 1990). Cells were transfected in six wells with PEI-complexed specific or nonspecific siRNAs as described above and 24 hr after transfection were trypsinized and counted. Cells (20,000) in 0.35% agar (Bacto Agar; Becton Dickinson, Franklin Lakes, NJ) were layered on top of 1 ml of a solidified 0.6% agar layer in a 35-mm dish. Growth medium with 2% FCS was included in both layers. After 2–3 weeks of incubation, colonies more than 50 μm in diameter were counted in a blinded fashion by at least two independent investigators.

RNA preparation and Northern blotting

Total RNA from tumors or cells or homogenized tissues was isolated with TRI reagent (PEQLAB Biotechnologie, Erlangen, Germany) according to the manufacturer's protocol, and 20 μg was separated, blotted, and probed for PTN as described (Fang *et al.*, 1992). After washing, blots were exposed to film, quantitated by phosphorimager analysis, and, to correct for variability in loading, stripped and reprobed with an 18S cDNA probe.

Pleiotrophin ELISA

PTN concentrations in U87 cells were determined from medium conditioned by the cells for 24–72 hr, using a specific PTN ELISA essentially as described previously (Aigner *et al.*, 2003). Briefly, a mouse anti-PTN monoclonal antibody (4B7, 100 μg/ml), diluted to 1 μg/ml in Tris-buffered saline (TBS), was incubated in covered 96-well ELISA plates (Life Technologies, Karlsruhe, Germany) at 4°C overnight. Wells were washed three times with TBS–0.5% Tween 20 (TBST), blocked with 200 μl of TBST–1% bovine serum albumin (BSA) for 2 hr, and washed again before the addition of conditioned and centrifuged medium (100 μl/well). After incubation for 1 hr and subsequent washing, biotinylated affinity-purified goat anti-human PTN detection antibody (100 μl/well; R&D Systems, Wiesbaden, Germany) was added at a concentration of 500 ng/ml and incubated for 1 hr, washed again, and incubated with streptavidin–alkaline phosphatase conjugate (100 μl/well [diluted 1:5000 in TBST]; Roche Diagnostics, Mannheim, Germany) for 1 hr. After a final washing, the plate was incubated in the dark with *p*-nitrophenyl phosphate substrate solution (100 μl/well) for 2 hr. Absorbance was measured in an ELISA reader at 405 nm. Recombinant human PTN (R&D Systems) served as the standard.

Determination of TNF-α and IFN-α serum levels

PEI-complexed PTN siRNA or PEI-complexed nonspecific control siRNA (0.6 nmol [8 μg]) was administered by intraperitoneal or subcutaneous injection to athymic or immunocompetent mice as indicated in Fig. 3c. After 48 hr, the treat-

ment was repeated before the termination of the experiment 6 hr after the last injection. As a positive control based on a previous study (Osburg *et al.*, 2002), a single intraperitoneal injection of 40 µg of lipopolysaccharide (LPS; Sigma, St. Louis, MO) in 200 µl of phosphate-buffered saline (PBS) was performed and the experiment was terminated after 2 hr. Blood was taken, allowed to clot overnight at 4°C, and centrifuged for 10 min at 5000 rpm. The serum was removed and stored at -20°C. Murine tumor necrosis factor- α (TNF- α) and interferon- α (IFN- α) serum levels were determined by ELISAs according to the manufacturer protocols (Cytimmune Sciences [Rockville, MD] and PBL Biomedical Laboratories [Piscataway, NJ], respectively). On the basis of data of previous studies (Judge *et al.*, 2005), the serum was diluted 1:1 (TNF- α) or 1:100 (IFN- α) in the respective sample diluent.

Atomic force microscopy

DNA and siRNA polyplexes were prepared as described above, and after 1 hr they were directly transferred onto a silicon chip by dipping the chip into the complex solution. Atomic force microscopy was performed on a digital NanoScope IV BioScope (Veeco Instruments, Santa Barbara, CA) as described in detail elsewhere (Oberle *et al.*, 2000; Anabousi *et al.*, 2005). The microscope was vibration-damped. Commercial pyramidal Si₃N₄ tips (NCH-W; Veeco Instruments) on a cantilever with a length of 125 µm, a resonance frequency of about 220 kHz, and a nominal force constant of 36 N/m were used. All measurements were performed in tapping mode to avoid damage to the sample. The scan speed was proportional to the scan size and the scan frequency was between 0.5 and 1.5 Hz. Images were obtained by displaying the amplitude signal of the cantilever in the trace direction, and the height signal in the retrace direction, both signals being simultaneously recorded. Results were visualized either in height or in amplitude mode. For the evaluation of complex size, section analyses were performed as depicted in Fig. 1b, with ~60 single determinations per micrograph.

Laser Doppler anemometry

The ξ potential of complexes freshly prepared as described above was determined with the standard capillary electrophoresis cell of the Zetasizer 3000 HS from Malvern Instruments (Malvern, UK) at 25°C. The average value \pm standard deviation was calculated on the basis of the data of six runs.

In vivo tissue distribution of PEI-complexed siRNAs

PTN-specific siRNAs (0.6 µg [0.05 nmol]) were ³²P end-labeled, using T4 polynucleotide kinase and [γ -³²P]ATP, before purification by microspin columns (Bio-Rad, Munich, Germany) to remove unbound radioactivity and complexation as described above. U87 glioblastoma cells, 3×10^6 in 150 µl of PBS, were injected subcutaneously into both flanks of athymic nude mice (*nude/nude*) and grown until they reached a size of ~8 mm in diameter. The complexes, or noncomplexed labeled siRNAs as a negative control, were dissolved in 200 µl of PBS and intraperitoneally injected. After 4 hr, mice were killed and samples, organs, and tissues as detailed in Fig. 3a were removed

and subjected to RNA preparation with TRI reagent (PEQLAB Biotechnologie) according to the manufacturer's protocol. Total RNA was dissolved in 200 µl of diethylpyrocarbonate (DEPC)-treated water and 10-µl samples were subjected to agarose gel electrophoresis before blotting and autoradiography (BioMax, Eastman Kodak, Rochester, NY). As controls, ³²P-labeled siRNAs were complexed or not complexed with PEI, and treated with RNase A at 37°C for 15 min as indicated in Fig. 3a. Sodium dodecyl sulfate (1%) was then added, and mixtures were heat denatured for 5 min at 100°C and analyzed as described above.

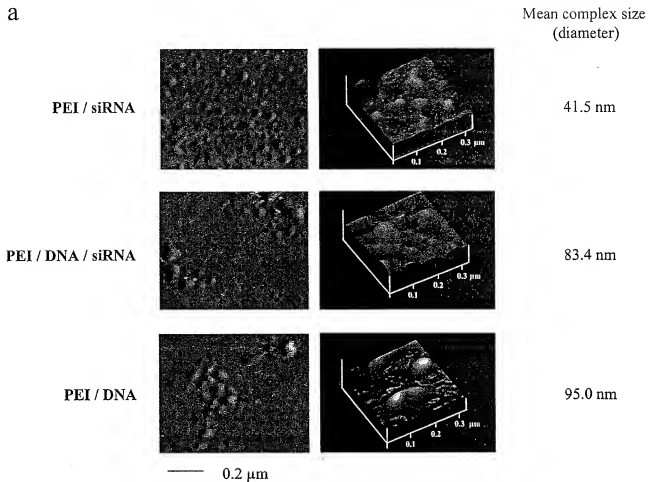
In vivo siRNA treatment in subcutaneous tumor models in mice and PEI detection

U87 glioblastoma cells (3×10^6 in 150 µl of PBS) were injected subcutaneously into both flanks of athymic nude mice (*nude/nude*). When solid tumors were established, mice were treated at various time points with 0.6 nmol (8 µg) of PEI-complexed specific or PEI-complexed nonspecific siRNA, administered by intraperitoneal injection or subcutaneous injection at a site along the median line more than 10 mm distant from both tumors. Tumor growth was monitored every 2–3 days, and tumor sizes were estimated from the product of the perpendicular diameters of the tumors. On termination of the experiment, mice were killed and tumors were removed. Pieces of each subcutaneous tumor representing at least half of the tumor mass were immediately fixed in 10% paraformaldehyde for paraffin embedding.

For detection of PEI, tumor-bearing mice were injected intraperitoneally with siRNA complexed with PEI-FluO (Qbiogene) or, as negative control, nonlabeled PEI/siRNA complexes as described above. The experiment was terminated 4 hr after injection, mice were killed, and tumor sections were analyzed by confocal microscopy. A Zeiss Axiovert microscope coupled to a Zeiss LSM 510 scanning device (Carl Zeiss, Göttingen, Germany) and an argon laser with an excitation wavelength of 488 nm were used. This experiment was performed with a long-pass filter of 505 nm for green fluorescence and a $\times 63/1.4$ oil lens.

Orthotopic glioma model in mice

Female 6- to 8-week-old nude mice (NMRI-*nude/nude*) were used. Institutional guidelines for animal welfare and experimental conduct were followed. A guide-screw system (Plastics One, Roanoke, VA) was used to perform the intracerebral tumor cell engraftment and subsequent intratumoral injections of PEI-complexed PTN-specific siRNA, PEI-complexed nonspecific siRNA, or sodium chloride solution. Guide screws were implanted as described previously (Brockmann *et al.*, 2003a,b). Briefly, mice were anesthetized by intraperitoneal administration of ketamine (100 mg/kg body weight) and xylazine (5 mg/kg body weight). A piece of the scalp and of the underlying periosteum were removed, and a 1-mm burrhole was drilled into the skull 3.5 mm lateral to the bregma. The guide screw was screwed into the burrhole and fixed with two-component adhesive. Two days after the implantation of guide screws, 7×10^5 U87 glioblastoma cells were injected through the screw into the basal ganglia of the mice, using a 26-gauge needle attached to a 25-µl Hamilton syringe. For the injection of test substances, mice were anesthetized as described above and received injec-



b

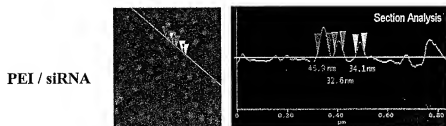


FIG. 1. (a) Analysis of PEI/siRNA, PEI/DNA/siRNA, and PEI/DNA complexes by atomic force microscopy (AFM). PEI/siRNA complexes (*top*) are ~2-fold smaller and more compact as compared with PEI/DNA complexes (*bottom*). The absence of free siRNA molecules, or molecule ends, indicates efficient complexation of the siRNAs. Hence, PEI/siRNA complexes completely cover and protect siRNAs. In size and shape (i.e., spherical, sufficiently large but still <200 nm in diameter), they are well suited for endocytic uptake. (b) Example of a line scan of the PEI/siRNA complex surface to evaluate complex size. For section analyses, ~60 single determinations per micrograph were performed; three examples are shown in (b). The spherical structures of PEI/siRNA complexes were determined to be ~41.5 nm in diameter.

tions of either PEI-complexed PTN-specific siRNA (15 pmol in 5 μ l of sodium chloride solution, reflecting the smaller distribution volume compared with systemic delivery as described above) or an equal amount of PEI-complexed nonspecific siRNA, or 5 μ l of sodium chloride solution. Treatments were initiated on day 1 after tumor cell implantation and were continued three times per week over 3 weeks, after which all animals were killed with CO₂.

Determination of size of orthotopic tumors

Mouse brains were removed from the cranial cavity, fixed in formalin overnight, bisected coronally, and embedded in paraffin. Serial sections (5 μ m thick) were stained with hematoxylin-eosin. The maximum cross-sectional area of the intracranial glioblastoma xenografts was determined by computer-assisted image analysis with a Leica Quantimet 500 system (Leica, Hamburg, Germany). Tumor volume was estimated according to the following formula: volume = (square root of maximal tumor cross-sectional area)³.

Immunohistochemistry

Immunostaining of paraffin sections of the tumors was performed essentially as described previously (Aigner *et al.*, 2002b). Briefly, after deparaffinization with xylene and rehydration with graded alcohols, sections were incubated in 10 mM citrate buffer (pH 7.4) at 90°C for 20 min, endogenous peroxidases were inactivated with 0.3% hydrogen peroxide at 4°C for 20 min, and slides were washed three times with PBS-0.1% Tween 20 (PBST). After blocking with 10% normal horse serum in PBST-2% BSA for 1 hr at room temperature, the slides were incubated with a mixture of goat anti-PTN antibodies (R&D Systems [Wiesbaden, Germany] and Santa Cruz Biotechnology [Santa Cruz, CA]) in PBST at 37°C for 1 hr in a wet chamber. After washing, a 1:500 diluted, biotinylated horse anti-goat IgG antibody (Vector Laboratories, Burlingame, CA) was applied as the secondary antibody for 1 hr before washing. Immunoreactivity on the sections was visualized with a streptavidin-biotin-peroxidase complex (VECTASTAIN ABC kit; Vector Laboratories) according to the manufacturer's instructions and revealed with the peroxidase substrate diaminobenzidine (brown). For the determination of PTN protein levels, hematoxylin counterstain was omitted and sections were mounted, scanned by light microscopy, and electronically analyzed for staining intensity (TILL Photonics and TILL Vision, Graefelfing, Germany). Each tumor was represented by at least two different sections originating from distant areas of the tumor mass, and for scanning and quantitation at least five fields per section were chosen. To analyze the proliferative activity of the tumor cells, sections were stained with the antibody MIB-1 directed against the Ki-67 antigen, using the VECTASTAIN kit as described above, and counterstained with hematoxylin. The percentage of MIB-1-positive nuclei was determined by counting immunoreactive tumor cell nuclei in three high-power fields in the most actively proliferating tumor area.

Data analysis

For statistical analysis, the Student unpaired, two-sided *t* test was used for comparisons between data sets (**p* < 0.05, ***p* <

0.01, ****p* < 0.005). *In vivo* experiments were performed with five to eight mice per group and one (orthotopic mouse model) or two (subcutaneous xenografts) tumors per mouse.

RESULTS

Characterization of PEI complexes by atomic force microscopy

For PTN gene targeting, we chose to approach the matter by direct application of a PEI-complexed siRNA that had been pre-selected according to criteria predicting high targeting efficacy and selectivity. Chemically synthesized, PTN-specific siRNA 473 was complexed with a commercially available low molecular weight polyethylenimine (jetPEI) at the optimal siRNA:PEI ratio (*N/P* ratio) of 10 as determined in pilot experiments for siRNAs (data not shown) and as suggested by the manufacturer for DNA transfection. Because this PEI complexation represents a rather novel approach for siRNA delivery, the resulting PEI/siRNA complexes were first analyzed by atomic force microscopy (AFM) regarding size, structure, and integrity. Furthermore, keeping in mind that jetPEI was introduced previously as a DNA plasmid transfection reagent, they were compared with PEI/DNA plasmid complexes. Analysis of the AFM data revealed that all complexes, that is, PEI/DNA, PEI/DNA/siRNA, and PEI/siRNA, were stable and uniform in size (Fig. 1a, left, and three-dimensional representation at higher magnification in Fig. 1a, right). PEI/siRNA complexes showed a mean complex diameter of ~41.5 nm (Fig. 1a, top) and see Fig. 1b for details of the analysis). More importantly, AFM allowed visualization of free, noncomplexed DNAs or siRNAs as thin fiber-like structures. The absence of free siRNA molecule ends, which otherwise would be visible as standing out from the round, well-shaped complexes, as well as the absence of free siRNA molecules, indicated the complete complexation of the siRNAs (Fig. 1a, top). PEI complexes with DNA plasmids were somewhat larger (Fig. 1a; compare upper and lower panels); however, the only ~2-fold increase in size (~95 nm) was much smaller than the differences in molecular weight between the siRNAs (22 bp) and the plasmid (>5000 bp), indicating, as expected, no direct correlation between the size of nucleic acids and the size of their complexes (see Discussion). Concomitantly, the PEI complexation of a 1:1 mixture of DNA plasmids and siRNAs led to the formation of complexes of intermediate size (83.4 nm; Fig. 1a, center). The comparison also revealed that PEI/siRNA complexes were spherical and more compact as compared with PEI/DNA complexes.

From these data we conclude that (1) in the complexes DNA and/or siRNAs were condensed effectively, that (2) PEI/siRNA complexes completely covered and protected siRNAs, and that (3) in size and shape (spherical, sufficiently large but still <200 nm in diameter) they were well suited for endocytotic uptake.

PEI/siRNA-mediated PTN targeting in vitro

When U87 glioblastoma cells were treated with PEI-complexed PTN-specific siRNAs *in vitro*, a profound (at least 60%) reduction of endogenous PTN gene expression, compared with treatment with PEI-complexed nonspecific siRNAs, was ob-

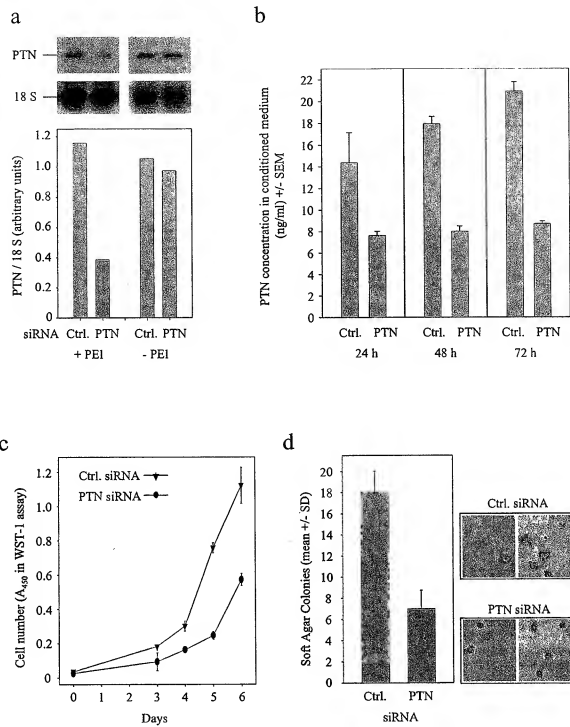


FIG. 2. Reduction of endogenous PTN gene expression in U87 glioblastoma cells at the mRNA level (a) and at the protein level (b) as shown by Northern blotting and ELISA, respectively. On PEI complexation, PTN-specific siRNAs efficiently reduce PTN levels, whereas PEI-complexed unrelated siRNAs show no effect. PTN downregulation was stable for several days. (c and d) Biological effects of PEI/siRNA-mediated PTN targeting on U87 glioblastoma cell proliferation. Treatment with PEI-complexed PTN-specific siRNAs results in reduced anchorage-dependent proliferation as compared with PEI-complexed unrelated siRNAs (c). The same is true for anchorage-independent proliferation, as shown by markedly decreased colony formation in soft agar assays (d; quantitation of colonies > 50 μm [left] and micrographs of representative colonies [right]).

served after only a single treatment. This was shown at the mRNA level by Northern blotting (Fig. 2a) as well as at the protein level by PTN-specific ELISA and was stable for several days (Fig. 2b). No PTN downregulation, however, was observed on treatment with naked PTN-specific or nonspecific siRNAs (Fig. 2a, right), indicating that PEI complexation is required for the delivery of intact siRNAs into cells.

Analysis of the *in vitro* proliferation of U87 glioblastoma cells demonstrated that our PTN gene-targeting approach through PEI-complexed PTN-specific siRNAs resulted in a robust ~50% reduction of anchorage-dependent cell proliferation (Fig. 2c). In soft agar assays, which monitor anchorage-independent cell proliferation and therefore resemble more closely the *in vivo* situation, an even more pronounced (>60%) reduction of colony formation was observed (Fig. 2d).

In vivo PEI/siRNA-mediated PTN targeting in subcutaneous glioblastomas

For the more relevant *in vivo* validation of our PEI/siRNA complexation method, and to test whether PEI/siRNA-mediated PTN targeting in glioblastomas exerts an antitumoral effect *in vivo*, we chose subcutaneous tumor xenografts, which are often used as a model system for *in vivo* tumors.

We first tested the delivery of intact siRNAs into tumor as well as into other tissues because this is critical for RNAi *in vivo*. U87 glioblastoma cells were injected subcutaneously into both flanks of athymic nude mice and, when they reached a size of ~8 × 8 mm, a single dose of ³²P-labeled siRNA was intraperitoneally injected. On termination of the experiment after 4 hr, total RNA prepared from the tissues was analyzed by gel electrophoresis, blotting, and autoradiography. Intact siRNA, represented by radioactive bands on the blot, was detected in several tissues including kidney, muscle, and, to a smaller extent, lung. Strong signals were observed in liver and, more importantly, in the tumor, whereas brain and blood were almost negative (Fig. 3a, left). As controls, PEI-complexed or noncomplexed siRNAs were analyzed by agarose gel electrophoresis, blotting, and autoradiography, showing identical bands (Fig. 3a, right). However, as described previously (Urban-Klein *et al.*, 2005), on RNase A-mediated degradation of siRNA molecules, no band was detected, demonstrating that the bands represent only end-labeled full-length siRNA rather than labeled nucleotides from degraded siRNAs. Consequently, the

lack of any signal on injection of noncomplexed siRNAs indicates the expected, extremely short half-lives due to excretion and degradation of the unprotected siRNA molecules (data not shown). From this experiment we concluded that, on PEI complexation, intact siRNAs are able to reach the tumor xenografts and hence their site of action.

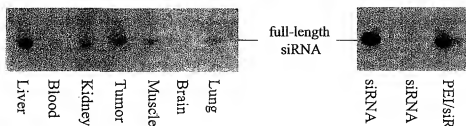
To evaluate whether PEI/siRNA particles indeed reached the tissues where siRNA signals were detected or whether free siRNA molecules, once liberated from the PEI/siRNA complexes, further diffused to other sites, we determined, in addition to siRNA molecules, the presence of labeled PEI in tumor xenografts. This is particularly relevant because the PEI/siRNA complexes used in this study were positively charged (ζ potential, 19.05 ± 1.46 mV) and, once injected, may aggregate, forming larger particles, with both charge and size possibly preventing diffusion. Four hours after intraperitoneal injection of PEI-FluoF/siRNA complexes, analysis of tumor sections by confocal microscopy revealed diffuse green fluorescence that was stronger than, and thus distinguishable from, the background tissue fluorescence in sections of PEI/siRNA-treated control tumors (Fig. 3b). Furthermore, in tumors treated with PEI-FluoF/siRNA complexes strongly fluorescing larger complexes with sizes in the low micrometer range were visible, which were absent in the PEI/siRNA control (Fig. 3b).

Sequence-dependent stimulation of the mammalian innate immune system by synthetic siRNAs has been previously described, and putative immunostimulatory motifs have been identified (Homung *et al.*, 2005; Judge *et al.*, 2005). To exclude that in our experiments any *in vivo* antitumor effects could be due to immunostimulatory processes rather than PTN gene inhibition, we tested for the induction of cytokines by PEI-complexed siRNAs after intravenous or intraperitoneal injection. We selected cytokines TNF- α and IFN- α , which have been reported previously to be upregulated in mice after administration of formulated immunostimulatory siRNAs (Homung *et al.*, 2005).

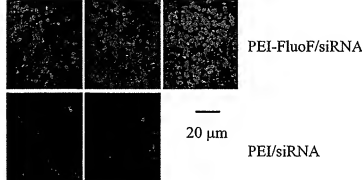
Athymic mice were treated twice with PEI-complexed siRNAs as indicated in Fig. 3c, with a 48-hr time interval between the injections. Six hours after the second treatment, analysis of serum cytokine levels revealed an upregulation of TNF- α neither in immunodeficient nor immunocompetent mice, whereas a short 2-hr treatment with 40 μ g of LPS led to a significantly higher TNF- α level as shown previously (Osburg *et al.*, 2002) and thus serving as a positive control. The absence

FIG. 3. PEI-complexed PTN-specific siRNAs are delivered to tumor xenografts and exert antitumoral effects in a subcutaneous *in vivo* mouse glioblastoma model. (a) ³²P-labeled siRNAs (0.05 nmol [0.65 μ g]), complexed with PEI, were injected intraperitoneally into tumor-bearing mice, and after 4 hr total RNA from various organ and tissue homogenates was prepared and subjected to agarose gel electrophoresis before blotting and autoradiography. The bands represent intact ³²P-labeled siRNAs, which were detected in several tissues including tumor. This indicates that, on PEI complexation, intact siRNAs are able to reach the tumor xenografts and hence their site of action. Right: Naked (left lane) and PEI-complexed (right lane) ³²P-labeled siRNAs as controls. On RNase treatment, naked ³²P-labeled siRNAs are completely degraded and no signal is observed (center lane). (b) Presence of PEI in tumor xenografts. Tumor sections were analyzed by confocal microscopy 4 hr after intraperitoneal injection of PEI-FluoF/siRNA (top) and reveal diffuse green fluorescence that is stronger and clearly distinguishable from background fluorescence in sections from tumors treated with unlabeled PEI/siRNA complexes (bottom). In addition, strongly fluorescing, larger PEI-FluoF/siRNA complexes with sizes in the low micrometer range are visible (top). (c) PEI/siRNA complexes do not exert any measurable effect on immunostimulatory processes. Athymic or immunocompetent mice were treated twice with PEI/siRNA complexes, as indicated. ELISA-based analysis of serum levels reveals no detectable upregulation of TNF- α (left) or IFN- α (right) levels independent of the siRNA, the mouse strain, or the administration route. LPS: Single treatment with lipopolysaccharide as positive control.

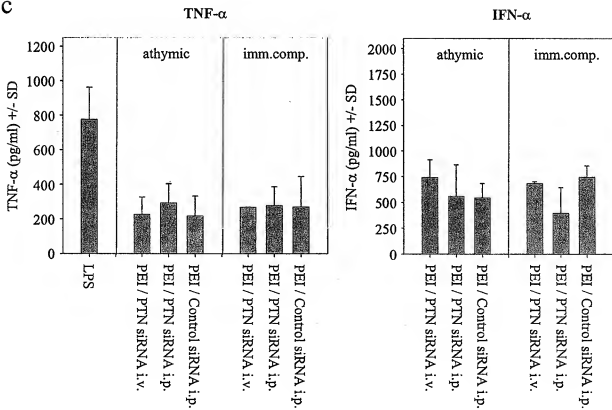
a



b



c



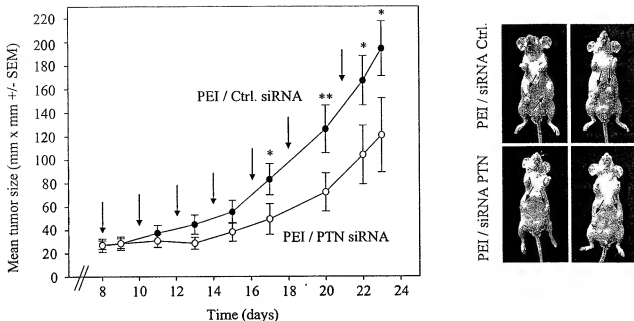


FIG. 4. Reduction of subcutaneous U87 glioblastoma tumor growth on intraperitoneal treatment with PEI-complexed PTN-specific siRNAs as compared with PEI-complexed unrelated control siRNA. *Left:* The corresponding growth curves show a statistically significant antitumoral effect of the treatment with PEI-complexed PTN-specific siRNAs (open circles) after 9 days. Arrows indicate the time points of treatment with 8 μ g (0.6 nmol) of PEI-complexed siRNA per injection. $n = 5$ animals per group. * $p < 0.05$; ** $p < 0.01$.

of a measurable immunostimulatory effect was true for both siRNAs and independent of the delivery route (intravenous or intraperitoneal). The dosing regimen selected here is in analogy to a previous study with a 6-hr interval between injection and serum level analysis (Judge *et al.*, 2005) and also resembles closely the treatment protocol to be used in our experiments with administration every 2–3 days.

Likewise, no detectable increase in IFN- α serum levels was observed under any treatment as indicated in Fig. 3c (right). From these data we conclude that our PEI/siRNA complexes do not exert a measurable immunostimulatory effect under the treatment conditions employed here.

Next, we monitored the antitumoral effects of PEI/siRNAs targeting PTN. U87 tumor cells were subcutaneously injected and, when solid tumors reached a size of $\sim 5 \times 6$ mm after 8 days, mice were intraperitoneally injected with 0.6 nmol of PEI-complexed PTN-specific siRNA every 2–3 days as indicated in Fig. 4. PEI/siRNA amounts were estimated from the previous *in vitro* results, and the same amount of PEI-complexed non-specific siRNA served as negative control. The intraperitoneal injection of PEI-complexed PTN-specific siRNAs resulted over 3 weeks in a $\sim 40\%$ reduction of tumor growth, which was statistically significant 9 days after the start of treatment (Fig. 4). Because at early time points tumors appeared flat, making it difficult to determine the tumor volume, the determination of tumor areas (length \times width) was chosen to monitor tumor growth although this somewhat underestimates the antitumoral effects visible at later time points (Fig. 4, right).

As an alternative treatment regimen, in the next experiment

subcutaneous injection of PTN-specific PEI/siRNA complexes was chosen. Complexes were subcutaneously injected at a distant site, that is, more than 10 mm from the tumors. Analysis of tumor sizes over 3 weeks demonstrated a profound ($>70\%$) reduction of tumor growth in the specific treatment group as compared with the control treatment with PEI-complexed non-specific siRNA (Fig. 5a). It should also be noted that in both experiments, comparison of the control treatment group with subcutaneous U87 wild-type cell tumors in untreated mice (described in a previous study; Grzelinski *et al.*, 2005) shows similar growth curves, indicating the absence of nonspecific PEI effects. On termination of the experiment, mice were killed and the tumors were removed for further analysis. Immunohistochemical staining of paraffin-embedded tumor sections for PTN revealed strong cytoplasmic staining (Fig. 5b, left), which allowed the determination of PTN levels through scanning and electronic analysis. To accurately measure the staining intensities representing the PTN protein concentration, a hematoxylin counterstain was omitted in these sections (Fig. 5b, center). The quantitation of at least five fields per section and two sections per tumor revealed a statistically significant ($\sim 70\%$) reduction of PTN protein levels in the tumors of the specific treatment group, as compared with the control group (Fig. 5b, right), indicating PTN siRNA-specific gene targeting. In contrast to the rather homogeneous PTN staining pattern within each section, blood vessel densities as determined by anti-von Willebrand factor staining showed considerable heterogeneity, which did not allow the determination of antiangiogenic effects of the PEI/siRNA-mediated PTN targeting (data not shown).

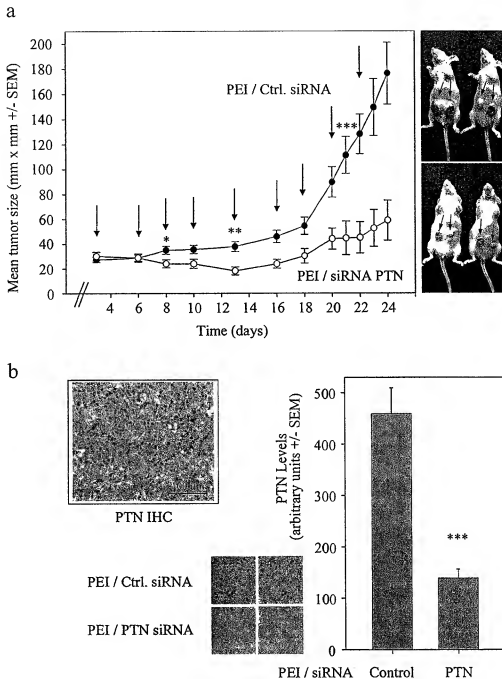


FIG. 5. (a) *In vivo* PTN targeting through subcutaneous injection of PEI-complexed PTN-specific siRNAs (open circles) leads to a marked decrease in U87 glioblastoma growth as compared with PEI-complexed unrelated control siRNA (solid circles). Arrows indicate the time points of injection, with 8 μ g (0.6 nmol) of PEI-complexed siRNA per injection. The reduction of tumor growth is statistically significant 5 days after the start of treatment (right: two representative mice of each group; tumors are indicated by arrows). (b) Immunohistochemical staining of paraffin-embedded tumor sections for PTN reveals strong cytoplasmic brown staining (left: sections are hematoxylin counterstained; scale bar, 100 μ m) allowing the quantitation of PTN by scanning and electronic analysis. For accurate determination of staining intensities the hematoxylin counterstain was omitted, and therefore sections do not show histological detail (center: two representative examples of each group). Quantitation of at least five fields per section and two sections per tumor reveals a ~70% reduction of PTN protein levels in the tumors of the specific treatment group, as compared with the control group, demonstrating PEI/siRNA-specific PTN gene targeting (right). $n = 5$ animals per group. * $p < 0.05$; ** $p < 0.01$; *** $p < 0.005$.

PEI/siRNA-mediated PTN targeting in an orthotopic glioblastoma model

The tumor model with the highest biological relevance for glioblastomas is in the CNS. We therefore employed an orthotopic glioblastoma mouse model to study the antitumoral effects of PEI/siRNA-mediated targeting of PTN. Tumor cells were intracerebrally grafted by injection through an implanted guide screw into the basal ganglia of mice (Fig. 6a). For PTN targeting, because it was shown previously that PEI complexes are unable to cross the blood-brain barrier (Urban-Klein *et al.*, 2005), we chose intracerebral delivery of PEI/siRNA complexes. The treatment was performed in anesthetized mice. Reflecting the smaller distribution volume, 0.015 nmol of PEI-complexed PTN-specific or, as a negative control, nonspecific siRNAs was injected three times per week.

Determination of tumor volumes at the end of the experiment (after 3 weeks) revealed a statistically significant (~50%) reduction of tumor growth on treatment with PEI-complexed, PTN-specific siRNA as compared with PEI-complexed, non-specific siRNA, indicating an siRNA-specific effect (Fig. 6b).

Because of the location of the orthotopic tumors in the CNS and the intracerebral application of siRNAs, this model is also sensitive to unwanted side effects and was therefore also chosen to demonstrate the absence of nonspecific effects of PEI or siRNAs. A comparison of tumors after PEI-complexed, non-specific siRNA treatment with tumors from the group injected with a physiological sodium chloride solution revealed no differences in tumor size (Fig. 6b, left column versus right column). This firmly establishes the absence of nonspecific antitumoral effects of PEI or of PEI-complexed siRNAs. Furthermore, on performance of any of the treatment regimens, in whole brain sections no gross histological changes were detected, and no behavioral alterations were observed in the animals, indicating that the treatment was well tolerated.

Further immunohistochemical analysis of the tumors also revealed a statistically significant reduction in the number of proliferating cells as determined by detection of the nuclear protein Ki-67, which is expressed in the active phases of the cell cycle and thus serves as a marker of cell proliferation (Fig. 6c). Immunohistochemical quantitation furthermore demonstrated the PTN siRNA-mediated downregulation of PTN. Despite the fact that, because of the higher staining heterogeneity within each tumor, this decrease did not reach statistical significance ($p < 0.06$), it nevertheless provides evidence that the observed effects on tumor growth and tumor cell proliferation were based on PTN targeting (Fig. 6d). From these data we conclude that the intracranial administration of PEI-complexed PTN-targeted siRNAs inhibits intracranial glioblastoma growth through the specific reduction of PTN expression.

DISCUSSION

Glioblastomas, which can arise *de novo* or progress from lower grade gliomas, are the most frequent and most malignant brain tumors, with thus far limited treatment options. To develop novel and more efficacious therapies against GBM, attractive target genes need to be defined and drug targeting strategies must be established *in vivo*. Because GBM tumor

growth relies on vasculature remodeling, destruction of the surrounding normal tissue, and migration and proliferation of tumor cells, factors that drive angiogenesis (e.g., VEGF; Jensen, 1998) or invasion and motility of tumor cells (e.g., cathepsin B; Gondi *et al.*, 2004) represent, among many others, attractive targets in GBM. Previous studies have shown that pleiotrophin, which was originally described as a developmentally regulated mitogenic, chemotactic, and angiogenic factor with a restricted expression pattern in adults, is markedly overexpressed in glioblastomas (Mentlein and Held-Feindt, 2002; Müller *et al.*, 2003; Ulbricht *et al.*, 2003; Lu *et al.*, 2005) and represents a functionally relevant molecule in GBM (Grzelinski *et al.*, 2005). This prompted us to speculate that PTN gene targeting may provide an avenue for new gene therapy approaches with clinical significance in glioblastomas.

Although all glioblastoma cell lines are positive for pleiotrophin, U87 cells express comparably high levels of PTN (Lu *et al.*, 2005) and have been widely used as a model system for glioblastoma multiforme. On initial formation of small nodules after xenografting into athymic nude mice, they show aggressive and rapid tumor growth. Thus, this tumor model makes high demands on any (gene) therapy approach and was chosen in this study.

Previously, we established polyethylenimine (PEI) as a reagent for the complexation of ribozymes or siRNAs, leading to their protection and cellular delivery *in vitro* and *in vivo* (Aigner *et al.*, 2002a; Urban-Klein *et al.*, 2005). This easy-to-use, nontoxic, and efficient method of siRNA delivery allows the use of siRNA molecules in a rather low-dose range and without any chemical modifications. Here, we explore the PEI/siRNA-mediated targeting of PTN as a putatively powerful, new therapeutic strategy in glioblastoma treatment.

We show by atomic force microscopy that PTN-specific siRNAs through PEI complexation are efficiently condensed, covered, and protected. The lack of a direct relation between the size of nucleic acids (5-kb plasmid DNA versus 22-bp siRNA) and the size of their complexes can be readily explained because the complexes contain many nucleic acid molecules each. Interestingly, however, *in vitro* our complexes were much smaller as compared with previous studies based on quasi-elastic light scattering, where complex sizes over 1 μm were detected (Goula *et al.*, 1998). Also, whereas our complexes appear stable and uniform in size, Goula *et al.* presented electron micrographs showing clumped, unstable, and irregularly shaped particles. The reason why our complexes resemble more closely PEI/DNA complexes prepared in 5% glucose (Goula *et al.*, 1998) rather than 150 mM sodium chloride remains to be elucidated. However, it should be noted that *in vivo*, larger aggregates were observed (see below).

We demonstrate that our PEI/siRNA complexes are delivered to cells *in vitro*, where they display full biactivity. The PTN downregulation at the mRNA and protein levels translates into markedly reduced glioblastoma cell proliferation *in vitro*. Although the PEI transfection is only transient, unpublished data from our laboratory (B. Urban-Klein and A. Aigner) show that PEI/siRNA effects are stable for at least 7 days, which may account for the fact that effects on colony formation can still be measured after 2–3 weeks in the soft agar assay. Taken together, these results confirm previous data in PTN-depleted cell lines on stable *in vitro* transfection with ribozyme expression

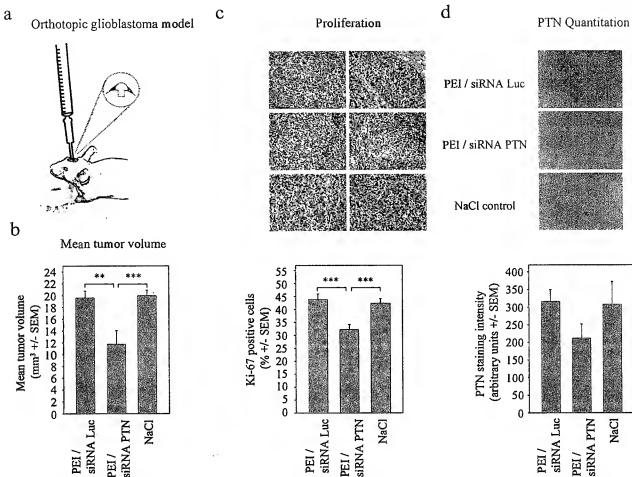


FIG. 6. Orthotopic *in vivo* mouse glioblastoma model to study the antitumoral effects of PEI-complexed PTN-specific siRNAs ($n = 5-7$ animals per group). (a) Schematic drawing of the free-hand injection technique, using a guide screw. The head of the mouse is placed on the lid of a 50-ml Falcon tube and the needle is cuffed with a sterile 2- to 10- μ l pipette tip. For the injections, the cannula is lowered into the guide screw, which is glued to the cranium of the mouse (arrow), and the cuff limits the penetration depth of the cannula during the injections (adopted from Brockmann *et al.*, 2003b). (b) Treatment with 0.2 μ g (0.015 nmol) of PEI-complexed PTN-specific siRNAs leads to a significant reduction of tumor growth as compared with mice treated with the same amount of PEI-complexed unrelated siRNAs or with buffer. (c) Ki-67 staining for proliferating cells. (d) PTN staining. To allow quantitation of PTN protein levels, these sections are not hematoxylin counterstained and thus do not show histological details. Quantitation reveals that the reduction in tumor volume (b) on treatment with PEI-complexed PTN-specific siRNAs correlates well with a decreased number of proliferating cells (c) and reduced PTN expression (d). ** $p < 0.01$; *** $p < 0.005$.

plasmids (Grzelinski *et al.*, 2005) and demonstrate the efficacy of the PEI/siRNA-based gene-targeting system employed here. They also set the standard for the effects expected in our *in vivo* mouse glioblastoma models.

More importantly, we show that PEI complexation allows the systemic *in vivo* application of PTN siRNAs in different glioblastoma models, leading to efficient PTN downregulation and to a significant decrease in tumor growth. Full-length siRNA molecules were detected in several tissues, but barely in the blood, indicating that (1) the signals represent siRNAs internalized into the tissue cells rather than floating in the blood stream and that (2) blood levels of siRNAs at any given time point are generally low. Furthermore, experiments with fluorescently labeled PEI reveal the presence of PEI, as well as of larger PEI-based particles, in the tumor xenografts. The notion

that intact PEI/nucleic acid complexes indeed reach target tissues despite their size and their positive charge is in agreement with previous studies on the organ distribution and pharmacokinetics of different double-labeled complexes comprising various PEIs and oligodeoxynucleotides (Fischer *et al.*, 2004).

However, our data also demonstrate the formation of aggregates as described previously, for example, under certain *in vitro* conditions (Goula *et al.*, 1998). Although these aggregates still show some *in vivo* mobility (as indicated by the fact that they are present in the tumor xenografts), it is tempting to speculate that they may also form a depot of complexed siRNAs, allowing the slow release of the noncovalently complexed siRNA molecules. This may also account for the fact that siRNA blood levels at any given time point are generally low (see above).

Because PEI-complexed unrelated siRNAs were employed as controls in several experiments, nonspecific effects based on PEI or siRNA (for review see Hannon and Rossi, 2004) can be excluded. This is also true for the sequence-dependent stimulation of the mammalian innate immune system by synthetic siRNAs, which has been described previously (Hornung *et al.*, 2005; Judge *et al.*, 2005). Despite the fact that our PTN siRNA contains a putative immunostimulatory motif (UGUG), under various conditions (see Results for details) we did not detect upregulation of the cytokines TNF- α and IFN- α , which have been reported previously to show increased serum levels in mice after administration of formulated immunostimulatory siRNAs (Hornung *et al.*, 2005; Judge *et al.*, 2005).

The lack of detectable immunostimulation even in the case of the siRNA containing a UGUG motif (1) may be due to a different formulation employed here, (2) may indicate insufficient immunostimulatory motifs on the siRNAs used in our study, and/or (3) may be based on the smaller siRNA amounts used in our experiments. In fact, Judge *et al.* employed more than 6-fold higher siRNA amounts per injection and performed liposome encapsulation rather than PEI complexation. Because this study also showed that, for example, the same amount of naked siRNAs did not induce an immune response in mice, the formulation seems to be of critical importance. In fact, it has been shown that the subcellular localization of siRNAs (cytoplasmic versus endosomal) seems to be of critical importance for the induction of an interferon response (for review see Sioud, 2006a), which further emphasizes the relevance of differences in siRNA delivery. Because cytoplasmic delivery of synthetic siRNAs by electroporation has been demonstrated not to induce either inflammatory cytokines or interferons, whereas the same sequences when delivered by lipid did (Sioud, 2005), our data further support the model of cytoplasmic siRNA release from PEI complexes. Furthermore, the siRNA amount per injection are certainly of relevance because an siRNA dose dependence of the immune response has already been shown (Judge *et al.*, 2005) and, because of a putative depot effect of larger PEI/siRNA particles, the actual siRNA concentrations may even be smaller in our study. Finally, it should be noted that single-stranded small interfering RNA molecules are more immunostimulatory than their double-stranded counterparts (Sioud, 2006b), again indicating a possible dependence of the immunostimulation on the siRNA formulation. Because LPS, serving here as a positive control, produced an immunostimulatory effect after only a short treatment time, we conclude from these data that our PEI/siRNA complexes do not exert a measurable immunostimulatory effect under these treatment conditions and that the antitumor effects are actually based on PTN downregulation.

The fact that comparably small amounts of PEI-complexed siRNAs were sufficient to achieve *in vivo* antitumoral effects may also account for the absence of any side effects of our treatment even on intracranial application. Subsequent analysis of the tumors reveals that the reduction in tumor volume correlates well with reduced PTN expression, confirming that the observed effects on tumor growth are based on specific PTN targeting. Hence we have established the antitumoral effect of *in vivo* PEI/siRNA-mediated PTN targeting in glioblastomas.

In future, the detailed characterization of an individual tumor based on gene expression analysis (e.g., by cDNA arrays)

will lead to more and more customized therapies and individual targeting strategies based on individual tumor expression profiles. To this end, it is essential to develop easy-to-use drug targeting strategies that allow rapid adaptation toward a novel set of target genes. In this regard, gene silencing by siRNA holds great promise and at the moment delivery of bioactive siRNAs into tumor cells seems to be the most challenging translational problem. This is especially true for GBM because the blood-brain barrier effectively inhibits the penetration of large and charged molecules such as siRNAs into the brain tissue. Thus, any siRNA-based treatment will rely on a direct application protocol into the tumor environment, which is technically demanding but feasible. One article showed in mice that the continuous intracranial delivery of plasmid-based vectors that drive the expression of siRNAs targeted against cathepsin B and urokinase plasminogen activator (uPA) by Alzet minipumps inhibited the tumor growth of established glioma xenografts (Gondi *et al.*, 2004). Although this study nicely demonstrated the feasibility of plasmid-based siRNA treatment of CNS tumors, gene therapy approaches with plasmid vectors carry specific risks and are not readily suitable for the development of customized therapies, as mentioned above. In another study, PEGylated polyethylenimine with an RGD peptide ligand was used to deliver siRNA with high tissue specificity to subcutaneous neuroblastoma N2A xenografts (Schiffelers *et al.*, 2004).

Here, we present the PEI complexation of siRNAs as a universally applicable platform for RNAi-based gene targeting, which will allow the use of various siRNAs directed against targets identified as optimal in a given tumor, and introduce PEI-complexed, PTN-specific siRNAs as an efficient tool for PTN targeting *in vitro* and *in vivo*. We firmly establish that, also in a complex and relevant orthotopic tumor model, intracranial application of therapeutic PTN-specific PEI/siRNA complexes significantly reduced intracranial U87 tumor growth, indicating the potential of this approach as a novel therapeutic option in GBM.

ACKNOWLEDGMENTS

The authors are grateful to Nicole Bader, Jan-Sebastian Grigoleit, Susanne Hamisch, Beate Junk, Helga Radler, and Andrea Wüstenhagen for expert help with the experiments, and to Marc Vigny for providing the PTN antibody (4B7). T.M. was supported by a scholarship from the Verein zur Förderung der Krebsforschung Heidelberg, e.V., and M.G. was supported by a stipend from the FAZIT Stiftung, Frankfurt. This work was supported in part by grants AI 245-1 (to A.A.) and WE 928-4-2 from the Deutsche Forschungsgemeinschaft (DFG).

REFERENCES

ABUHARBEID, S., APEL, J., SANDER, M., FIEDLER, B., LANGER, M., ZUZARTE, M.L., CZUBAYKO, F., and AIGNER, A. (2004). Cytotoxicity of the novel anti-cancer drug rViscum depends on HER-2 levels in SKOV-3 cells. *Biochem. Biophys. Res. Commun.* 321, 403-412.

AIGNER, A. (2006). Gene silencing through RNA interference (RNAi) *in vivo*: Strategies based on the direct application of siRNAs. *J. Biotechnol.* 124, 12–25.

AIGNER, A., FISCHER, D., MERDAN, T., BRUS, C., KISSEL, T., and CZUBAYKO, F. (2002a). Delivery of unmodified bioactive ribozymes by an RNA-stabilizing polyethylenimine (LMW-PEI) efficiently down-regulates gene expression. *Gene Ther.* 9, 1700–1707.

AIGNER, A., RAY, P.E., CZUBAYKO, F., and WELLSTEIN, A. (2002b). Immunolocalization of an FGFR-binding protein reveals a widespread expression pattern during different stages of mouse embryo development. *Histochem. Cell Biol.* 117, 1–11.

AIGNER, A., BRACHMANN, P., BEYER, J., JAGER, R., RAULAS, D., VIGNY, M., NEUBAUER, A., HEIDENREICH, A., WEINKNECHT, S., CZUBAYKO, F., and ZUGMAIER, G. (2003). Marked increase of the growth factor pleiotrophin and fibroblast growth factor-2 in serum of testicular cancer patients. *Ann. Oncol.* 14, 1525–1529.

ANABOUDI, S., LAUE, M., LEHR, C.M., BAKOWSKY, U., and EHRHARDT, C. (2005). Assessing transferrin modification of liposomes by atomic force microscopy and transmission electron microscopy. *Eur. J. Pharm. Biopharm.* 60, 295–303.

BEHR, J.P. (1997). The proton sponge: A trick to enter cells the viruses did not exploit. *Chimia* 51, 34–36.

BOUSSIF, O., LEZOUALCH'F, ZANTA, M.A., MERGNY, M.D., SCHERMAN, D., DEMENEIX, B., and BEHR, J.P. (1995). A versatile vector for gene and oligonucleotide transfer into cells in culture and *in vivo*: Polyethylenimine. *Proc. Natl. Acad. Sci. U.S.A.* 92, 7297–7301.

BOWDEN, E.T., STOICA, G.E., and WELLSTEIN, A. (2002). Anti-apoptotic signaling of pleiotrophin through its receptor, anaplastic lymphoma kinase. *J. Biol. Chem.* 277, 35862–35868.

BROCKMANN, M.A., PAPADIMITRIOU, A., BRANDT, M., FILLBRANDT, R., WESTPHAL, M., and LAMSZUS, K. (2003a). Inhibition of intracerebral glioblastoma growth by local treatment with the scatter factor/hepatocyte growth factor-antagonist NK4. *Clin. Cancer Res.* 9, 4578–4585.

BROCKMANN, M.A., WESTPHAL, M., and LAMSZUS, K. (2003b). Improved method for the intracerebral engraftment of tumour cells and intratumoural treatment using a guide screw system in mice. *Acta Neurochir. (Wien)* 145, 777–781; discussion 781.

CHAUDHURI, R., ZHANG, H.T., DONNINI, S., ZICHE, M., and BICKNELL, R. (1997). An angiogenic role for the neurokinins midkine and pleiotrophin in tumorigenesis. *Cancer Res.* 57, 1814–1819.

COURTY, J., DAUCHEL, M.C., CARUELLE, D., PERDERISET, M., and BARRITAULT, D. (1991). Mitogenic properties of a new endothelial cell growth factor related to pleiotrophin. *Biochem. Biophys. Res. Commun.* 180, 145–151.

CZUBAYKO, F., SCHULTE, A.M., MISSNER, S.C., HSIEH, S.S., COLLEY, K.J., and WELLSTEIN, A. (1995). Molecular and pharmacologic targeting of angiogenesis factors: The example of pleiotrophin. *Breast Cancer Res. Treat.* 36, 157–168.

CZUBAYKO, F., SCHULTE, A.M., BERCHEM, G.J., and WELLSTEIN, A. (1996). Melanoma angiogenesis and metastasis modulated by ribozyme targeting of the secreted growth factor pleiotrophin. *Proc. Natl. Acad. Sci. U.S.A.* 93, 14753–14758.

DAVIS, F.G., KUPELIAN, V., FREELS, S., MCCARTHY, B., and SURAWICZ, T. (2001). Prevalence estimates for primary brain tumors in the United States by behavior and major histology groups. *J. Neurooncol.* 3, 152–158.

ELBASHIR, S.M., HARBORTH, J., LENDECKEL, W., YALCIN, A., WEBER, K., and TUSCHL, T. (2001). Duplexes of 21-nucleotide RNAs mediate RNA interference in cultured mammalian cells. *Nature* 411, 494–498.

FANG, W.J., HARTMANN, N., CHOW, D., RIEGEL, A.T., and WELLSTEIN, A. (1992). Pleiotrophin stimulates fibroblasts, endothelial and epithelial cells, and is expressed in human cancer. *J. Biol. Chem.* 267, 25889–25897.

FISCHER, D., OSBURG, B., PETERSEN, H., KISSEL, T., and BICKEL, U. (2004). Effect of poly(ethylene imine) molecular weight and pegylation on organ distribution and pharmacokinetics of polyplexes with oligodeoxynucleotides in mice. *Drug Metab. Dispos.* 32, 983–992.

GONDI, C.S., LAKKA, S.S., DINH, D.H., OLIVERO, W.C., GUJRALI, M., and RAO, J.S. (2004). RNAi-mediated inhibition of cathepsin B and uPAR leads to decreased cell invasion, angiogenesis and tumor growth in gliomas. *Oncogene* 23, 8486–8496.

GOULIA, D., REMY, J.S., ERBACHER, P., WASOWICZ, M., LEVI, G., ABDALLAH, B., and DEMENEIX, B.A. (1998). Size, diffusibility and transfection performance of linear PEI/DNA complexes in the mouse central nervous system. *Gene Ther.* 5, 712–717.

GRZELINSKI, M., BADER, N., CZUBAYKO, F., and AIGNER, A. (2005). Ribozyme-targeting reveals the rate-limiting role of pleiotrophin in glioblastoma. *Int. J. Cancer* 117, 942–951.

HANNON, G.J., and ROSSI, J.J. (2004). Unlocking the potential of the human genome with RNA interference. *Nature* 431, 371–378.

HOLLAND, E.C. (2000). Glioblastoma multiforme: The terminator. *Proc. Natl. Acad. Sci. U.S.A.* 97, 6242–6244.

HORNUNG, V., GUENTHER-BILLER, M., BOURQUIN, C., ABLASER, A., SCHLEE, M., UEMATSU, S., NORONHA, A., MANOHarAN, M., AKIRA, S., DE FOUGEROLLES, A., ENDRES, S., and HARTMANN, G. (2005). Sequence-specific potent induction of IFN- α by short interfering RNA in plasmacytoid dendritic cells through TLR7. *Nat. Med.* 11, 263–270.

HOWARD, K. (2003). Unlocking the money-making potential of RNAi. *Nat. Biotechnol.* 21, 1441–1446.

JENSEN, R.L. (1998). Growth factor-mediated angiogenesis in the malignant progression of glial tumors: A review. *Surg. Neurol.* 49, 189–195; discussion 196.

JUDGE, A.D., SOOD, V., SHAW, J.R., FANG, D., McCLINTOCK, K., and MACLACHLAN, I. (2005). Sequence-dependent stimulation of the mammalian innate immune response by synthetic siRNA. *Nat. Biotechnol.* 23, 457–462.

KICHLER, A. (2004). Gene transfer with modified polyethylenimines. *J. Gene Med.* 6(Suppl. 1), S3–S10.

KURTZ, A., SCHULTE, A.M., and WELLSTEIN, A. (1995). Pleiotrophin and midkine in normal development and tumor biology. *Crit. Rev. Oncog.* 6, 151–177.

LAAROUBL, K., DELBE, J., VACHEROT, F., DESGRANGES, P., TARDIEU, M., JAYE, M., BARRITAULT, D., and COURTY, J. (1994). Mitogenic and *in vitro* angiogenic activity of human recombinant heparin apafin regulatory peptide. *Growth Factors* 10, 89–98.

LI, Y.S., MILNER, P.G., CHAUHAN, A.K., WATSON, M.A., HOFFMAN, R.M., KODNER, C.M., MILBRANDT, J., and DEUEL, T.F. (1990). Cloning and expression of a developmentally regulated protein that induces mitogens and neurite outgrowth activity. *Science* 250, 1690–1694.

LU, K.V., JONG, K.A., KIM, G.Y., SINGH, J., DIA, E.Q., YOSHIMOTO, K., WANG, M.Y., CLOUGHESY, T.F., NELSON, S.F., and MISCELL, P.S. (2005). Differential induction of glioblastoma migration and growth by two forms of pleiotrophin. *J. Biol. Chem.* 280, 26953–26964.

MALERZYK, C., SCHULTE, A.M., CZUBAYKO, F., BELLON, L., MACEJAK, D., RIEGEL, A.T., and WELLSTEIN, A. (2005). Ribozyme targeting of the growth factor pleiotrophin in established tumors: A gene therapy approach. *Gene Ther.* 12, 339–346.

MENTLEIN, R., and HELD-PEINDT, J. (2002). Pleiotrophin, an angiogenic and mitogenic growth factor, is expressed in human gliomas. *J. Neurochem.* 83, 747–753.

MILNER, P.G., LI, Y.S., HOFFMAN, R.M., KODNER, C.M., SIEGEL, N.R., and DEUEL, T.F. (1989). A novel 17 kD heparin-binding growth factor (HBGF-8) in bovine uterus: Purification and N-terminal amino acid sequence. *Biochem. Biophys. Res. Commun.* 165, 1096–1103.

MOOG-LUTZ, C., DEGOUTIN, J., GOUZI, J.Y., FROBERT, Y., BRUNET-DE CARVALHO, N., BUREAU, J., CREMINON, C., and VIGNY, M. (2005). Activation and inhibition of anaplastic lymphoma kinase receptor tyrosine kinase by monoclonal antibodies and absence of agonist activity of pleiotrophin. *J. Biol. Chem.* **280**, 26039–26048.

MULLER, S., KUNKEL, P., LAMSZUS, K., ULRICH, U., LORENTE, G.A., NELSON, A.M., VON SCHACK, D., CHIN, D.J., LOHR, S.C., WESTPHAL, M., and MELCHER, T. (2003). A role for receptor tyrosine phosphatase ζ in glioma cell migration. *Oncogene* **22**, 6661–6668.

MURAMATSU, T. (2002). Midkine and pleiotrophin: Two related proteins involved in development, survival, inflammation and tumorigenesis. *J. Biochem. (Tokyo)* **132**, 359–371.

OBERLE, V., BAKOWSKY, U., ZUHORN, I.S., and HOEKSTRA, D. (2000). Lipoplex formation under equilibrium conditions reveals a three-step mechanism. *Biophys. J.* **79**, 1447–1454.

OSBURG, B., PEISER, C., DOMLING, D., SCHOMBURG, L., KO, Y.T., VOIGT, K., and BICKEL, U. (2002). Effect of endotoxin on expression of TNF receptors and transport of TNF- α at the blood-brain barrier of the rat. *Am. J. Physiol. Endocrinol. Metab.* **283**, E899–E908.

POWERS, C., AIGNER, A., STOICA, G.E., McDONNELL, K., and WELLSTEIN, A. (2002). Pleiotrophin signaling through anaplastic lymphoma kinase is rate-limiting for glioblastoma growth. *J. Biol. Chem.* **277**, 14153–14158.

RAUVALA, H. (1989). An 18-kD heparin-binding protein of developing brain that is distinct from fibroblast growth factors. *EMBO J.* **8**, 2933–2941.

SATYAMOORTHY, K., OKA, M., and HERLYN, M. (2000). An antisense strategy for inhibition of human melanoma growth targets the growth factor pleiotrophin. *Pigment Cell Res.* **13**(Suppl. 8), 87–93.

SCHIFFELERS, R.M., ANSARI, A., XU, J., ZHOU, Q., TANG, Q., STORM, G., MOLEMA, G., LU, P.Y., SCARIA, P.V., and WOODLE, M.C. (2004). Cancer siRNA therapy by tumor selective delivery with ligand-targeted sterically stabilized nanoparticle. *Nucleic Acids Res.* **32**, e149.

SHANKAR, P., MANJUNATH, N., and LIEBERMAN, J. (2005). The prospect of silencing disease using RNA interference. *JAMA* **293**, 1367–1373.

SIoud, M. (2005). Induction of inflammatory cytokines and interferon responses by double-stranded and single-stranded siRNAs is sequence-dependent and requires endosomal localization. *J. Mol. Biol.* **348**, 1079–1090.

SIoud, M. (2006a). RNA interference below the immune radar. *Nat. Biotechnol.* **24**, 521–522.

SIoud, M. (2006b). Single-stranded small interfering RNA are more immunostimulatory than their double-stranded counterparts: A central role for 2'-hydroxy uridines in immune responses. *Eur. J. Immunol.* **36**, 1222–1230.

ULBRICH, U., BROCKMANN, M.A., AIGNER, A., ECKERICH, C., MULLER, S., FILLBRANDT, R., WESTPHAL, M., and LAMSZUS, K. (2003). Expression and function of the receptor protein tyrosine phosphatase ζ and its ligand pleiotrophin in human astrocytomas. *J. Neuropathol. Exp. Neurol.* **62**, 1265–1275.

UPRICHARD, S.L. (2005). The therapeutic potential of RNA interference. *FEBS Lett.* **579**, 5996–6007.

URBAN-KLEIN, B., WERTH, S., ABUHARBEID, S., CZUBAYKO, F., and AIGNER, A. (2005). RNAi-mediated gene-targeting through systemic application of polyethylenimine (PEI)-complexed siRNA *in vivo*. *Gene Ther.* **12**, 461–466.

WAGNER, B., KIRCHEIS, R., and WALKER, G.F. (2004). Targeted nucleic acid delivery into tumors: New avenues for cancer therapy. *Biomed. Pharmacother.* **58**, 152–161.

WELLSTEIN, A., LUPU, R., ZUGMAIER, G., FLAMM, S.L., CHEVILLE, A.L., DELLI BOVI, P., BASILICO, C., LIPPMAN, M.E., and KERN, F.G. (1990). Autocrine growth stimulation by secreted Kaposi's fibroblast growth factor but not by endogenous basic fibroblast growth factor. *Cell Growth Differ.* **1**, 63–71.

WELLSTEIN, A., FANG, W.J., KHATRI, A., LU, Y., SWAIN, S.S., DICKSON, R.B., SASSE, J., RIEGEL, A.T., and LIPPMAN, M.E. (1992). A heparin-binding growth factor secreted from breast cancer cells homologous to a developmentally important cytokine. *J. Biol. Chem.* **267**, 2582–2587.

ZHANG, N., and DEUEL, T.F. (1999). Pleiotrophin and midkine, a family of mitogenic and angiogenic heparin-binding growth and differentiation factors. *Curr. Opin. Hematol.* **6**, 44–50.

Address reprint requests to:

Dr. Achim Aigner

Department of Pharmacology and Toxicology

Philipps-University Marburg,

School of Medicine

Karl-v.-Frisch-Strasse 1

D-35033 Marburg, Germany

E-mail: aigner@staff.uni-marburg.de

Received for publication January 14, 2006; accepted after revision May 21, 2006.

Published online: June 21, 2006.

EXHIBIT 12

Cholesteryl Oligoarginine Delivering Vascular Endothelial Growth Factor siRNA Effectively Inhibits Tumor Growth in Colon Adenocarcinoma

Won Jong Kim,¹ Lane V. Christensen,¹ Seongbong Jo,¹ James W. Yockman,¹ Ji Hoon Jeong,¹ Yong-Hee Kim,² and Sung Wan Kim^{1,*}

¹Center for Controlled Chemical Delivery, Department of Pharmaceutics and Pharmaceutical Chemistry, 205 2030 E RM 205 BPRB, University of Utah, Salt Lake City, UT 84112-5820, USA

²Department of Bioengineering, College of Engineering, Hanyang University, Seoul 133-791, Korea

*To whom correspondence and reprint requests should be addressed. Fax: +1 801 581 7848. E-mail: rburris@pharm.utah.edu.

Available online 12 June 2006

Vascular endothelial growth factor (VEGF) is a multifunctional angiogenic growth factor that is a primary stimulant of the development and maintenance of a vascular network in the vascularization of solid tumors. It has been reported that a blockade of VEGF-mediated angiogenesis is a powerful method for tumor regression. RNA interference represents a naturally occurring biological strategy for inhibition of gene expression. In mammalian systems, however, the *in vivo* application of small interfering RNA (siRNA) is severely limited by the instability and poor bioavailability of unmodified siRNA molecules. In this study, we tested the hypothesis that hydrophobically modified protein transduction domain, cholesteryl oligo-D-arginine (Chol-R9), may stabilize and enhance tumor regression efficacy of the VEGF-targeting siRNA. The noncovalent complexation of a synthetic siRNA with Chol-R9 efficiently delivered siRNA into cells *in vitro*. Moreover, in a mouse model bearing a subcutaneous tumor, the local administration of complexed VEGF-targeting siRNA, but not of scrambled siRNA, led to the regression of the tumor. Hence, we propose a novel and simple system for the local *in vivo* application of siRNA through Chol-R9 for cancer therapy.

Key Words: VEGF, angiogenesis, RNA interference, oligoarginine, gene therapy

INTRODUCTION

The phenomenon of RNA interference (RNAi) or posttranscriptional gene silencing is an evolutionarily conserved biological response to double-stranded RNA (dsRNA) for degradation of the sequence-specific homologous mRNA. RNAi is initiated by the dsRNA-specific endonuclease, Dicer, which promotes processive cleavage of long dsRNA into double-stranded fragments between 21 and 23 nucleotides long, termed small interfering RNA (siRNA). This siRNA binds to the RNA-induced silencing complex, which recognizes target mRNA to be degraded [1–4]. Recently, it has become a useful tool for specific gene silencing and analysis of gene function.

To improve the efficiency of siRNA function, delivery systems need to be developed to condense siRNA effectively into small particles, thereby enhancing the cellular uptake and protection from enzymatic degradation. Ideas for siRNA delivery vehicles based upon the designs of polymeric delivery systems for plasmid DNA [5–9] have begun to flourish [10,11]; therefore, enhancement of the

transfection efficiency *in vitro* and *in vivo* has progressed rapidly. In fact, numerous attempts to enhance siRNA function have been made based on cationic lipopeptide [12], steroid and lipid conjugates of siRNA [13,14], and block copolymer-coated calcium phosphate nanoparticles [15]. Recently, to enhance the cellular uptake and transfection efficiency, arginine-rich cell-penetrating peptides (CPPs) such as human immunodeficiency virus (HIV-1) TAT and antennapedia have been developed as gene delivery vehicles [16,17]. In cell culture, a conjugate of an antisense oligonucleotide and the antennapedia peptide was able to inhibit the translation of amyloid precursor protein at a concentration of 40 nM [18]. In a separate study, the antennapedia peptide-conjugated oligonucleotide against Cu/Zn superoxide dismutase showed a 100-fold higher efficiency in culture than did the oligonucleotide itself [19]. Furthermore, arginine oligopeptides have been modified with several hydrophobic lipid molecules to enhance plasmid gene transfection [20]. The mechanism of internalization of CPPs is

not well understood and has recently been the subject of discussion. Most cellular uptake studies of CPPs in the literature based on fluorescence microscopy of fixed cells and/or flow cytometry analysis report that internalization of CPPs does not involve endocytosis [21–25]. These studies have been recently revisited by the mechanism of cellular uptake being reevaluated. More current evidence shows that the internalization of CPPs is an energy-dependent process involving classical adsorptive endocytosis [26–28].

We have reported an effective water-soluble lipopolymer (WSLP) by combining the cationic headgroup of branched polyethylenimine (bPEI; M_w , 1.8 kDa) with a hydrophobic lipid anchor, cholesterol chloroformate [6]. WSLP showed low cytotoxicity and enhanced transfection efficacy *in vitro* and *in vivo* [6,29–31]. The effectiveness of WSLP over bPEI was due to the modification of the inherent structural DNA complex to enhance the interaction with plasma membrane and facilitate the endosomal escape.

In this study, we synthesized a cholesteryl oligo-D-arginine (nine residues) conjugate (Chol-R9) as a siRNA delivery vehicle for vascular endothelial growth factor (VEGF) silencing. VEGF is a growth factor most consistently found in a wide variety of conditions associated

with angiogenesis [32]. It has been reported that impairing the function of VEGF could inhibit tumor growth and metastasis by preventing its own vascularization in a variety of animal models [33–35]. We investigated the potency of the Chol-R9 conjugate as a siRNA delivery vehicle *in vitro* and *in vivo* in a mouse tumor model.

RESULTS

Synthesis of Chol-R9

We successfully modified oligoarginine (R9) with cholesterol chloroformate (Fig. 1). The ^1H NMR spectrum of Chol-R9 showed characteristic cholesterol methyl proton peaks ranging from 0.5 to 1.0 ppm (Fig. 2A). R9 proton peaks are also shown in the spectrum. Especially the methine proton peak of R9 (protons at α -carbons), which represents nine protons, appeared at 4.2 ppm. We determined the coupling yield of cholesterol chloroformate to R9 from the cholesterol methyl proton peak at 0.5 ppm, which represents three protons, and the proton peak of arginine α -carbon at 4.2 ppm using the equation coupling yield (%) = $(3 \times A_{0.5\text{ ppm}})/A_{4.2\text{ ppm}} \times 100$, where $A_{0.5\text{ ppm}}$ and $A_{4.2\text{ ppm}}$ stand for integrations of proton peaks at 0.5 and 4.2 ppm in the NMR spectrum of

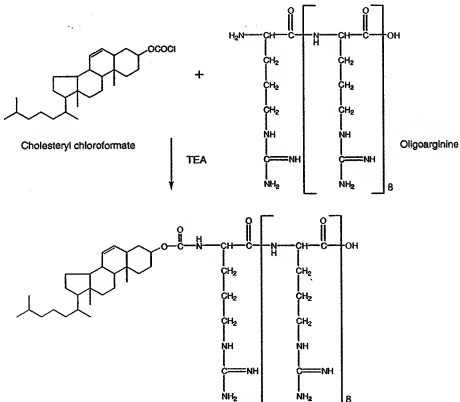


FIG. 1. Synthesis scheme of Chol-R9 conjugate.

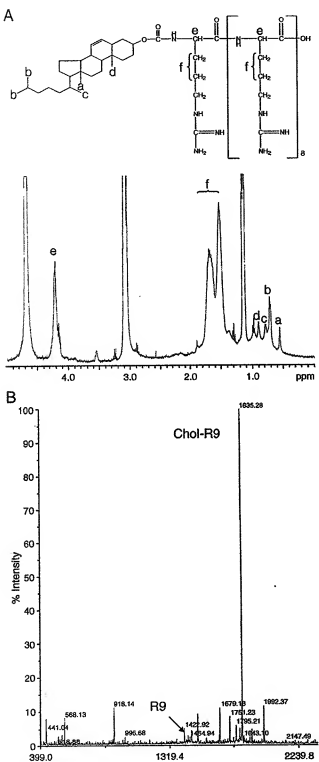


FIG. 2. Chol-R9 conjugate characterized using ¹H NMR and MALDI-TOF mass spectroscopy. (A) ¹H NMR spectrum of Chol-R9. (B) MALDI-TOF mass spectra of Chol-R9.

Chol-R9, respectively. The calculated coupling yield in this study was 50.3%. The matrix-assisted laser desorption time-of-flight (MALDI-TOF) mass spectrum of Chol-R9 showed a predominant peak at 1835.28 (*m/z*), which can be assigned as (M-H) (Fig. 2B). The electrospray ionization (ESI) mass spectrum also showed dominant peaks of Chol-R9 and R9, indicating an absence of any free cholesterol chloroformate (data not shown). These results reaffirm the fact that the polymer product contains only a mixture of Chol-R9 and R9.

Complex Formation of Chol-R9 with Plasmid DNA
To identify the characteristics of Chol-R9 to act as an efficient nonviral gene carrier, we carried out DNA complex formation on agarose gel electrophoresis at different *N/P* ratios, i.e., the ratio of concentration of total nitrogen atoms (*N*) of the polycation to that of the phosphate groups (*P*) of reporter plasmid DNA. The movement of plasmid in the gel was retarded as the amount of the Chol-R9 conjugate was increased, demonstrating that the conjugate binds to negatively charged DNA, neutralizing its charge (Fig. 3A, top). Complete complex formations were achieved at *N/P* ratios equal to and above 8:1 (lane S), similar to unmodified oligoarginine (Fig. 3A, bottom).

Cell Toxicity and *In Vitro* Transfection Efficiency of Chol-R9/DNA Complex

We investigated the cytotoxicity of Chol-R9/DNA complexes using the 3-(4,5-dimethylthiazol-2-yl)-2,5-diphenyltetrazolium bromide (MTT) assay (Fig. 3B) on 293T cells. We prepared Chol-R9/DNA complexes at various *N/P* ratios from 8 to 72, while we made bPEI/DNA complexes at an *N/P* ratio of 5. The complex of Chol-R9/DNA showed at least 90% cell viability at the *N/P* ratios of 8 to 48.

We evaluated the transfection efficiency of the synthesized Chol-R9 *in vitro* using 293T cell lines. For the transfection experiments, we formulated various Chol-R9/pCMV-Luc or R9/pCMV-Luc complexes with a fixed amount of pCMV-Luc (50 µg/ml). Chol-R9/pCMV-Luc complexes showed higher transfection efficiency than R9/pCMV-Luc complexes at a range of *N/P* ratios between 20 and 40 (Fig. 3C). The conjugation of cholesterol to R9 suggests enhanced cellular uptake of complexes and increased transfection efficiency.

Complex Formation of Chol-R9 Conjugate with siRNA
To identify the formation of Chol-R9/siRNA complexes, we performed polyacrylamide gel electrophoresis (PAGE) at different *N/P* ratios. The positively charged R9 of the Chol-R9 conjugate makes complexes with the negatively charged phosphate ions on the base backbone on siRNA. When the value of the *N/P* ratio of Chol-R9/siRNA reached 40, free siRNA was not detected on the PAGE (Fig. 4B).

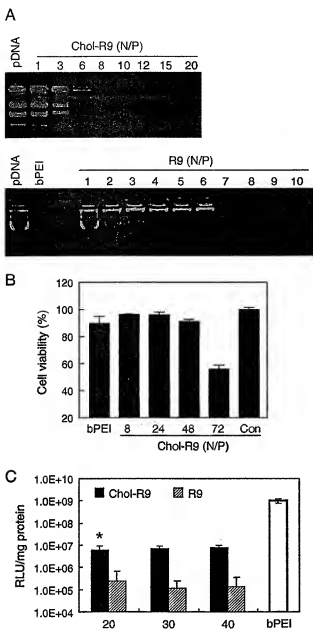


FIG. 3. Complex formation, cell viability, and transfection profiles of Chol-R9/bPEI and R9/bPEI. (A) Electrophoretic patterns of plasmid DNA complexes with Chol-R9 (top) and R9 (bottom). (B) Cytotoxicity of bPEI/pCMV-Luc and Chol-R9/pCMV-Luc for 293T cells. The data are expressed as mean values \pm standard deviation of three experiments. (C) Luciferase expression of Chol-R9 conjugates compared to unmodified R9 and a bPEI control. The graph represents mean values \pm standard deviation of experiments run in triplicate. * $P < 0.05$ compared to unmodified R9.

VEGF Silencing Effect of Chol-R9/siRNA Complex *in Vitro*

To evaluate the biological significance of these systems, we investigated the inhibitory activity of siRNA against the expression of VEGF in CT-26 cells. We evaluated the

inhibitory effect from the relative silencing of the VEGF assayed by enzyme-linked immunosorbent assay (ELISA). Obviously, we observed appreciable silencing of the VEGF for the bPEI/siVEGF complex at the N/P ratio of 10, while scrambled (sc) VEGF showed no effect (Fig. 5A). As shown in Fig. 5B, Chol-R9/siVEGF complex suppressed the VEGF production by 55% compared with the untreated control, whereas the unmodified R9/siVEGF complex did not silence the expression of VEGF with the same amount of siRNA.

Inhibition of Tumor Growth with Chol-R9/siRNA Complex *in Vivo*

We injected CT-26 cells (1×10^6) sc into the flank of mice. By 2 weeks, visible tumors had developed at the injection sites (mean tumor volume 74.18 mm^3). To determine the therapeutic effectiveness of VEGF siRNA, we started intratumoral treatment with Chol-R9/siVEGF or Chol-R9/scVEGF and repeated every 4 days for a total of six times. As shown in Figs. 6A and 6B, Chol-R9/siVEGF complex markedly suppressed the tumor growth compared with Chol-R9/scVEGF complex ($P < 0.05$) or 5% glucose solution as a control. To assess the relationship between the therapeutic effects of Chol-R9/siRNA and VEGF in tumors, we quantified the amount of VEGF in tumors. We observed a dramatically lower level of VEGF in tumors treated with Chol-R9/siVEGF at 17 days after the first injection, whereas the tumors treated with Chol-R9/scVEGF showed higher level of VEGF (Fig. 7A). We then examined the vascularization in tumors by immunostaining with an anti-CD31 antibody. The vascularization in tumors observed in the Chol-R9/siVEGF-treated group was significantly reduced compared with tumors from the Chol-R9/scVEGF-treated group (Fig. 7B). Based on the above observations, we believe that the antitumor effect of Chol-R9/siVEGF was due mainly to the antiangiogenic effect of Chol-R9/siVEGF, which was confirmed by VEGF quantification (Fig. 7A) and histological examination (Fig. 7B).

DISCUSSION

Since siRNAs play a pivotal role in gene silencing, the critical factors that will determine the success of RNA interference approaches are the ability to deliver intact siRNAs efficiently into the appropriate cells. In an attempt to enhance the function of siRNA, numerous studies have used DNA vectors that, upon viral or nonviral transfection, lead to intracellular expression of double-stranded RNA [36–40]. While this approach often results in robust downregulation of gene expression *in vitro*, it suffers *in vivo* from problems including low transfection efficiency, poor tissue penetration, and toxicity to the host.

Bioactive arginine-rich peptides derived from HIV-1 TAT and antennapedia homeodomain capable of con-

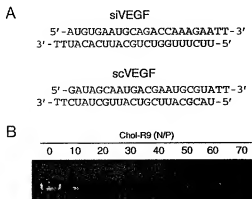


FIG. 4. Sequences of siRNA and complex formation profile. (A) Sequences of siRNA targeting VEGF, siVEGF, and scrambled siRNA, scVEGF. (B) Electrophoretic patterns of siRNA complexes with Chol-R9 conjugates.

densing nucleic acids have attracted considerable attention as parts of DNA and siRNA delivery vectors because of a highly reproducible and scalable production and an inherent specific biological activity [16–20]. Cellular uptake of these peptides has been ascribed in the literature to an energy- and receptor-independent mechanism that does not involve endocytosis [21–25]. Recently, however, it has been demonstrated that cell fixation, even under mild conditions, leads to the artifactual uptake of these peptides [26]. Moreover, a number of studies questioned the validity of the predominant mechanisms and suggested that the internalization of arginine-rich peptides is a temperature- and energy-dependent process involving endocytosis [26–28]. When used alone, small arginine-rich peptides usually exhibit lower cytotoxicity and are also weaker activators of the complement system than high-molecular-weight polycations such as bPEI. However, the polyelectrolyte complexes formed with short arginine-rich peptides lack sufficient stability to survive in the blood circulation and showed lower cellular uptake.

Small peptides of a distinctive structure, such as oligoarginine, have been studied less extensively compared with other cationic polymers as a DNA or siRNA delivery vehicle. Wender *et al.* reported that short oligomers of arginine were indeed more efficiently taken up into cells than TAT peptide [41]. This was quantified further by Michaelis-Menten kinetics analysis that showed that the arginine oligomers (R9) had K_m values 20- and 100-fold greater than that found for TAT. Prompted by this potential value of oligoarginine to enhance cellular entry, we initiated modification of oligoarginine to improve its transfection ability further.

Previously, the conjugation of the hydrophobic lipid anchor cholesterol to cationic polymers of polyethylenimine was reported to enhance the cellular uptake of DNA from the cell surface [6,7,29–31,42]. This WSLP con-

denses DNA and enhances endosomal release due to its tertiary amines, while the lipid coating on the DNA increases its permeability through cell membranes. To magnify advantages of the cell-penetrating oligoarginine and cholesterol lipid, we conjugated the cholesterol lipid anchor to R9 covalently as a gene and siRNA delivery vehicle.

For gene transfer, bPEI of high-molecular-weight (M_w 25 kDa) is commonly used, but is highly toxic to the cells even at low N/P ratios. Addition of the cholesterol to R9 did not adversely affect cell viability even at higher N/P ratios, though it increased transfection efficiency significantly in 293T cells (Figs. 3B and 3C). This higher

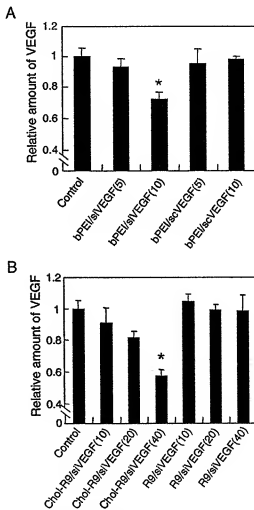


FIG. 5. VEGF silencing with a complex of siRNAs (siVEGF, VEGF siRNA; scVEGF, VEGF scrambled siRNA) and various carriers in CT-26 cells. (A) Sequence specificity of siRNAs. Cells were transfected with bPEI/siVEGF and bPEI/sciVEGF at the N/P ratios of 5 and 10. (B) Comparison of Chol-R9 with unmodified R9. Cells were transfected with Chol-R9/siVEGF and R9/siVEGF at the N/P ratios of 10 to 40. VEGF concentration in the conditioned medium was determined by ELISA for mouse VEGF. * $P < 0.02$ compared to untreated control.

transfection efficiency suggests enhanced cellular uptake of complexes.

To test for the bioactivity of Chol-R9 complexed with siRNAs, we performed a study of the inhibition of tumor angiogenesis by siRNA. A number of growth factors have been identified as potential positive regulators of angiogenesis. Among them, VEGF has been thoroughly studied as a target for antiangiogenic therapy [8,33–35]. Recently, inhibition of VEGF production by siRNA was reported as an effective and useful method for tumor antiangiogenic therapy *in vitro* and *in vivo* [43–45].

In this study, we found that the combination of two independent agents (oligoarginine and cholesterol) can produce synergistic effects and not only inhibit the production of VEGF in CT-26 cells *in vitro* but also suppress tumor growth *in vivo*. The higher bioactivity of Chol-R9/siRNA might be due to the ionic and hydrophobic interactions between Chol-R9 and siRNA, while the precise mechanism is not still clear. In a recent report,

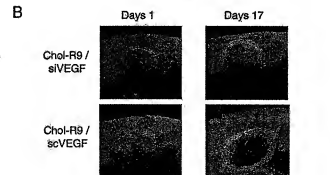
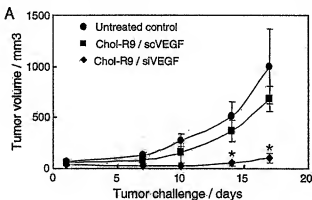


FIG. 6. Antitumor effect of siRNAs *in vivo*. (A) Tumor growth curves. VEGF siRNA (10 μ M siVEGF) or VEGF scrambled siRNA (10 μ M scVEGF) was mixed with Chol-R9 conjugate at the N/P ratio of 40, and 50 μ l of each mixture was injected into the tumor region subcutaneously. As a control, 5% glucose solutions were injected. Day 1 corresponds to 2 weeks after inoculation of cells when the tumor volume was approximately 70 mm^3 . Tumor diameters were measured at a regular interval for up to 17 days with calipers, and the tumor volume was calculated. Results represent the means \pm standard deviation ($n = 5$ tumors). * $P < 0.05$ compared to Chol-R9/scVEGF. (B) Images of CT-26 allografts. On days 1 and 17 CT-26 tumors were taken.

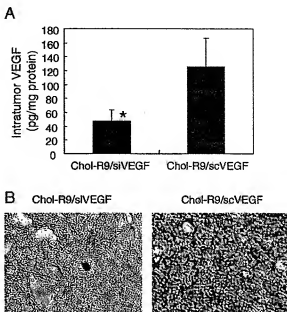


FIG. 7. Intratumor VEGF contents and vascularization. (A) VEGF levels in tumors at 17 days after injection. The excised tumors were homogenized in PBS with protease inhibitor (Sigma Chemical Co.) and then centrifuged. The amount of VEGF in each supernatant was measured by ELISA. * $P < 0.05$ compared to Chol-R9/scVEGF. (B) Immunohistochemical staining of the subcutaneous tumors with CD31 antibody. Representative images of Chol-R9/siVEGF-treated tumors (left) and Chol-R9/scVEGF-treated tumors (right).

higher cellular association of the stearyl-R8/DNA than R8/DNA was observed by Khalil *et al.* [46]. They suggested that with the aid of both the cationic charges and the hydrophobic interactions the stearyl-R8/DNA complexes would be adsorbed at high levels to the cell surface and then internalized via endocytosis. Conjugation of hydrophobic moieties to peptides has also been described to enhance the transfection efficiency by causing the compaction of DNA/carrier complexes [6,7,29–31,47,48].

Taken together, we suggest that the combination of the cholesterol moiety and cationic cell-penetrating peptides may enhance the cellular uptake of Chol-R9/siRNA complexes and transfection efficiency via endocytosis. Further study is needed to investigate the precise internalizing mechanisms of Chol-R9 or Chol-R9/siRNA complexes, including the intracellular location and fate of Chol-R9/siRNA complexes. Moreover, a variety of lipid moieties might be conjugated to arginine-rich peptides to test their enhancing ability for siRNA delivery.

MATERIALS AND METHODS

Synthesis of cholesterol oligoarginine conjugate. Chol-R9 was synthesized by reacting cholesterol chloroformate (Aldrich Chemical Co.) and oligo-D-arginine (nine residues) (Genemed Synthesis, Inc., San Francisco, CA, USA) in the presence of triethylamine (TEA) (Fig. 1). Oligoarginine (15.4 mg, 10.8 μ mol) was dissolved in 5 ml of anhydrous dimethylformamide,

After 15.08 μ l of TEA was added into the oligoarginine solution, cholesterol chloroformate (24.3 mg, 54 μ mol) in 5 ml of anhydrous tetrahydrofuran was slowly added at room temperature. The reaction mixture was stirred overnight. Upon completion of the reaction, solvents were removed by purging dry nitrogen gas through a glass transfer pipette. The remaining cholesterol chloroformate and TEA were rinsed off three times with 15 ml of diethyl ether each time. The crude precipitate was purified for 2 days by dialysis (MWCO 500; Spectrum) against deionized distilled water to remove free cholesterol. Fourteen milligrams of Chol-R9 was finally collected after freeze drying. Synthesized Chol-R9 was characterized by 1 H NMR spectroscopy, MALDI-TOF, and ESI mass spectrophotometer.

Gel retardation assay. Chol-R9/plasmid DNA complex formation were confirmed by the agarose gel retardation assay. Chol-R9/pCMV-Luc complexes were formed at different *N/P* ratios by incubating in 5% glucose solution at room temperature for 30 min. Each sample was then analyzed by electrophoresis on a 1% agarose gel with ethidium bromide (EtBr; 0.1 μ g/ml). Complex formation of Chol-R9/siRNA was monitored by the polyacrylamide gel retardation assay. siRNA targeting mouse VEGF (siVEGF) and scrambled siRNA (scVEGF) were purchased from IDT Technologies, Inc. (Coralville, IA, USA). Sequences of siRNA are shown in Fig. 4A. We selected siRNA sequences as reported by Filleur et al. [45]. Various amounts of Chol-R9, ranging from 0 to 44.5 ng, were added to 7 ng of siRNA at Chol-R9/siRNA *N/P* ratios from 0 to 70 in 5% glucose solution and incubated for 30 min at room temperature. After incubation, each sample was electrophoresed on 13% polyacrylamide gel (w/v) for 1 h at 100 V, TBE (89 mM Tris-borate, 2 mM EDTA) buffer was used as electrophoresis buffer. Following EtBr (0.1 μ g/ml) staining, the gel was illuminated with a UV illuminator to show the location of the siRNA.

Cell toxicity and *in vitro* transfection assay. The cytotoxicity of Chol-R9/DNA complexes was investigated using a tetrazolium-based calorimetric assay as previously reported [49]. In this test, viability of cells is assessed by the metabolism of a water-soluble tetrazolium dye, MTT, into insoluble formazan salts (Sigma) (Fig. 3B). Briefly, 293T cells were plated in 24-well plates at 60,000 cells per well and allowed to incubate for 24 h. Polymer/DNA complexes were added in triplicate to the wells at 0.5 μ g reporter plasmid DNA per well at varying *N/P* ratios. The bPEI (M4, 25 kDa) control was prepared at a 5:1 *N/P* ratio. After 44 h of incubation, the cell viability was determined, in which viability was compared to cells that received 5% glucose instead of polyplex dispersion.

Luciferase expression using different *N/P* ratios of R9 and Chol-R9 was observed by using a pCMV-Luc reporter plasmid. When cells reached ~80% confluence, transfections were performed at the total DNA concentration of 50 μ g/ml. Transfection experiments were carried out on 293T cells in six-well plates maintained in DMEM (GIBCO) medium at 37°C in a humidified atmosphere containing 5% CO₂. After 4 h of incubation, medium was replaced with 2 ml of fresh medium supplemented with 10% fetal bovine serum (FBS; Hyclone) and the cells were cultured for 48 h. Luciferase expression was quantitated using the Luciferase Assay System (Promega) normalized by milligrams of protein.

ELISA. CT-26 colon adenocarcinoma cells were grown to 80% confluence in 24-well plates and transfected with cationic substance/siRNA complexes. Following 24-h incubation, the level of mouse VEGF produced in the medium was determined by using a mouse VEGF ELISA kit (R&D Systems, Inc., Minneapolis, MN, USA) according to the recommendation of the manufacturer's protocol. Briefly, the 96-microwell plate (provided in the kit), coated with mouse polyclonal anti-VEGF antibody, was washed with wash buffer. Cell supernatant samples were diluted 1:4 by calibrator diluent, and 50 μ l of the sample was added into the designated wells. Similarly, VEGF standards ranging from 7.8 to 500 pg/ml, also diluted in calibrator diluent, were added to the microwell plates. The calibrator diluent alone was added in a blank well and incubated at room temperature for 2 h. After being washed four times with wash buffer, 100 μ l of polyclonal antibody against VEGF conjugated to horseradish peroxidase was added and incubated at room temperature for 2 h. After the wells were washed again four times, tetramethylbenzidine substrate

solution was added and incubated at room temperature for 30 min. The enzymatic reaction was stopped by adding 100 μ l of stop solution to the wells, and absorbance was determined by spectrophotometric reading at 450 nm. The VEGF concentration in the cell supernatant samples was calculated based on the standard curve.

Cell culture. 293T and CT-26 colon adenocarcinoma cell lines were grown and maintained in DMEM and RPMI 1640, respectively, which were supplemented with 10% FBS at 37°C and humidified 5% CO₂.

VEGF silencing with Chol-R9/siRNA complex *in vitro*. CT-26 cells were seeded in 24-well tissue culture plates at 8 \times 10⁴ cells per well in 10% FBS containing RPMI 1640 medium. Cells achieved 80% confluence within 24 h after which they were transfected with cationic substance/siRNA complexes prepared at different *N/P* ratios ranging from 5 to 40. The total amount of siRNA loaded was maintained constant at 0.7 μ g/well. The transfection was carried out in the absence of serum. The cells were allowed to incubate at 37°C in the presence of complexes for 4 h in a CO₂ incubator followed by replacement of 1 ml of RPMI 1640 containing 10% FBS. Thereafter, the cells were incubated at 37°C for additional 24 h. Cell supernatants were collected for analysis of the amount of VEGF produced by ELISA.

Tumor therapy. To generate tumors, 4- to 5-week-old female BALB/c mice were injected subcutaneously in the middle of the right flank with 100 μ l of a single-cell suspension containing 1 \times 10⁶ CT-26 cells. Tumor size was measured using a vernier caliper across its longest (*a*) and shortest (*b*) diameters and its volume was calculated using the formula $V = 0.5ab^2$. Treatment of the tumors was started after 10-15 days when the tumor size reached approximately 70 mm³. Chol-R9/siRNA complexes (*N/P* ratio of 40) were prepared in 5% glucose and 50 μ l of the complexes was injected directly into the tumor of BALB/c mice at a dose of 3.5 μ g siRNA/mouse. The tumors were measured every 4 days and mice were examined for appearance and growth of necrosis as well as decreased physical activity. Tumor progression was reported in terms of tumor volume over a period of 2 weeks.

Statistical analysis. Results are reported as means \pm SD. The statistical analysis between groups was determined using a nonpaired *t* test. $P < 0.05$ was considered significant.

ACKNOWLEDGMENT

This work was supported by National Institutes of Health Grant CA10707.

RECEIVED FOR PUBLICATION NOVEMBER 10, 2004; REVISED MARCH 14, 2006; ACCEPTED MARCH 20, 2006.

REFERENCES

- Zamore, P. D., Tuschl, T., Sharp, P. A., and Bartel, D. P. (2000). RNA: double-stranded RNA directs the ATP-dependent cleavage of mRNA at 21 to 23 nucleotide intervals. *Cell* 101: 25–33.
- Ebishti, S. M., Lendeckel, W., and Tuschl, T. (2001). RNA Interference is mediated by single- and double-nucleotide RNAs. *Nature Revs Dev* 15: 188–200.
- Opalka, J. B., and Gewirtz, A. M. (2002). Nucleic-acid therapeutics: basic principles and recent applications. *Nat Rev Drug Discov* 1: 503–514.
- Ebishti, S. M., Harbooth, J., Lendeckel, W., Yalcin, A., Weber, K., and Tuschl, T. (2001). Duplexes of 21-nucleotide RNAs mediate RNA interference in cultured mammalian cells. *Nature* 411: 494–498.
- Kim, J.-S., Maruyama, A., Akaike, T., and Kim, S. W. (1997). In vitro gene expression on smooth muscle cells using a terpolymer delivery system. *J. Controlled Release* 47: 51–59.
- Kim, S., Mehato, R. I., and Kim, S. W. (2001). Water-soluble lipopolymer for gene delivery. *Bioconjugate Chem* 12: 337–345.
- Ferguson, D. Y., Chan, W. S., Yockman, J. W., and Kim, S. W. (2003). Modified linear poly(ethylene-glycol)-cholesterol conjugates for DNA complexation. *Bioconjugate Chem* 14: 840–847.
- Kim, J. W., et al. (2005). Soluble Flt-1 gene delivery using PEG-g-PEG-RGD conjugate for anti-angiogenesis. *J. Controlled Release* 106: 224–234.
- Jeong, J. H., et al. (2005). Anti-GAD antibody targeted non-viral gene delivery to islet beta cells. *J. Controlled Release* 107: 562–570.
- Bologna, J. C., Dom, G., Natt, F., and Weiler, J. (2003). Linear poly(ethyleneimine) as a

tool for comparative studies of antisense and short double-stranded RNA oligonucleotides. *Nucleic Acids Nucleotides Nucleic Acids* 23: 1729–1731.

- Urban-Klein, R., Werth, S., Abuhabib, S., Czubayko, F., and Aigner, A. (2005). RNA-mediated gene targeting through systemic application of polyethylenimine (PEI)-complexed siRNA in vivo. *Gene Ther.* 12: 461–466.
- Unnammal, N., Kang, B. G., and Lee, W. S. (2004). Cationic oligopeptide-mediated delivery of dsRNA for post-transcriptional gene silencing in plant cells. *FEBS J.* 566: 307–310.
- Lorenz, C., Hadwiger, P., John, M., Vornlocher, H.-P., and Unverzagt, C. (2004). Steroid and lipid conjugates of siRNAs to enhance cellular uptake and gene silencing in liver cells. *Bioorg. Med. Chem. Lett.* 14: 4975–4977.
- Spagnoli, S., Miller, A. D., and Keller, M. (2004). Lipidic carriers of siRNA: differences in the formulation, cellular uptake, and delivery with plasmid DNA. *Biochemistry* 43: 13348–13356.
- Kakizawa, Y., Furukawa, S., and Kataoka, K. (2004). Block copolymer-coated calcium phosphate nanoparticles targeting intracellular environment for oligodeoxynucleotides and siRNAs delivery. *J. Controlled Release* 97: 345–356.
- Rudolph, C., et al. (2003). Oligomers of the arginine-rich motif of the HIV-1 Tat protein are capable of transferring plasmid DNA into cells. *J. Biol. Chem.* 278: 11411–11418.
- Mankani, D. S., Blight, H. S., Wan, L., Man, G., and Chlipacki, D. (2005). Influence of TAT-peptide polymerization on properties and transfection activity of TAT/DNA complexes. *J. Controlled Release* 102: 293–304.
- Alliquant, S., Hantraye, P., Malleix, P., Moya, K., Boulot, C., and Prochiantz, A. (1995). Downregulation of amyloid precursor protein inhibits neurite outgrowth in vitro. *J. Cell Biol.* 128: 919–927.
- Troy, C. M., Derossi, D., Prochiantz, A., Greene, L. A., and Sheslanski, M. L. (1996). Downregulation of Cu/Zn superoxide dismutase leads to cell death via the nitric oxide-peroxynitrite pathway. *J. Neurosci.* 16: 253–261.
- Futaki, S., et al. (2001). Steady-state arginine-rich peptides: a new class of transfection systems. *Bioconjugate Chem.* 12: 1005–1011.
- Suzuki, T., Futaki, S., Niwa, M., Tanaka, S., Ueda, K., and Sugiyama, Y. (2002). Possible existence of membrane-penetrating mechanisms among arginine-rich peptides. *J. Biol. Chem.* 277: 2437–2443.
- Tordjilin, V. P., Ramrohaman, R., Weisz, V., and Levenchko, T. S. (2001). Tat peptide on the surface of liposomes affords their efficient intracellular delivery even at low temperature and in presence of metabolic inhibitors. *Proc. Natl. Acad. Sci. USA* 98: 8786–8791.
- Futaki, S., et al. (2001). Arginine-rich peptides: an abundant source of membrane-permeable peptides having potential as carriers for intracellular protein delivery. *J. Biol. Chem.* 276: 5836–5840.
- Vives, E., Brodin, P., and Lebleu, B. (1997). A truncated HIV-1 Tat protein basic domain rapidly translocates through the plasma membrane and accumulates in the cell nucleus. *J. Biol. Chem.* 272: 16010–16017.
- Derossi, D., Chassing, G., and Prochiantz, A. (1998). Trojan peptides: the penetration system for intracellular delivery. *Trends Cell Biol.* 8: 84–87.
- Richard, J. P., et al. (2003). Cell-penetrating peptides: a reevaluation of the mechanism of cellular uptake. *J. Biol. Chem.* 278: 585–590.
- Leclerc, J. A., Hankins, S., and Whittaker, J. L. (2003). Full-length proteins attached to the HIV tat protein translocation domain are neither transduced between cells, nor exhibit enhanced immunogenicity. *Gene Ther.* 10: 1422–1428.
- Difesa, G., Cottini, S., Blanc, E., Rees, A. R., and Temsamani, J. (2003). Studies on the internalization mechanism of cationic cell-penetrating peptides. *J. Biol. Chem.* 278: 31192–31201.
- Yockman, J. W., Maheshwari, A., Han, S., and Kim, S. W. (2003). Tumor regression by repeated intratumoral delivery of water soluble lipopolymers/p2CMVml12 complexes. *J. Controlled Release* 87: 177–186.
- Lee, M., Rentz, J., Han, S., Bull, D. A., and Kim, S. W. (2003). Water-soluble lipopolymer as an efficient carrier for gene delivery to myocardium. *Gene Ther.* 10: 585–593.
- Lee, M., Rentz, J., Bakram, M., Han, S., Bull, D. A., and Kim, S. W. (2003). Hypoxia-inducible VEGF gene delivery to ischemic myocardium using water-soluble lipopolymer. *Gene Ther.* 10: 1535–1542.
- Leung, D. W., Cachianes, G., Kuang, W. J., Goeddel, D. V., and Ferrara, N. (1989). Vascular endothelial growth factor is a secreted angiogenic mitogen. *Science* 246: 1306–1309.
- Kim, K. J., et al. (1993). Inhibition of vascular endothelial growth factor-induced angiogenesis suppresses tumor growth in vivo. *Nature* 362: 841–844.
- Brekken, R. A., et al. (2000). Selective inhibition of vascular endothelial growth factor (VEGF) receptor signaling by a monoclonal anti-VEGF antibody blocks tumor growth in mice. *Cancer Res.* 60: 5117–5124.
- Hohsi, J., et al. (2002). VEGF-Trap: a VEGF blocker with potent antitumor effects. *Proc. Natl. Acad. Sci. USA* 99: 11393–11398.
- Xia, H., Mao, Q., Paulson, H. L., and Davidson, B. L. (2002). siRNA-mediated gene silencing in vitro and in vivo. *Nat. Biotechnol.* 20: 1006–1010.
- McCaffrey, A. P. (2003). Inhibition of hepatitis B virus in mice by RNA interference. *Nat. Biotechnol.* 21: 639–644.
- Jacque, J.-M., Triques, K., and Stevenson, M. (2002). Modulation of HIV-1 replication by RNA interference. *Nature* 418: 435–438.
- Coburn, G. A., and Cullen, B. R. (2002). Potent and specific inhibition of human immunodeficiency virus type 1 replication by RNA interference. *J. Virol.* 76: 9225–9231.
- Kapadia, S. S., Brinkley-Andersen, A., and Chisari, F. V. (2003). Interference of hepatitis C virus RNA replication by short interfering RNA. *Proc. Natl. Acad. Sci. USA* 100: 2014–2018.
- Wender, P. A., et al. (2000). The design, synthesis, and evaluation of molecules that enable or enhance cellular uptake: peptoid molecular transporters. *Proc. Natl. Acad. Sci. USA* 97: 13005–13010.
- Kimura, M., Yokota, M., and Ohano, T. (2000). Transfection efficiency increases by incorporating hydrophobic monomer units into polymeric gene carriers. *J. Controlled Release* 68: 1–8.
- Li, P. Y., Xie, F. Y., and Woodle, M. C. (2003). siRNA-mediated antithrombogenicity for drug target validation and therapeutics. *Curr. Opin. Mol. Ther.* 5: 221–234.
- Takei, Y., Kadonatsu, K., Yuzava, Y., Matsuo, S., and Muramatsu, T. (2004). A small interfering RNA targeting vascular endothelial growth factor as cancer therapeutic. *Cancer Res.* 64: 3365–3370.
- Filleur, S., et al. (2003). siRNA-mediated inhibition of vascular endothelial growth factor severely limits tumor resistance to antiangiogenic thrombospondin-1 and slows tumor vascularization and growth. *Cancer Res.* 63: 3919–3922.
- Khalil, I. A., et al. (2004). Mechanism of improved gene transfer by the N-terminal stearylation of octaarginine: enhanced cellular association by hydrophobic core formation. *Gene Ther.* 11: 636–644.
- Blessing, T., Remy, J. S., and Behr, J. P. (1998). Monomeric collapse of plasmid DNA into stable virus-like particles. *Proc. Natl. Acad. Sci. USA* 95: 1427–1431.
- Carney, D. J., et al. (2000). Long chain arginine esters: a new class of catonic delivery agents for preparation of hydrophobic ion-paired complexes. *Biochim. Cell Biol.* 78: 59–65.
- Lee, M., Nah, J.-W., Kwon, Y., Koh, J. J., Ko, K. S., and Kim, S. W. (2001). Water-soluble and low molecular weight chitosan-based plasmid DNA delivery. *Pharm. Res.* 18: 427–431.

EXHIBIT 13

A Small Interfering RNA Targeting Vascular Endothelial Growth Factor as Cancer Therapeutics

Yoshifumi Takei,¹ Kenji Kadomatsu,¹ Yukio Yuzawa,² Seiichi Matsuo,² and Takashi Muramatsu¹

¹Departments of ¹Biochemistry and ²Clinical Immunology of Internal Medicine, Nagoya University Graduate School of Medicine, 65 Tsurumai-cho, Showa-ku, Nagoya, Japan

Abstract

Vascular endothelial growth factor (VEGF) plays a critical role during normal embryonic angiogenesis and also in the pathological angiogenesis that occurs in a number of diseases, including cancer. We developed a novel VEGF blockade system using RNA interference. The small interfering RNA (siRNA) targeting human VEGF almost completely inhibited the secretion of VEGF in a human prostate cancer cell line, PC-3, whereas the control scramble siRNA showed no effects. The VEGF siRNA with atelocollagen dramatically suppressed tumor angiogenesis and tumor growth in a PC-3 s.c. xenograft model. Atelocollagen provided a beneficial delivering means by which stabilization and efficient transfection of the siRNA injected into the tumors were achieved.

Introduction

Several RNA interference (RNAi) methodologies are rapidly being established and hold promise to specifically inhibit gene expression in mammals (1). RNAi is the sequence-specific, posttranscriptional gene silencing method initiated by double-stranded RNAs, which are homologous to the gene being suppressed. Double-stranded RNAs are processed by Dicer, a cellular RNase III, to generate duplexes of ~21 nt with 3'-overhangs [small interfering RNA (siRNA)], which mediate sequence-specific mRNA degradation (1, 2). RNAi technology, especially chemically synthesized siRNA, is currently being evaluated not only as an extremely powerful instrument for functional genomic analyses but also as a potentially useful method to develop highly specific gene-silencing therapeutics. However, there are only a few studies on the application of siRNA to the organismal level. This study was performed to suppress tumor angiogenesis by siRNA. There is compelling evidence indicating that uncontrolled angiogenesis is a major contributing factor in both tumor growth and metastasis (3–5). A number of growth factors have been identified as potential positive regulators of angiogenesis. Among them, vascular endothelial growth factor (VEGF) is the only growth factor most consistently found in a wide variety of conditions associated with angiogenesis (6). Inhibition of VEGF activity or disabling the function of its receptors has been shown to inhibit both tumor growth and metastasis in a variety of animal tumor models (7–9). We planned to suppress the synthesis of VEGF in the human prostate carcinoma cell line, PC-3, using siRNA and to evaluate its therapeutic significance in a xenograft model. For *in vivo* treatment, we used a new gene transfer method using a biomaterial, atelocollagen, prepared from bovine dermis (10). Atelocollagen is unique in that it is a liquid at 4°C and a gel at 37°C. Therefore, we expected atelocollagen to increase cellular uptake,

nuclease resistance, and prolonged release of the siRNA administered into the tumor as has been shown in the case of plasmid DNA (10) and antisense oligodeoxynucleotide modified with a phosphorothioate backbone (11).

Materials and Methods

Preparation of siRNAs. Five siRNAs targeting human VEGF and one scrambled siRNA (used for a positive control) with the following sense and antisense sequences were used: VEGF siRNA no. 1 (bases 131–149), 5'-UGAU-GUCUA-CAGCGGCA-GdTdT-3' (sense), 5'-CUGC-CGGU-GAU-GACAU-CAC-dTdT-3' (antisense); VEGF siRNA no. 2 (bases 149–167), 5'-CAUC-AUCGCC-AUCCAU-UAGG-dTdT-3' (sense), 5'-UCGA-UUGGU-GAGCG-CAGUAG-CGdTdT-3' (antisense); VEGF siRNA no. 3 (bases 189–207), 5'-GGAGU-GACCC-GAU-GAGAUCdTdT-3' (sense), 5'-GAUCUCAUCAGGGU-AUCCCGGA-UAUUdTdT-3' (antisense); VEGF siRNA no. 4 (bases 290–308), 5'-CUGAG-GAGU-GCCA-CAU-CACdTdT-3' (sense), 5'-GUGAUGU-GGACUCCUCA-GdTdT-3' (antisense); VEGF siRNA no. 5 (bases 336–354), 5'-CAAGGCCAGCACAU-AGGG-dTdT-3' (sense), 5'-UCCUAU-GUGCG-GCCUUGGdTdT-3' (antisense), and VEGF siRNA no. 3-SCR, 5'-ACGCCGU-AACCCGGGA-UAUUdTdT-3' (sense), 5'-AAAUUCCCGGGUUAACGGGU-dTdT-3' (antisense). All siRNAs were designed by B-Bridge International, Inc. (Sunnyvale, CA) and synthesized by Dharmacore, Inc. (LaJolla, CA) using 2'-bis (acetoxyethoxy)-methyl ether (ACE) protection chemistry. We selected siRNA sequences as reported by Elsharif et al. (12). Thus, we (a) searched for sequences 5'-AA(N19) or 5'-NA(N19), where N is any nucleotide, in the intended mRNA sequence (within an open reading frame and preferably 50–100 nt downstream of the start codon) and choose those with 47 or 52% G/C content; (b) Blast-searched the selected siRNA sequences against expressed sequence tag libraries to ensure that only a single gene is targeted; and (c) checked a predicted secondary structure of the intended mRNA to avoid a steric hindrance for its binding. Each freeze-dried siRNA was reconstituted with RNase-free water to prepare a 20 μM stock solution. The targeting sequence and its location of each siRNA in VEGF cDNA is shown in Fig. 1*A*. To inhibit the synthesis of all five alternative splicing variants of human VEGF, all target sites in this study were selected within exons 3 and 4. We also used fluorescein (F-) or ³²P-labeled VEGF siRNA no. 3-SCR to monitor the stability of siRNA upon injection into tumors grown in nude mice. To verify the sequence specificity of the RNAi system, VEGF siRNA no. 3 with one or two mismatches was also synthesized (Fig. 1*B*).

Cell Culture Conditions and Transfection of siRNAs. PC-3 cells (American Type Culture Collection, Manassas, VA) derived from human prostate adenocarcinomas were cultured in Ham's F-12 medium modified by Prostate (F-12K) with 10% heat-inactivated fetal bovine serum at 37°C in a humidified atmosphere of 5% CO₂. Cells were plated at a density of 2 × 10³ cells/35-mm tissue culture dish. After 20 h and 70–80% confluence, the cells were transfected with siRNAs in serum-free medium using LipofectAMINE PLUS (Invitrogen, Carlsbad, CA). Then, 5 μl of each siRNA stock solution (20 μM) and the PLUS reagent (10 μl) were mixed in Opti-MEM (85 μl, Invitrogen) in a small sterile tube. After immediate mixing and incubation at room temperature for 15 min, the LipofectAMINE reagent (4 μl) in Opti-MEM (100 μl) was added, and the mixture was left at room temperature for 15 min. Then, 0.8 ml of F-12K was added to generate the siRNA-lipid complex. The PC-3 culture medium was removed, and the siRNA-lipid complex (1 ml total volume) was added. After incubation for 4 h at 37°C, 1 ml of F-12K with 10% fetal bovine

Received 8/27/03; revised 3/15/04; accepted 3/26/04.

Grant support: Ministry of Education, Science, Sports and Culture of Japan Grants-in-Aid 15CE2006 and 21st Century Grand and Japan Society for the Promotion of Science Grants-in-Aid 12004272 and 15390103.

The costs of publication of this article were defrayed in part by the payment of page charges. This article must therefore be hereby marked *advertisement* in accordance with 18 U.S.C. Section 1734 solely to indicate this fact.

Requests for reprints: Yoshifumi Takei, Department of Biochemistry, Nagoya University Graduate School of Medicine, 65 Tsurumai-cho, Showa-ku, Nagoya 466-8550, Japan. Phone: 81-52-744-2064; Fax: 81-52-744-2065; E-mail: takei@med.nagoya-u.ac.jp.

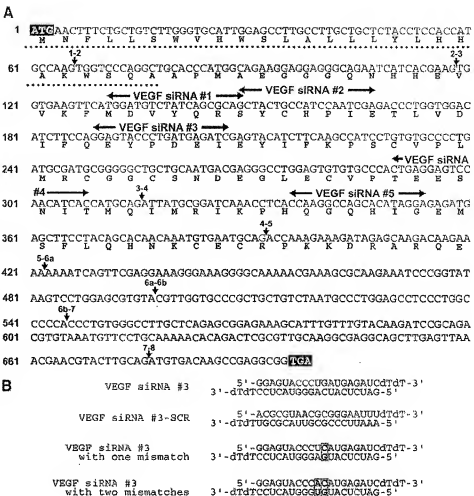


Fig. 1. *A*, design of vascular endothelial growth factor (VEGF) small interfering RNAs (siRNAs). Locations of VEGF siRNA nos. 1, 2, 3, 4, and 5 examined in this study are shown by horizontal arrows. ATG (**■**), the translation initiation site; TGA (**▲**), the translation terminal site; \rightarrow , the signal peptide; \leftarrow , vertical arrow, exon-intron junctions (number indicates exon numbers). *B*, structures of VEGF siRNA no. 3 determined as the most effective siRNA to human VEGF secretion in this study and its scrambled control (VEGF siRNA no. 3-SCR). We also used two siRNAs to verify the sequence specificity of VEGF siRNA no. 3. Structures of VEGF siRNA no. 3 with one mismatch and two mismatches were also shown. Mismatch site(s) was shown in box(es).

serum was added, and incubation was continued for 6 h. The medium was then replaced with fresh F-12K with heparin (20 μ g/ml). After 16 h of incubation, conditioned medium was collected for ELISA.

VEGF ELISA. Secretion of VEGF into the cell culture supernatant and tumor contents of VEGF in the PC-3 xenografts were determined using a Quantikine human VEGF Immunoassay kit (R&D Systems, Minneapolis, MN) according to the manufacturer's instructions.

Quantifying mRNA of VEGF. The concentrations of human VEGF mRNA were determined with a Quantikine mRNA colorimetric quantitation kit (R&D Systems) according to the manufacturer's instructions. Total RNA samples (5 μ g) from PC-3 cells transfected with various siRNAs were assayed using human VEGF gene-specific biotin-labeled capture oligonucleotide probes and digoxigenin-labeled detection probes. The concentration of human VEGF mRNA was calculated by interpolation of a standard calibration curve.

Semi quantitative Reverse Transcription-PCR Analysis for VEGF Family Gene Expression. Reverse transcription-PCR was performed with the isolated total RNA (1 μ g) using Omniscript RT kit and HotStarTaq PCR kit (Qagen) according to the manufacturer's instructions. Two primer set to detect VEGF-B (13), VEGF-C (14), VEGF-D (14), and placenta growth factor (13) was used, respectively. Details in conditions for PCR reaction were reported previously (13, 14).

Preparation of 32 P-Labeled siRNA. VEGF siRNA no. 3-SCR were labeled at the 5'-end by T4 polynucleotide kinase (Takara Shuzo Co. Ltd.) and [32 P]ATP (Amersham Bioscience) in 50 μ l of reaction mixture. Thus, 5 μ l of VEGF siRNA no. 3-SCR stock solution (20 μ M), RNase-free water (30 μ l), 10 \times kinase buffer (5 μ l; Takara), 5 μ l of T4 polynucleotide kinase (10 units/ μ l), and 5 μ l of [32 P]ATP (6000 Ci/mmol) were incubated at 37°C for 2 h. The reaction mixture was placed in the upper chamber of Microcon YM3 (cutoff value M_r 3000, Millipore Corp.). After adding 200 μ l of RNase-free

water, it was centrifuged (4000 \times g), and the procedure was repeated four times. Material remaining in the upper chamber was regarded as 32 P-labeled VEGF siRNA (200 μ M). Analysis of 32 P-labeled VEGF siRNA by PAGE (15% acrylamide) followed by autoradiography gave a single band.

Cellular Uptake of 32 P-Labeled siRNA. PC-3 cells were transfected with 32 P-labeled VEGF siRNA (100 nM; 213,965 cpm/dish) using LipofectAMINE PLUS as described above. On the next day, the cells were vigorously washed with PBS to remove incorporated 32 P-labeled siRNA on the cell surface and were lysed with Celllytic-MT Mammalian Tissue Lysis/Extraction Reagent (Sigma Chemical Co.). After centrifugation, radioactivity in the supernatant was determined by a liquid scintillation counter (Beckman). Then, the efficiency for transfection was calculated.

Tumor Therapy. A total of 3.0×10^6 PC-3 cells were s.c. inoculated in 0.3 ml of serum-free F-12K medium through a 24-gauge needle into the lower flank of 8-week-old athymic nude mice obtained from SLC (Tokyo, Japan) as described previously (11, 15). After 3 weeks when the tumors had reached an average volume of $\sim 50 - 60$ mm³, the tumor-bearing nude mice were treated with VEGF siRNA no. 3 with stelocollagen (Koken Co. Ltd., Tokyo, Japan). The final concentration of stelocollagen was 1.75% and that of the siRNA is described in Fig. 3. siRNAs were used after dilution with PBS. As positive controls, PBS mixed with stelocollagen was injected. Each therapeutic reagent was injected into the tumors every 10 days after the first injection as indicated in Fig. 3. Tumor diameters were measured at regular intervals with digital calipers, and the tumor volume in mm³ was calculated by the formula: volume = (width)² \times length/2 (16). Data are presented as mean \pm SE. Animal experiments in the present study were performed in compliance with the guidelines of the Institute for Laboratory Animal Research, Nagoya University Graduate School of Medicine.